CLEAN WATER
WATER POLLUTION CONTROL RESEARCH SERIES ●
16130 FSU 12/71

# SURFACE DISCHARGE OF HEATED WATER

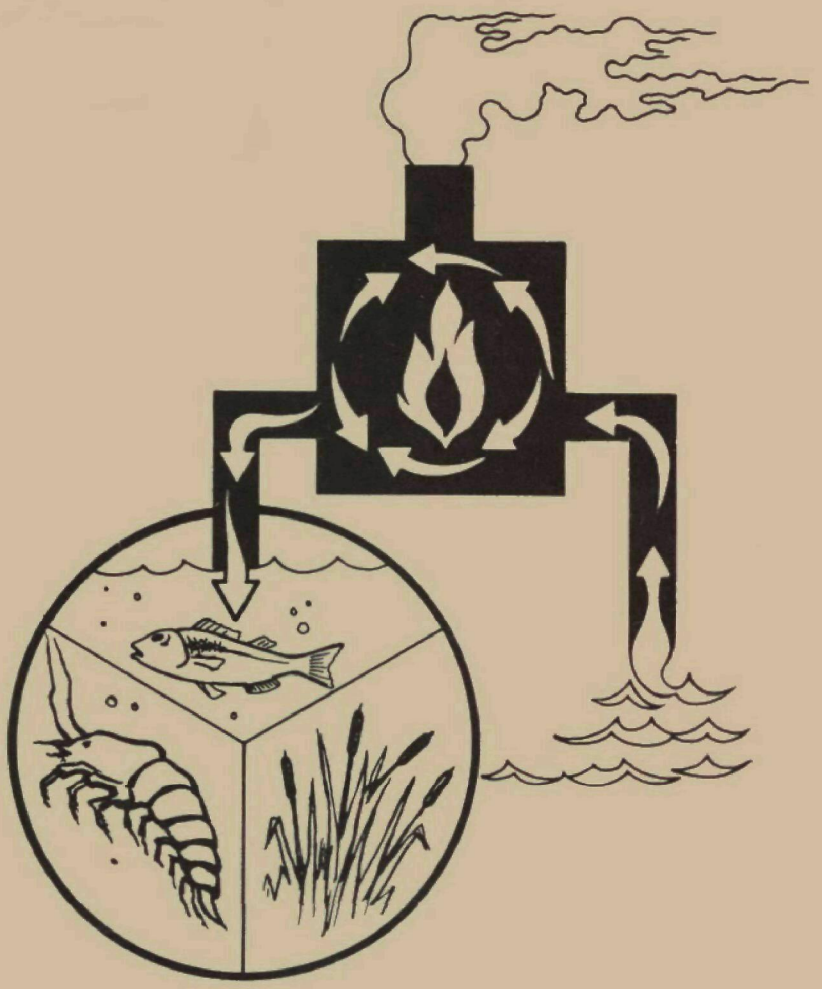

U.S. ENVIRONMENTAL PROTECTION AGENCY

## WATER POLLUTION CONTROL RESEARCH SERIES

The Water Pollution Control Research Series describes the results and progress in the control and abatement of pollution in our Nation's waters. They provide a central source of information on the research, development and demonstration activities in the Environmental Protection Agency, through inhouse research and grants and contracts with Federal, State, and local agencies, research institutions, and industrial organizations.

Inquiries pertaining to Water Pollution Control Research Reports should be directed to the Chief, Publications Branch (Water), Research Information Division, R&M, Environmental Protection Agency, Washington, D.C. 20460.

# SURFACE DISCHARGE OF HEATED WATER

by

H. Stefan,
N. Hayakawa,
and
F.R. Schiebe

University of Minnesota
St. Anthony Falls Hydraulic Laboratory
Mississippi River at 3rd Avenue S.E.
Minneapolis, Minnesota 55414

for the

Office of Research and Monitoring
ENVIRONMENTAL PROTECTION AGENCY

Project #16130 FSU

December 1971

For sale by the Superintendent of Documents, U.S. Government Printing Office, Washington, D.C., 20402 - Price $2

EPA Review Notice

This report has been reviewed by the Environmental Protection Agency and approved for publication. Approval does not signify that the contents necessarily reflect the views and policies of the Environmental Protection Agency nor does mention of trade names or commercial products constitute endorsement or recommendation for use.

# PREFACE

The dissipation of heat from cooling water rejected by power generating plants has become a problem of great concern because of its ecological impact. Research efforts in the area of thermal pollution, thermal addition, calefaction, or whatever name may be used have been tremendously increased over the past decade. The St. Anthony Falls Hydraulic Laboratory has participated in these efforts, and several reports on related topics have preceded this one.

This volume is divided into three parts, each of which contains its own conclusions and recommendations, table of contents, series of figures and tables, and list of bibliographical references. The parts are as follows:

Part I: "Three-Dimensional Jet-Type Surface Plumes in Theory and in the Laboratory," by H. Stefan (Project Report No. 126, St. Anthony Falls Hydraulic Laboratory, University of Minnesota, December 1971), pages I-i through I-129 plus Appendices A and B.

Part II: "The Two-Dimensional Buoyant Surface Jet and the Internal Hydraulic Jump," by H. Stefan and N. Hayakawa (Project Report No. 127, St. Anthony Falls Hydraulic Laboratory, University of Minnesota, August 1971), pages II-i through II-55.

Part III: "Field Measurements in a Three-Dimensional Jet-Type Surface Plume," by H. Stefan and F. R. Schiebe (Project Report No. 128, St. Anthony Falls Hydraulic Laboratory, University of Minnesota, December 1971), pages III-i through III-35.

From these titles it is clear that the report deals with one particular aspect of the very complex thermal pollution problem. Emphasis is on flow, entrainment, and dilution of heated water effluents near surface outlets. The results are of significance for open-cycle operating systems and may also find application in the operation of cooling ponds and mixing chambers.

# Part I: Three-Dimensional Jet-Type Surface Plumes in Theory and in the Laboratory

by

H. Stefan

December 1971

## ABSTRACT

The steady flow of heated water from a channel into a reservoir or lake has been studied analytically and experimentally. A three-dimensional buoyant-jet-type model has been developed to predict the main trajectory, velocity, and temperature distributions in that portion of the plume in which the flow is dominated by the momentum and the buoyancy of the discharge and has free boundaries. The interaction between turbulent mixing, buoyant spreading, and surface cooling, which are crucial for the development of any thermal plume, can be illustrated with the aid of the model. The effects of weak cross currents and weak wind on the development of a surface plume are also incorporated into the model. The model does not apply to heated water discharges which cling to a shoreline due to a particular shoreline configuration or to wind or current conditions. The effects of cold water wedge penetration into an outlet channel can be accommodated by the model.

Experimental results on temperature and velocity distributions in free-jet-type three-dimensional thermal plumes have been used to verify some of the assumptions made in the numerical model, particularly those regarding Gaussian velocity and temperature distributions and lateral spread coefficients. In addition, the measurements have been used to illustrate changes in total flow rate, total heat storage, and dimensions of a surface plume. The distribution of temperatures, velocities, and Richardson numbers in an experimental surface plume has been illustrated using different types of contour plots. There is reasonable agreement between the results of the experiments and the proposed analytical prediction method.

CONTENTS

LIST OF FIGURES AND TABLES

## LIST OF SYMBOLS AND UNITS

| | |
|---|---|
| $a$ | Standard deviation of velocity distribution in vertical plane through main trajectory [ft] |
| $b$ | Standard deviation of velocity distribution at water surface [ft] |
| $C$ | Drag coefficient [-] |
| $C$ | Heat content [BTU] |
| $c_1$, $c_2$, $c_3$ | Coefficients related to various functions for entrainment coefficient [-] |
| $c_4$ | Coefficient designating turbulent spread of non-buoyant, circular, submerged jet [-] |
| $c_5$ | Coefficient designating buoyancy induced lateral spread of plume [-] |
| $c_6$ | = exp (-0.5) |
| $c_7$ | Coefficient related to initial spread of contour of plume |
| $c_p$ | Specific heat of water [BTU slugs$^{-1}$ $^{o}F^{-1}$] |
| $D$ | Drag force [lbs] |
| $D_o$ | Hydraulic diameter of discharge channel [ft] |
| $d$ | Depth [ft] |
| $d_o$ | Depth at discharge channel [ft] |
| $F$ | densimetric Froude number [-] |
| $F$ | Force [lbs] |
| $f_1$, $f_2$, $f_3$, $f_4$, $f_5$ | Values of specified integrals [-] |

| | |
|---|---|
| $g$ | Acceleration of gravity (32.2 ft $sec^{-2}$) |
| $H$ | Heat flux [BTU $sec^{-1}$] |
| $K$ | Entrainment coefficient [-] |
| $K_s$ | Surface heat transfer coefficient [BTU $ft^{-2}$ $^oF^{-1}$ $hr^{-1}$] |
| $k$ | Constant concentration [-] |
| $M$ | Momentum flux [lbs] |
| $m$ | Number limiting depth of plume [-] |
| $N$ | Number of steps |
| $N_p$ | Number of positive values in a profile [-] |
| $n$ | Number limiting width of plume [-] |
| $Q$ | Volumetric flow rate [$ft^3$ $sec^{-1}$] |
| $R$ | Radius of curvature of plume in horizontal plane [ft] |
| Re | Reynolds number |
| Ri | Richardson number |
| $r$ | Distance from and perpendicular to main trajectory [ft] |
| $s$ | Distance from virtual origin along main trajectory [ft] |
| $T$ | Temperature [$^oF$] |
| $t$ | Time [sec] |
| $U_o$ | Average discharge velocity [ft $sec^{-1}$] |
| $U_s$ | Constant stream or current velocity [ft $sec^{-1}$] |
| $u$ | Flow velocity tangent to main trajectory [ft $sec^{-1}$] |
| $v$ | Flow velocity perpendicular to main trajectory [ft $sec^{-1}$] |
| $W$ | Wind velocity [ft $sec^{-1}$] |
| $w_o$ | Width of discharge channel [ft] |
| $x$ | Coordinate in direction perpendicular to current [ft] |
| $y$ | Coordinate in direction of current [ft] |
| $z$ | Depth [ft] |

| | |
|---|---|
| $\alpha$ | Angle between plume trajectory and current [degrees] |
| $\beta$ | Angle between wind and current [degrees] |
| $\delta$ | Halfwidth to depth ratio of plume [-] |
| $\epsilon$ | Error |
| $\lambda$ | Similarity parameter [-] |
| $\mu$ | Dynamic viscosity [lb sec $ft^{-2}$] |
| $\varrho$ | Density of water [slugs $ft^{-3}$] |
| $\tau$ | Wind shear stress [lb $ft^{-2}$] |
| $\phi$ | Spread angle of contour [degrees] |

Subscripts

| | |
|---|---|
| a | air |
| c | contour |
| D | drag |
| E | equilibrium |
| e | experimental |
| f | friction |
| h | horizontal |
| i | control volume |
| i | element along main trajectory |
| j | element along vertical profile |
| $\ell$ | lake or ambient |
| n | net value |
| o | initial value |
| o | neutrally buoyant (for K only) |
| r | in r-direction |
| s | in s-direction |
| T | temperature |
| th | theoretical |
| u | velocity |
| v | vertical |
| w | wind |

Superscript * differential with reference to ambient water

# SECTION I

## CONCLUSIONS

The study reported in Part I deals with the steady flow of heated water from a channel into a reservoir or lake. A three-dimensional buoyant-jet-type analytical model has been developed and compared with laboratory data. The model is based on the observation that a heated water surface discharge is initially dominated by the momentum and the buoyancy of the discharge. The absence of solid boundaries and the unhindered spread of the heated water are essential. The model will predict the main trajectory, the depth, and the width of the plume and the centerline velocities and temperatures in the plume. The model includes the effect of cold water wedge penetration into an outlet channel.

The method of calculation is such that the geometrical extent of the flow field which can be legitimately covered by a jet-type model (the nearfield) becomes apparent from the results. The experimental data which are reported and analyzed have been valuable as a guide to a physically meaningful analytical description of the flow. A spread parameter was used and its possible magnitude derived from experimental data.

Results obtained with the analytical model and from experiments show substantial initial dilution of effluents even when buoyancy and stratification are strong.

## SECTION II

## RECOMMENDATIONS

It is recommended that the effects of solid boundaries and strong winds on thermal plumes be further investigated both analytically and experimentally. A substantial change in the flow and turbulent mixing processes is induced when heated water is injected into strong cross currents or onshore winds. Further attention should be given to these circumstances.

## SECTION III

## INTRODUCTION

The possibility of ecological stresses on the aquatic environment produced by discharges of large quantities of heated water from industrial plants, particularly power generating plants, has been discussed by numerous authors. References [1,2,3,4,5]* are examples of such discussions. A large amount of information on the effects of heat on organisms is becoming available, and it indicates that future site selection and operating policy for power plants will be much more complex in the light of their variable impact on water ecology.

Temperature standards have been set by individual states under the guidance and supervision of the federal government. These standards have an important bearing on power plant site selection and mode of operation, especially when the standards are very restrictive. Mixing zones are often allowed near the heated water outfalls. Temperature standards are frequently defined in terms of a temperature increment between an ambient water temperature and the outlet temperature and in terms of a maximum discharge temperature, both of which must be met at the end of the mixing zone. It is therefore necessary to be able to predict in the planning stage the temperature decay in a mixing zone. The present investigation was concerned with that problem.

Heated water can be discharged into a natural body of water in many different ways. Frequently the discharge is from an open channel, and attention will be focused on this case.

---

*References for Part I are listed on pages I-125 through I-129.

## SECTION IV

## PREVIOUS STUDIES ON THERMAL PLUMES

The problem of heat dispersion in a body of water has been attacked theoretically, experimentally, and through site studies. A general solution method according to which point temperatures and velocities in all thermal plumes could be calculated has not been found. A few theoretical approaches have been tried, with some success, and laboratory and field measurements have been accumulated and interpreted. More such data will certainly be forthcoming.

### Theoretical Studies

The surface plume problem has generally been treated theoretically as either a passive dispersion problem, as in Refs. [6,7,8], or a two-dimensional turbulent jet problem as in Refs. [9,10,11,12]. The plume has also been treated theoretically as a purely buoyant surface jet [13] and as a three-dimensional surface jet [14]. These theories apply to the near field only, where turbulence is generated by shear between discharge and ambient fluid. Both jet-type dispersion and passive dispersion in a free turbulent field are treated with various simplifying assumptions in Ref. [15]. There have also been a number of studies dealing with non-buoyant two- or three-dimensional jet discharges into cross-currents or co-current streams; Refs. [16] and [17] are examples.

### Experimental Studies

Experiments with three-dimensional surface discharges of heated water into cold water tanks have produced temperature data in plumes for a great variety of outlet conditions. Numerous case studies have been made of specific power plants, as a recent compilation [18] shows, and there have also been a few investigations dealing with idealized geometrical boundary conditions and more fundamental aspects of plume formation [13,14,16,17,19,20,21,22]. In this context it is also pertinent to cite studies concerned with fresh water flows into saline bodies of water [23,24].

Model studies of specific power plant sites are, of course, useful in dealing with complicated geometrical boundary conditions. Although scale effects on turbulent mixing and entrainment are beyond control, each experimental plume can be considered a plume in its own right. Therefore, laboratory data are as useful as field measurements when they are used to formulate and examine deterministic prediction methods.

### Field Measurements

Field measurements usually consist of sets of temperature data [25,26, 27,28,29]. In a few instances, current measurements have been carried out simultaneously [29]. Such measurements are, of course, very useful in the development of prediction techniques, especially if the discharge, ambient water, and meteorological conditions are measured simultaneously.

## SECTION V

## THEORETICAL STUDY

### Concept of Analytical Plume Model

Power plants operating with open cooling water supply systems withdraw the cooling water from natural sources such as rivers, lakes, and the ocean. They use it once and discharge it at elevated temperatures back into the environment. The present study was concerned with the flow and dissipation of heat in the receiving body of water, with emphasis on lakes. The effects of currents and wind, surface cooling, and mixing are combined in a comprehensive numerical model.

Condenser cooling water temperatures generally range from $10^{\circ}$ to $35^{\circ}$F above intake temperatures. Flow rates are of the order of from several hundred to several thousand cfs for the largest power plants presently in operation or under construction. When such large quantities of heated water are discharged into a lake, a so-called thermal plume is formed. If the environmental impact of heated water discharges is to be assessed, it is necessary to be able to predict the size of the plume, its temperature, and its flow characteristics.

At the point of discharge, usually at the end of an outlet channel, a heated water plume is basically a turbulent, incompressible jet of very large dimensions. It is characterized by an initial mass flux, momentum flux, buoyancy flux, and energy flux. As the water moves away from the surface outlet into a larger and colder body of water it will display some features which are familiar from high speed jet flows, such as entrainment of surrounding fluid by turbulent mixing. In the absence of both solid boundaries near the jet and external forces, the momentum flux will be conserved. Sometimes the effects of solid boundaries on the jet are felt rather strongly, however, and the conservation of momentum assumption does not apply. As the flow volume increases and the velocities in the jet decrease, the characteristics of the receiving body of water--in particular its currents and its turbulence--will be imprinted more and more on the jet. Eventually the jet flow will be altered to such an extent that the initial characteristics will be unrecognizable.

Simultaneously with the jet's development, the atmosphere has its effect on the thermal plume. There is an energy flux, reversible in direction, across any air-water interface. Usually heat energy is transmitted by evaporation, conduction, convection, and long-wave backradiation from the plume to the atmosphere, with the result that the heat flux carried by the plume decreases with distance from its point of discharge. Sometimes the direction of the heat flux is reversed. The water surface is also where the transfer of mechanical energy provided by wind takes place. Shear stresses at the water surface, wave generation, currents, and turbulence are very closely associated with the action of wind. From field studies it is well known that wind has an influence on the shape and extent of thermal plumes.

A third and very important aspect of thermal plumes is that of buoyancy and stratification. Since the density of fresh water decreases when the temperature is raised above 39.2°F, heated water will generally float when surrounded by colder water. This is also the case when sea water is used as a source of cooling water. Buoyancy will cause lateral spread of a plume beyond that produced by turbulent mixing. It will also tend to reduce or eliminate vertical mixing between a thermal plume and the underlying water. The thermal plume will thus display certain features which are typical for stratified flows.

Experimental studies and field measurements have revealed quite clearly the dual character of thermal plumes as turbulent jets and stratified flows. A simplified mathematical formulation will be given for the heated water plume problem in terms of a buoyant jet flow into a slow cross current under the effects of wind and surface cooling. The model will predict the main trajectory, the depth, the width, and the temperature distribution of the plume as well as the rate of heat dispersion.

Since the geometry of heated water outlet channels and shoreline configurations varies from one discharge to another, it is often advantageous to consider separately an outlet region, a near field, and a far field. In the outlet region, channel and lake shore geometries have a major effect on the flow and mixing in addition to the source characteristics of momentum and buoyancy flux. If the outlet and shore geometries are complicated, it may be necessary to study this zone separately using analytical or numerical methods or even physical model studies. The model which will now be discussed begins at the point from which solid boundaries have a negligible effect on the plume and considers essentially the flow in the near field.

The near field is that portion of the plume in which the dynamics are controlled by the momentum of the discharge and by external forces such as wind, shear, and well defined currents. The far field is that portion of the plume where the heated effluent is dispersed essentially by turbulent mixing and heat transfer mechanisms which are controlled by the overall hydrodynamic and thermodynamic characteristics of the receiving body of water, including specifically large-scale turbulence, existing stratification, and overall velocity patterns.

The theory to be presented considers a three-dimensional half-jet and the essential forces and processes contributing to its development. Since at the present time turbulent flow and transport processes are not understood completely enough to permit an exact solution for the three-dimensional turbulent flow in a thermal plume, the problem is formulated in terms of experimentally supported and mostly well documented semi-empirical relationships. Several of these are drawn from previous studies, but some new ones are also proposed. All relationships together constitute a mathematical model of the thermal plume.

Basic Equations

The theory approximates the real plume by a three-dimensional horizontal half-jet discharging at some angle $\alpha_o$ into an existing current as shown in Fig. 1. A finite shear stress produced by wind is assumed to exist at the water surface. The behavior of the heated water jet in a body of water of infinite extent will be examined. A real outlet is usually located at the shore, and the last assumption will be satisfied only if the current and wind patterns allow the jet to move away from the shoreline. A strong initial momentum and an offshore wind will generally help to produce such a situation.

In the analysis the thermal plume is described in terms of its main trajectory and its velocity and temperature distributions in cross sections perpendicular to the main trajectory. The main trajectory is the streamline through all points with maximum velocity at the water surface. The plume in this study is characterized by velocities and temperatures in excess of those of the surrounding water. The situation is shown schematically in Fig. 2.

The excess velocity and excess temperature distributions in a plane perpendicular to the main trajectory are assumed to be similar to each other when normalized with respect to centerline values (for velocity and temperature) and standard deviations (for distances from the main trajectory), respectively. The practical evaluations will be carried through with Gaussian distributions in both vertical and horizontal directions, although other distributions can be used as well without changing the essence of the procedure. Gaussian profiles approximate experimental data on submerged jets quite well [30,31,32] and have been used before in numerical models [9,11,30]. The velocity distribution is shown schematically in Fig. 2. Temperature and velocity measurements in surface plumes [20,21,22] support to some degree the use of Gaussian distributions in the description of three-dimensional plumes. An analysis of experimental data to this effect will be presented in a later section. Because of the complicated interaction between buoyancy and turbulence in a horizontally stratified flow, it is thought that under close scrutiny the similarity principle does not hold rigorously for the vertical distributions. This serious theoretical defect is fully realized, but appears not to be of overwhelming significance for the overall picture of a plume.

The spread of these Gaussian distributions, as measured by standard deviations, will be different in the horizontal and vertical directions because of buoyancy as evidenced by experimental and field data. The relative velocity and temperature distributions are therefore described by the equations

$$\frac{u^*(s,r,z)}{u^*(s,0,0)} = \exp\left[-\frac{1}{2}\left(\frac{r}{b}\right)^2\right] \exp\left[-\frac{1}{2}\left(\frac{z}{a}\right)^2\right] \tag{1}$$

$$\frac{T^*(s,r,z)}{T^*(s,0,0)} = \exp\left[-\frac{1}{2}\left(\frac{r}{\lambda_h b}\right)^2\right] \exp\left[-\frac{1}{2}\left(\frac{z}{\lambda_v a}\right)^2\right] \tag{2}$$

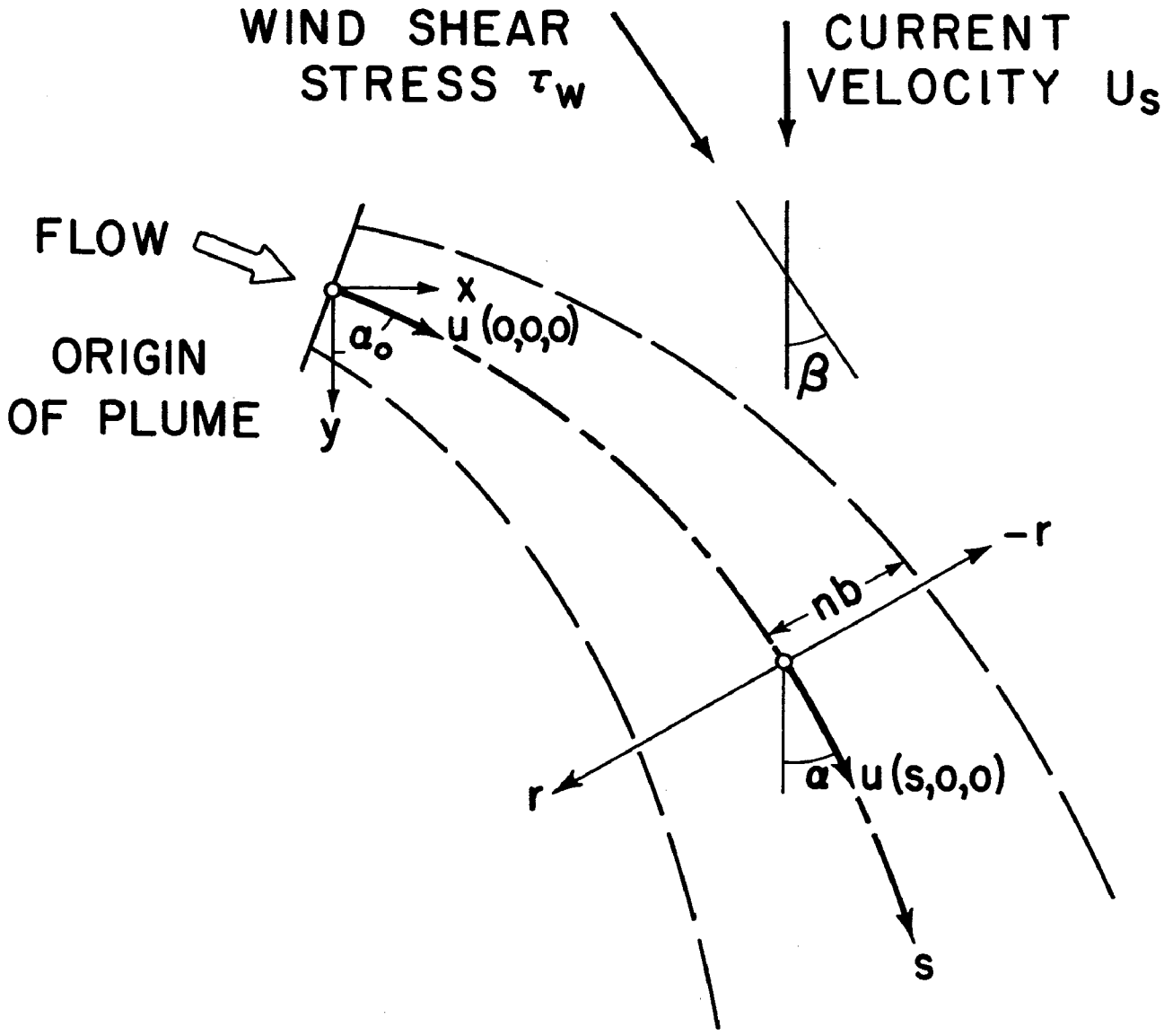


Fig. 1 - Definition Sketch - Plan View of Buoyant Surface Jet

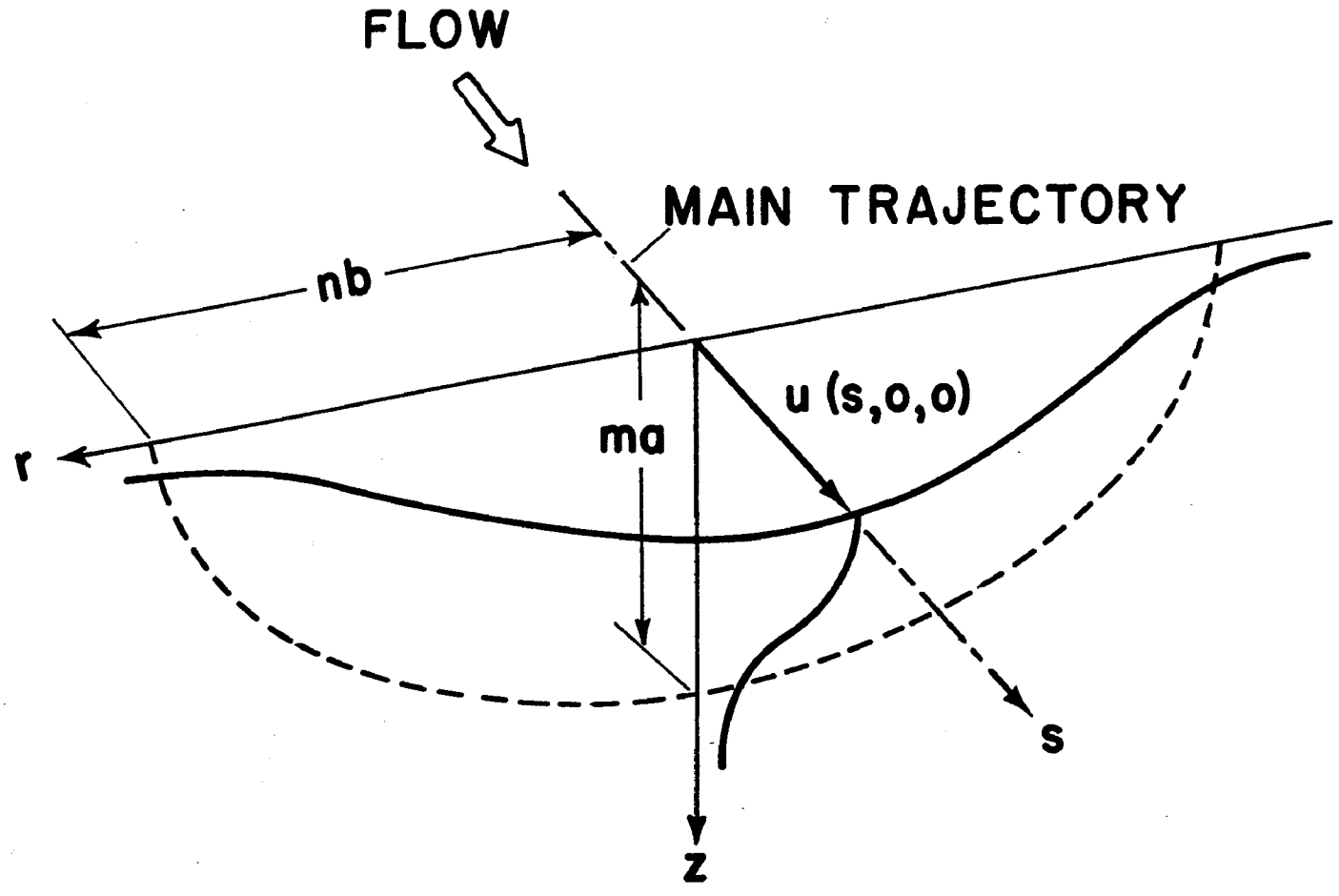


Fig. 2 - Definition Sketch - Cross Section of Buoyant Surface Jet

where $u^*(s,r,z)$ is the velocity at a point with the coordinates $(s,r,z)$ relative to the surrounding fluid; $u^* = u - U_s \cos\alpha$, where $u$ is the absolute local velocity in the plume, $U_s$ is the velocity of a uniform current surrounding the jet, and $\alpha$ is the jet angle relative to the current; the thermal plume is assumed to move imbedded in the current; $s$ is the distance from the beginning of the buoyant jet field which is usually located at or downstream from the actual outlet; $r$ is the normal distance from the main trajectory; $z$ is the depth below the water surface; and $T^*(s,r,z)$ is the water temperature at the same point as $u^*$ relative to the surrounding water. Thus $u^*(s,0,0)$ and $T^*(s,0,0)$ are the relative velocities and temperatures, respectively, on the main trajectory and $a(s)$ and $b(s)$ are standard deviations indicating the lateral or vertical spread of the distributions; $T^* = T - T_\ell$ where $T_\ell$ is the water temperature in the impoundment.

All velocities in a cross section perpendicular to the main trajectory are assumed to be parallel to the tangent on the main trajectory, and $\lambda_v$ and $\lambda_h$ are similarity parameters. In the absence of buoyancy and for fully submerged axisymmetric jets $\lambda_v = \lambda_h = 1.16$ has been used in Ref. [30]. In buoyant surface jets the horizontal spread of momentum is produced in a somewhat different way than the vertical spread. The vertical spread is essentially by turbulent mixing, including the effects of buoyancy; the horizontal spread is by turbulent mixing plus buoyant spread. In a later section an analysis of some experimental data will be given. As will be explained, there is not enough justification at this time for choosing values of $\lambda_h$ and $\lambda_v$ different from each other or much different from unity. It is therefore tentatively proposed to use $\lambda_v = \lambda_h = 1.05$.

The local buoyancy force per unit weight will follow a distribution quite similar to that of the temperature. If the temperature range covered by a specific temperature profile is not too wide, the density relationship $\varrho = \varrho(T)$ can be approximated by a straight line and the density deficit distribution is then

$$\frac{\varrho^*(s,r,z)}{\varrho^*(s,0,0)} = \exp\left[-\frac{1}{2}\left(\frac{r}{\lambda_h b}\right)^2\right] \exp\left[-\frac{1}{2}\left(\frac{z}{\lambda_v a}\right)^2\right] \qquad (3)$$

Here $\varrho^* = \varrho_\ell - \varrho$ where $\varrho$ is the actual local density and $\varrho_\ell$ is the density of the surrounding colder fluid (lake).

The density difference between the heated water in the jet and the cold water in the lake produces a loss in axisymmetry in a plane perpendicular to the main trajectory. In addition, the curvature of the main trajectory of a high-speed turbulent jet due to a cross current should result in a loss of symmetry with respect to a vertical plane (Fig. 3a) as shown in Refs. [34] and [35]. In buoyant and slowly moving surface jets (half-jets) with large radius of curvature of the main trajectory, however, the latter effect should be small. The

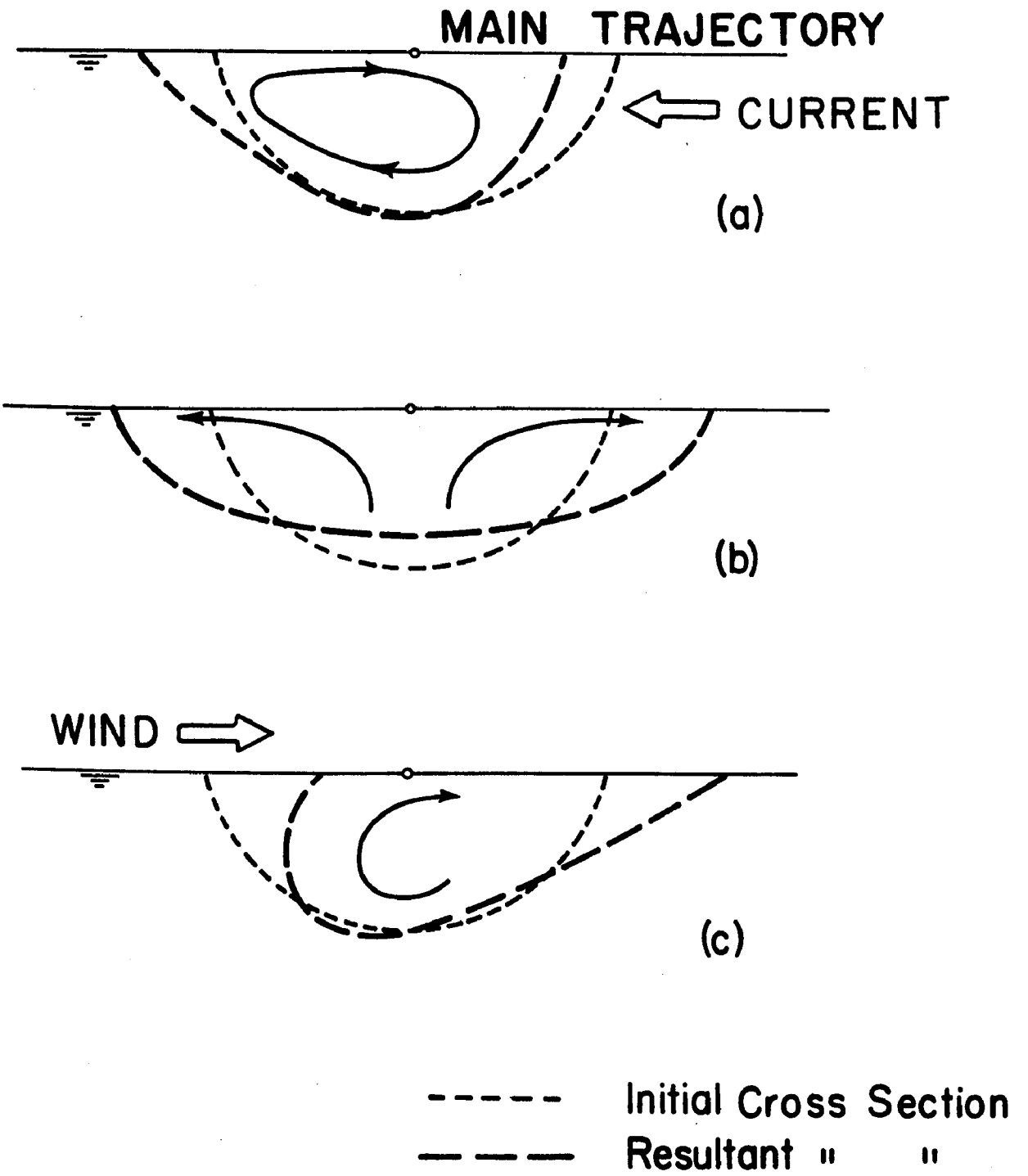


Fig. 3 - Deformation of Cross Section of Plume by (a) current, (b) buoyancy, (c) wind - Schematic

following analysis will therefore be concerned mainly with situations without vortex formation in the wake of the surface jet. This means in part that there is enough turbulence at a small enough scale remaining from the initial momentum of the jet or produced by external currents, as well as enough buoyancy at any cross section, to compensate for the current- or wind-produced destruction of the symmetry of a plume.

Because a thermal plume is also a density stratified flow, it may have features which are well known from open channel flow. In particular it is possible that the thickness of the plume is controlled from downstream rather than upstream. The conditions under which such a control exists in a two-dimensional plume have been discussed in Refs. [15] and [36]. It has been shown [36] that the value of the densimetric Froude number in a given cross section is the controlling dimensionless parameter. If the value of this number is larger than the critical value, a downstream control does not exist. The present model applies to flows for which the densimetric Froude number, as defined later in Eq. (4), remains larger than critical. This is likely to be the case under various natural conditions if there is a current, substantial wind drift, or simply sufficient heat transfer through the water surface. It may not hold true in a lake in which the surface cooling is temporarily very slow or if the wind drift is in direct opposition to the direction of discharge. An internal backwater effect will then become apparent as shown by Fig. 9c of Ref. [36] and by Fig. 12 of Ref. [20]. The internal Froude number can be defined as

$$F = F^* + F_s$$

where

$$F^* = \frac{u^*(s,0,0)}{\left[\frac{\varrho^*(s,0,0)}{\varrho}\, g\, \lambda_v\, a\right]^{1/2}} \quad \text{and} \quad F_s = \frac{U_s \cos\alpha}{\left[\frac{\varrho^*(s,0,0)}{\varrho}\, g\, \lambda_v\, a\right]^{1/2}} \tag{4}$$

To arrive at the basic equations it is necessary to examine the volumetric flux $Q$, the heat flux $H$, and the momentum flux $M$ in cross sections perpendicular to the main trajectory of the plume. Since the fluid is incompressible and since the Boussinesq assumption can also be made because temperature-induced density differences are very small, the volumetric flux $Q$ is used instead of the mass flux.

$$Q(s) = \int_{-\infty}^{\infty}\int_{0}^{\infty} u(s,r,z)\, dzdr \tag{5}$$

$$H(s) = \int_{-\infty}^{\infty}\int_{0}^{\infty} u(s,r,z)\ c_p \varrho T^*(s,r,z)\ dzdr \tag{6}$$

$$M(s) = \int_{-\infty}^{\infty}\int_{0}^{\infty} \varrho u^2(s,r,z)\ dzdr \tag{7}$$

These fluxes are of course absolute values. The limits of integration of Eqs. (5), (6), and (7) must match the velocity and temperature distributions of Eqs. (1) and (2), which provide for infinite width and depth of the jet. The real jet is limited in width, and therefore the limits of integration should be replaced by $-nb$ and $+nb$ for the r-direction and by zero and $ma$ for the z-direction where $n$ and $m$ are finite numbers. The visual spreading angle of non-buoyant axisymmetric jets is of the order of $14^\circ$ to $19^\circ$ according to Refs. [37] and [38]. It is therefore physically meaningful to limit $n$ and $m$ values to $n = m = 3$.

The volumetric flux increases in the flow direction as a consequence of entrainment. The process is very complex. In the initial stage of the plume's development, turbulence is produced mostly by the shearing motion between the heated water jet and the surrounding cold water. In such a flow it has been shown [32] that the rate of entrainment is proportional to the velocity of the main jet relative to its surroundings. Application of the entrainment principle to the buoyant half-jet yields

$$\frac{dQ(s)}{ds} = K\, u^*(s,0,0)\, \frac{(a+b)\pi\sqrt{2}}{2} \tag{8}$$

The eddies which produce this kind of mixing are on the same geometrical scale as the jet itself. For a neutrally buoyant, fully submerged, axisymmetric turbulent air jet $K = 0.057$ was found to match experimental data [33] best, while a study with liquid jets [38] resulted in $K = 0.059$. $K = 0.082$ is adequate for axisymmetric buoyant plumes with vertical axes [31]. The same value was used in Ref. [33] to match experiments on buoyant plumes with curvilinear main trajectories. $K = 0.089$ has been used for buoyant slot jets [30]. In both two- and three-dimensional situations $K$ was independent of distance from the source, and a comparison of experimentally measured flow rates with the predicted ones was used in support of this hypothesis. In addition, the same amount of entrainment occurred per unit length of jet contour in a given cross section because of the axisymmetry of the flow. Neither of these assumptions is applicable to the horizontal buoyant surface jet, because its entrainment is a function not only of the centerline velocity, but also of the degree of stratification. It is believed that the entrainment principle is still useful, but it must be applied in a

modified form. A variable entrainment coefficient along the contour of the jet must be used. Equation (8) specifies a semi-elliptical contour of the half-jet. Vertical entrainment through the bottom part of the surface jet is inhibited by buoyancy, while horizontal entrainment through the sides of the half-jet is not. Since the real distribution of K values along the contour is unknown, an approximation is used. It is proposed to use a constant horizontal entrainment parameter $K_h = 0.059$. Because density stratification inhibits turbulence, vertical entrainment must be equal to or smaller than the horizontal entrainment, dependent on some stratification parameter. It has been shown [39,40,41] that an overall Richardson number in terms of an overall depth, average velocity, and average density differential is an adequate stratification parameter. Since this number, raised to the power (-2), is equivalent to a densimetric Froude number, the dimensionless parameter $F^*$ as defined in Eq. (4) has been retained as a stratification parameter in this model. Experimental data on the effects of stratification on vertical entrainment are relatively scarce. The field data reported in [41] and the laboratory data reported in [42] and [43] are probably the best known, and various ways of fitting these have been proposed. A short review made in 1969 [44] shows that relationships of the form

$$\left.\begin{aligned} K_v/K_o &= \left(1 + \frac{c_1}{(F^*)^2}\right)^{-a_1} \\ K_v/K_o &= \left(1 - \frac{c_2}{(F^*)^2}\right)^{a_2} \end{aligned}\right\} \qquad (9)$$

$$K_v/K_o = e^{-c_3/(F^*)^2}$$

have been used as best fits with available measurements. Here $a_1$, $a_2$, $c_1$, $c_2$, and $c_3$ are positive real numbers and $K_o$ is the eddy exchange coefficient in neutrally buoyant flow. A restriction on Eq. (9) is, of course, that $0 < K_v/K_o < 1.0$. The relationship retained in this study, which fits experimental data from Ref. [42], is, as shown in Fig. 4,

$$\frac{K_v}{K_h} = 1.0 - 1.33 \log \left(\frac{6.32}{F^*}\right) \qquad (10)$$

where $K_h$ is the horizontal entrainment parameter. It is applied in the range $1.12 < F^* < 6.32$ and covers the transition of the entrainment coefficient in the range $0 < K_v/K_h < 1.0$. In Fig. 4 $K_v/K_h$ was plotted on a linear scale because it is believed that the customary logarithmic

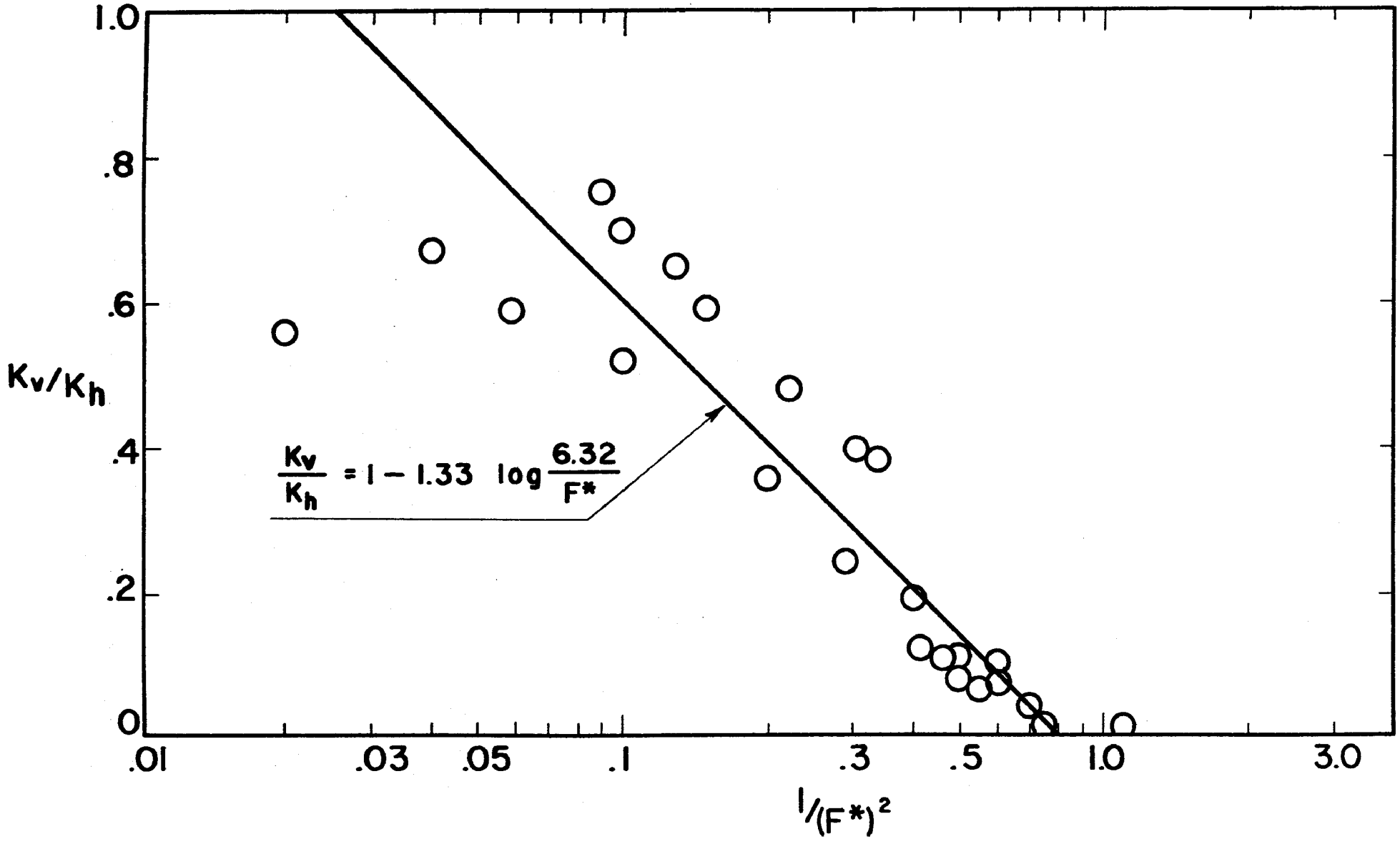


Fig. 4 - Fit of Equation for Vertical Entrainment Coefficient with Experimental Data from Ellison and Turner [42]

distortion of that scale tends to result in too much emphasis on the low values in the fitting process. It is believed that the horizontal entrainment also depends to some extent on the degree of stratification. For lack of experimental data it was not found possible to express this relationship in quantitative form.

If the driving force producing vertical entrainment is not the momentum of the jet, but the shear stress produced by wind blowing over the water surface, Eq. (10) can no longer be applied. It has been shown in Refs. [43] and [45] how an entrainment coefficient can be obtained in that particular situation.

Another change must be made in the horizontal entrainment coefficient to accommodate the turbulence inherent in the ambient current in which the thermal plume is embedded. An entrainment parameter related to the characteristics of the ambient current must then be used. Experiments on jet discharges into co-current streams indicate that entrainment is larger than for jets discharged into stagnant environments, but it appears very difficult at this time to express observations in quantitative form.

Circular jets discharged into a cross current have been found to entrain much more ambient fluid than jets discharged into stagnant fluid. Entrainment coefficients as high as 0.4 and 0.5 have been reported [46]. The increase is caused by a pair of large vortices which form in the cross section of the plume perpendicular to the main trajectory as shown, for example, in Ref. [34]. In a surface jet only one vortex exists, as shown in Fig. 3a. The cross current, which causes the deflection of the main trajectory of the plume, is responsible for the internal vortex-type circulation in the plume. A horizontal entrainment coefficient variable with the radius of curvature of the main trajectory may therefore be used. Based on available experimental and field data, an approximate relationship $K_h = K_h(R)$ may be formulated. When such a relationship is applied to a surface plume, however, there is an additional complication, because buoyancy will oppose the onset of an internal vortex-type circulation pattern. After the internal circulation occurs, the assumed Gaussian distributions of temperature and velocity will be destroyed. This analysis is therefore restricted to situations with sufficient buoyancy or large enough radii of curvature to prevent internal circulation. Tentative bounds are $F^* < 6.3$ and $R/b > 100$, with smaller values of $R/b$ acceptable as $F^*$ decreases.

It is proposed to calculate an average entrainment coefficient $K$ for each cross section from the relationship

$$K = \frac{K_h a + K_v b}{a + b} \tag{11}$$

where $a(s)$ and $b(s)$ are used as measures of the relative depth and width of the plume, respectively.

As the plume moves away from the outlet, the total flow rate increases by turbulent entrainment, and the plume dimensions also increase. It is proposed to use the relationships

$$\left(\frac{db}{ds}\right)_T = c_4 \frac{u^*(s,0,0)}{u^*(s,0,0) + U_s \cos \alpha} \tag{12}$$

and

$$\left(\frac{da}{ds}\right)_T = \left(\frac{K_v}{K_h}\right)^{1/2} \left(\frac{db}{ds}\right)_T \tag{13}$$

to describe the increase in geometrical size of the plume cross section. The first equation implies that the lateral, turbulence-induced spread of the plume is the same as that for non-buoyant jets except that the absolute spreading angle is distorted by the velocity of the surrounding current into which the plume is being injected. The second equation implies that the vertical and horizontal spreading ratio is closely related to the vertical and horizontal mixing ratio. This hypothesis is an extension of non-buoyant jet results to buoyant surface jets. The coefficient $c_4$ is the spreading angle of a jet in a stagnant reservoir without buoyancy effects. In a three-dimensional jet $c_4 = 0.081$ [37].

The thermal plume will spread laterally not only by turbulent mixing, but also under the effect of buoyancy, as shown in Fig. 3b. In this process some fluid is removed from the center of the plume and moved laterally toward the edges of the plume. An internal circulation pattern with a horizontal peak velocity at some distance from the main trajectory will result (Fig. 3b). Buoyancy may tend to restore the symmetry of the flow lost due to current or wind action. The rate of lateral spread due to buoyancy can be approximated using an equation of the form

$$\left(\frac{db}{dt}\right)_B = c_5 \left[ g\, a\, \lambda_v \frac{\rho^*(s,0,0)}{\rho} \right]^{1/2} \tag{14}$$

which is analogous to that used in the analysis of unsteady density currents [47]. This equation has been used before to describe the lateral spread [12].

At a distance $b$ from the main trajectory the forward velocity is $u(s,b,0)$. The horizontal buoyancy-induced angle of spread at this point should be

$$\left(\frac{db}{ds}\right)_B = \left(\frac{db}{dt}\right)_B \frac{1}{u(s,b,0)} \tag{15}$$

Hence
$$\left(\frac{db}{ds}\right)_B = \frac{c_5}{u(s,b,0)}\left[g\, a\lambda_v \frac{\rho^*(s,0,0)}{\rho_o}\right]^{1/2} \tag{16}$$

Since
$$u(s,b,0) = c_6\, u(s,0,0) = c_6(u^*(s,0,0) + U_s \cos\alpha) \tag{17}$$

where $c_6 = \exp(-0.5)$ is a coefficient related to the Gaussian velocity distribution, the above equation reduces, using Eq. (4), to

$$\left(\frac{db}{ds}\right)_B = \frac{c_5}{c_6}\frac{1}{F} \tag{18}$$

Conservation of mass in a cross section requires that as the width of the plume increases at the rate given by Eq. (13), the depth decreases; this requirement is satisfied by the relationship

$$\left(\frac{da}{ds}\right)_B = -\frac{a}{b}\left(\frac{db}{ds}\right)_B \tag{19}$$

Equations (18) and (19) represent, respectively, the lateral and the vertical spread due to buoyancy.

The interaction between spread by buoyancy and spread by mixing is complicated. It is proposed to consider the possibility that the effects of turbulence and buoyancy on spreading are additive. It is conceivable that the lateral spreading process also influences the formation of turbulence in the shear zone between the jet fluid and the surrounding fluid, but if this is the case it is impossible to take it into consideration at the present time. The total spread of the jet in the surrounding fluid must be of the order of

$$\frac{db}{ds} = \left(\frac{db}{ds}\right)_B + \left(\frac{db}{ds}\right)_T \tag{20}$$

$$\frac{da}{ds} = \left(\frac{da}{ds}\right)_B + \left(\frac{da}{ds}\right)_T \tag{21}$$

The half-width-to-depth ratio of the plume after a step length ds will have changed from b/a to

$$\delta = \frac{b + db}{a + da} \tag{22}$$

The rate of change of the heat flux is equal to the rate of heat loss to the atmosphere. The unit rate of surface heat transfer can be found [48] from a relationship of the form

$$H_n = K_s[T(s,r,0) - T_E] \tag{23}$$

where the coefficient of surface heat transfer $K_s$ and the equilibrium temperature $T_E$ are essentially functions of the prevailing meteorological conditions: solar radiation, wind velocity, air temperature, and relative humidity. The gradient of the total heat flux in the main direction of the trajectory must be balanced by the heat flux through the water surface:

$$-\frac{dH(s)}{ds} = \int_{-nb}^{nb} H_n \, dr = K_s \int_{-nb}^{nb} [T(s,r,0) - T_E] dr \tag{24}$$

In addition to mixing, spreading, and cooling, the momentum flux must be considered separately with regard to its components in the x- and the y-direction or in the s- and r-directions, all of which are shown in Fig. 1. The rate of change of momentum flux in the s- and r-directions is equal to the force components (forces per unit length) acting on the control volume.

$$\left.\begin{aligned} \frac{dM_s}{ds} &= \Sigma F_s \\ \frac{dM_r}{dr} &= 0 = \Sigma F_r \end{aligned}\right\} \tag{25}$$

External forces which cause changes in momentum flux are produced by wind shear stress at the water surface, dynamic pressures due to the ambient current, and frictional forces which do not result in entrainment. The latter restriction is necessary, as illustrated by the different effects of free and solid boundaries on submerged jets. On a free boundary, frictional forces are translated into entrainment, and no loss in total momentum results from frictional action. A solid boundary does not allow entrainment and will cause a loss in total momentum flux.

A plume without any turbulent entrainment must be laminar in character on all its boundaries. If the resultant shear force in this case is $D_{f\ lam}$, the shear force for the partially mixing plume is approximately

$$D_f = D_{f\ lam} \frac{K_h - K}{K_h} \tag{26a}$$

The lower and upper bounds for $D_f$ are thus zero and $D_{f\ lam}$. The value of $D_{f\ lam}$ can be approximated using Newton's shear law in conjunction with the maximum velocity gradients perpendicular to the contour of the plume to find local shear stresses. Integration of the shear stresses along the contour will result in a force per unit length

$$D_{f\ lam} = -\ 1.965\ \mu\ e^{-1/2}\ (\frac{a}{b} + \frac{b}{a})u^*(s,0,0) \tag{26b}$$

Most often this force will be small compared to other external forces.

The external force resulting from the wind shear stress $\tau_w$ on a surface strip of unit length is found from the relationship

$$F_w = 2nb\ \tau_w \tag{27}$$

Numerous empirical relationships have been reviewed for the calculation of wind shear stress from wind velocity data [49,50], and these can be selectively incorporated into the model. A surface stress due to wind transverse to the main trajectory will also tend to stretch the width of the plume. A large-scale eddy with water velocities at the surface in the direction of the wind shear stress will be produced as schematically shown in Fig. 3c. If such a circulation appears, it will tend to destroy the assumed temperature distribution in the model. It is therefore not included in this analysis. It should be mentioned that the wind may blow at any angle $\beta$ with reference to the x-axis, as is shown in Fig. 1.

Equation (27) does not include wind effects on the cold water, because these are contained in the specifications of the external current into which the heated water is discharged. This is meaningful for two reasons. First, the cold water currents in a body of water receiving thermal effluents frequently depend not only on wind, but also on the shore and bottom topography. In fact, the relationship between currents and wind is quite complex and must be investigated apart from the thermal plume problem. The plume itself is considered to be embedded in the cold water and subject to separate wind action. The second reason is the observation that the cold water current sometimes represents a much larger mass flux than the heated water discharge. The longshore currents in the Great Lakes and the flow in impounded rivers can be cited as examples. These masses of water are less susceptible to motion by wind than the buoyant surface jet which frequently spreads out as a thin layer on top of such a current. A substantial amount of

time is required to reach a steady wind generated current in a large lake.

The current into which a plume discharges produces a dynamic pressure normal to the direction of the main trajectory and also a shear stress parallel to it. If the thermal plume is approximated by a solid body somewhat similar to a bent half-cylinder, the dynamic pressure forces will produce a form drag

$$D_D = C_D \frac{\varrho(U_s \sin \alpha)^2}{2} a \tag{28}$$

perpendicular to the main trajectory and a friction drag

$$D_f = C_f \frac{\varrho(u^*(s,0,0))^2 (b + a)\pi\sqrt{2}}{2} \tag{29}$$

parallel to the main trajectory. The friction forces given in Eqs. (26a) and (29) are of course the same. Equation (26a) may be easier to use than Eq. (29) because of the friction coefficient $C_f$. The form drag coefficient $C_D$ in Eq. (28) was taken as equal to unity because of the semi-elliptical shape of the plume.

The change in momentum flux must also account for the original momentum of the entrained fluid, meaning $\frac{dQ}{ds} \varrho U_s \cos \alpha$ in the s-direction and $\frac{dQ}{ds} \varrho U_s \sin \alpha$ in the r-direction.

Pressure (buoyancy) forces in the direction of the main trajectory are not included in the analysis. The buoyancy force in any cross section is $g \int_0^{ma} \int_{-nb}^{nb} \varrho^*(s,r,z)\, z\, dz$ and can be calculated from the density deficit distribution given in Eq. (3). It can be shown that this value is also equal to $0.33\, g\lambda_v f_5\, \varrho^*(s,0,0)\, ab$. The value of this quantity is usually less than one per cent of the momentum flux of the jet. The net longitudinal buoyancy force acting on a control volume in the plume is $0.33\, g\lambda_v f_5 \frac{d[\varrho^*(s,0,0)ab]}{ds}$ which is usually negligible in relation to the momentum flux.

Summarizing, the momentum equations in terms of all external forces are

$$\frac{dM}{ds} = D_f + F_w \cos(\beta - \alpha) + \frac{dQ}{ds} \varrho U_s \cos \alpha \tag{30}$$

$$\frac{dM}{dr} = -\frac{dQ}{ds} \varrho U_s \sin \alpha = -\frac{M}{R} + D_D - F_w \sin(\beta - \alpha) \tag{31}$$

The radius of curvature of the main trajectory is

$$R = \left[\frac{1 + (y')^2}{y''}\right]^{3/2} \tag{32}$$

where $y(x)$ is the equation of the main trajectory in the x-y-plane.

The curvature of the main trajectory is also associated with a change of the flow direction $\alpha$. Considering a length element $ds$,

$$d\alpha = \frac{ds}{R} \tag{33}$$

will be a good approximation for the change in angle.

All secondary circulation patterns shown in Fig. 3 tend to destroy the Gaussian velocity and temperature distributions. It can be speculated that the result will often be a more uniform temperature distribution within the plume, but there is no proof of this. Certainly, all the above circulation patterns are superimposed on the main motion of the plume along the main trajectory, and frequently on each other as well. Thus a theoretical argument for the use of symmetrical temperature and velocity profiles such as those used in the preceding section cannot be given. However, experiments in the laboratory and in the field support the assumption.

Solutions of the Basic Equations

The basic equations of the previous sections are solved by an explicit, finite-difference, forward-stepping method. Calculations of the volumetric, heat, and momentum fluxes as defined previously were made using the following formulations:

$$Q_i = u_i a_i b_i f_1 + \frac{\pi}{2} U_s \cos \alpha_i \, ma_i \, nb_i \tag{34}$$

$$H_i = T_i u_i s_i b_i f_2 + T_i U_s \cos \alpha_i \, a_i b_i \, f_4 \tag{35}$$

$$M_i = \rho u_i^2 \, a_i b_i \, f_3 + 2\rho U_s \cos \alpha_i \, u_i \, a_i b_i \, f_1 + \rho \frac{\pi}{2} U_s^2 \cos^2 \alpha_i ma_i nb_i \tag{36}$$

where the subscript $i$ refers to a particular cross section at distance $s$ from the origin of the plume, $u_i$ is equal to the excess-centerline velocity $u^*(s,0,0)$, $T_i$ is equal to the excess-centerline temperature $T^*(s,0,0)$, and the coefficients $f_1$ through $f_4$ are constants equivalent to the following definite integral values:

$$f_1 = \frac{1}{a_i b_i} \int_{-nb_i}^{nb_i} \int_{0}^{ma_i} \left\{ \exp\left[ -\frac{1}{2} \left( \frac{r}{b_i} \right)^2 \right] \exp\left[ -\frac{1}{2} \left( \frac{z}{a_i} \right)^2 \right] \right\} dr dz$$

$$= \pi \, \mathrm{erfn} \left( \frac{n}{\sqrt{2}} \right) \mathrm{erfn} \left( \frac{m}{\sqrt{2}} \right) \tag{37}$$

$$f_2 = \frac{1}{a_i b_i} \int_{-nb_i}^{nb_i} \int_{0}^{ma_i} \left\{ \exp\left[-\frac{1}{2}\left(\frac{r}{b_i}\right)^2\right] \exp\left[-\frac{1}{2}\left(\frac{z}{a_i}\right)^2\right] \exp\left[-\frac{1}{2}\left(\frac{r}{\lambda_h b_i}\right)^2\right] \right.$$

$$\left. \exp\left[-\frac{1}{2}\left(\frac{z}{\lambda_v a_i}\right)^2\right] \right\} dr\,dz = f_1 \frac{\lambda_v \lambda_h}{\lambda_v \lambda_h + 1} \tag{38}$$

$$f_3 = \frac{1}{a_i b_i} \int_{-nb_i}^{nb_i} \int_{0}^{ma_i} \left\{ \exp\left[-\frac{1}{2}\left(\frac{r}{b_i}\right)^2\right] \exp\left[-\frac{1}{2}\left(\frac{z}{a_i}\right)^2\right] \right\}^2 dr\,dz$$

$$= \frac{\pi}{2} \operatorname{erfn}(n) \operatorname{erfn}(m) \tag{39}$$

$$f_4 = \frac{1}{a_i b_i} \int_{-nb_i}^{nb_i} \int_{0}^{ma_i} \left\{ \exp\left[-\frac{1}{2}\left(\frac{r}{\lambda_h b_i}\right)^2\right] \exp\left[-\frac{1}{2}\left(\frac{z}{\lambda_v a_i}\right)^2\right] \right\} dr\,dz$$

$$= f_1 \lambda_v \lambda_h \tag{40}$$

Values of $f_1$ through $f_4$ can also be calculated if other than Gaussian velocity and temperature distributions are used.

Basic input parameters include the initial flow rate $Q_o$, the initial depth $a_o$, the initial momentum flux $M_o$, the outlet temperature $T_o$, the lake temperature $T_\ell$, the current velocity $U_s$, and the outlet angle $\alpha_o$ with respect to the current direction. If there is wind, its direction $\beta$ and the shear stress on the water surface $\tau_w$ which it produces are specified. Since $\tau_w$ must be calculated from wind speed, it is possible to include such calculations in the program. The wind speed $W$ at a specified altitude (e.g., 30 ft) is then an input variable.

Prediction of surface heat loss requires specification of the equilibrium temperature $T_E$ and the surface heat transfer coefficient $K_s$. These can be calculated from semi-empirical relationships [51]. If the actual calculations are again transferred into the program, the necessary input values must include solar radiation $H_s$, dew point temperature $T_D$, and wind speed $W$.

The step length $d_s$ and the number of steps must be chosen. Values approximately equivalent to the outlet depths were chosen for the step length. The number of steps depends, of course, on the size of the flow field to be investigated.

The set of equations can be solved numerically in a meaningful manner and at little cost in computer time by extrapolating forward from one cross section to another starting at the outlet. The process is the same as that used in backwater profile computations in supercritical channel flows. The procedure is justified by the fact that a heated water surface jet as described herein is an internally supercritical (or at least critical) three-dimensional flow. The heated water surface jet may lose this property at some distance downstream from the outlet. The centerline densimetric Froude number defined in Eq. (4) can be used as an indicator. Anticipating results to be shown later, it appears that the critical densimetric Froude number value is in the vicinity of 3.0. The analysis of the thermal plume using a heated jet type model and the procedure described herein should not be carried on if the densimetric Froude number values are less than critical. The physical significance of this statement is relatively simple: The flow should not be considered a jet flow if its momentum has become small compared to the buoyant forces. The magnitude and direction of external forces thus have great influence on the size of the area in which the analytical jet-type flow model can be applied. By definition, the area is considered equivalent to the nearfield. Onshore wind or currents may reduce the nearfield considerably, while longshore currents and offshore winds may stretch it.

Effects of the farfield or downstream controls on heated water surface jets have been reported for two-dimensional flows [15,36,52] and will be further investigated in Part II of this report.

Details of the numerical computations can be gathered from the computer program given in Appendix A. The following explanations will be helpful: The initial conditions as described above are used to compute an initial plume width $b_o$ and centerline velocity $u_o$ such that the initial flow rate and the initial momentum flux are as specified. Equations (34) and (36) are used for that purpose. Then the equations given earlier are solved in a specific order. First the entrainment is found from Eq. (8) with the aid of Eqs. (10) and (11). Then $Q_{i+1} = Q_i + dQ_i$. The heat loss $dH_i$ is found from Eq. (24) in the form

$$-dH_i = [T_i b_i f_5 + 2(T_\ell - T_E) n b_i] \frac{K_s ds}{c_p \varrho} \tag{41}$$

where $$f_5 = \frac{1}{b_i} \int_{-nb_i}^{nb_i} \exp\left[-\frac{1}{2}\left(\frac{r}{\lambda_h b_i}\right)^2\right] dr = \lambda_h \sqrt{2\pi}\, \mathrm{erfn}\left(\frac{n}{\sqrt{2}}\right) \tag{42}$$

Then $H_{i+1} = H_i + dH_i$. Equation (30) is then used to evaluate the change in momentum flux in the direction of the main trajectory and Eq. (31) to find the radius of curvature of the main trajectory $R_i$. Then $M_{i+1} = M_i + dM_i$ and with the radius of curvature from Eq. (31), the change in the trajectory angle $d\alpha_i$ can be calculated using Eq. (33).

$$d\alpha_i = R_i \, ds \tag{43}$$

Then $\alpha_{i+1} = \alpha_i + d\alpha_i$.

The plume characteristics in the (i+1)-th cross section--in particular the standard deviations $a_{i+1}$ and $b_{i+1}$, the centerline velocity $u_{i+1}$, and the centerline temperature excess $T_{i+1}$--can be found from the previously calculated fluxes $Q_{i+1}$, $M_{i+1}$, and $H_{i+1}$ in conjunction with the spread characteristics of Eqs. (20), (21), and (22). Simultaneous solution of Eqs. (34) and (36) for the (i+1)-th values instead of the i-th gives $u_{i+1}$ and the area $(a_{i+1}\ b_{i+1})$, and the individual values of the (i+1)-th standard deviations are then found using Eq. (22). Prior to this, Eqs. (12) through (21) must be solved for each individual step. The centerline temperature $T_{i+1}$ can then be found directly from Eq. (35). After completion of all these calculations, the orientation of the main trajectory and the velocity and temperature distributions in the (i+1)-th cross section are known. If the calculations are repeated for N steps, the characteristics of a whole plume can be found. The described process is simple and explicit, and changes in step lengths have little effect on the results if the step length remains of the order of the initial depth.

The limitations of the model described lie, of course, in the assumptions made initially: similarity of all profiles, specific lateral spreading patterns regardless of wind and current conditions, and absence of solid boundaries. The coefficients used are derived from a rather small number of experiments.

To facilitate interpretation of the output, the numerical program was extended by a contour plotting program which is a modified version of program CONTOUR from the University of Michigan. As a result, an output consisting of isotherm patterns can be obtained; Fig. 31 is an example. The point of discharge is at the center bottom of the picture, and there is no wind or current. The plot shows surface temperatures. Near the outlet the contour interpolation is slightly erroneous because of the large grid sizes and the interpolation procedure in the contour plotting package.

To determine the accuracy of the method, predicted temperatures were compared with measurements in the field and under laboratory conditions. Results and comparisons with laboratory data will be given in the following section.

## Non-Dimensional Analysis and Results

The procedure described in the previous section will produce results for an individual plume under individual ambient conditions. However, dimensionless quantitative information on, for example, temperature decay, spread, and flow velocities in a plume in terms of all the relevant parameters influencing the behavior of the thermal plume is also desirable. Such information would greatly aid in making generalized predictions of the character of the plume for different field conditions. Attempts to provide such general information have failed owing to the large number of factors affecting the plume characteristics as well as the interaction and mutual interference among these parameters. If the initial plume characteristics $u_o = u(0,0,0)$ and $a_o = a(0)$ and the initial water temperature excess ${}^{o}T_o - T_\ell = T(0,0,0) - T_\ell$ are chosen as reference values, the independent variables can be written as

$$\frac{b_o}{a_o},\quad F_o,\quad \frac{U_s}{u_o},\quad \frac{W}{u_o},\quad \frac{T_E - T_\ell}{T_o - T_\ell},\quad \frac{K_s(T_o - T_E)}{u_o\,\varrho\,c_p},\quad \alpha_o,\quad \beta$$

in which $F_o$ is the initial densimetric Froude number. The dependent variables are

$$\frac{u}{u_o},\quad \frac{T - T_\ell}{T_o - T_\ell},\quad \frac{a}{a_o},\quad \frac{b}{b_o},\quad \frac{Q}{Q_o},\quad \frac{H}{H_o},\quad \frac{\alpha}{\alpha_o},\quad \frac{y}{a_o},\quad \frac{x}{a_o}$$

where the subscript zero again refers to the initial cross section at $(s = 0)$. It has not been found possible to produce dimensionless results for the dependent variables in terms of all the independent parameters. However, it was found that the initial behavior of most of the heated water surface jets investigated is controlled mainly by the hydrodynamic and turbulent convective processes. For purposes of illustration it is therefore justifiable and useful to eliminate those independent variables which refer to heat transfer through the water surface by setting $T_\ell = T_E$ and $K_s = 0$. The results will then refer to the mixing zone near the point of discharge only. The remaining independent variables then are

$$\frac{b_o}{a_o},\quad F_o,\quad \frac{U_s}{u_o} \text{ and } \frac{W}{u_o},\quad \alpha_o,\quad \beta$$

The effects of several combinations of these dimensionless parameters on dependent variables were investigated in two groups: plumes in wind without cross currents $(U_s = 0)$ and plumes in cross currents without wind $(W = 0)$. The wind or current was assumed to be at right

angles to the discharge ($\alpha_o = \pi/2$ or $\beta = 0$). The results of those investigations are shown in Figs. 5 through 20.

Figures 5 through 20 are largely self-explanatory. The first four figures refer to a low Froude number discharge ($F_o = 3.75$) into wind. The deflection of the main trajectory as shown in Fig. 5 is more substantial for the semicircular jet ($b_o/a_o = 1$) than for a wide semi-elliptical one ($b_o/a_o = 4$). The reason is that the circular discharge has a smaller initial flow rate and initial momentum than the wider one. There is substantial dilution of the discharge (Fig. 6), resulting in a significant temperature drop (Fig. 7) despite significant stratification. The second set of four figures refers to a higher Froude number discharge ($F_o = 15$). The deflection of the main trajectory is larger than before for identical $W/u_o$ ratios (Fig. 9). The reason is the larger amount of entrainment of the faster jet, which is associated with larger plume dimensions, including surface areas exposed to wind. There is a substantial difference in the dilution of the circular ($b_o/a_o = 1$) and the wide elliptical ($b_o/a_o = 4$) discharge. The centerline temperature decay by turbulent mixing with ambient lake water is overwhelming. Figure 12 shows very nicely the initial jet regime followed by a stratified flow process. It can also be noted that wind will tend to sustain turbulent entrainment (Fig. 10) and further growth of the plume's thickness (Fig. 12). The third and fourth sets of figures refer to heated surface jet discharges at right angles into cross-currents at a low densimetric Froude number ($F_o = 3.75$) and a high densimetric Froude number ($F_o = 15.0$), respectively

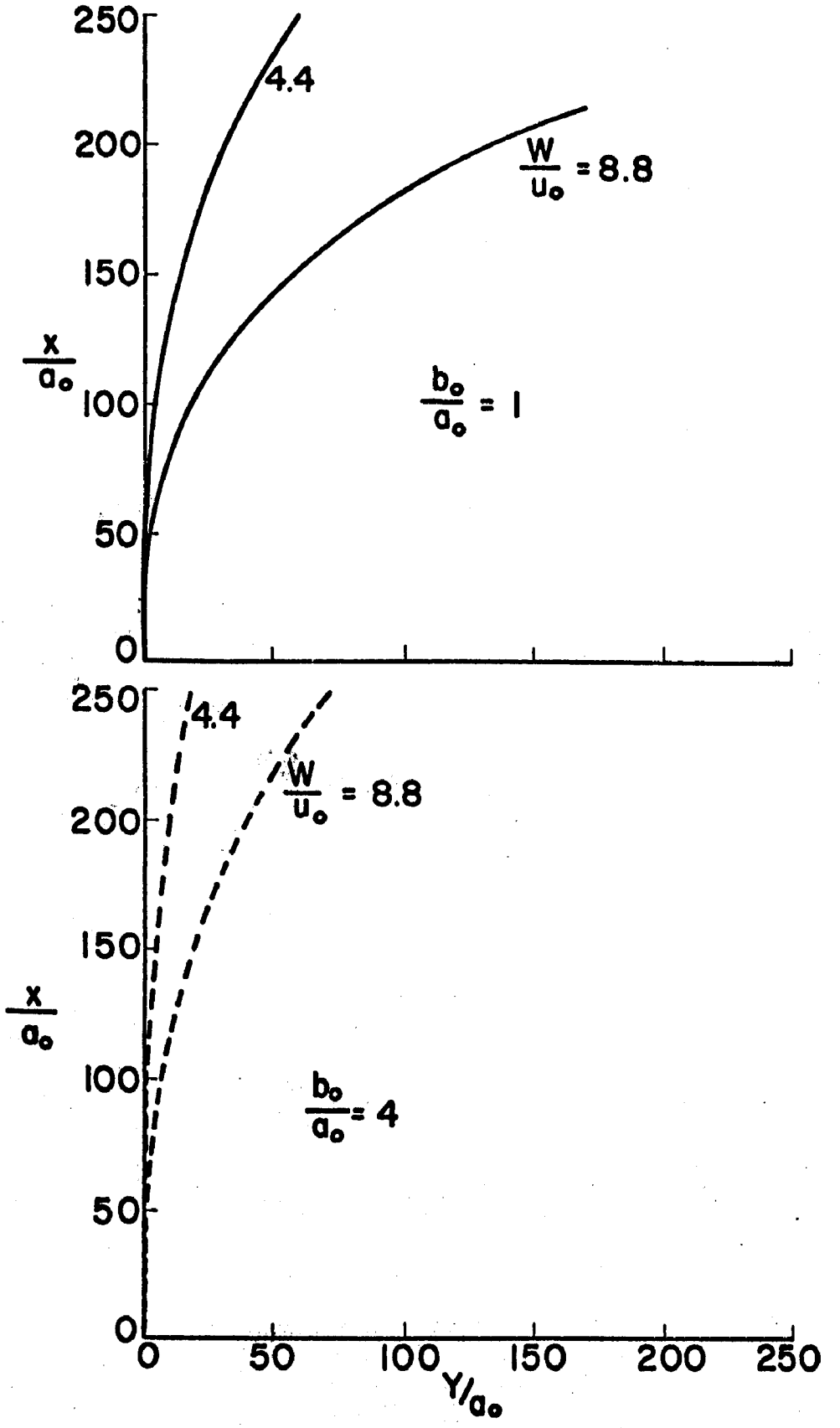


Fig. 5 - Plume Trajectory in Cross-wind Perpendicular to Discharge. $\alpha_o = 90^o$, $\beta = 0$, $F_o = 3.75$, $U_s = 0$, $K_s = 0$

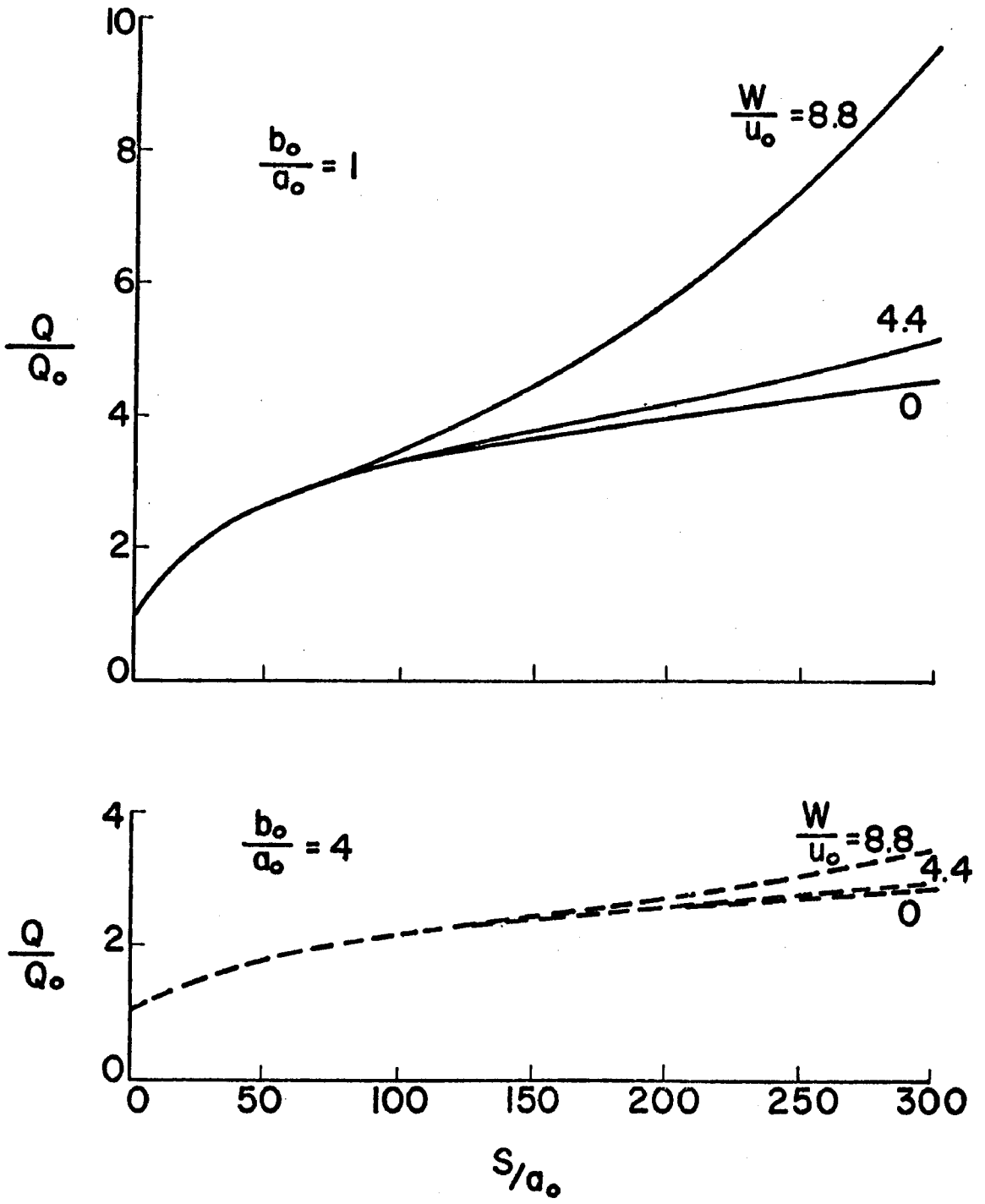


Fig. 6 - Total Volumetric Flow Rate versus Distance of Travel. Plume in Cross-wind perpendicular to Discharge. $\alpha_o = 90^o$, $\beta = 0$, $F_o = 3.75$, $U_s = 0$, $K_s = 0$

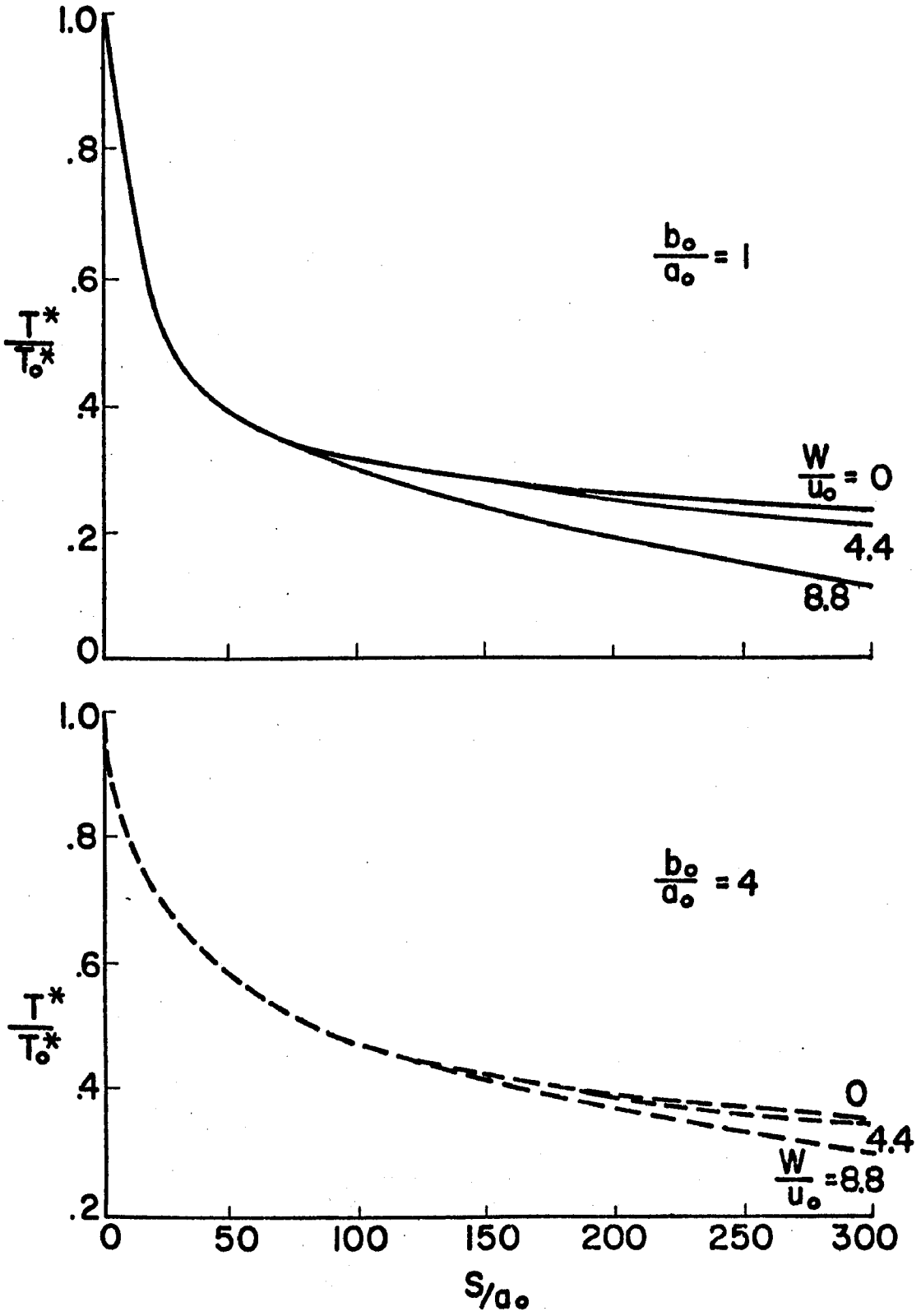


Fig. 7 - Excess Temperature above Ambient along Main Trajectory. Plume in Cross-wind Perpendicular to Discharge. $\alpha_o = 90^\circ$, $\beta = 0$, $F_o = 3.75$, $U_s = 0$, $K_s = 0$

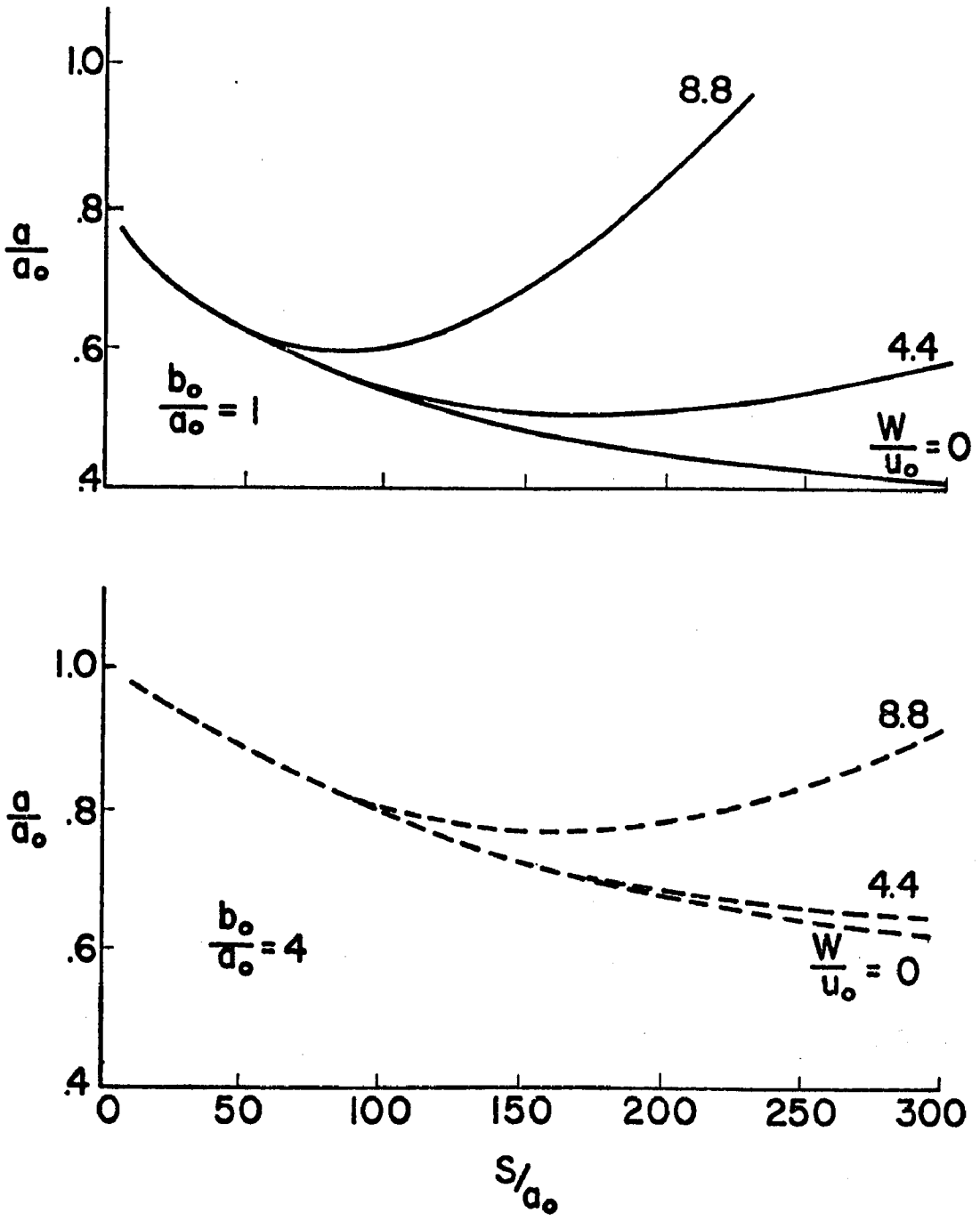


Fig. 8 - Depth of Thermocline below Water Surface along Main Trajectory. Plume in Cross-wind Perpendicular to Discharge. $\alpha_o = 90^o$, $\beta = 0$, $F_o = 3.75$, $U_s = 0$, $K_s = 0$

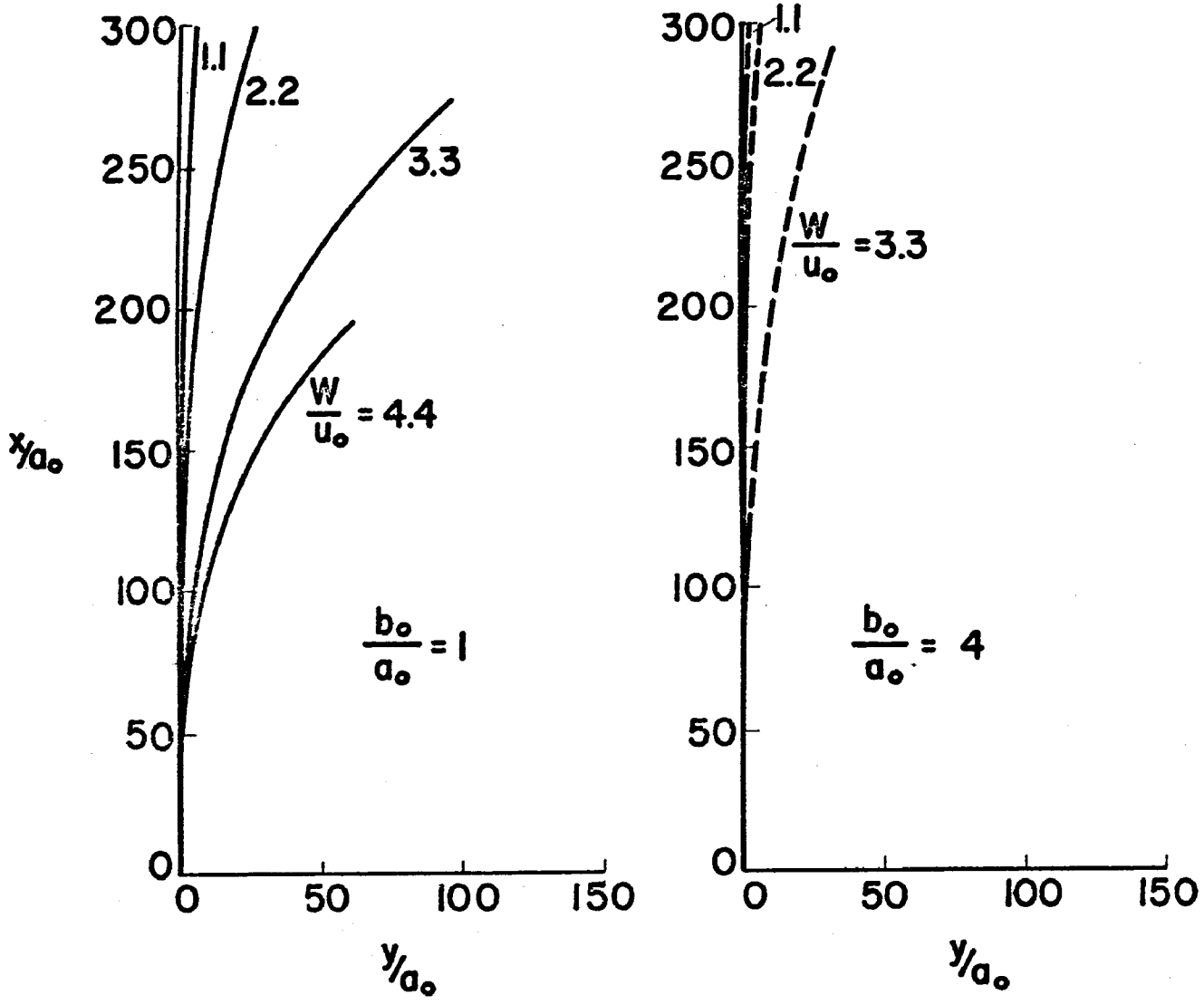


Fig. 9 - Plume Trajectory in Cross-wind Perpendicular to Discharge.
$\alpha_o = 90^o$, $\beta = 0$, $F_o = 15.0$, $U_s = 0$, $K_s = 0$

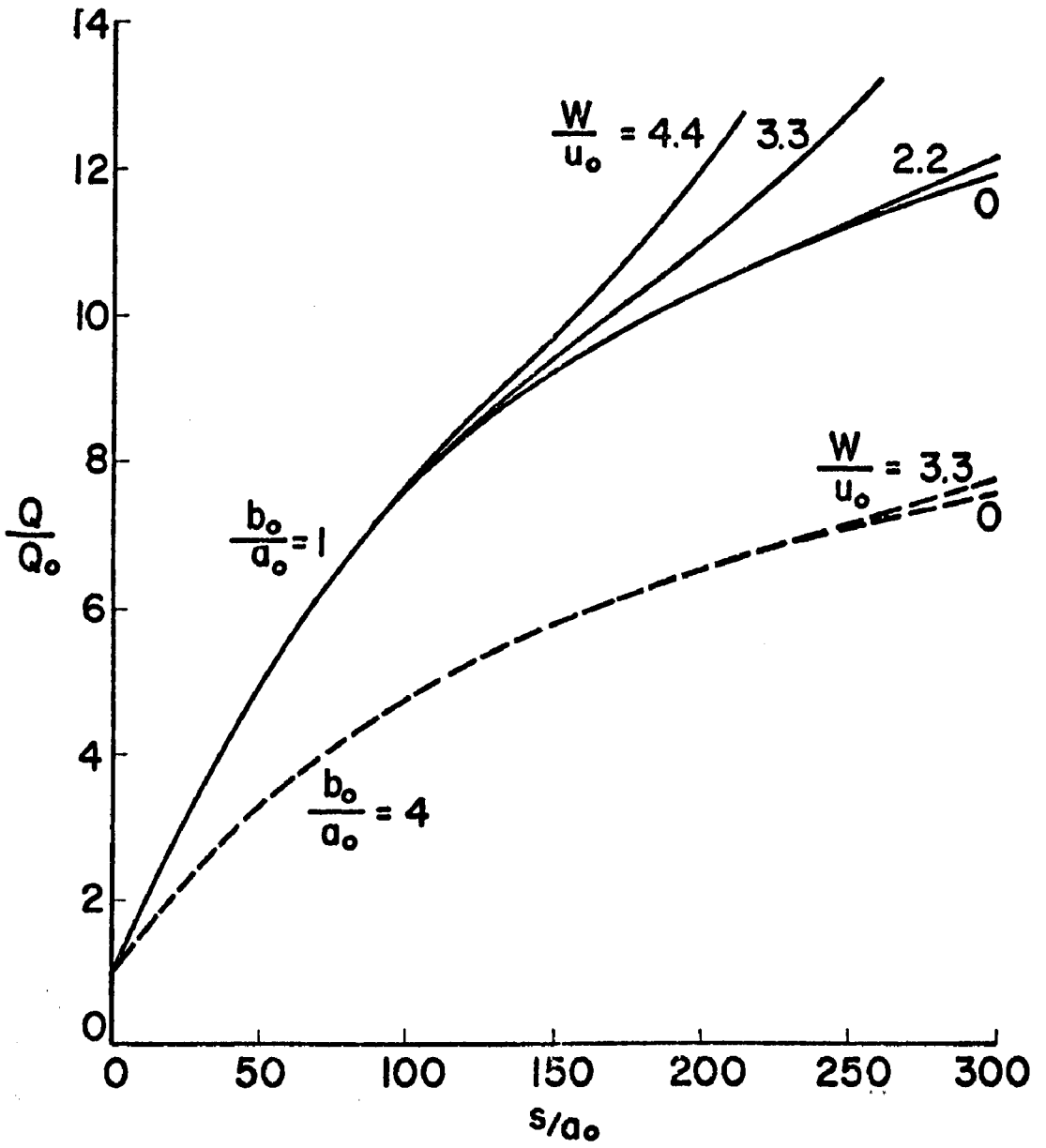


Fig. 10 - Total Volumetric Flow Rate versus Distance of Travel. Plume in Cross-wind Perpendicular to Discharge. $\alpha_o = 90^\circ$, $\beta = 0$, $F_o = 15.0$, $U_s = 0$, $K_s = 0$

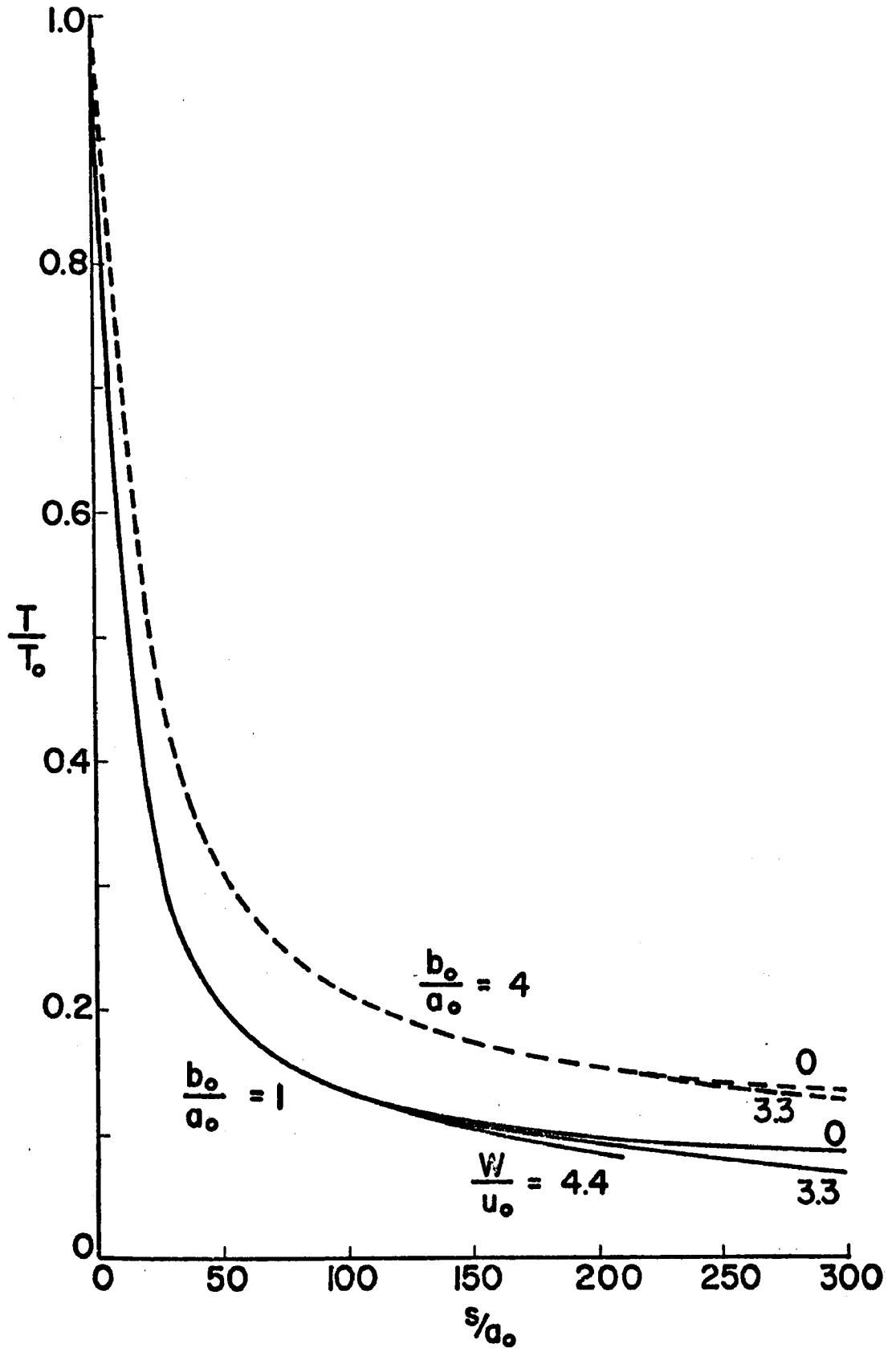


Fig. 11 - Excess Temperature above Ambient along Main Trajectory. Plume in Cross-wind perpendicular to Discharge. $\alpha_o = 90^o$, $\beta = 0$, $F_o = 15.0$, $U_s = 0$, $K_s = 0$

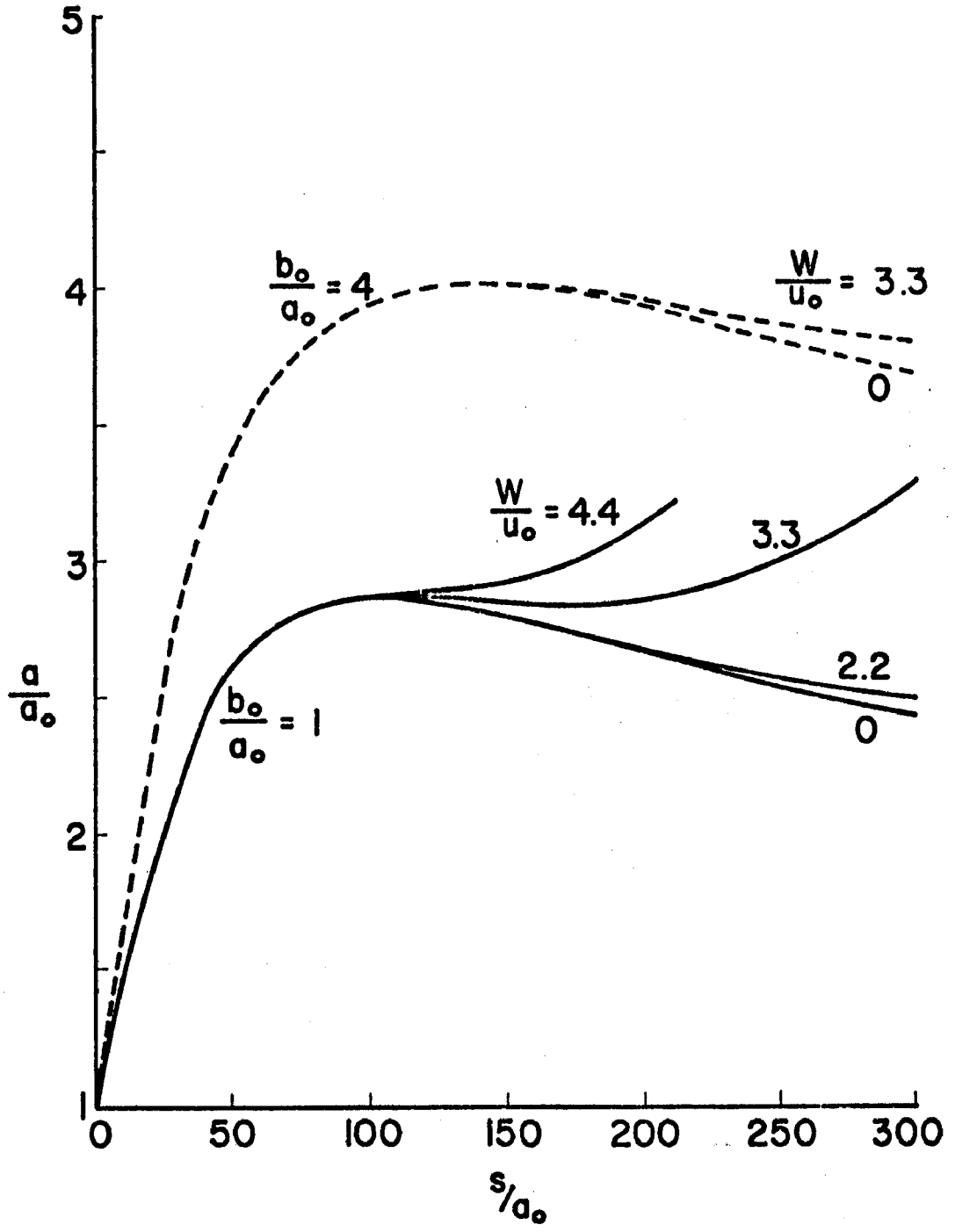


Fig. 12 - Depth of Thermocline below Water Surface along Main Trajectory. Plume in Cross-wind perpendicular to Discharge. $\alpha_o = 90^o$, $\beta = 0$, $F_o = 15.0$, $U_s = 0$, $K_s = 0$

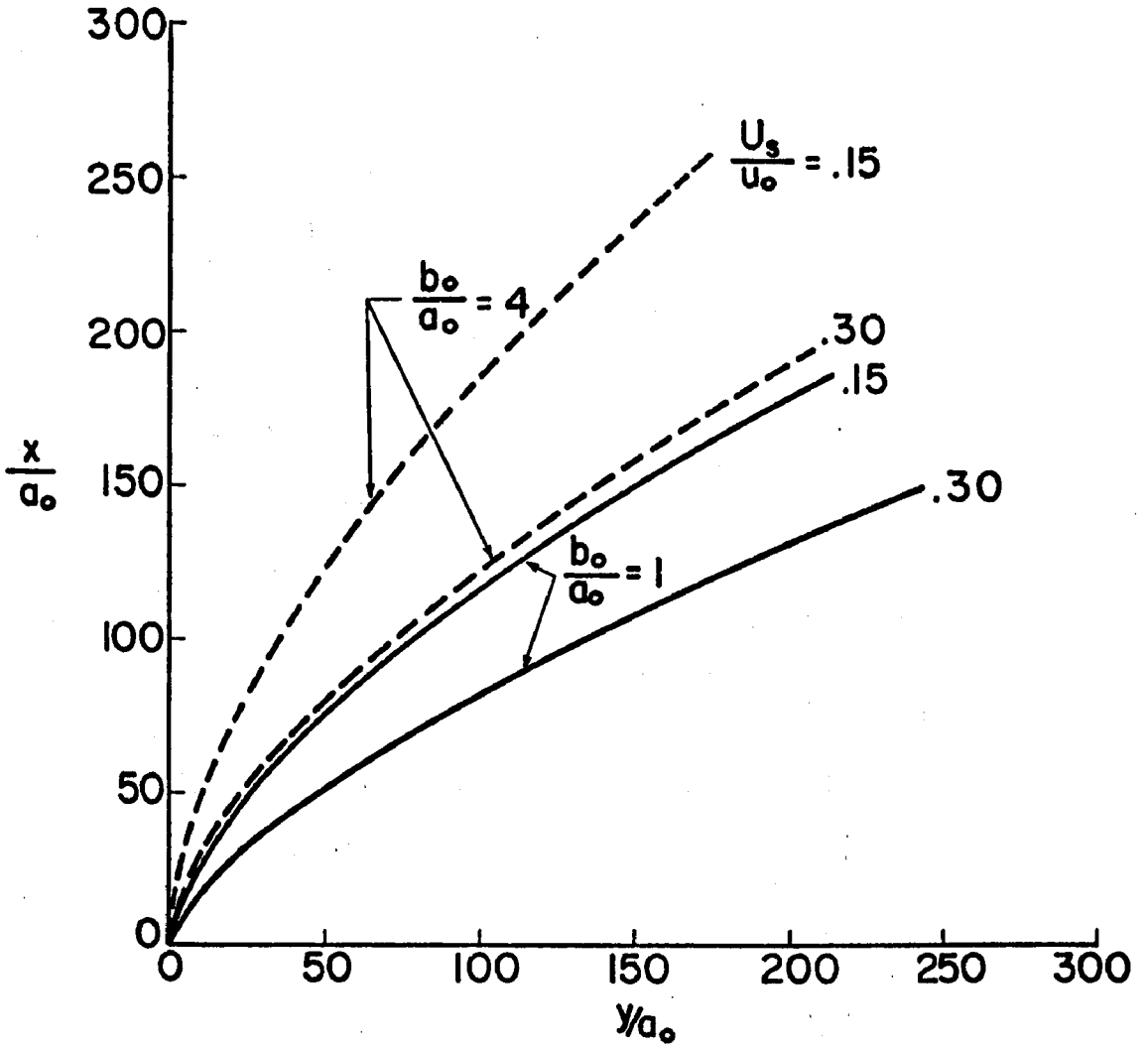


Fig. 13 - Plume Trajectory in Cross-current Perpendicular to Discharge. $\alpha_o = 90^o$, $F_o = 3.75$, $W = 0$, $K_s = 0$

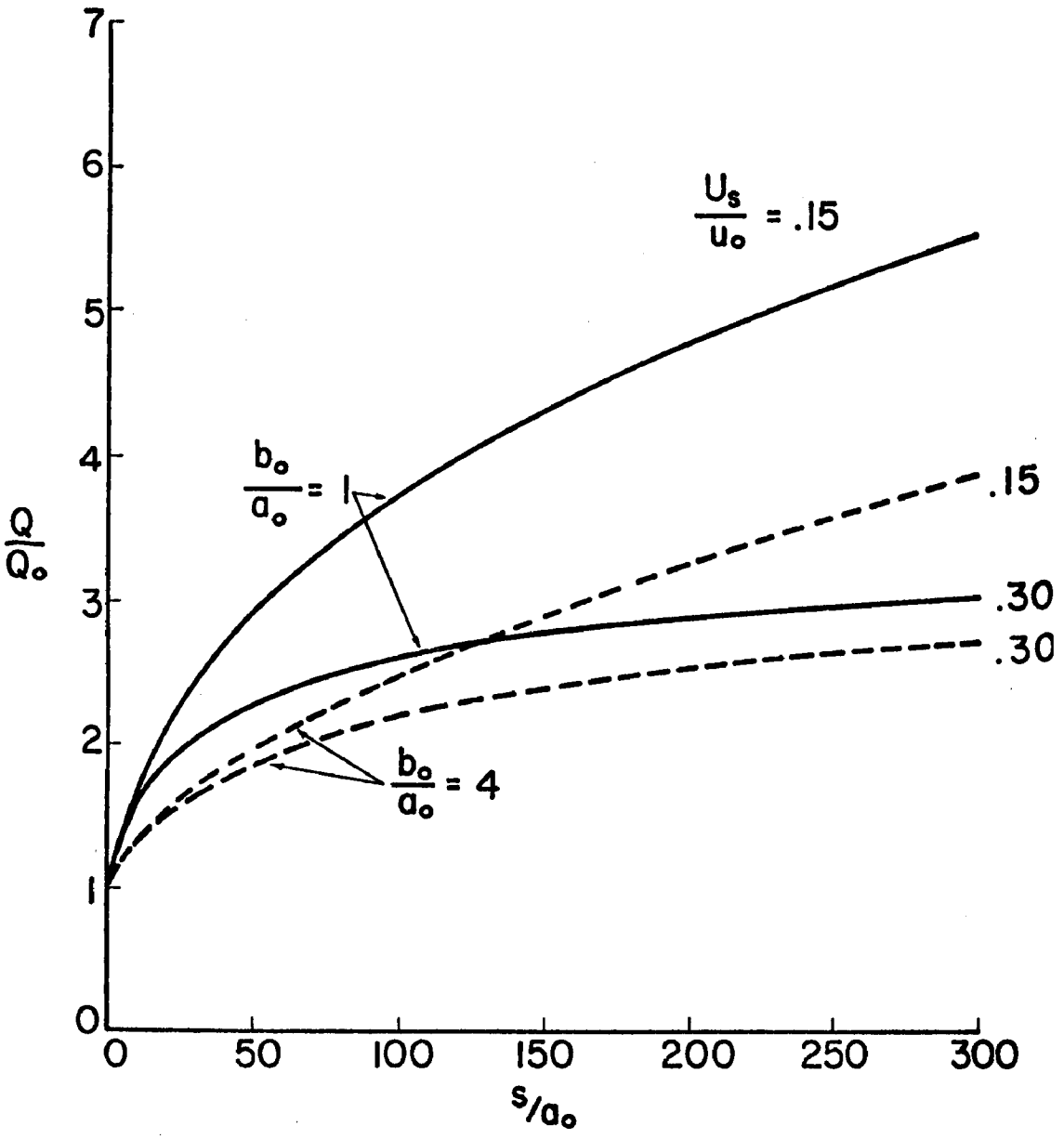


Fig. 14 - Total Volumetric Flow Rate versus Distance of Travel. Plume in Cross-current Perpendicular to Discharge. $\alpha_o = 90^o$, $F_o = 3.75$, $W = 0$, $K_s = 0$

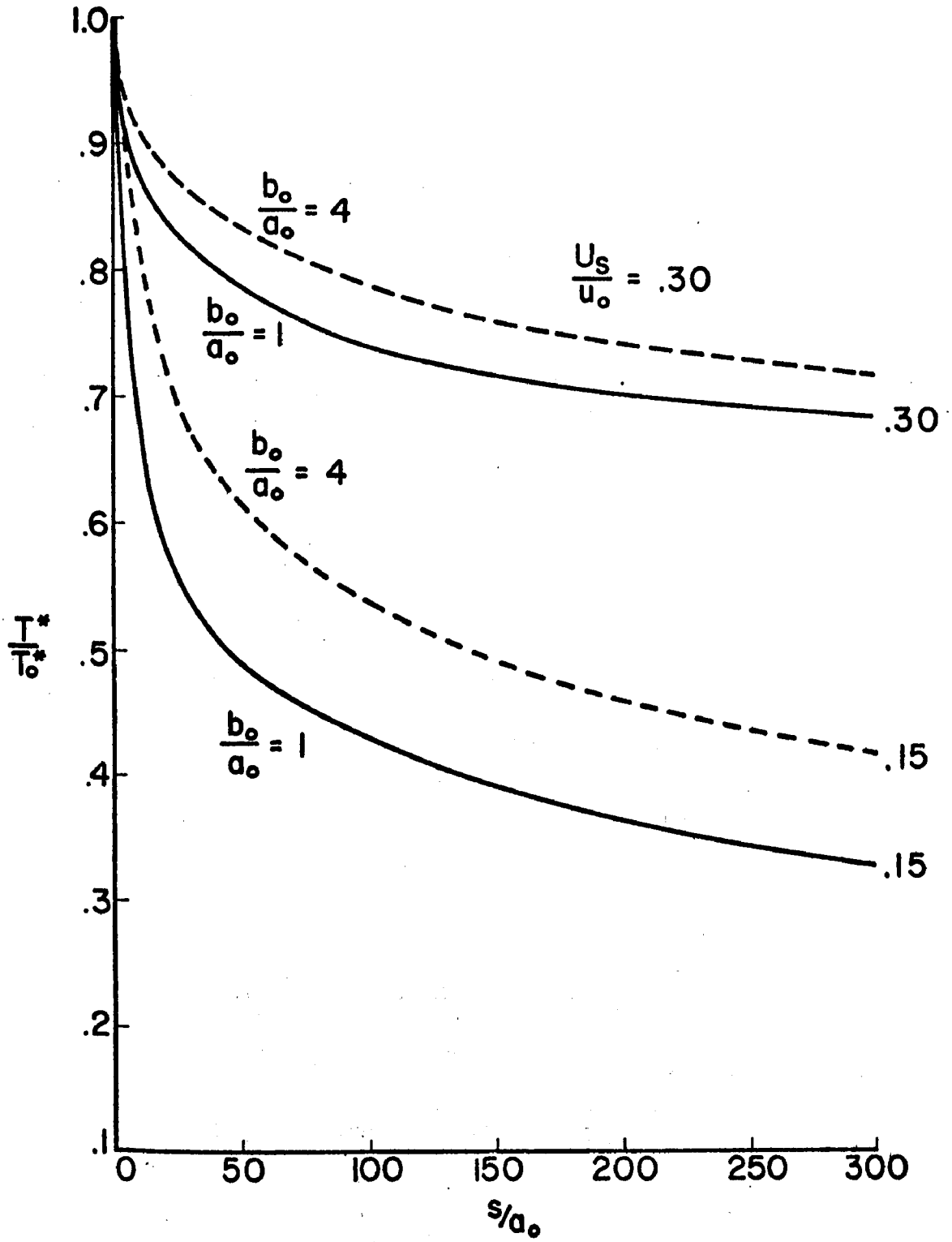


Fig. 15 - Excess Temperature above Ambient along Main Trajectory. Plume in Cross-current perpendicular to Discharge. $\alpha_o = 90^o$, $F_o = 3.75$, $W = 0$, $K_s = 0$

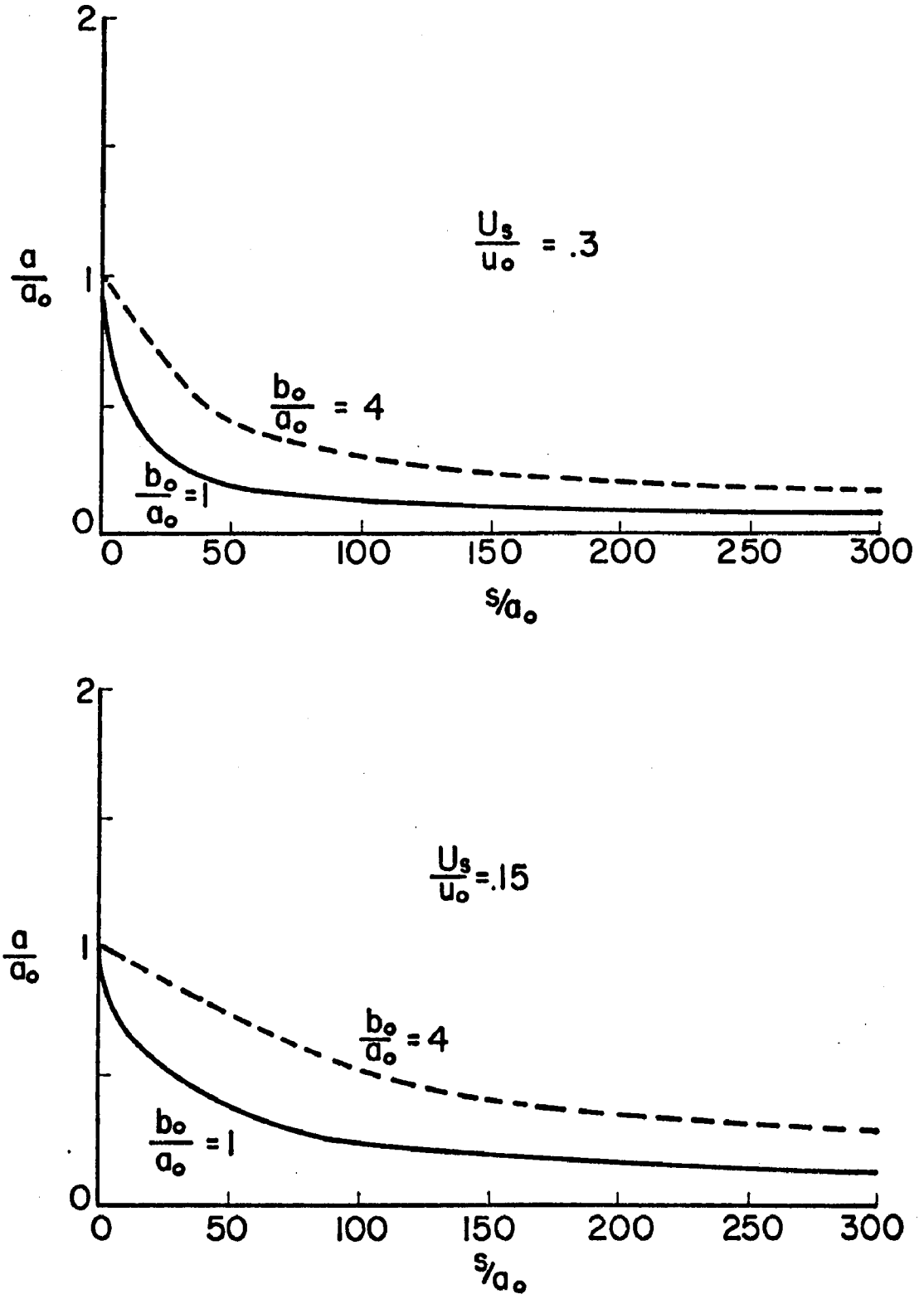


Fig. 16 - Depth of Thermocline below Water Surface along Main Trajectory. Plume in Cross-current perpendicular to Discharge. $\alpha_o = 90^o$, $F_o = 3.75$, $W = 0$, $K_s = 0$

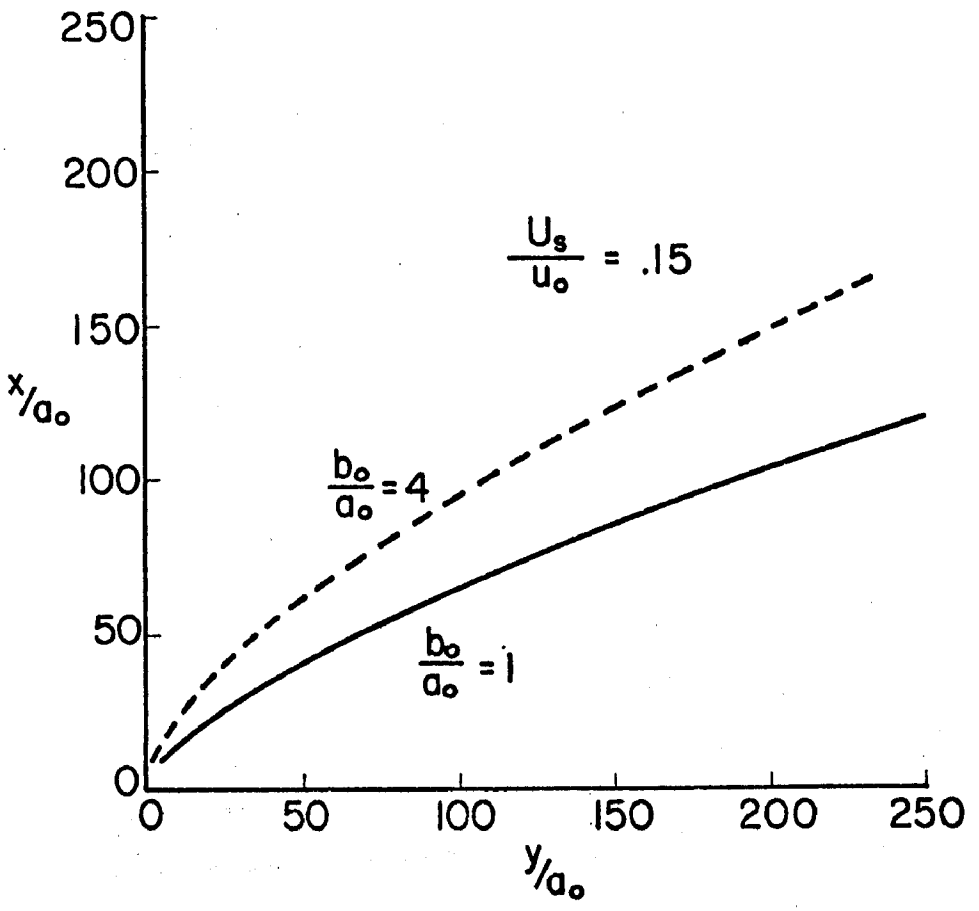


Fig. 17 - Plume Trajectory in Cross-current perpendicular to Discharge. $\alpha_o = 90^o$, $F_o = 15.0$, $W = 0$, $K_s = 0$

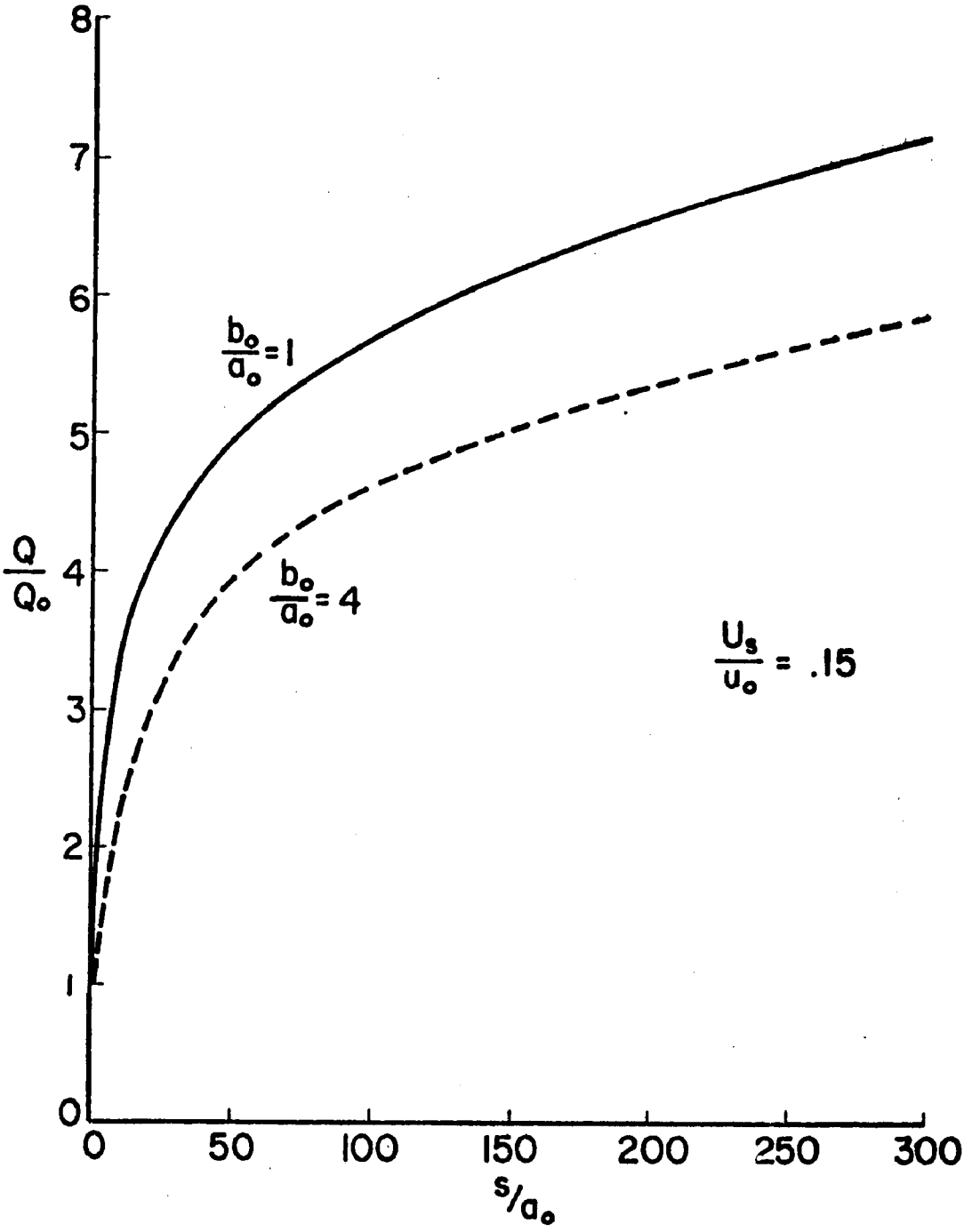


Fig. 18 - Total Volumetric Flow Rate versus Distance of Travel. Plume in Cross-current Perpendicular to Discharge. $\alpha_o = 90^o$, $F_o = 15.0$, $W = 0$, $K_s = 0$

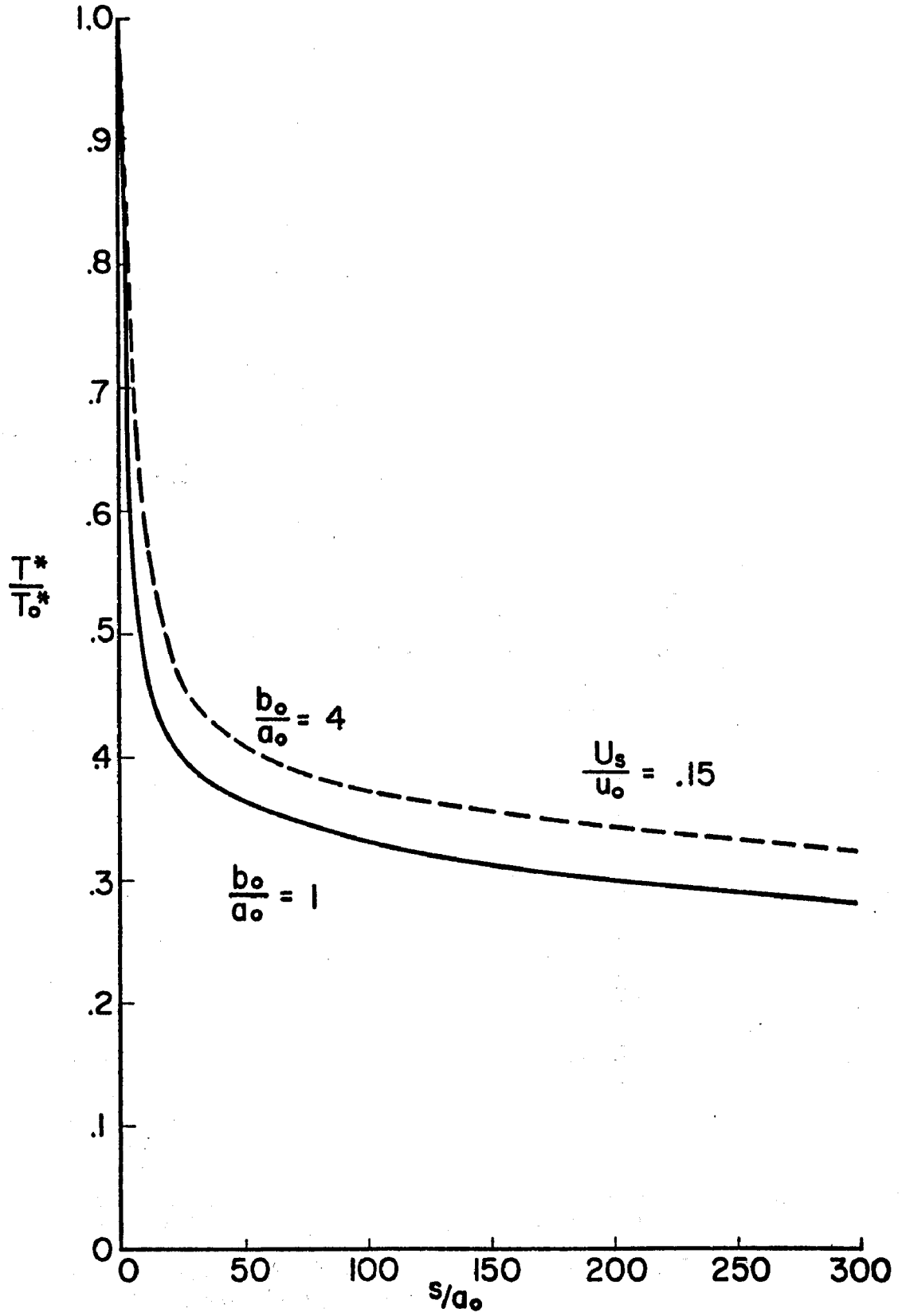


Fig. 19 - Excess Temperature above Ambient along Main Trajectory. Plume in Cross-current perpendicular to Discharge. $\alpha_o = 90^\circ$, $F_o = 15.0$, $W = 0$, $K_s = 0$

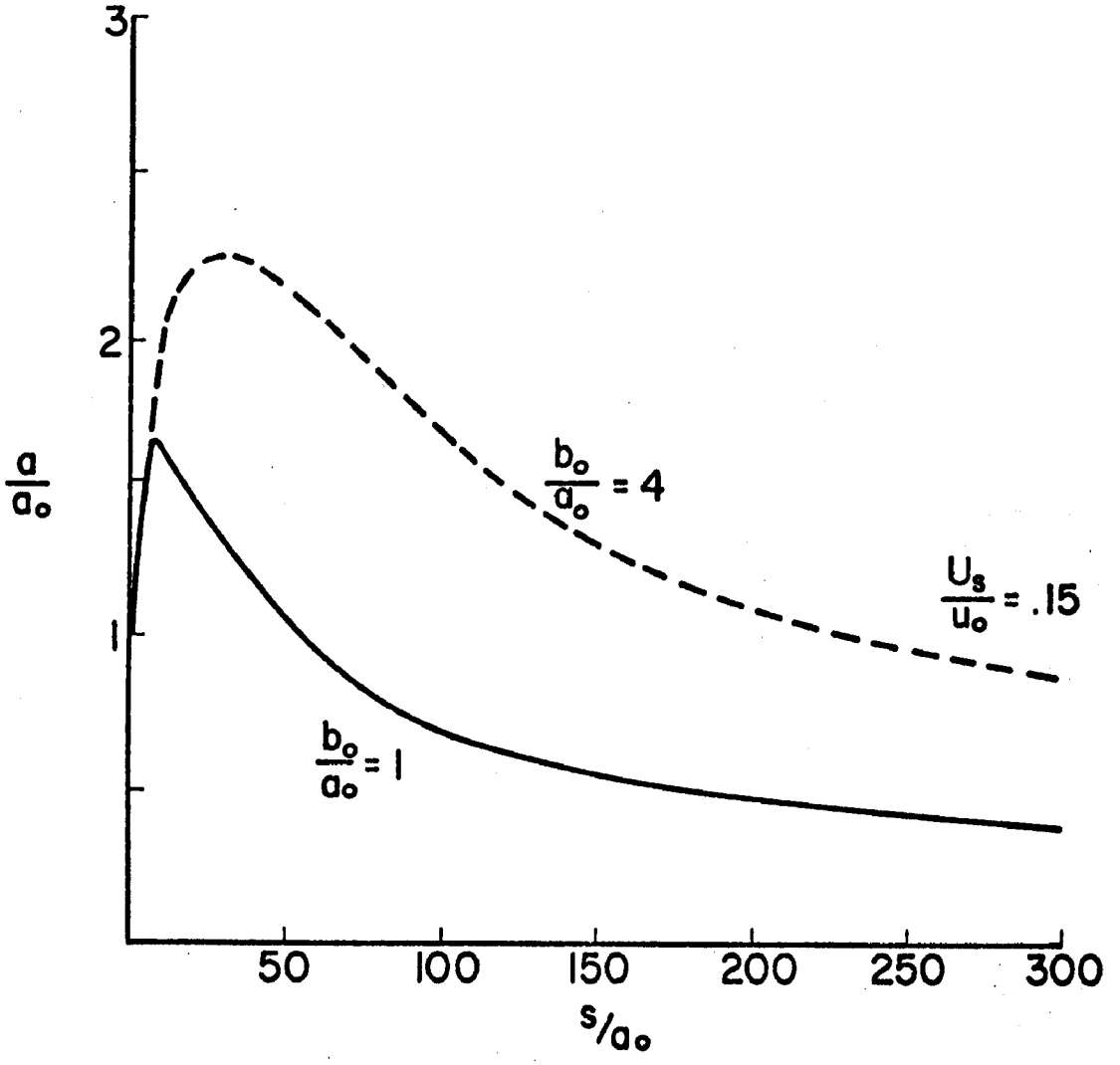


Fig. 20 - Depth of Thermocline below Water Surface along Main Trajectory. Plume in Cross-wind Perpendicular to Discharge. $\alpha_o = 90^0$, $F_o = 15.0$, $W = 0$, $K_s = 0$

## SECTION VI

## EXPERIMENTAL STUDY

### Apparatus and Data Acquisition

The experimental apparatus consisted of a large rectangular tank 17 ft wide, 40 ft long, and 2 ft deep. Hot water was discharged from a channel 6 inches wide and approximately 1.6 inches deep at right angles into the tank, which was filled with cold water. Point measurements of temperature and velocity were taken in the vicinity of the outlet with the aid of a combined temperature-velocity probe described in Ref. [22]. To assure steady-state conditions, cold water was fed into the tank constantly at very low velocity. The excess flow drained over a weir at the downstream end of the tank. Cross-currents and wind were absent in the experiments. More information on the experimental apparatus is given in Ref. [22].

### Data Preparation

The experimental data obtained by the procedures outlined in Ref. [22] consisted of velocity and temperature measurements at variable depth $z$ at a given location $(x,y)$ in the tank. Figure 21 will serve as a definition sketch. Velocity components in the x-direction (u-component) and in the y-direction (v-component) were measured. Usually fifteen to thirty measurements per profile were available. Temperature and velocity were usually not measured at the same depth $z$ because of the particular configuration of the tethered sphere probe used. Therefore 51 equidistant data points at 0.01 ft vertical spacing were obtained by interpolation for each vertical profile. Temperature profiles were approximated using a third order polynomial between any three given measurements, and the interpolation was carried out numerically. For the velocity profiles a graphical interpolation was preferred because the data had more scatter and smoother velocity distributions were desirable.

Table 1 summarizes the conditions for which experimental data were available. "FLUSH" signifies that the discharge channel terminated in the wall of the tank, while "PROJ." means that the outlet channel projected 4.8 ft into the tank. $Q_o$ is the heated water discharge rate, $d_o$ is the depth of the outlet channel, $T_o$ is the outlet water temperature, $T_\ell$ is the cold water temperature in the tank (lake), $T_a$ is the air temperature, and $Re_o$ is the outlet Reynolds number defined as

$$Re_o = \frac{U_o d_o}{\nu_o} = \frac{Q_o}{w_o \nu_o} \tag{44}$$

Table 1 - SUMMARY

| EXP. NO. | OUTLET TYPE | $Q_o$ (cfs) | $d_o$ (ft) | $T_o$ (°F) | TANK $T_\ell$ (°F) | AIR $T_a$ (°F) | $Re_o$ (-) | $F_o$ (-) |
|---|---|---|---|---|---|---|---|---|
| 215 | FLUSH | .00645 | .162 | 91.0 | 70.0 | 78 | 1,590 | .62 |
| 207 | FLUSH | .0131 | .165 | 76.5 | 51.5 | 78 | 2,700 | 1.38 |
| 216 | FLUSH | .0376 | .162 | 92.0 | 73.0 | 81 | 9,370 | 3.73 |
| 214 | PROJ. | .00645 | .155 | 87.0 | 68.0 | 80 | 1,520 | .72 |
| 211 | PROJ. | .0141 | .159 | 84.0 | 60.0 | 76 | 3,190 | 1.43 |
| 217 | PROJ. | .0376 | .155 | 92.5 | 73.5 | 81 | 9,400 | 3.98 |

OF EXPERIMENTS

| $T_o-T_a$ ($^oF$) | $T_o-T_\ell$ ($^oF$) | $\frac{T_o-T_a}{T_o-T_\ell}$ (-) | $H_o$ ($ft^{3o}F/sec$) | $C_o$ ($^oF\ ft^2$) | $D_o$ (ft) |
|---|---|---|---|---|---|
| 13 | 21 | .619 | .135 | 1.70 | .40 |
| -1.5 | 25 | -.060 | .328 | 2.06 | .40 |
| 11 | 19 | .578 | .715 | 1.54 | .40 |
| 7 | 19 | .369 | .123 | 1.47 | .40 |
| 8 | 24 | .333 | .339 | 1.91 | .40 |
| 11.5 | 19 | .605 | .715 | 1.47 | .40 |

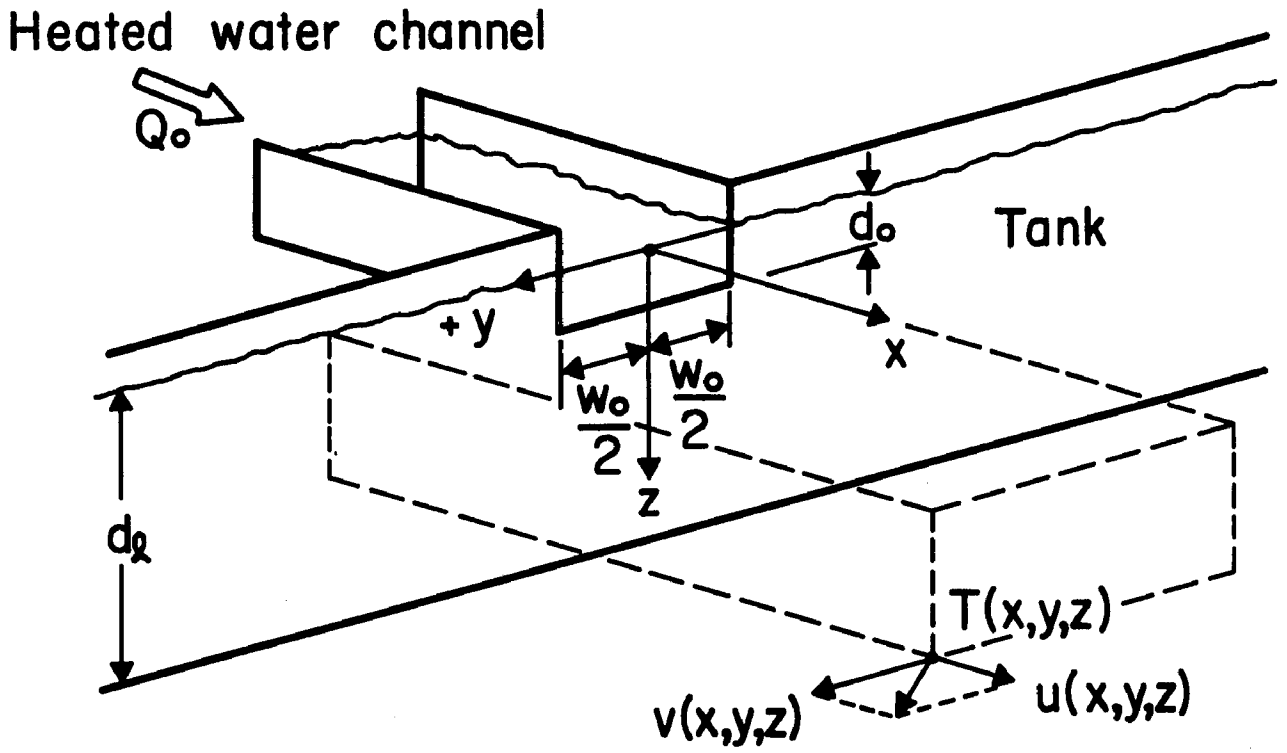


Fig. 21 - Definition Sketch - Surface Discharge into Experimental Tank

where $U_o$ is the average discharge velocity, $w_o = 0.5$ ft is the width of the outlet channel, and $\nu_o$ is the kinematic viscosity at the outlet. $F_o'$ is the outlet densimetric Froude number, defined as

$$F_o = U_o(g'd_o)^{-1/2} = Q_o(g'w_o d_o^3)^{-1/2} \tag{45}$$

where $g' = \frac{\Delta\varrho_o}{\varrho} g$ is a reduced acceleration of gravity. The outlet heat discharge (heat flux) into the tank is

$$H_o = \varrho c_p Q_o(T_o - T_\ell) \tag{46}$$

and the relative heat content in the outlet cross section is

$$C_o = \varrho c_p d_o w_o(T_o - T_\ell) \tag{47}$$

$D_o$ is the hydraulic diameter of the outlet cross section defined as

$$D_o = 4d_o w_o(2d_o + w_o)^{-1} \tag{48}$$

## Data Processing

### Distribution Functions

Each temperature or velocity profile measured in a vertical section was graphed using a scaleplot subroutine (SCLPLT) from the CDC 6600 system library of the University of Minnesota Computer Center. The graphs obtained were of course nearly identical to those obtained with the raw data and reported in Refs. [22] and [53]. Mere inspection of the output showed that the measured profiles were similar to each other and to normal distribution functions only in first approximation. As stated in Ref. [53], there appears to be no unique function which rigorously describes all distributions in a plume. A sample of measured velocities in Fig. 22 may illustrate this point.

The standard deviations identified as $a$ and $\lambda a$ in Eqs. (1) and (2), respectively, were calculated for each temperature and velocity profile. The standard deviation for the velocity profiles was found from the relationship

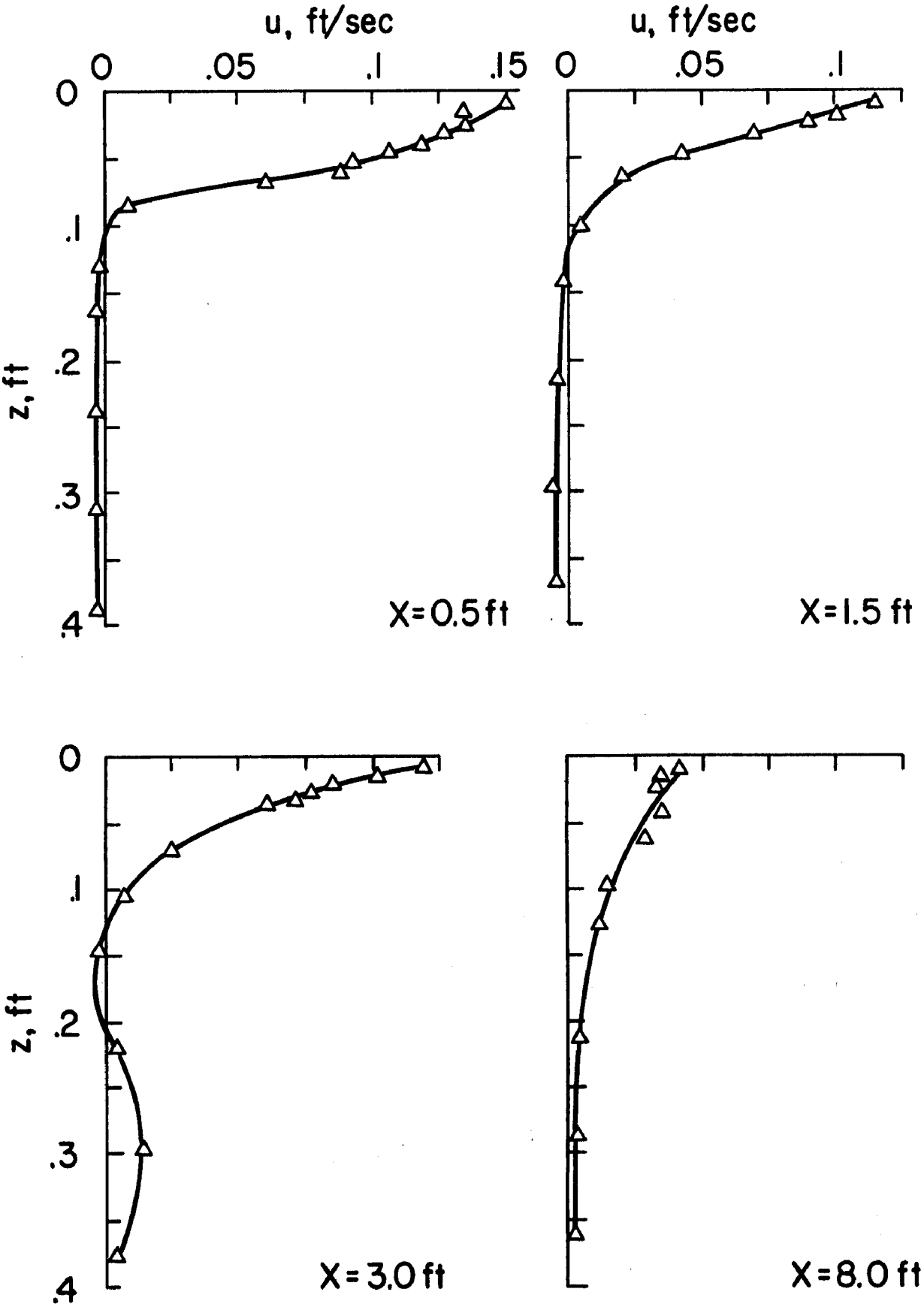


Fig. 22 - Variation of Velocity Component u with Depth at Various Distances from the Outlet along Centerline of tank. Exp. 215

$$a_u = a = \left[ \frac{\sum_{j=1}^{N_p} u_j z_j^2}{\sum_{j=1}^{N_p} u_j} \right]^{1/2} \tag{49}$$

where $u_j$ is the velocity component in the x-direction at a point and $N_p$ is the number of positive measurements in a profile. A vertical profile consisted of no more than $N_p = 51$ points. Similarly, the standard deviation for temperature profiles was calculated from

$$a_T = \lambda_v a = \left[ \frac{\sum_{j=1}^{N_p} (T_j - T_\ell)\, z_j^2}{\sum_{j=1}^{N_p} (T_j - T_\ell)} \right]^{1/2} \tag{50}$$

The calculated values of $a_T$ and $a_u$ showed dependence on location. Figure 23 gives values for all six experiments as a function of distance from the outlet. Predictions made with the aid of the analytical model are shown as solid lines. There is a substantial amount of scatter in the experimental data, particularly those derived from velocity measurements. The analytical model predicted the measured standard deviations, especially those for temperatures, reasonably well.

The vertical distortion parameter $\lambda_v = a_T/a_u$ was assumed to be calculable from the standard deviations for temperature and velocity. It was found to vary considerably from one location to another. This is shown in Fig. 24. Values of $\lambda_v$ less than unity mean that the temperature profile reached smaller depths than the velocity profile, a situation which characterizes fast momentum transfer and slow heat transfer, as would be typical for a very stably stratified shear flow. Values of $\lambda_v$ larger than unity indicate that the temperature profile covered a larger depth than the velocity profile, a situation which could be produced by the accumulation of warm water in the experimental tank before it flowed over the weir at the downstream end of the tank. It is known that this condition existed in the downstream portion of the tank for those experiments using the largest flow rates. Heat conduction could also be responsible for the temperature distributions' reaching larger depths than the velocity distributions. Considering the residence times of the heated water in the upstream portion of the

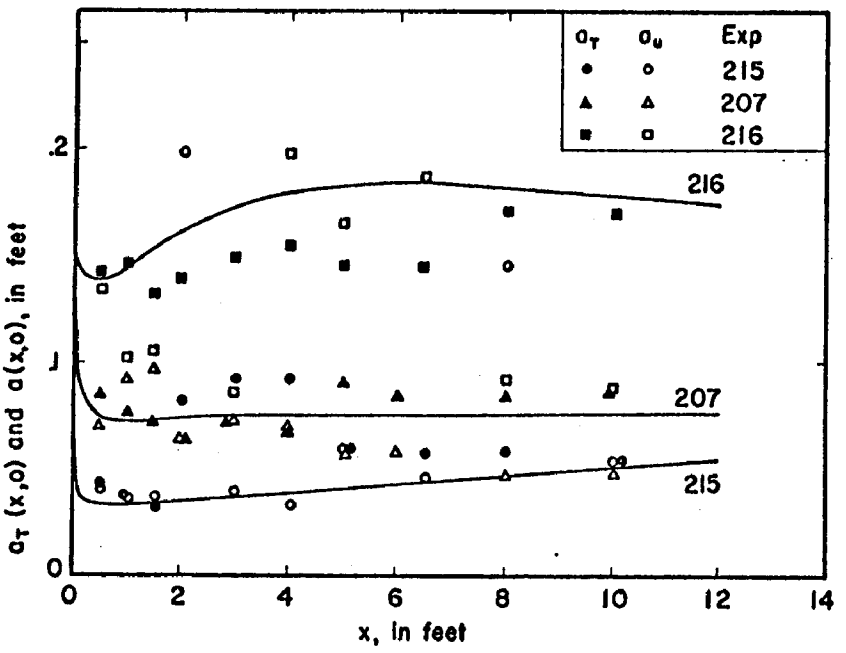


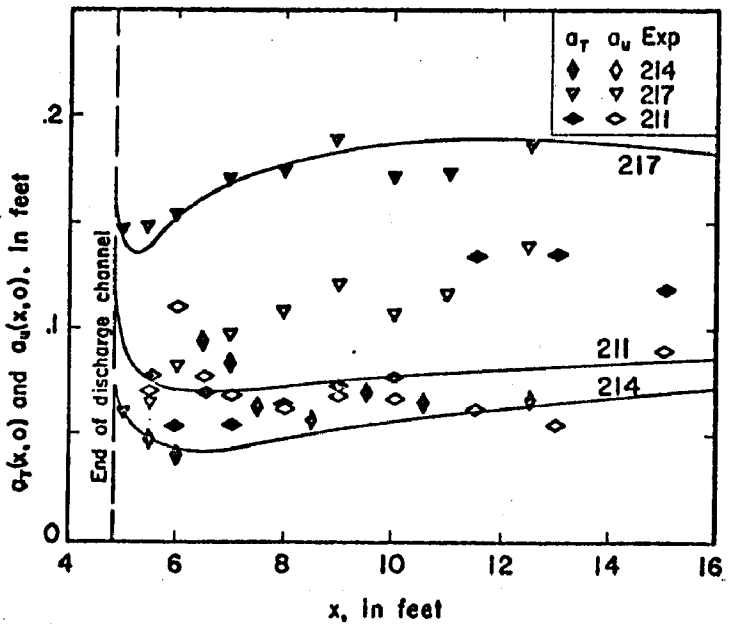


Fig. 23 - Standard Deviations $\sigma_u$ and $\sigma_T$ of Velocity Component u and Temperature T respectively as derived from Velocity and Temperature Profiles measured at Selected Locations along Main Trajectory of the Heated Water Surface Jet. Comparison with Predictions of Analytical Model (solid lines)

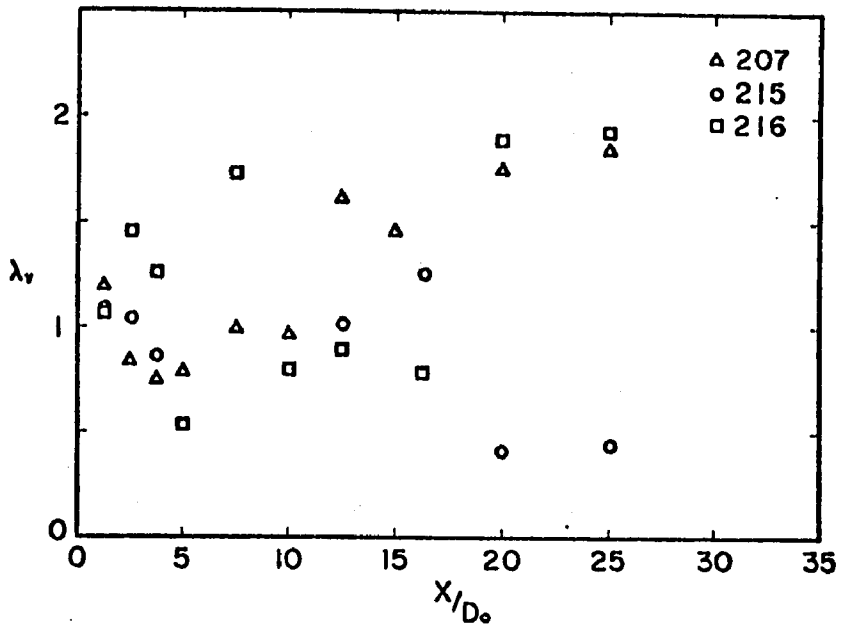


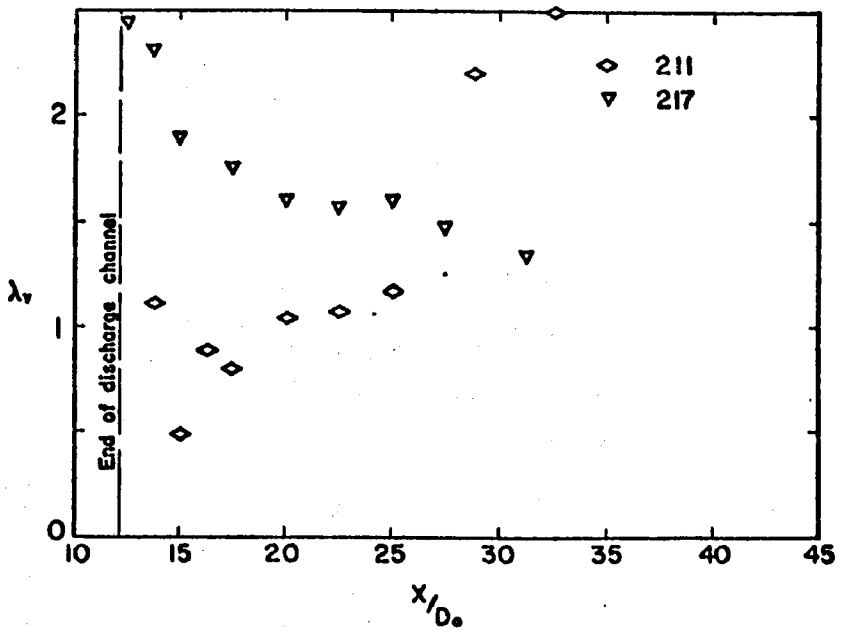


Fig. 24 - Similarity Parameter $\lambda_v$ versus Distance along Main Trajectory from Discharge Point

tank, however, this is only a remote possibility. While the above mechanisms can be cited to explain whatever trend can be detected in the data, much of the scatter in Fig. 24 is due to experimentation, particularly the difficulties encountered in measuring small velocities in a thin layer of heated water.

The way in which the similarity parameter $\lambda_v$ varied in cross sections perpendicular to the main trajectory was also examined. The results presented in Fig. 25 show that there is a slight tendency for $\lambda_v$ values to increase toward the edges of the jet. This is the result of an existing temperature stratification in the tank outside the heated water jet, as illustrated by Fig. 31f. It may also be noted that $\lambda_v$ is usually in the range $1 < \lambda_v < 2$. For the above reasons it was not really possible to accurately assess the value of $\lambda_v$, but it appears justified to use a value of $\lambda_v$ close to 1 for a heated jet into a non-stratified environment.

To determine how well the measured temperature and velocity profiles agreed with assumed Gaussian distributions, a standard error was calculated for each vertical profile. The error is defined for a velocity profile as

$$\epsilon_u(x,y) = \left[\frac{1}{N_p}\sum_{j=1}^{N_p}\left(u_e(x,y,z_j) - u_{th}(x,y,z_j)\right)^2\right]^{1/2} \tag{51}$$

where $u_e$ and $u_{th}$ refer to experimental (measured) and theoretical (calculated) velocities, respectively. The theoretical value $u_{th}$ was calculated from Eq. (1), in which $x$ and $y$ were substituted for $s$ and $r$, respectively, because of the absence of wind and cross-currents, and $a_u(x,y)$ was used as the standard deviation. Thus

$$u_{th}(x,y,z_j) = u_e(x,y,0)\,\exp\left[-\frac{1}{2}\left(\frac{z_j}{a_u(x,y)}\right)^2\right] \tag{52}$$

For easier interpretation a dimensionless standard error $\epsilon_u^*(x,y)$ was actually calculated

$$\epsilon_u^*(x,y) = \frac{\epsilon_u(x,y)}{u_e(x,y,0)} \tag{53}$$

The results given in Fig. 26 show no specific effect of distance. Standard errors average out to nearly 0.1. This is a good result considering that the standard error computation has nothing to do with a best fit, but is rather an evaluation of the shape of the velocity distribution in which the measured surface value is used as a reference.

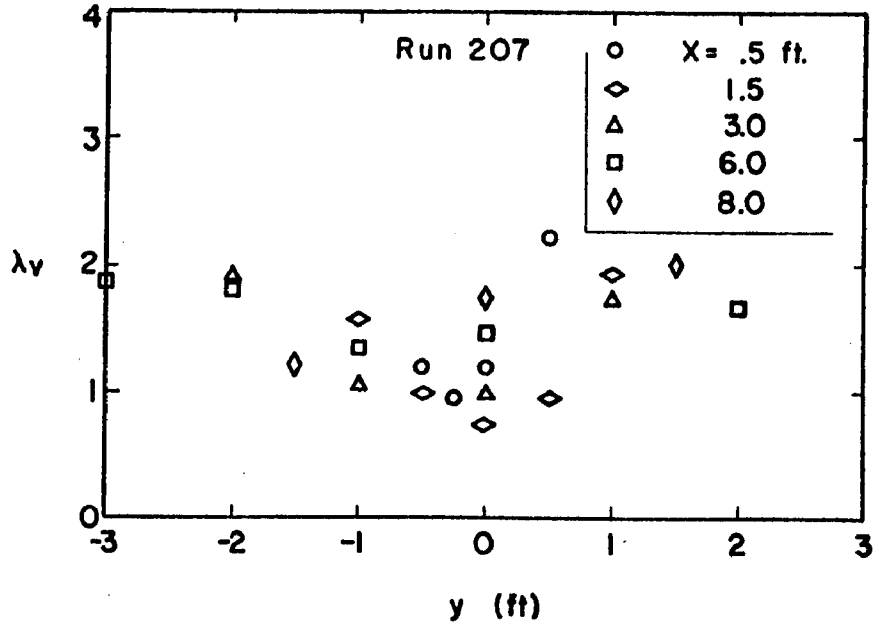


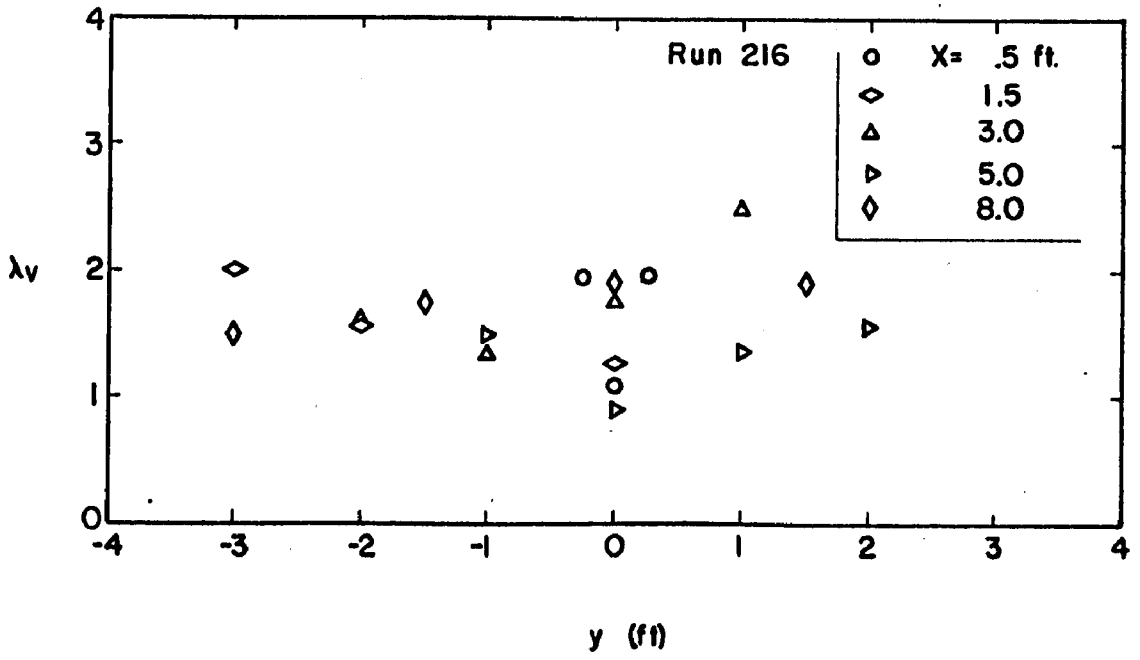


Fig. 25 - Similarity Parameter $\lambda_v$ versus Distance from Main Trajectory

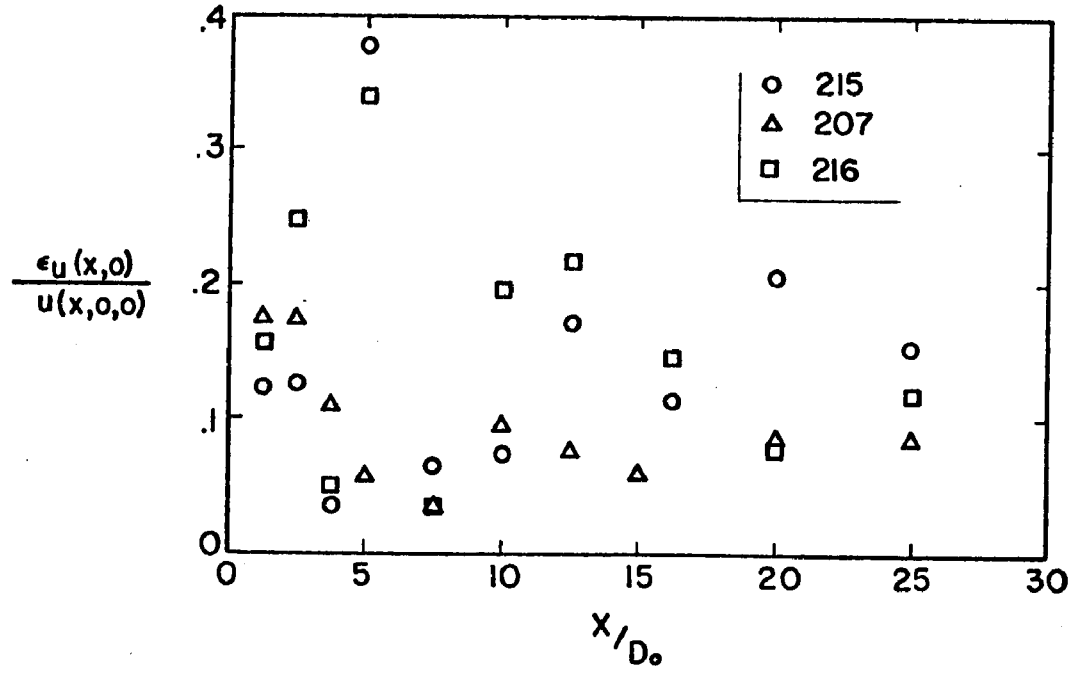


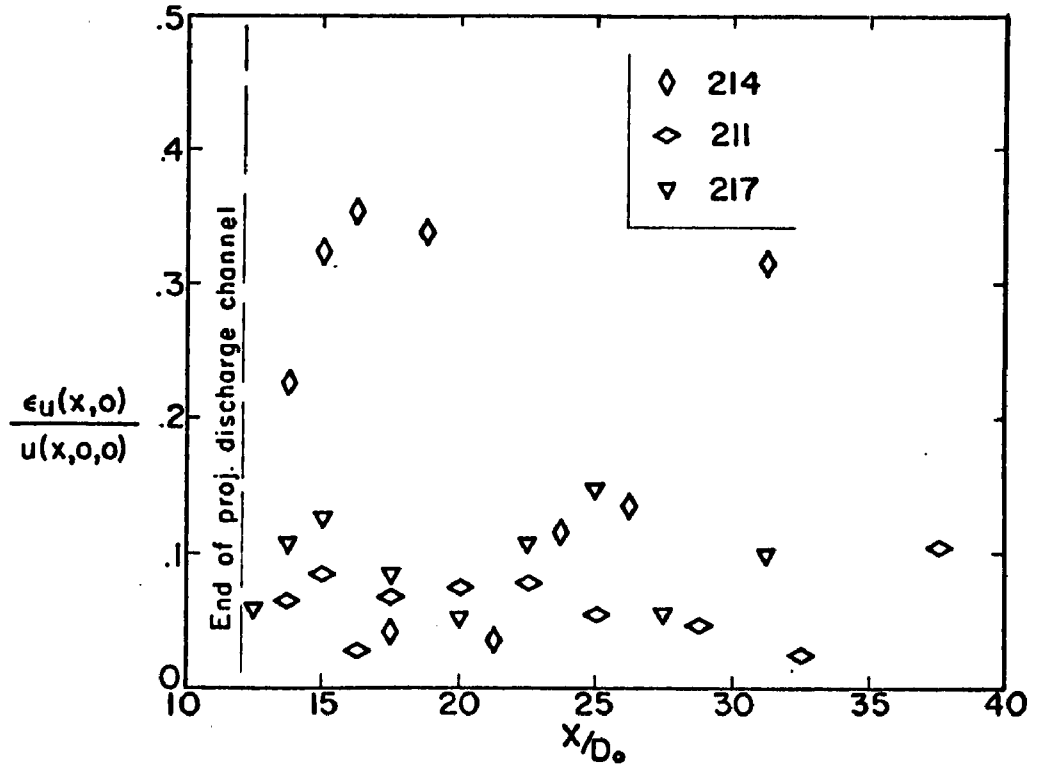


Fig. 26 - Standard Error between Normal Distribution Functions and Experimental Velocity Profiles Measured along Main Trajectory

Standard errors were also calculated for the temperature data or, more precisely, the excess temperature $T^*(x,y,z_j)$ above the cold water temperature. The final equation used is

$$\frac{\epsilon_T(x,y)}{T_e^*(x,y,0)} = \left[\frac{1}{N_p}\sum_{j=1}^{N_p}\left[\frac{T_e^*(x,y,z_j)}{T_e^*(x,y,0)} - \exp\left[-\left(\frac{1}{2}\frac{z_j}{a_T(x,y)}\right)^2\right]\right]^2\right]^{1/2} \tag{54}$$

where $T_e^* = T_e - T_\ell$. The results were plotted in Fig. 27. They are quite consistent with those in Fig. 26. The results for the temperature data seem to suggest certain trends with distance (plotted in dimensionless form with the hydraulic diameter $D_o = 0.4$ ft as a reference length), but there are not really enough data to warrant analysis of this detail.

The previous discussions centered around vertical distributions of temperature and velocity components in the x-direction. The analytical model described also specifies the horizontal distributions as Gaussian. There were not enough data in any horizontal section to really check this hypothesis. No more than seven measurements were taken in a horizontal cross section at a constant depth. The raw data reported in Ref. [53] suggest that normal distribution functions should be descriptive of what was observed. No further analysis is possible. It was noted that the widths of the velocity and excess temperature distributions were very similar, suggesting that the horizontal similarity parameter $\lambda_h$ must also have a value close to 1.

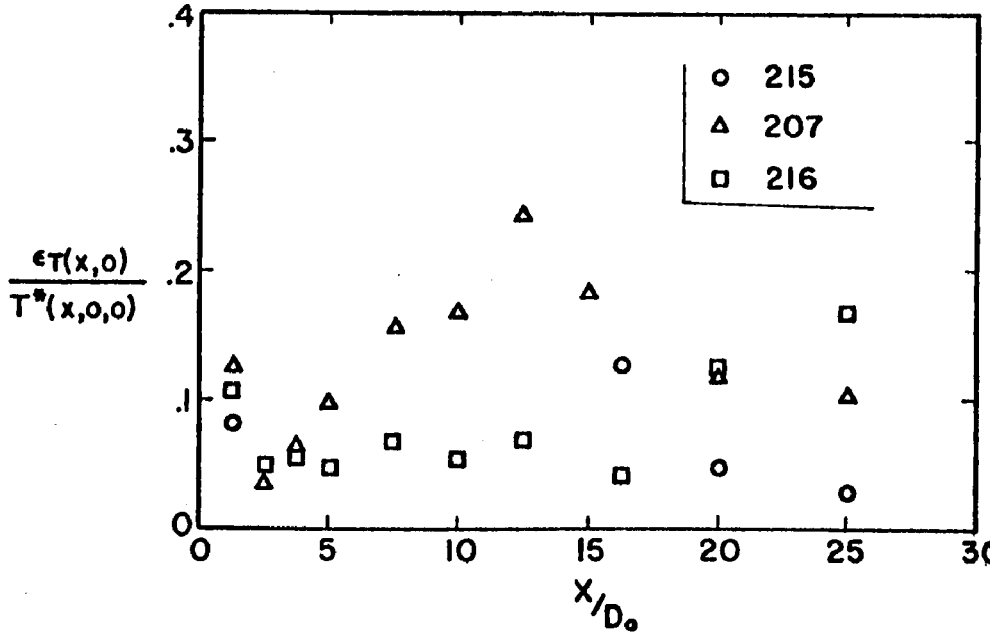


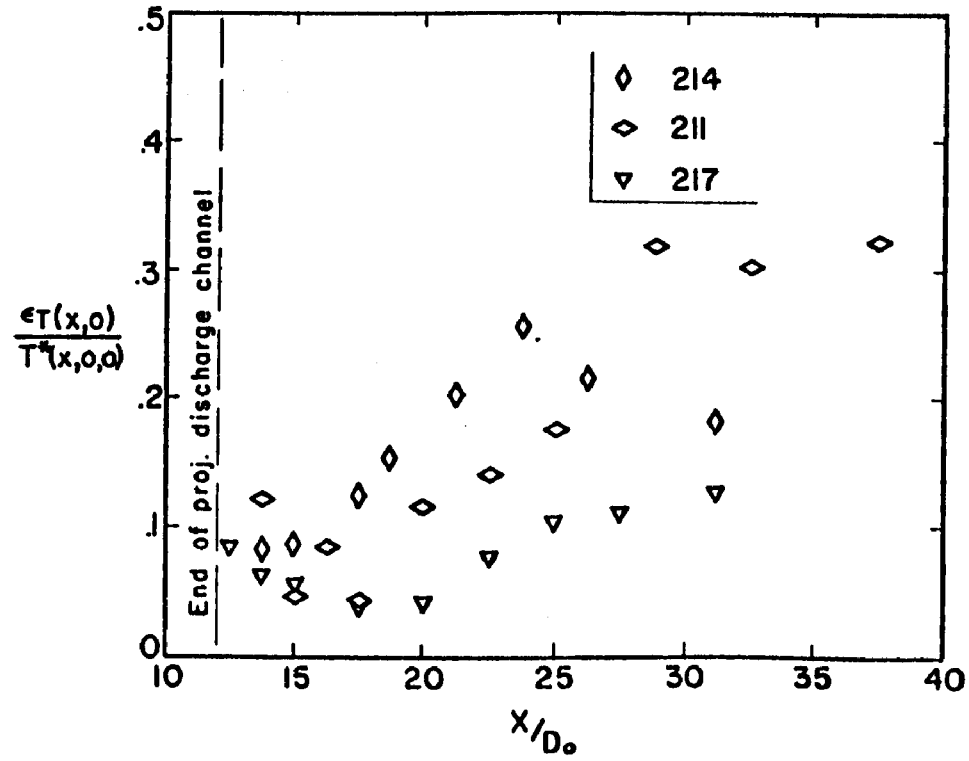


Fig. 27 - Standard Error between Normal Distribution Functions and Experimental Temperature Profile measured along Main Trajectory

## Spread

A second major objective was to obtain information on the horizontal and vertical spread of the plume after discharge. Spread was evaluated in several different ways using

a) Velocity
b) Spread of isotherm patterns
c) Spread of velocity distributions
d) Visual spread

Spread Velocities -- The velocity component v perpendicular to the main trajectory is probably the most direct measure of lateral spread. In the analytical model it was assumed to be related to a densimetric Froude number for the centerline section. Plots of lateral (spread) velocity components v are given in Fig. 28 as an example. Apparently surface lateral spread velocities reach a maximum at a distance approximately one-third of the total width of the plume from the main trajectory. In the analytical model this point would be represented by $y = b$, where b is the standard deviation defined in Eq. (1). The lateral spread velocity changes with depth. It reverses direction at some distance from the water surface. Outward spread velocities (away from the main trajectory) are found near the water surface and inward flow at some depth below. Figure 29 shows examples of measurements. The reversal in flow direction occurs at a depth approximately equal to the thermocline or standard deviation a in Eq. (1). The inward flow appears to provide the necessary fluid for entrainment and also for the replacement of warm water when lateral spread reduces the depth of the thermocline. The observation of an inward flow thus supports the displacement (spread) equation (19) in the analytical model.

Equation (18) suggests that the buoyancy-induced surface lateral spread velocity at a distance $y = b$ from the main trajectory is related to the centerline densimetric Froude number. The spread velocities v reported in Figs. 28 and 29 are totals produced by turbulence and buoyancy. According to Eq. (21) the two effects are additive. In Ref. [37] it has been shown that the centerline velocity u in a fully developed non-buoyant, axisymmetric jet varies according to

$$\frac{u(x,0,0)}{u(0,0,0)} \frac{x}{D_o} = 6.2 \qquad (x > 6.2\ D_o) \tag{55}$$

using the notations of this paper. The lateral spread velocity was found [37] to have a maximum of

$$\frac{v(x,b,0)}{u(0,0,0)} \frac{x}{D_o} = 0.35 \tag{56}$$

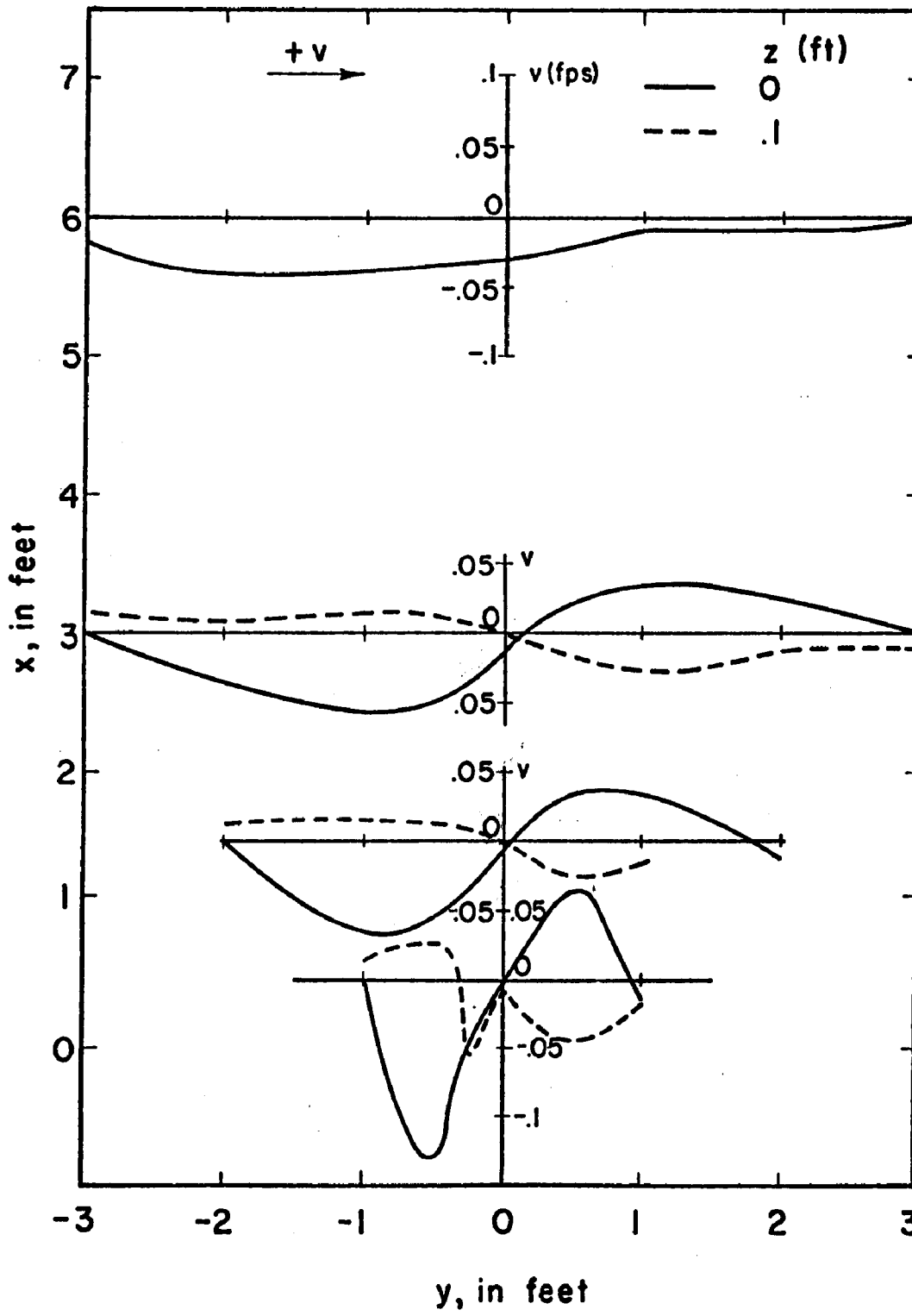


Fig. 28 - Lateral Spread Velocities v at Two Depths (z = 0 and z = 0.1 ft) for Exp. 207

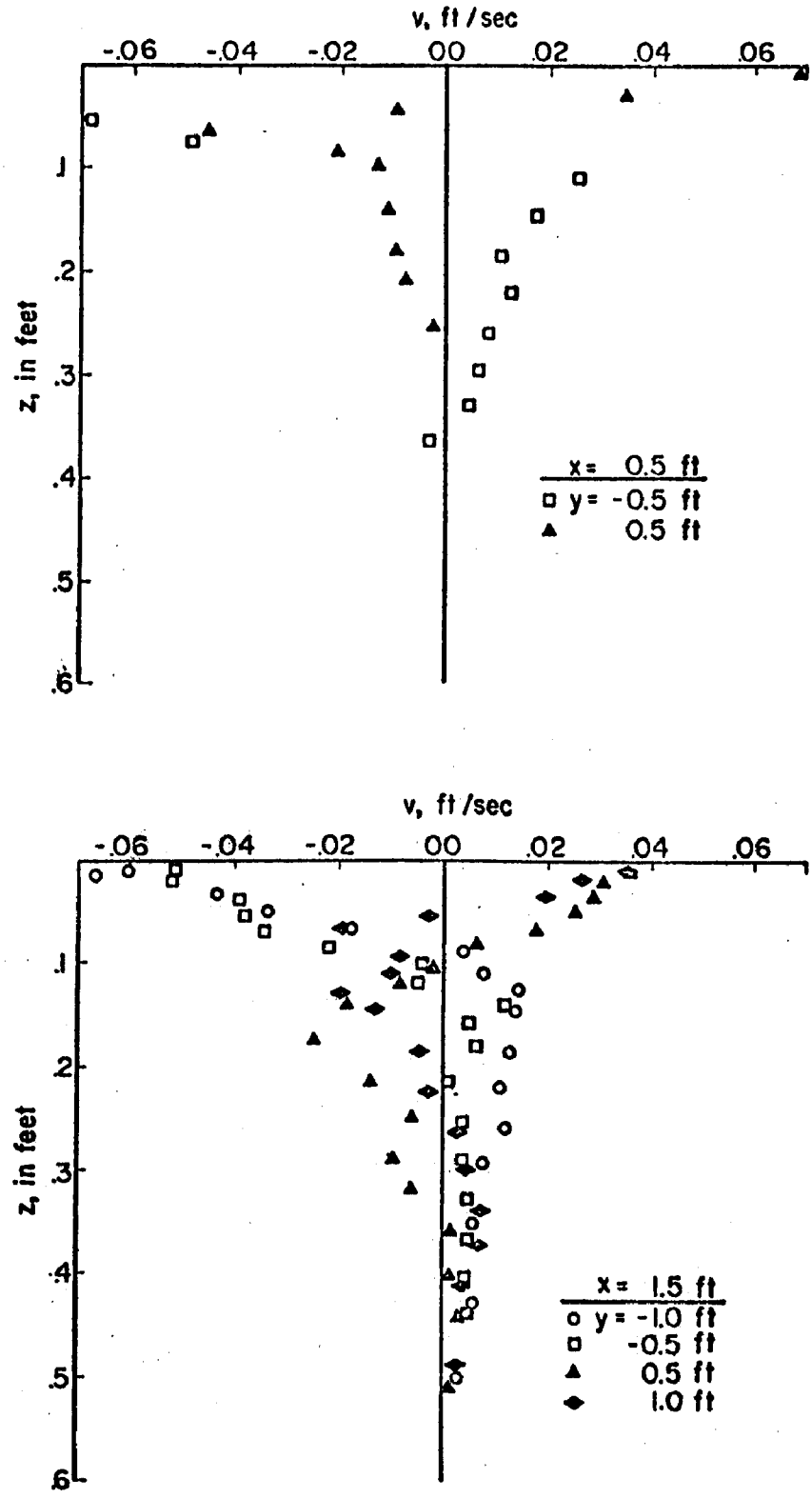


Fig. 29 - Variation of Velocity Component v with Depth at Various Distances from the Outlet and the Main Trajectory. Exp. 207

Thus the turbulence-induced spread in dimensionless form has a value of

$$\frac{(db/dt)_T}{u(x,0,0)} = \frac{v(x,b,0)}{u(x,0,0)} = \frac{0.35}{6.2} = 0.0565 \tag{57}$$

The buoyancy-induced spread according to Eqs. (14) and (4) is

$$\left(\frac{db}{dt}\right)_B = c_5 \frac{u(x,0,0)}{F^*} \tag{58}$$

which in the absence of both a cross current and wind is also equal to

$$\frac{(db/dt)_B}{u(x,0,0)} = \frac{c_5}{F} \tag{59}$$

To evaluate the coefficient $c_5$, measured maximum spread velocities (Fig. 28) were reduced to dimensionless form and a value of 0.0565 subtracted. The resulting values were plotted in Fig. 30 versus $1/F$. The results suggest that $c_5 \approx 0.5$.

Spread of Isotherm Patterns -- Another, more descriptive way to illustrate the spread of the heated water surface jet is to graph isotherms in various sections. Isotherm patterns in vertical planes along the main trajectory and perpendicular to it have been given in Refs. [22] and [53]. The results indicated in Ref. [53] are also reflected in the data of Fig. 23 of this report. The standard deviations of temperature profiles (and velocity profiles) as plotted in Fig. 23 can be used as measures of vertical spread. It is quite apparent that temperature induced buoyancy caused the heated water to spread on the surface of the tank without significant penetration into it.

To obtain a picture of the horizontal spread of the surface jet a different kind of graph was used. Figure 31 gives examples. Program CONTOUR was used to do the plotting. The outlet is at the bottom center of each map and the flow is from the bottom to the top of the map. Coordinates are given in feet with reference to the upstream end of the tank (bottom of picture) and the centerline of the tank, respectively. Alternate contours are printed. The numbers inside the map are dimensionless excess temperatures of the form $T^*(x,y,z)/T^*(0,0,0)$ multiplied by a factor of 10. Examination of the maps reveals a number of features. First, in each run a "typical" plume temperature distribution is formed around the outlet. The depth $d_T$ at which the pattern disappears has been plotted versus the densimetric outlet Froude number in Fig. 32. The results can be approximated by the relationship

$$\frac{d_T}{do} = \sqrt{\frac{F_o}{2}}$$

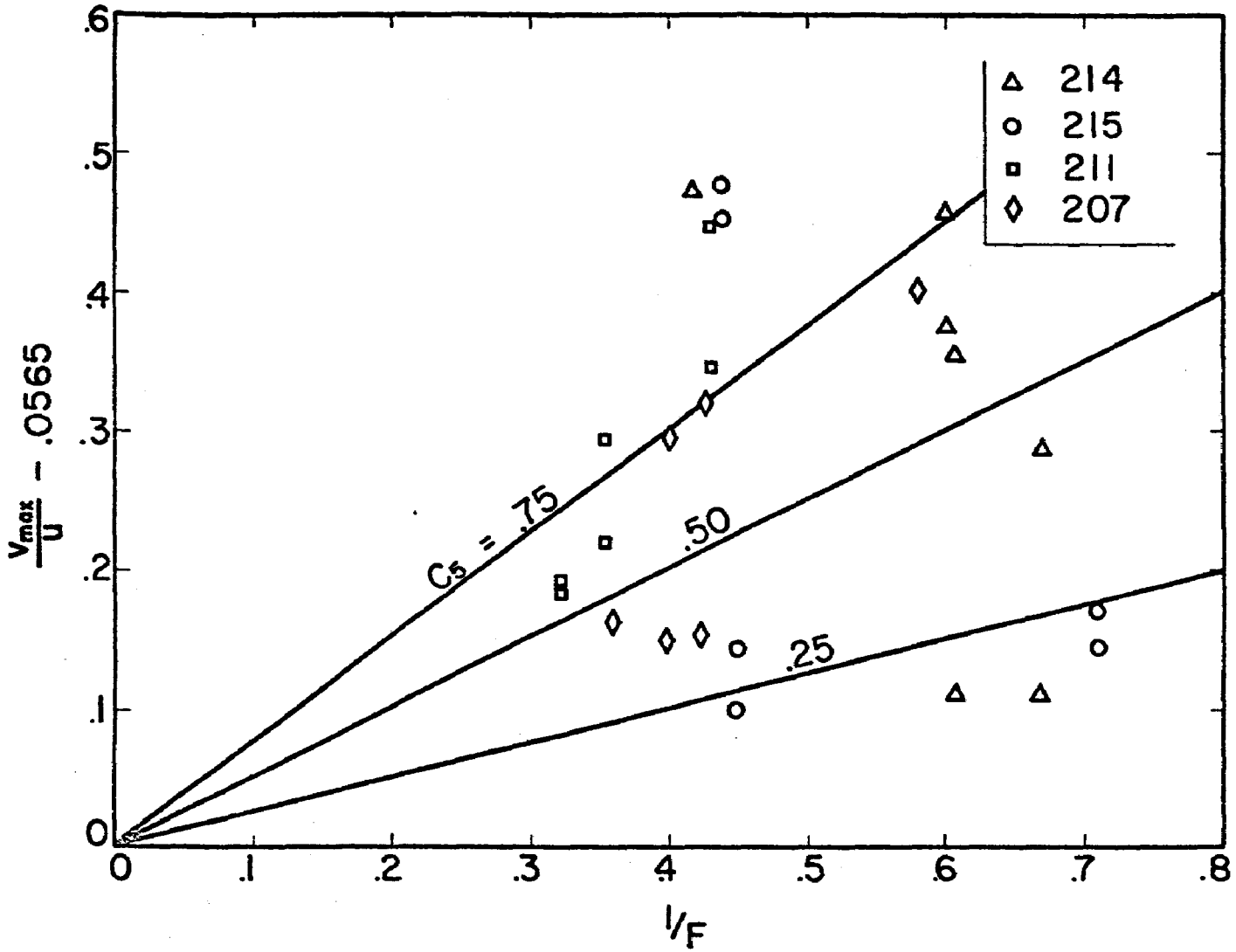


Fig. 30 - Maximum Spread Velocities versus Centerline Densimetric Froude Numbers for Individual Cross Sections Perpendicular to the Main Trajectory

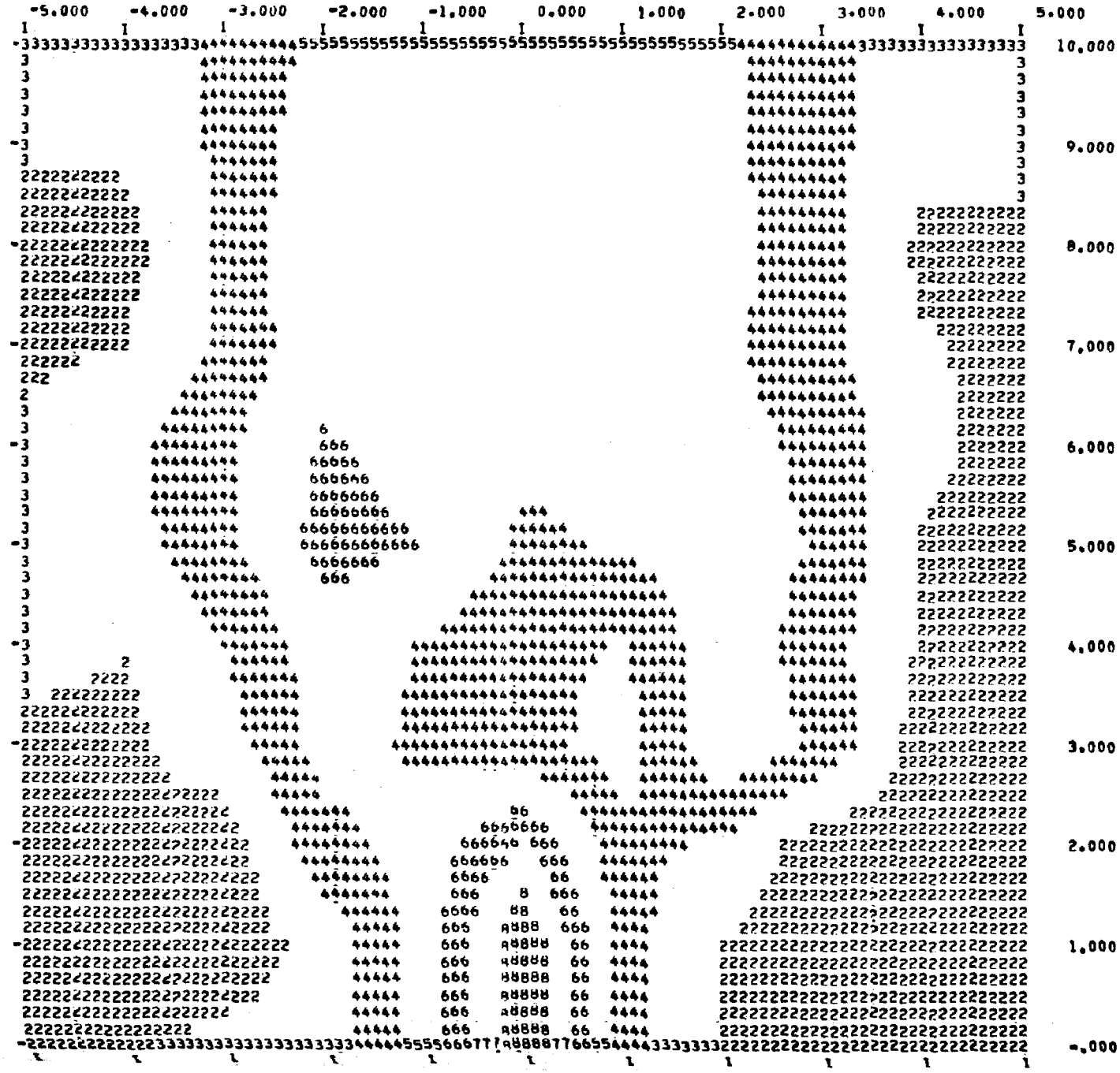




Fig. 31a - Isotherms for Run 215 (Horizontal section for depth z = 0.01 ft)

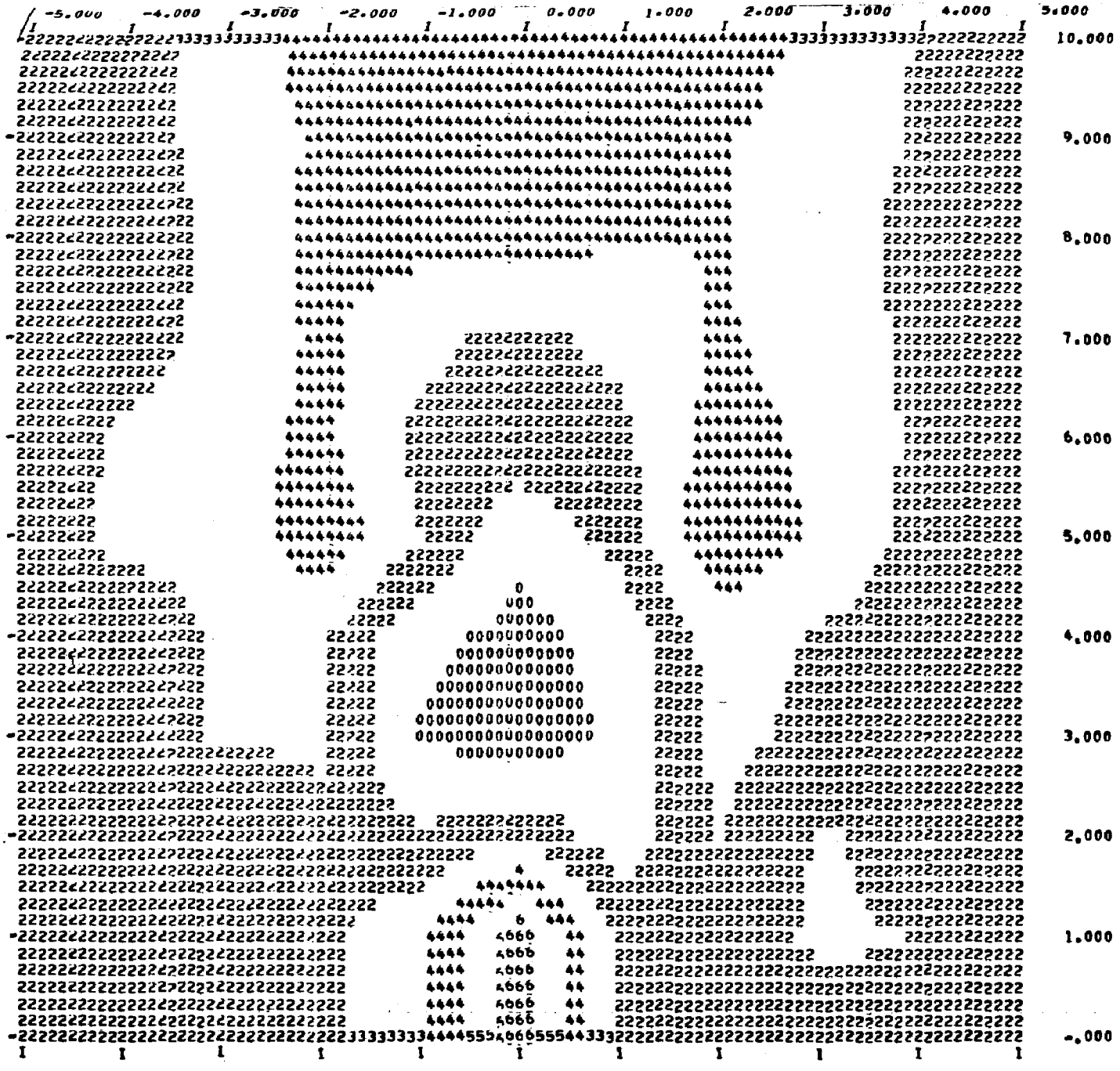


Fig. 31b - Isotherms for Run 215 (Horizontal section for depth z = 0.03 ft)

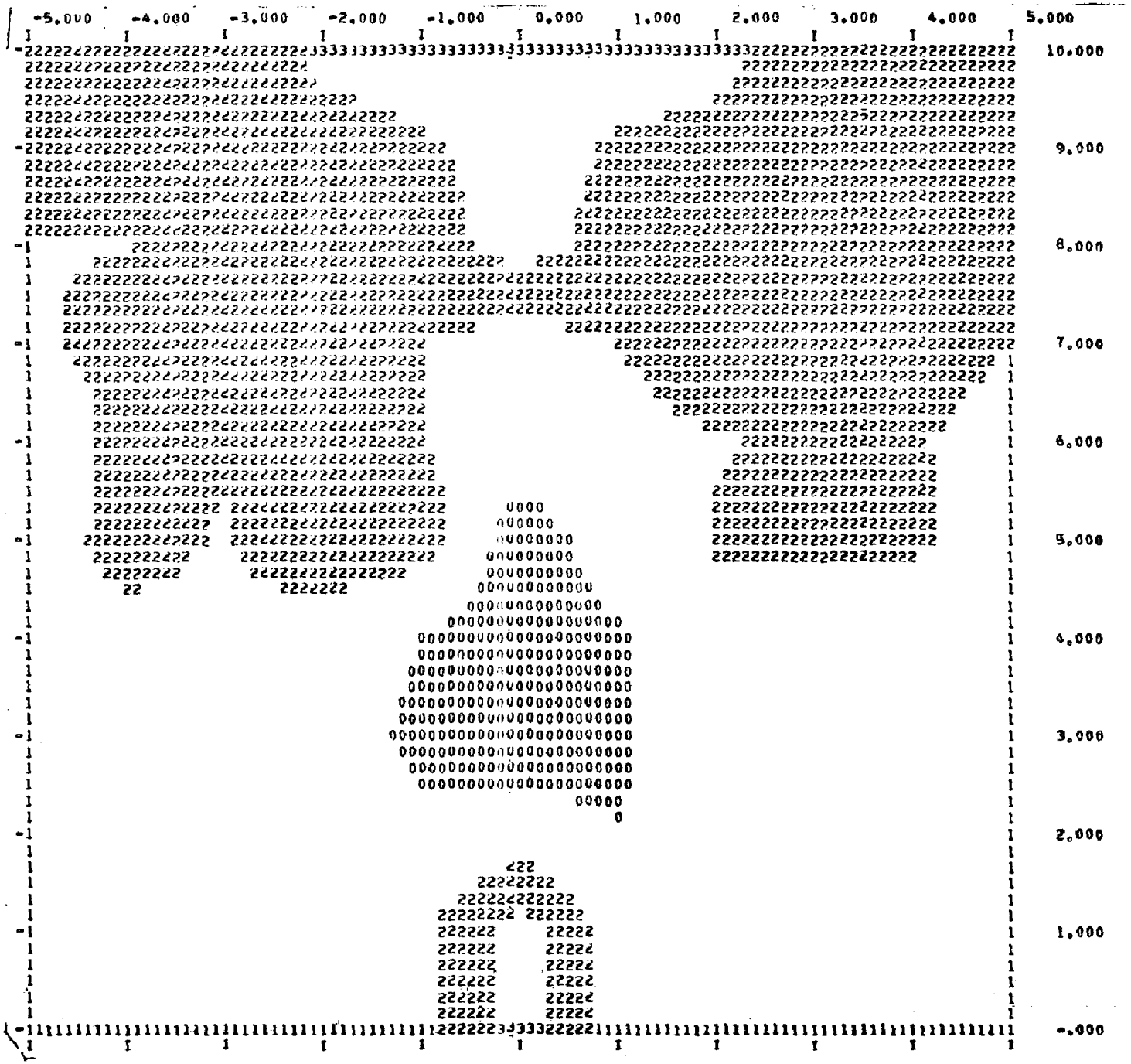




Fig. 31c - Isotherms for Run 215 (Horizontal section for depth z = 0.05 ft)

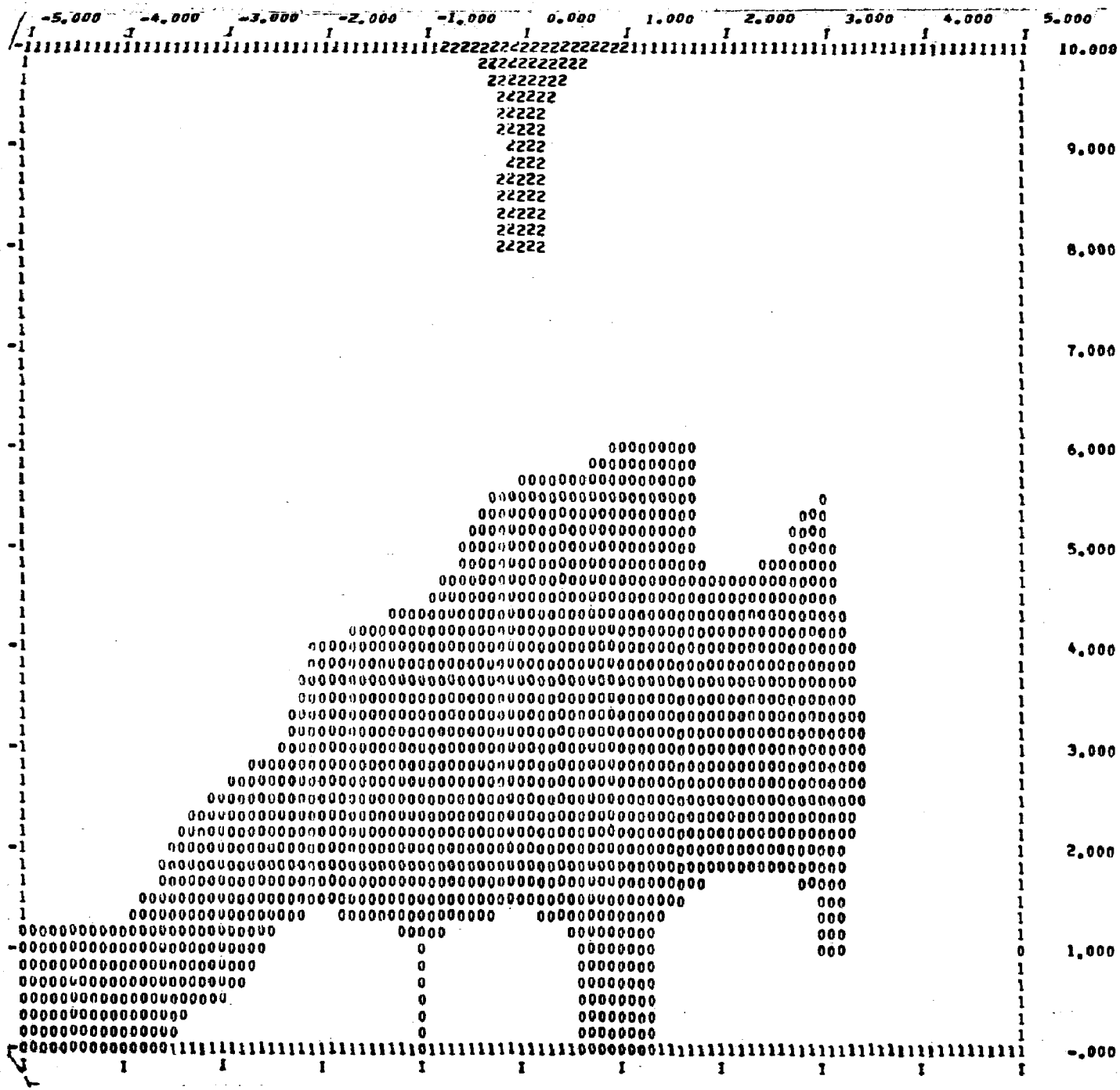


Fig. 31d - Isotherms for Run 215 (Horizontal section for depth z = 0.07 ft)

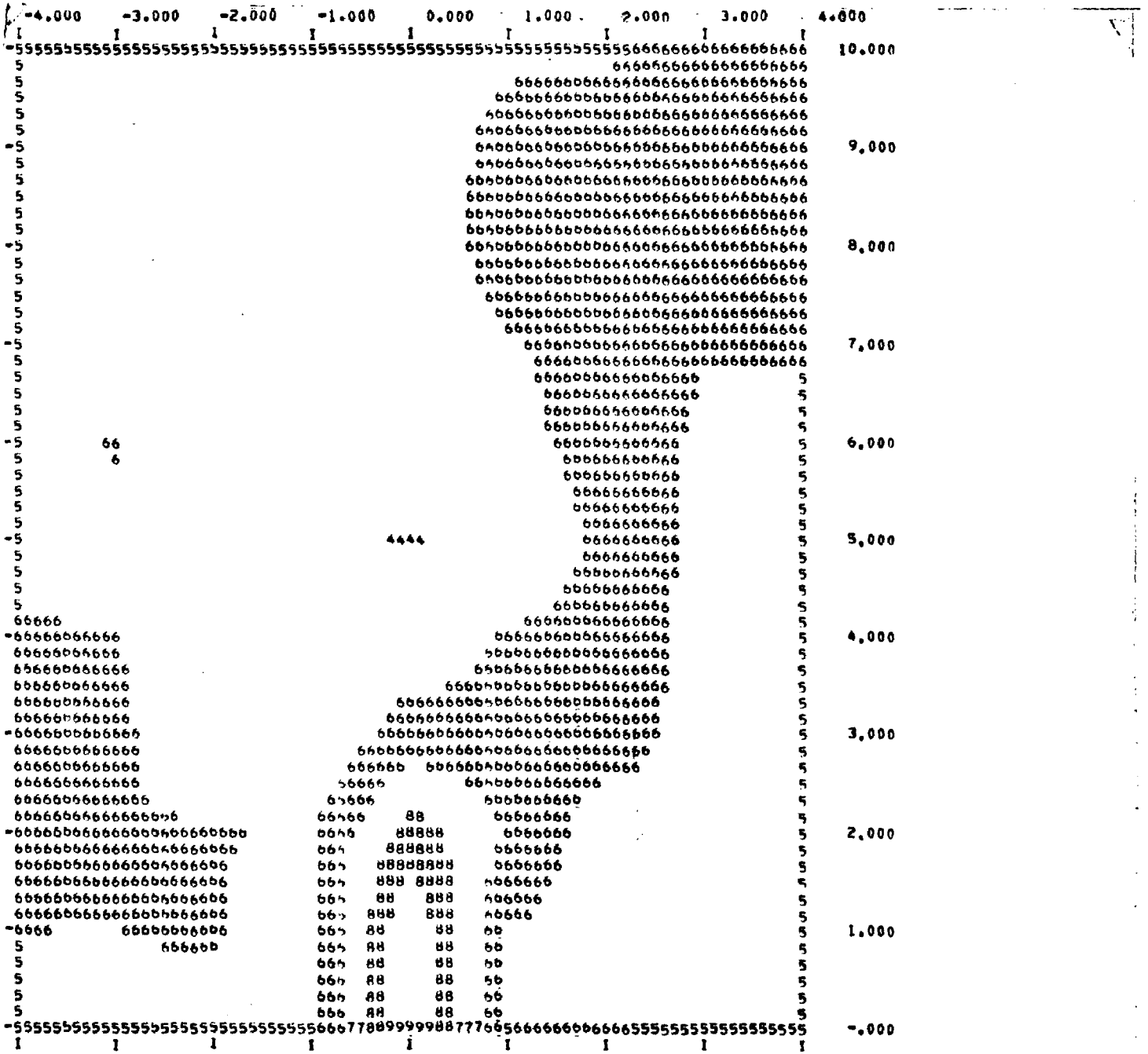




Fig. 31e - Isotherms for Run 207 (Horizontal section for depth z = 0.01 ft)

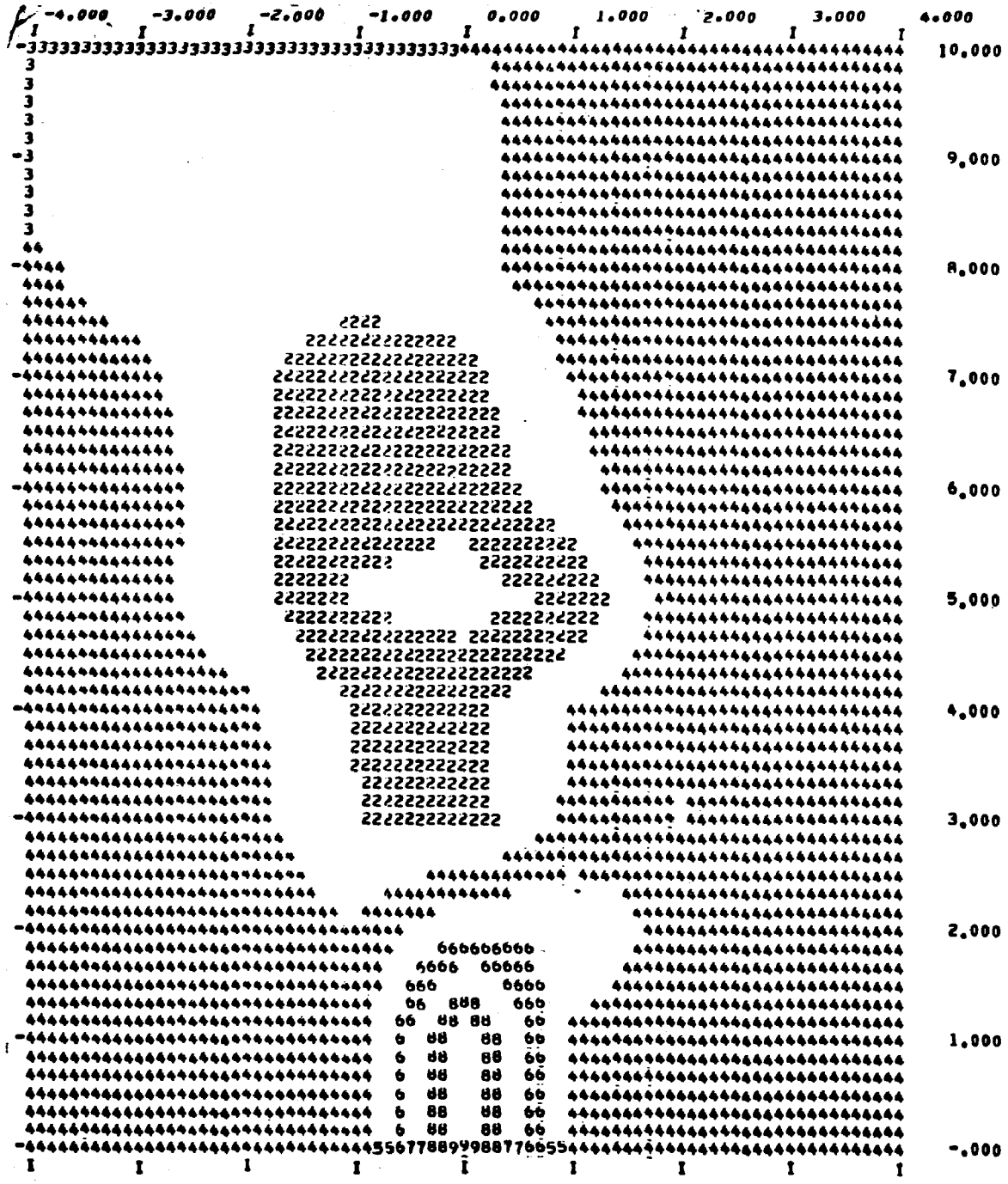




Fig. 31f -
Isotherms for Run 207
(Horizontal section
for depth z = 0.05 ft)

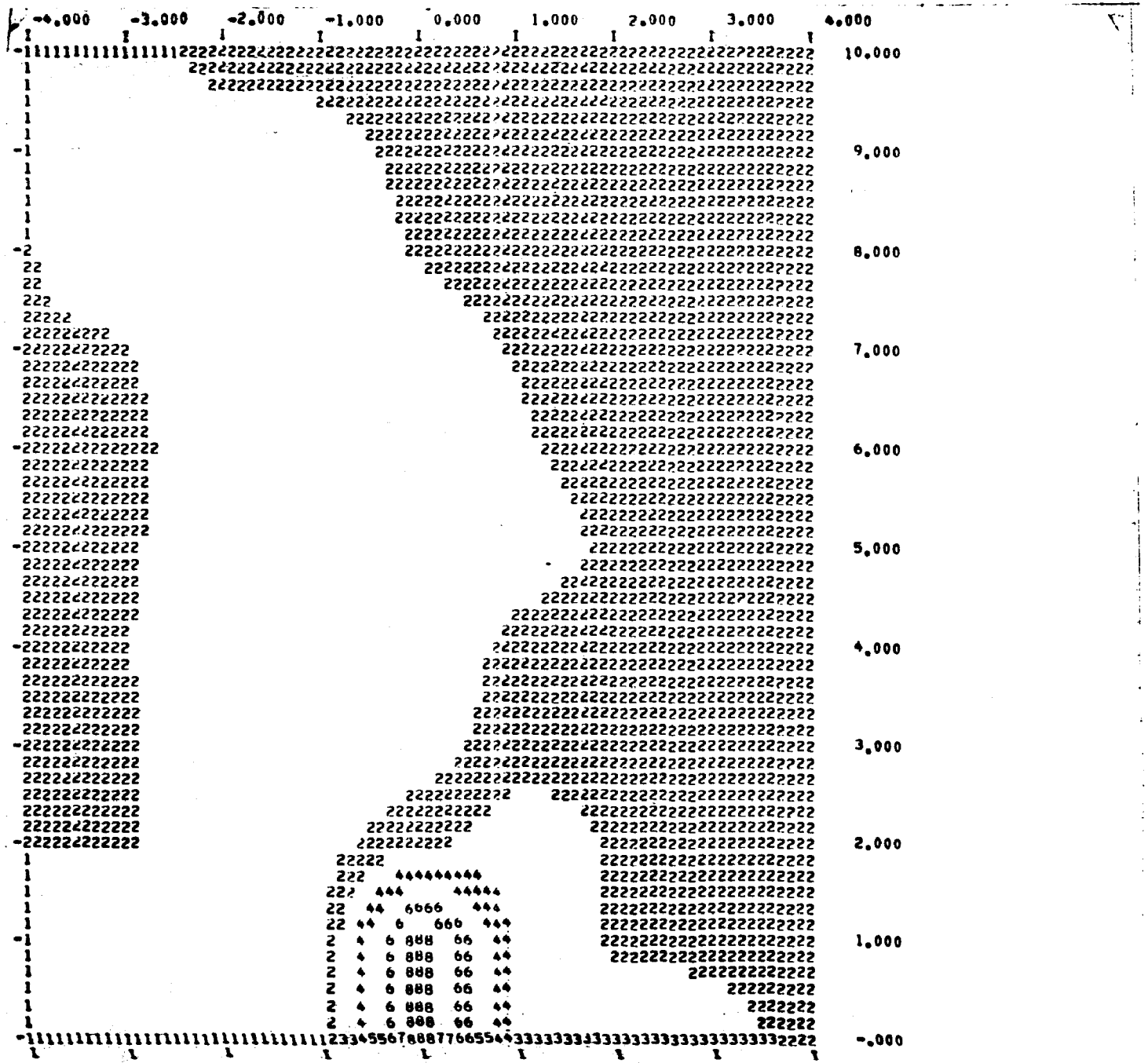




Fig. 31g -
Isotherms for Run 207
(Horizontal section
for depth z = 0.10 ft)

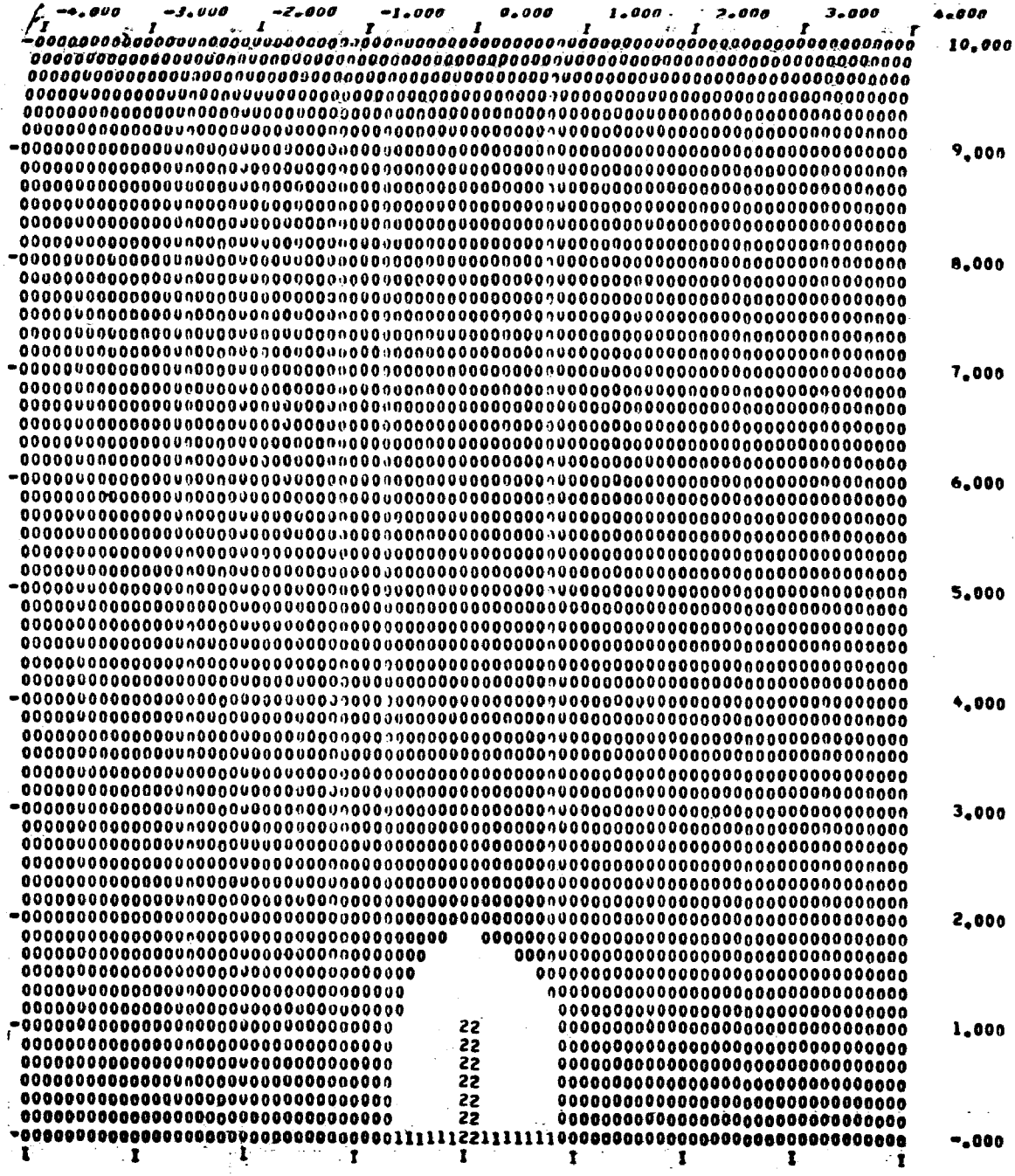


Fig. 31h - Isotherms for Run 207 (Horizontal section for depth z = 0.16 ft)

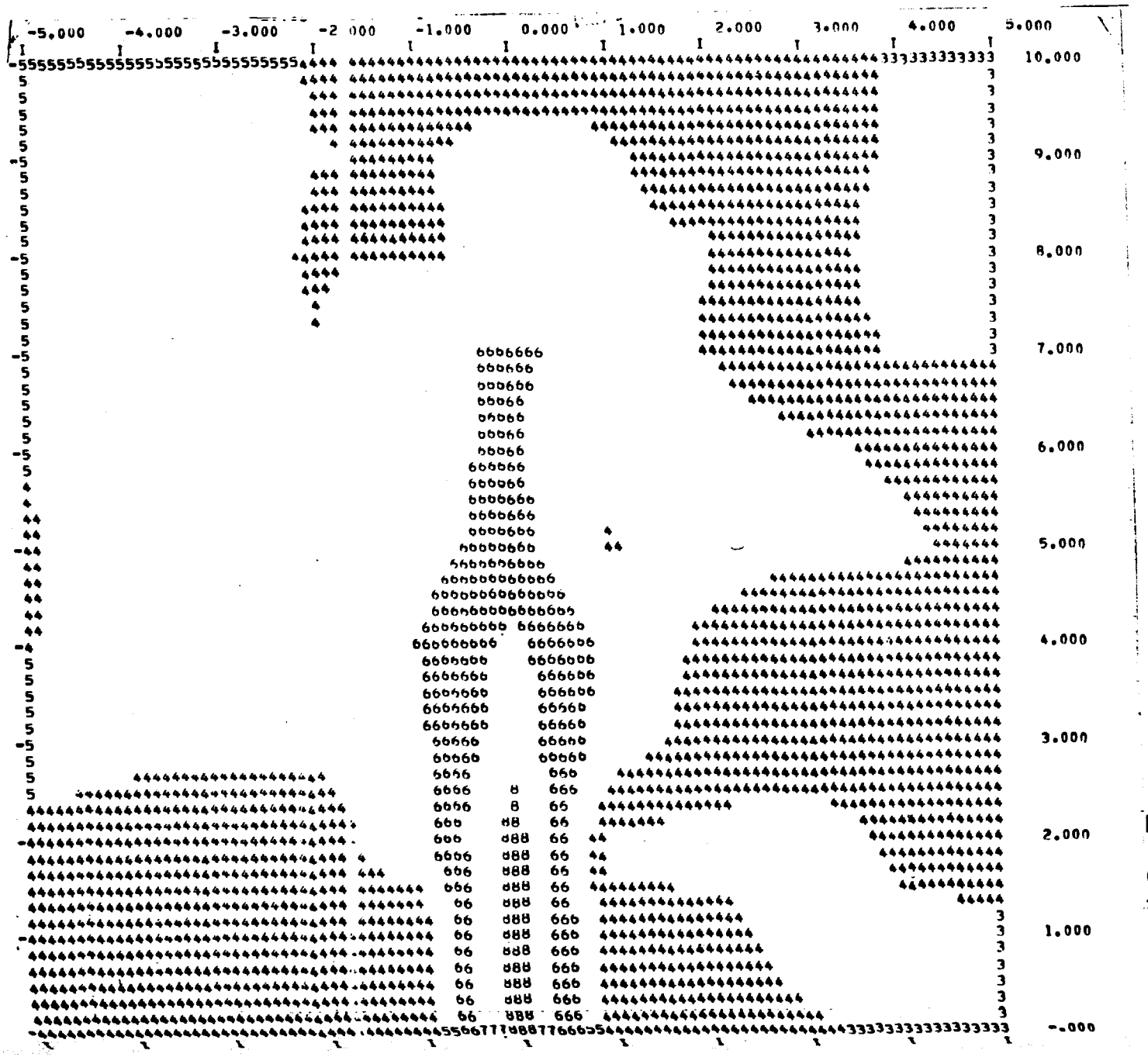




Fig. 31i - Isotherms for Run 216 (Horizontal section for depth z = 0.01 ft)

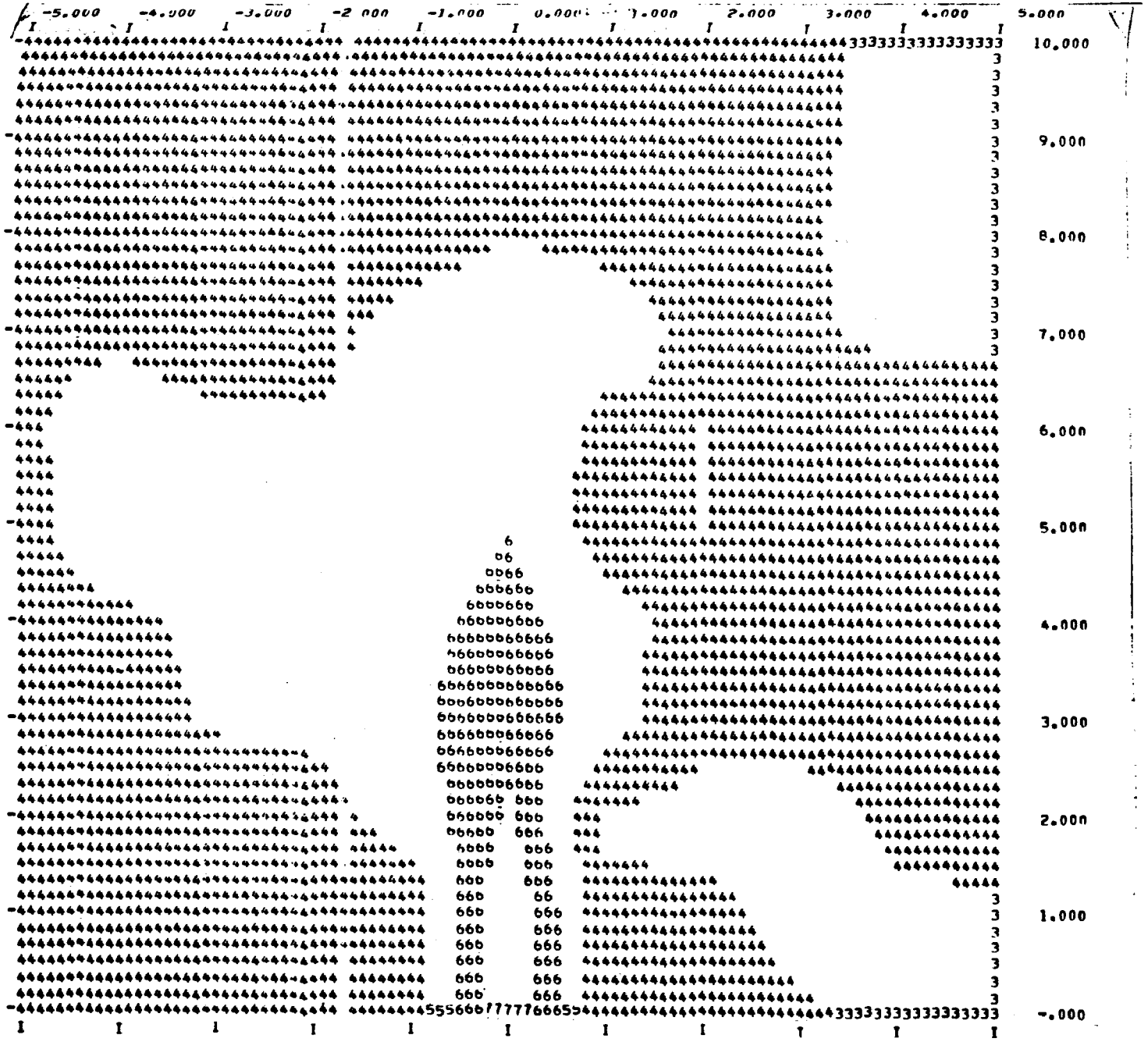


Fig. 31j -
Isotherms for Run 216
(Horizontal section
for depth z = 0.05 ft)

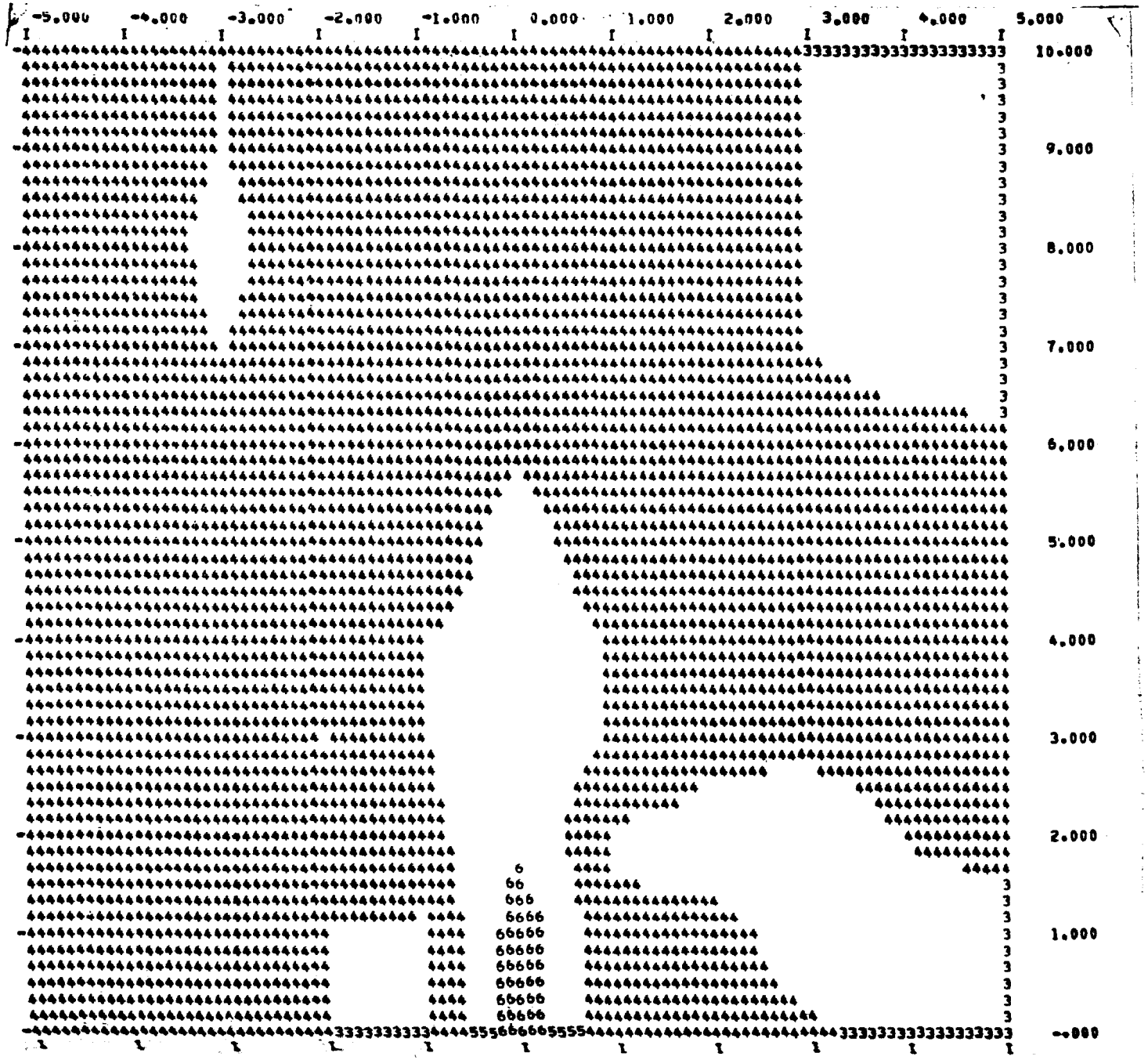




Fig. 31k -
Isotherms for Run 216
(Horizontal section
for depth z = 0.10 ft)

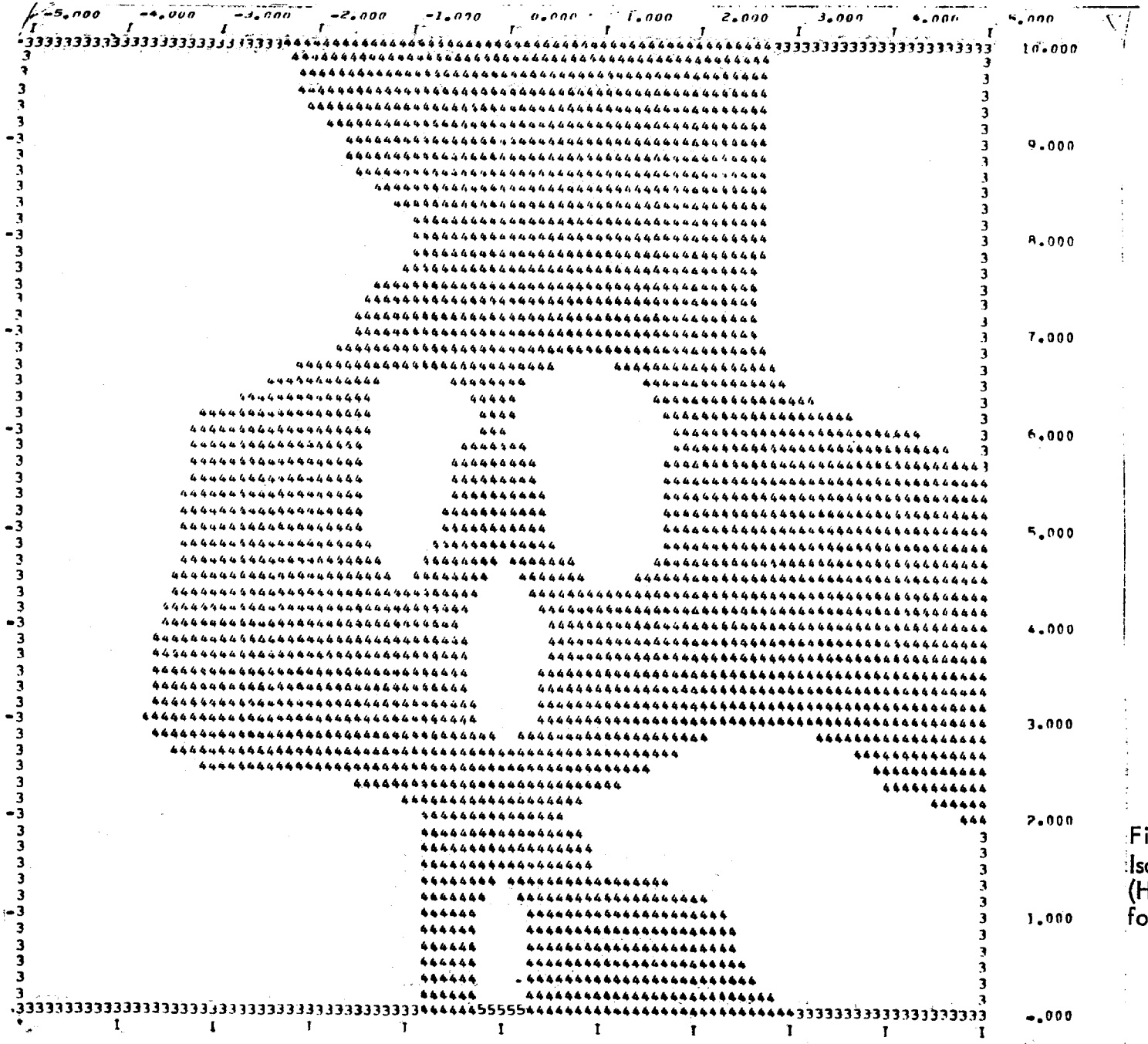


Fig. 31ℓ - Isotherms for Run 216 (Horizontal section for depth z = 0.14 ft)

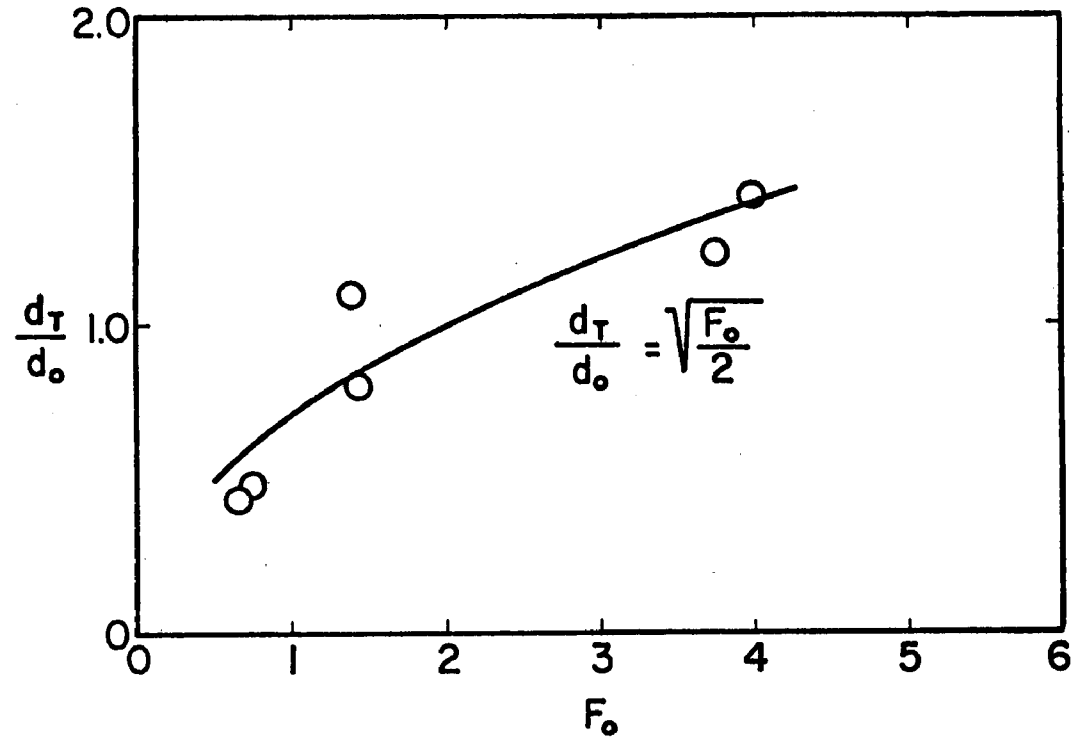


Fig. 32 - Depth of Penetration $d_T$ of Heated Water Surface Jet as derived from Isotherm Patterns

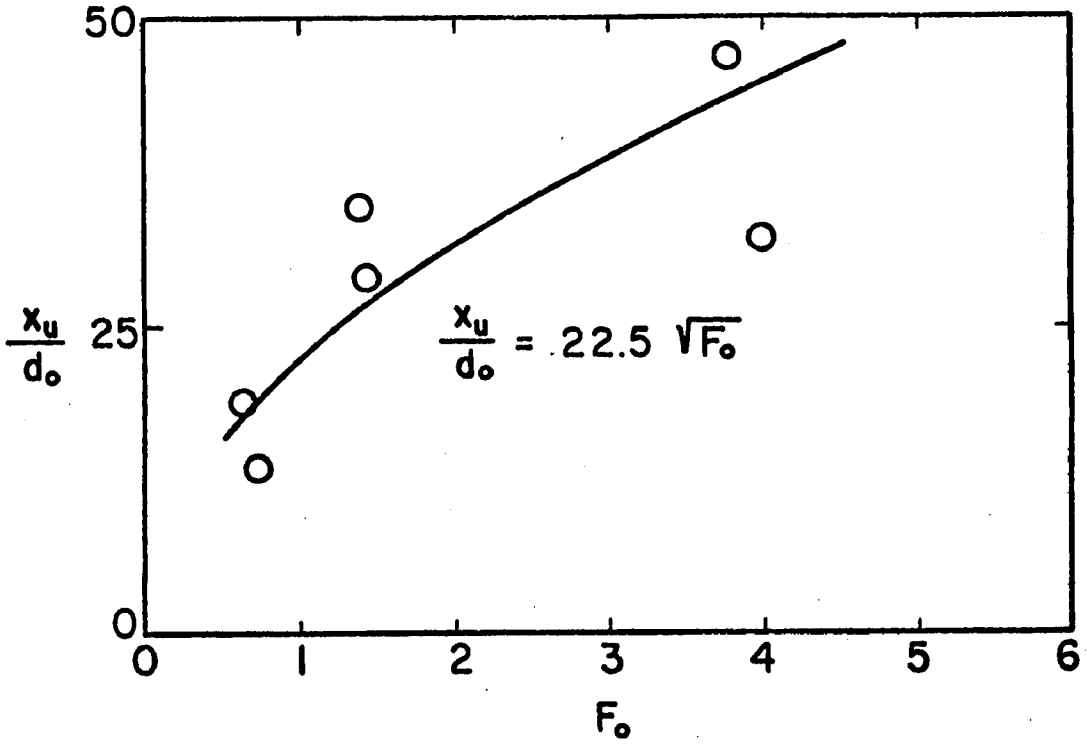


Fig. 34 - Length $x_T$ of Identifiable Jet Type Flow as derived from Velocity-Concentration Patterns

with $0.7 < F_o < 4.0$. The depth $d_m$ can be considered a measure of the depth to which the outlet (jet) flow penetrates into the ambient water.

The second observation pertains to the temperatures in the water surrounding the surface jet pattern. The ambient surface temperatures are not those of the cold water, but have some intermediate value. The heated water is discharged into a tank with an unintended existing (weak) temperature stratification which has been produced by flow conditions established through the boundaries of the tank and by the heat loss from the tank surface to the atmosphere. The tank had an overflow weir placed at the downstream end and vertical walls on either side. In the absence of any currents in a prototype a similar situation can exist.

A third observation regards the shape of the plume as shown by the isotherm patterns. The near surface patterns ($z = 0.01$ ft) generally consist of a very nearly uniform flow over a short distance (one foot) beyond the outlet followed by a gradual lateral expansion. The angle of lateral spread can be seen to depend somewhat on the outlet densimetric Froude number.

A fourth observation regards the randomness in the temperature distribution patterns. From a theoretical point of view all temperature distributions should be symmetrical with reference to the centerline of the tank. But except for a small area near the outlet, measurements do not show such perfect symmetry, because the tank is not a perfectly quiescent pool. The low-velocity inflow of cold water at the bottom of the tank, the free surface flow over the weir at the end of the tank, and the pair of very large and very slow eddies forming frequently on either side of the outlet all contributed to some very slow and barely detectable flow patterns on which the heated water jet flow and the free shear turbulence associated with it were superimposed. Near the outlet the jet mechanism was dominant, but at larger distance from the outlet more randomness in the patterns became clearly apparent. This investigation dealt only with the buoyant jet-type flow mechanism near the outlet and did not cover anything beyond. Motion of the ambient fluid exists in any bounded experimental tank with throughflow. The relevance of measurements very far downstream from the outlet must therefore be questioned.

Prototype plumes also break up into complex velocity and temperature patterns, usually by passive diffusion in currents. Wind frequently contributes to the disappearance of the typical plume patterns.

Spread of Iso-Velocity Concentrations -- Rather than temperature measurements, velocity measurements could be used to obtain maps similar to those of Fig. 31. Velocity components in the x-direction (u-component) were used for that purpose. Local measurements were reduced to dimensionless velocity concentrations using the average discharge velocity as a reference value. Thus velocity concentrations are defined as $u(x,y,z)/U_o$, where $U_o = Q_o/(w_o d_o)$. Figure 33 shows

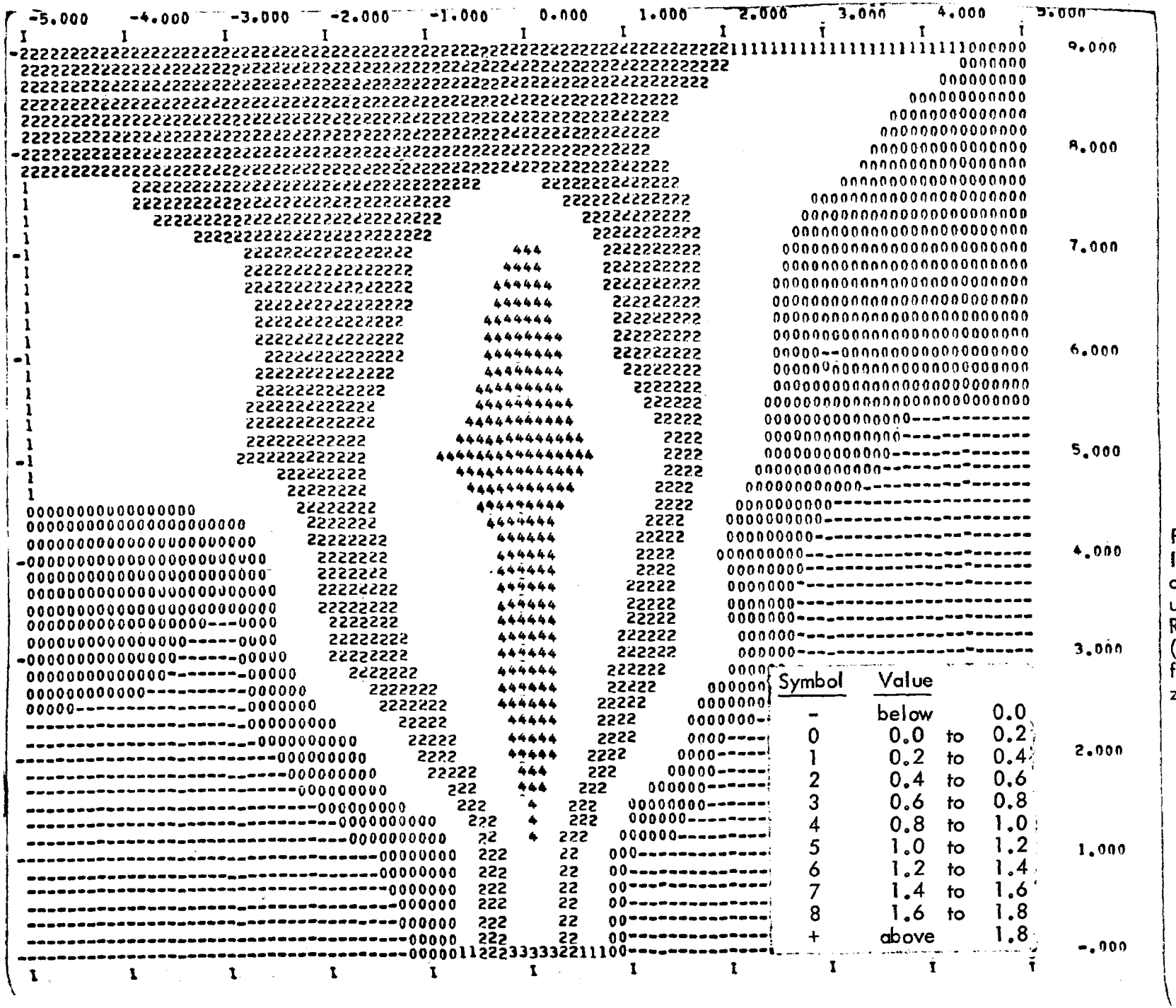


Fig. 33a - Iso-velocity concentrations of u-component for Run 207 (horizontal section for depth z = 0.01 ft)

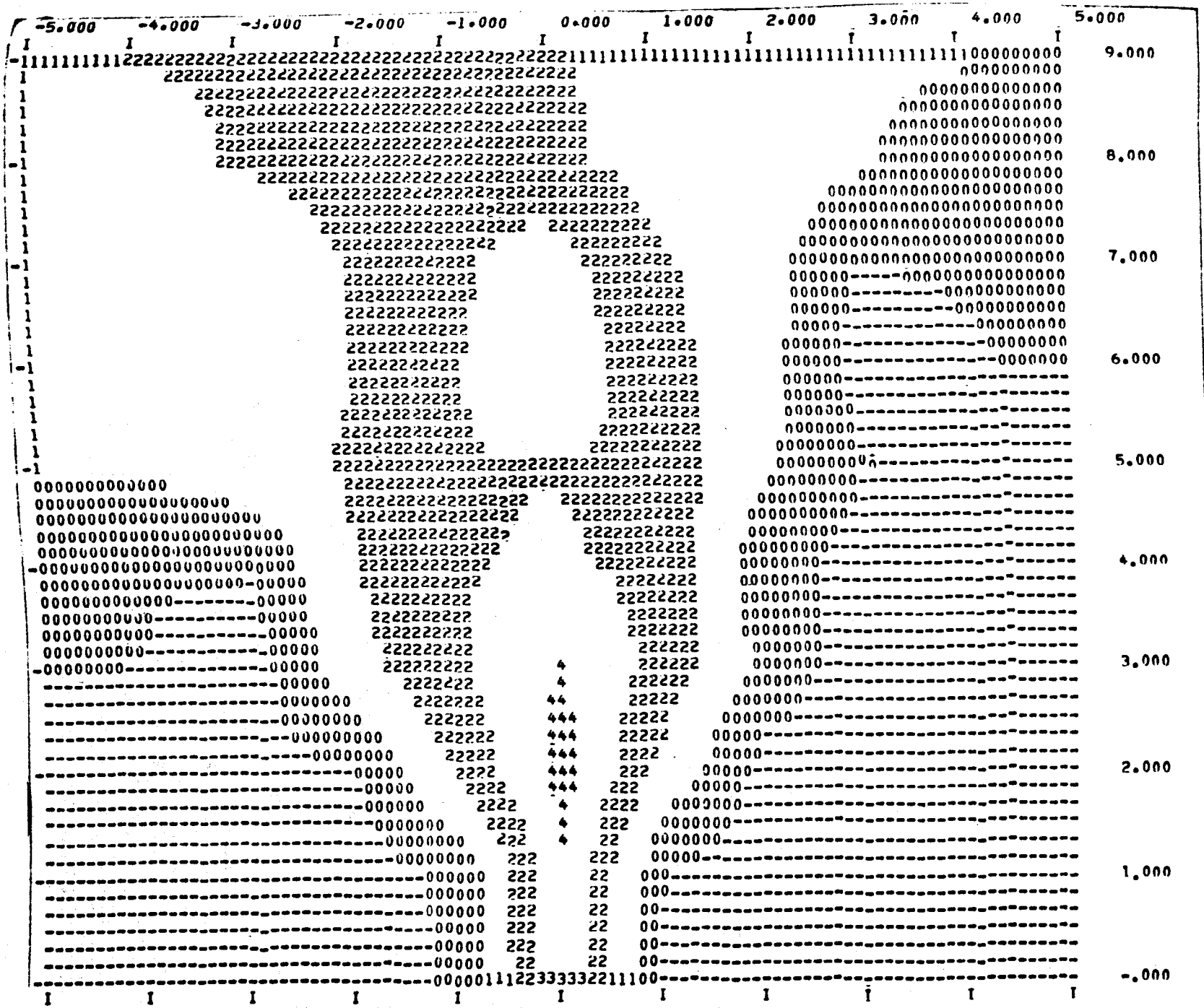


Fig. 33b - Iso-velocity concentrations of u-component for Run 207 (horizontal section for depth z = 0.03 ft)

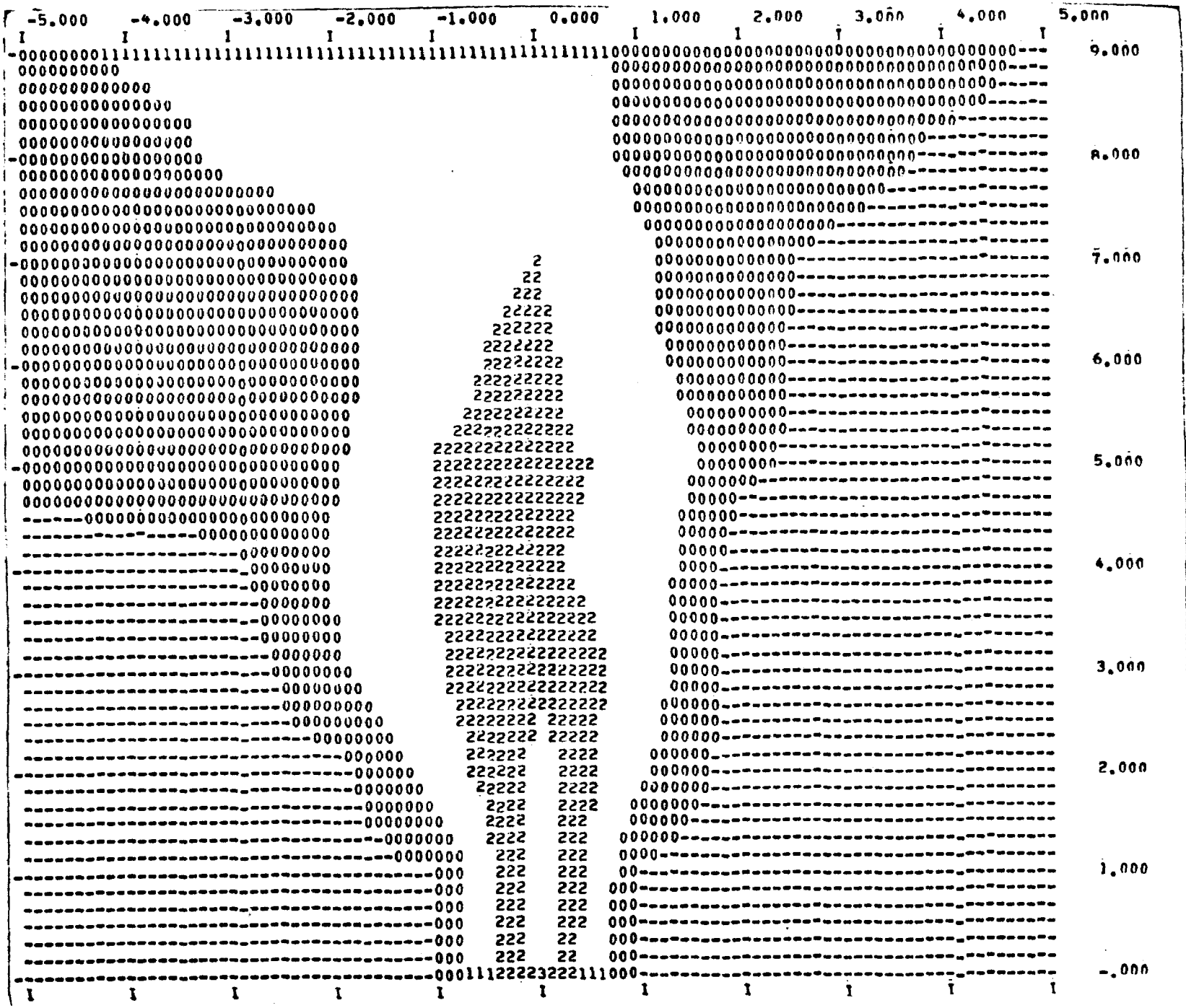




Fig. 33c - Iso-velocity concentrations of u-component for Run 207 (horizontal section for depth z = 0.07 ft)

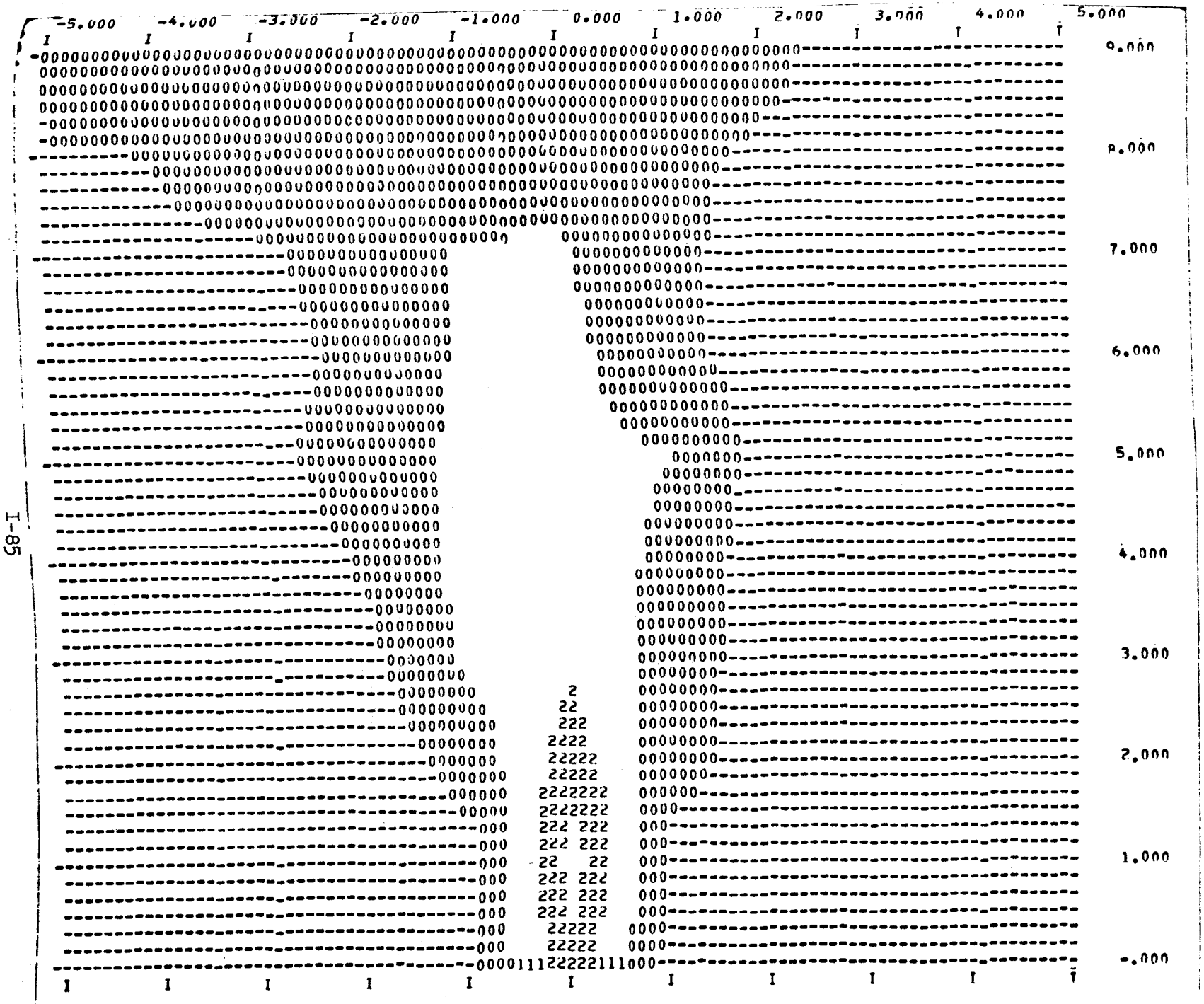


Fig. 33d - Iso-velocity concentrations of u-component for Run 207 (horizontal section for depth z = 0.10 ft)

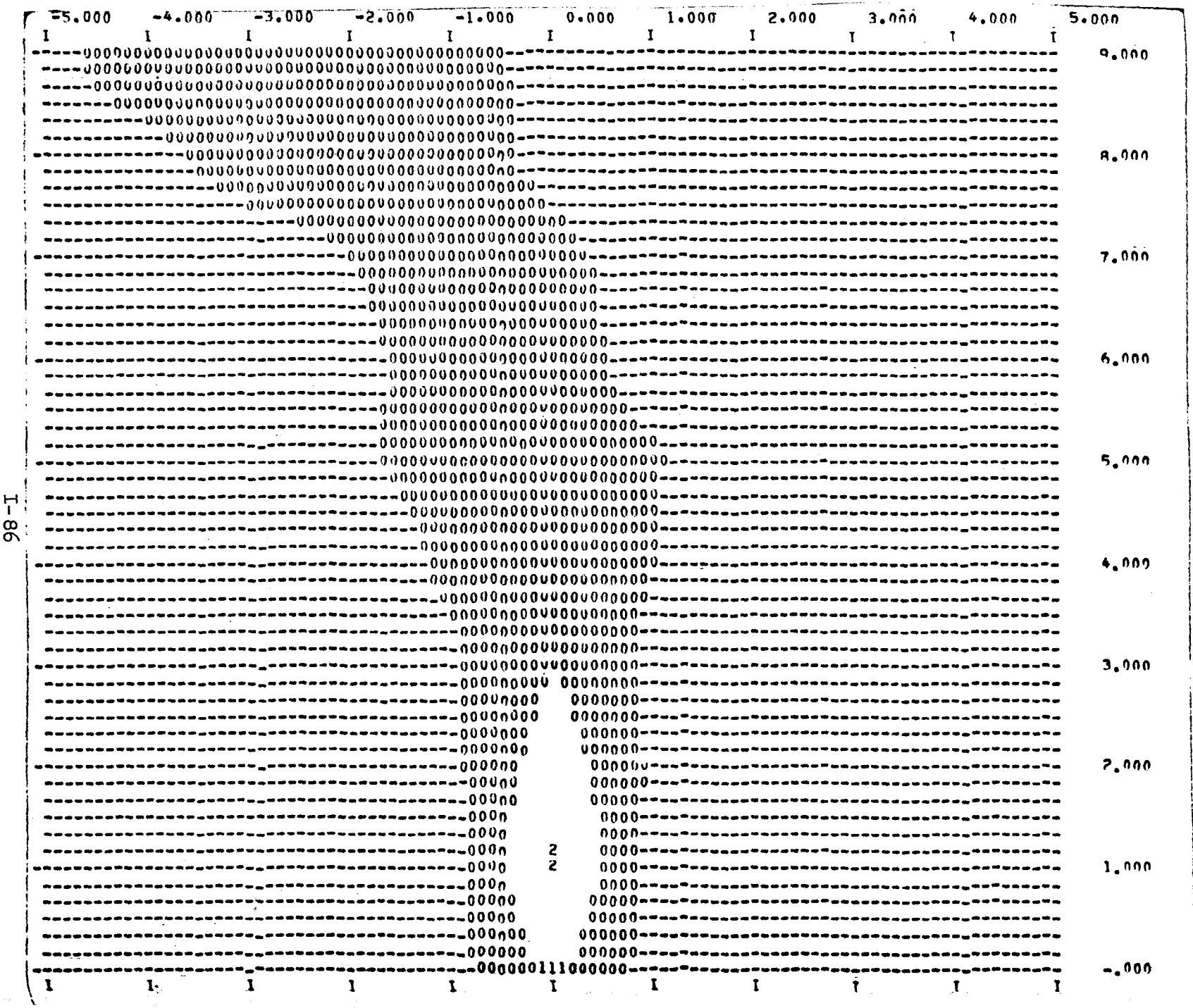




Fig. 33e - Iso-velocity concentrations of u-component for Run 207 (horizontal section for depth z = 0.14 ft)

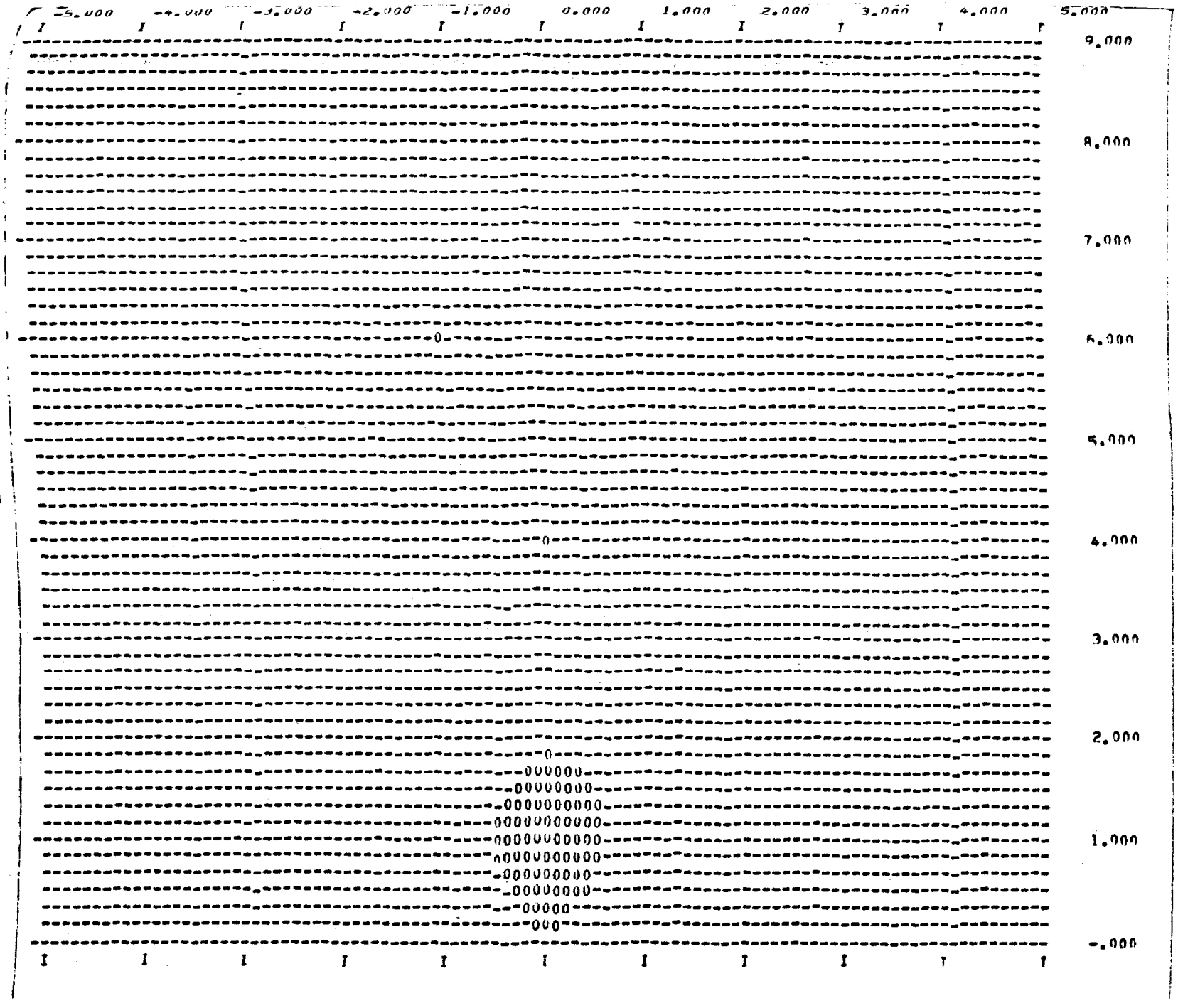


Fig. 33f - Iso-velocity concentrations of u-component for Run 207 (horizontal section for depth z = 0.20 ft)

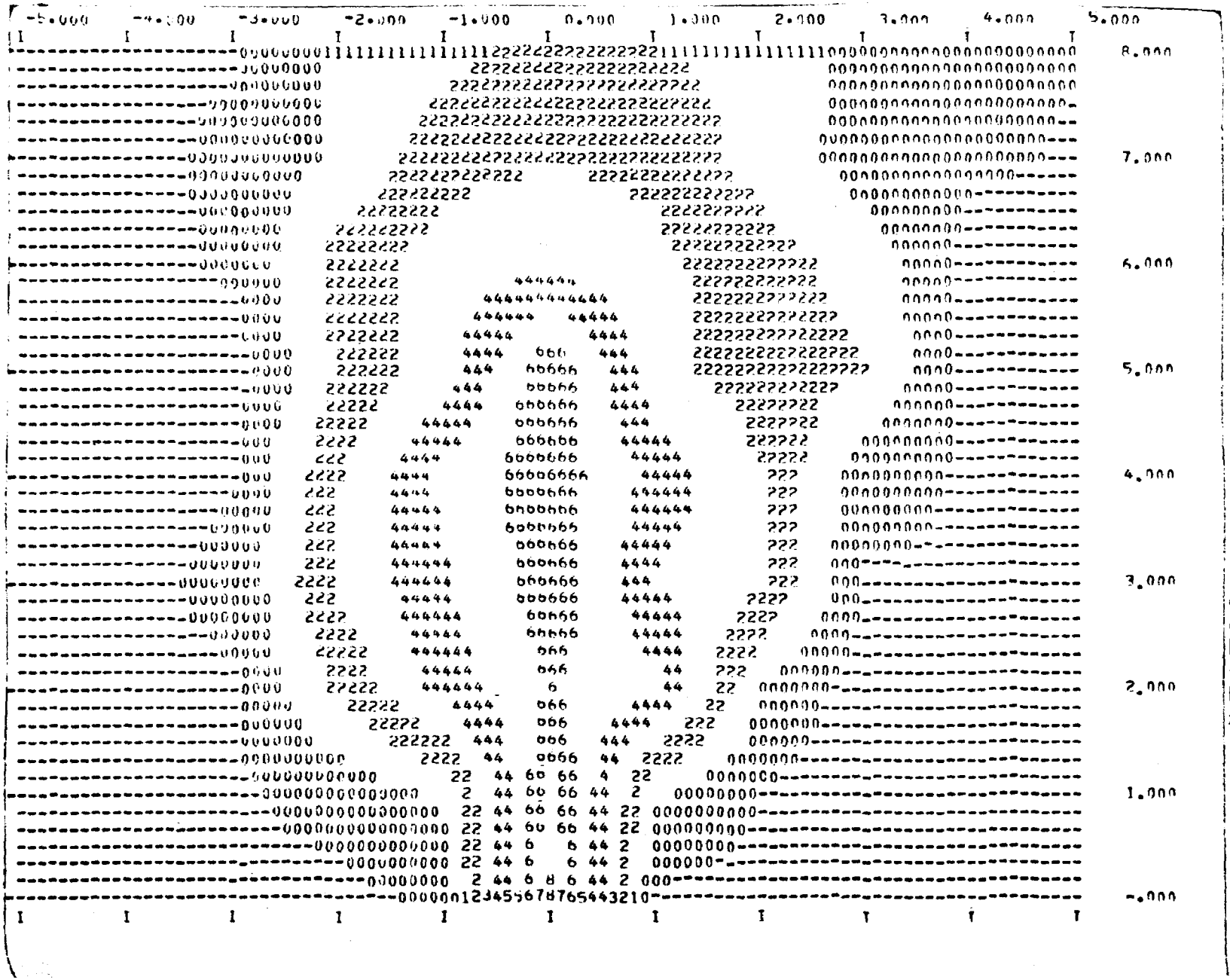


Fig. 33g - Iso-velocity concentrations of u-component for Run 215 (horizontal section for depth z = 0.01 ft)

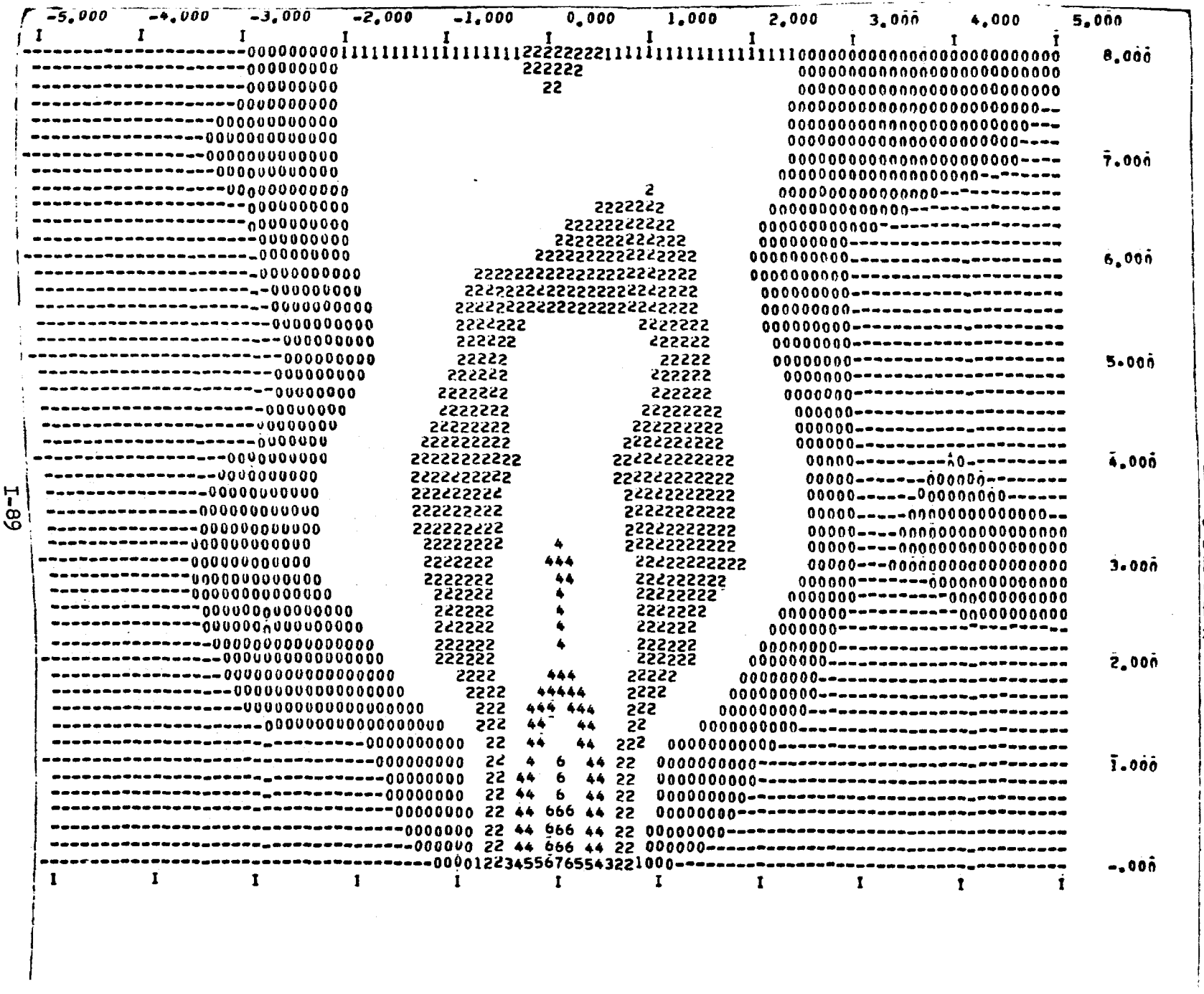


Fig. 33h - Iso-velocity concentrations of u-component for Run 215 (horizontal sectic for depth z = 0.03 ft)

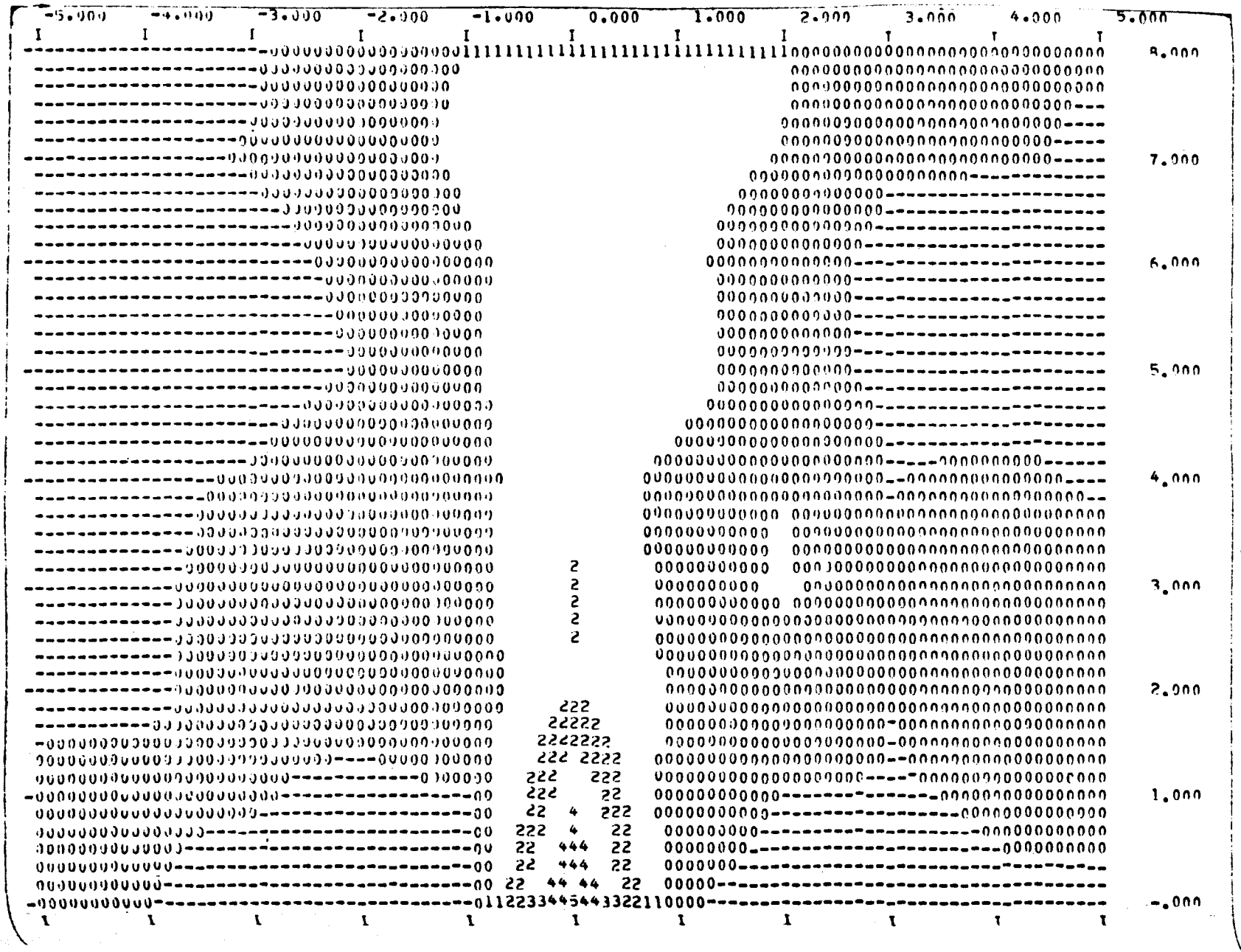


Fig. 33i - Iso-velocity concentrations of u-component for Run 215 (horizontal section for depth z = 0.05 ft)

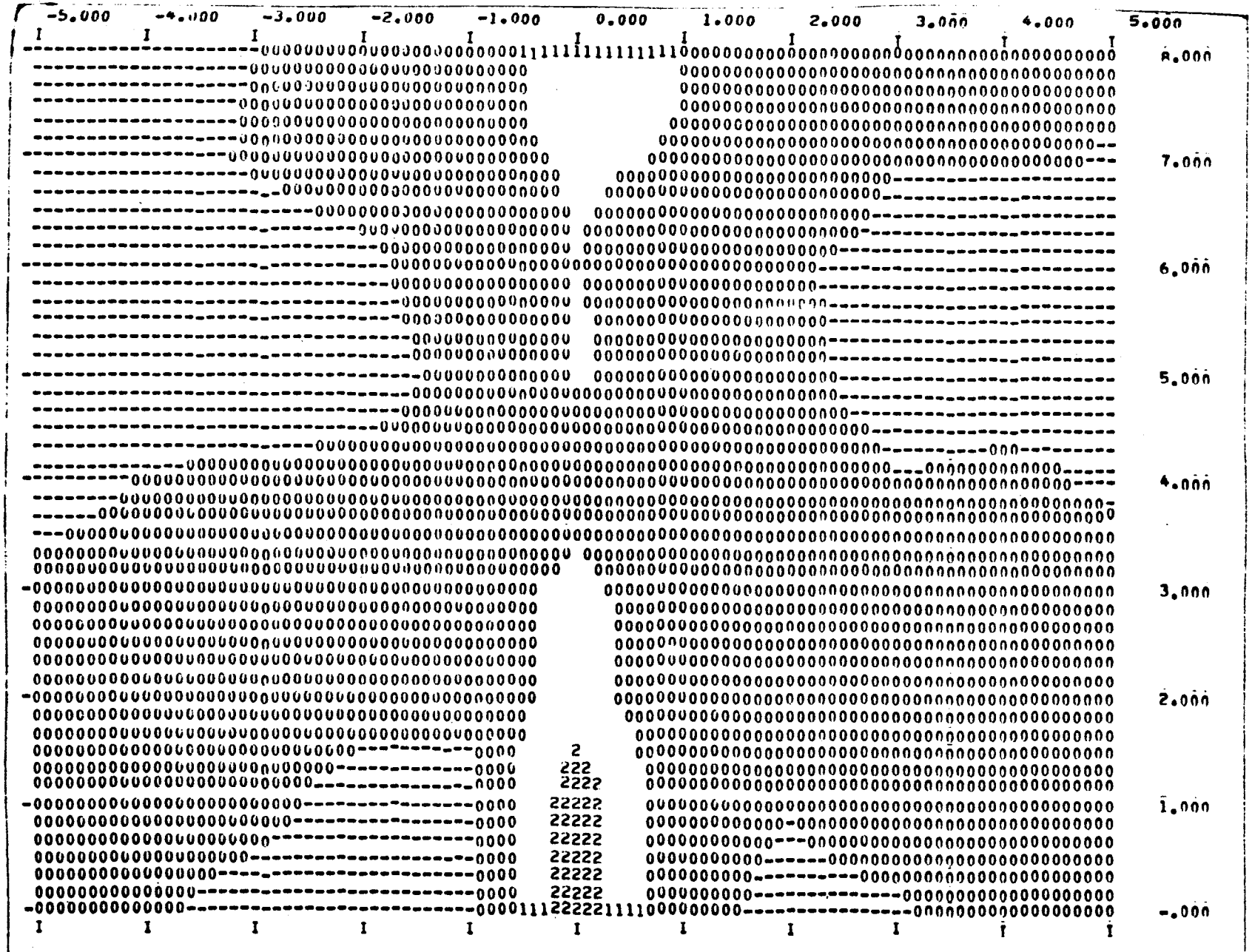


Fig. 33j - Iso-velocity concentrations of u-component for Run 215 (horizontal section for depth z = 0.07 ft)

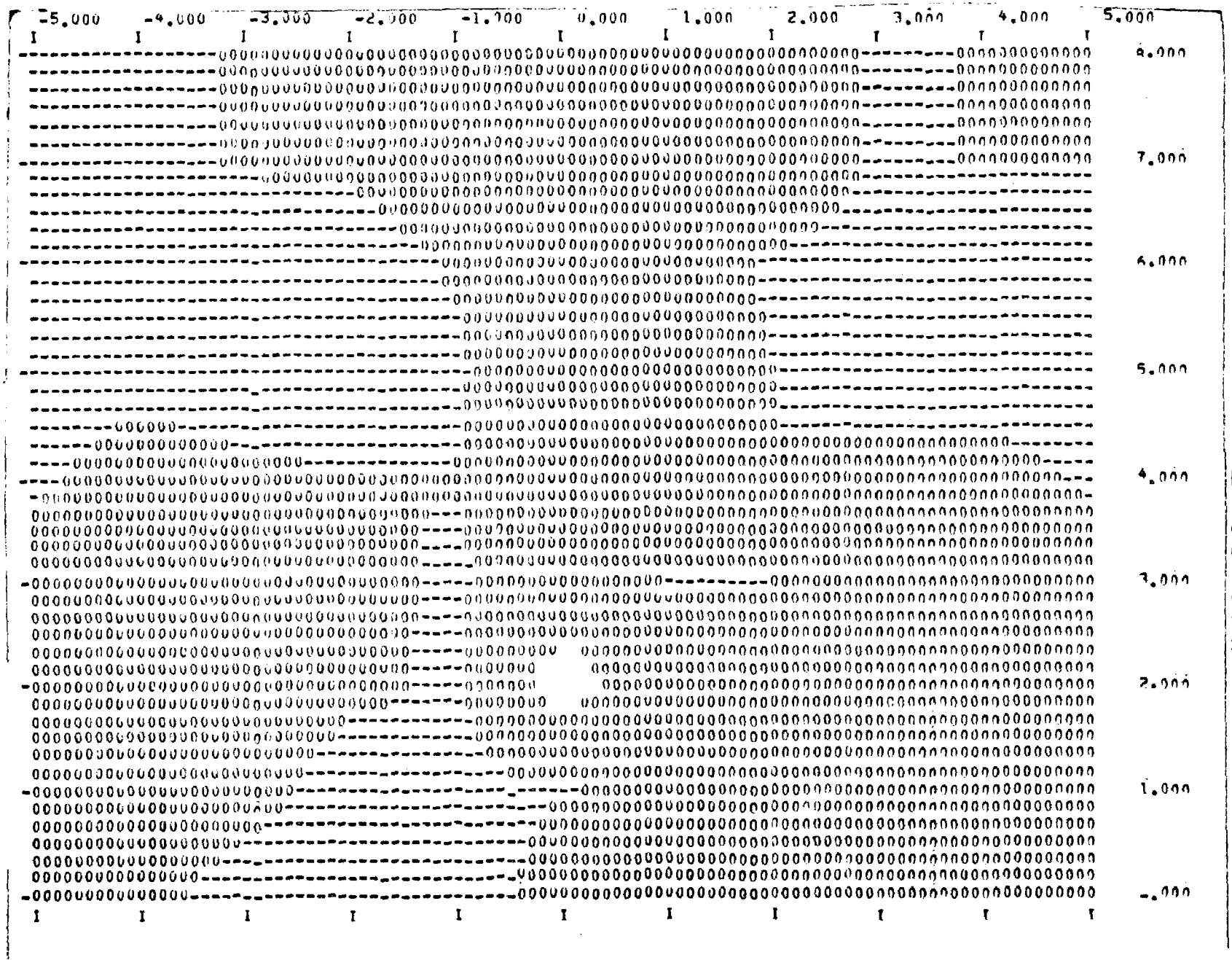


Fig. 33k - Iso-velocity concentrations of u-component for Run 215 (horizontal section for depth z = 0.10 ft)

velocity concentrations plotted by CONTOUR for horizontal planes. Again the discharge is at the bottom center of each figure and flow is from the bottom to the top. The symbol table in Fig. 33a gives the significance of each printed number.

The spreading patterns described by iso-velocity-concentration lines are quite similar to those found for iso-temperature concentrations. The following observations can be made:

> Near the outlet the surface jet is surrounded by a flow field with negative velocity. These velocities are part of a large eddy which forms on either side of the warm water jet. Lateral spread appears to depend on outlet densimetric Froude numbers. Smaller numbers are associated with faster spread.
>
> The horizontal shear stresses which the jet exerts on the underlying temperature-stratified fluid appear to produce a sort of low-amplitude standing wave pattern at certain depths. The phenomenon was also apparent in some of the temperature concentration patterns shown in Fig. 31. The distance $x_u$ over which the velocity distribution could be clearly identified as a jet-type flow was estimated and graphed versus $F_o$ in Fig. 34. The results are approximated by the relationship

$$\frac{x_u}{d_o} = 22.5 \sqrt{F_o} \tag{61}$$

> Although the measurements leading to Figs. 32 and 34 are only very crude estimates, it is worthwhile to note that the depth of penetration did not exceed two times the outlet depth and the spreading jet-type flow patterns persisted only over a relatively short distance of fifty times the outlet depth or less.

Iso-velocity concentrations have also been plotted in vertical cross sections perpendicular to the main axis of the experimental tank. Again only u-components of velocities were used. Examples are given in Fig. 35. The profiles show quite nicely the decrease in depth and the lateral spreading of the surface jet with distance. The shape of the profiles justifies Eq. (1).

A velocity concentration map for a vertical section through the main trajectory is given in Fig. 36. Flow is from left to right and distances are given in feet. The stratification is quite apparent.

To obtain velocity concentrations it is necessary to reduce each measurement by a reference velocity. The average discharge velocity at the outlet was chosen as such a value. The resulting concentration

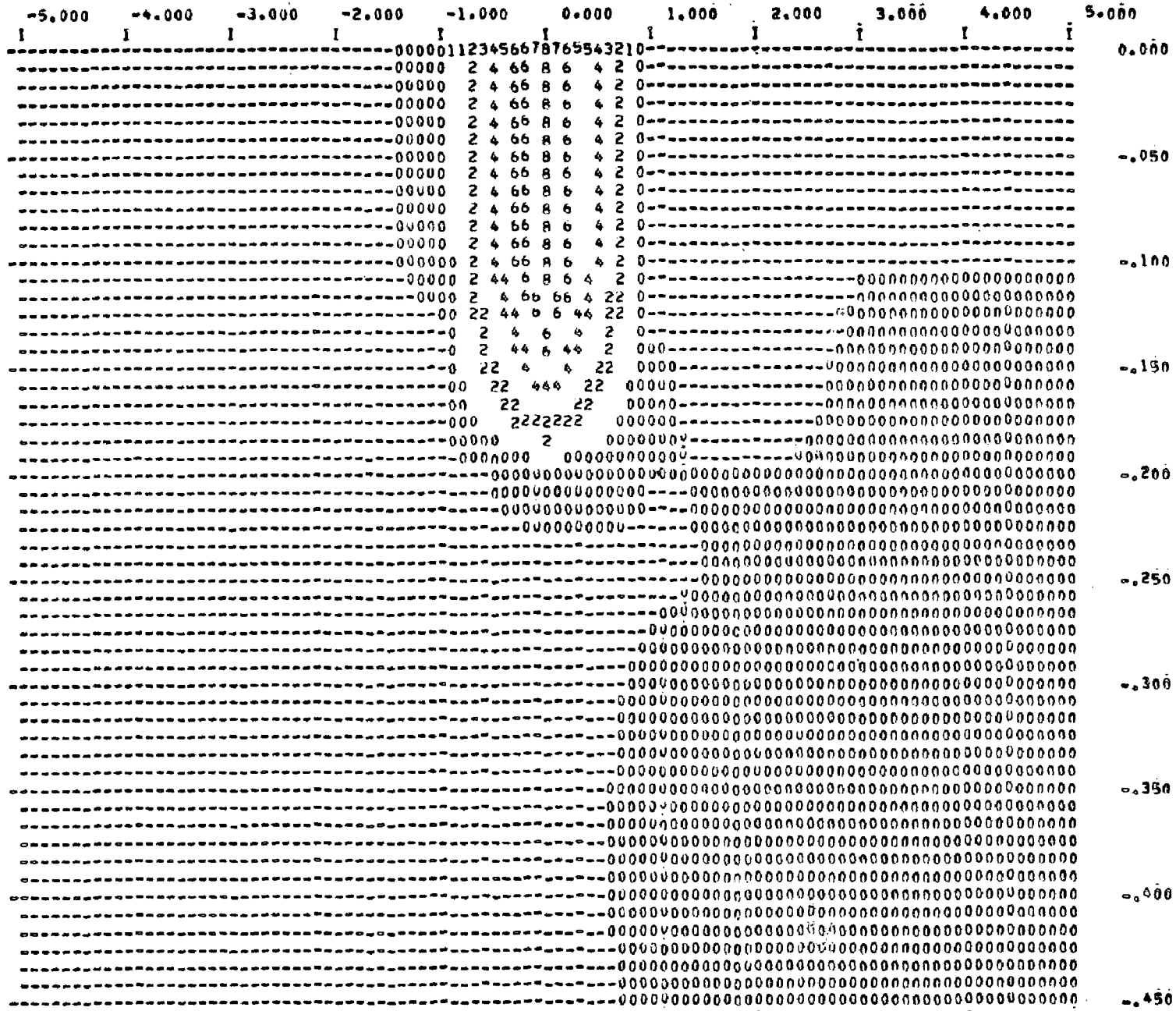


Fig. 35a - Iso-velocity concentrations for Run 215. (Vertical section at x = .5 ft)


Fig. 35b - Iso-velocity concentrations for Run 215. (Vertical section at x = 1.5 ft)

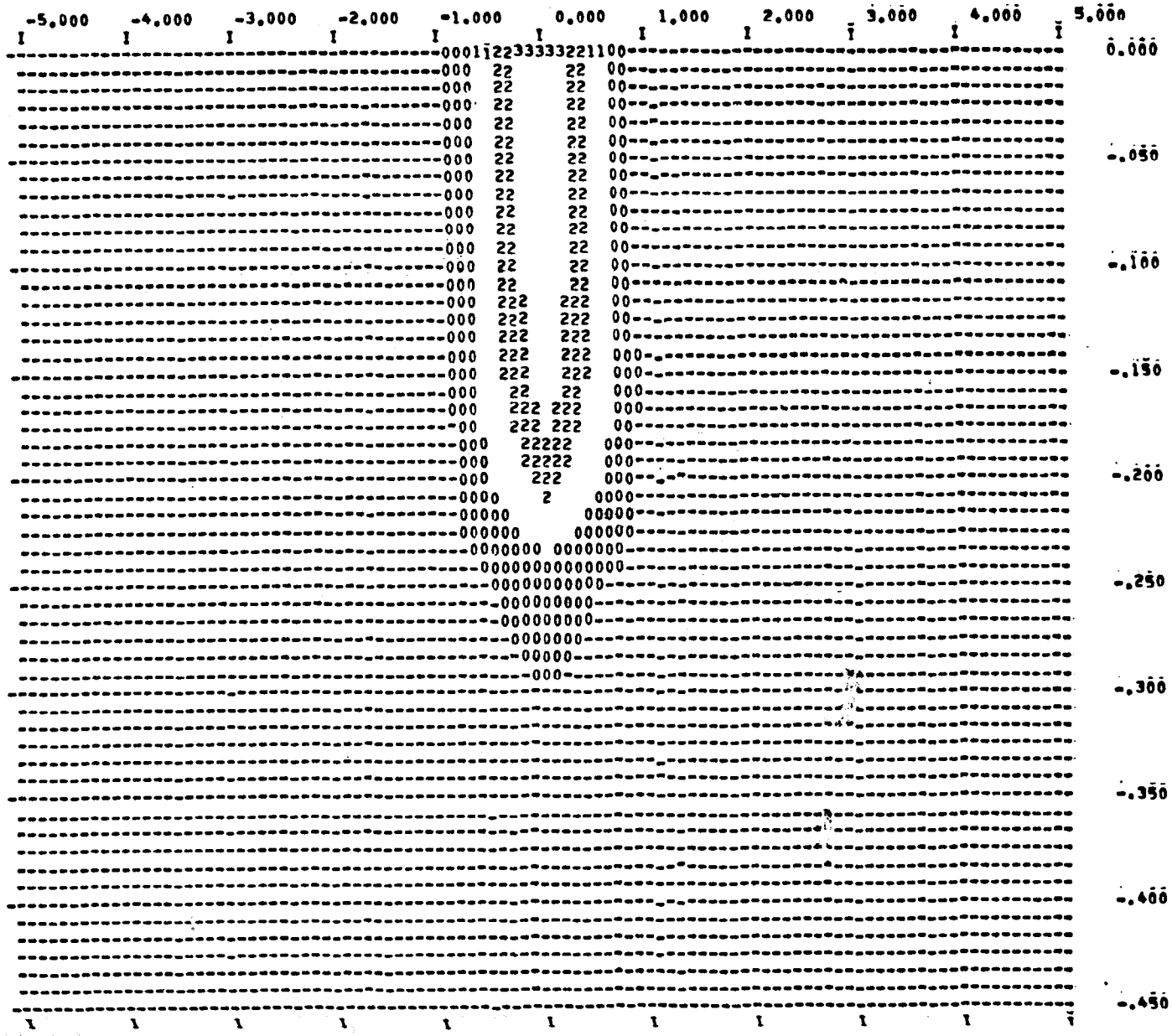




Fig. 35c - Iso-velocity concentrations for Run 207. (Vertical section for x = 0.5 ft)

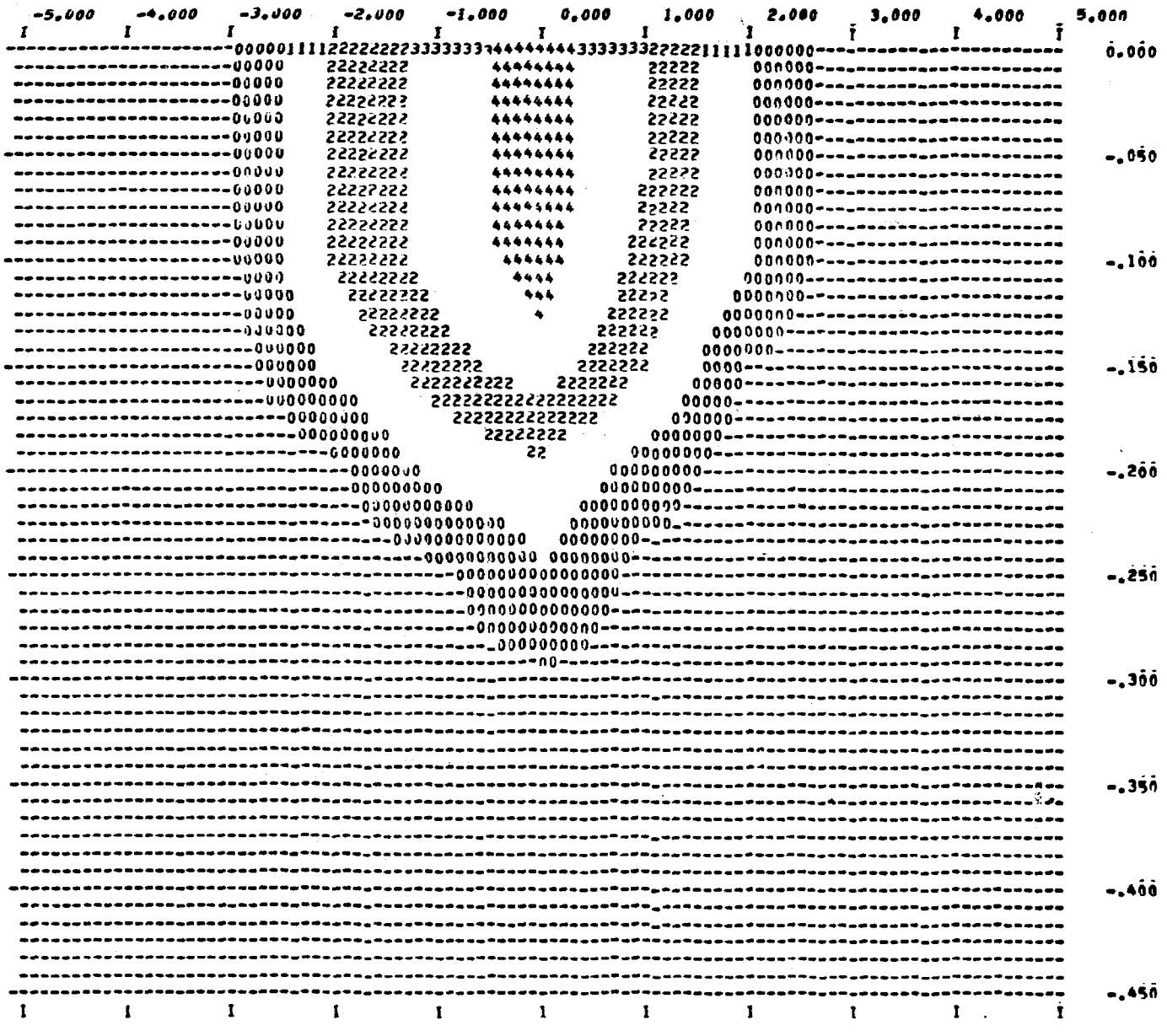




Fig. 35d - Iso-velocity concentrations for Run 207. (Vertical section for x = 3.0 ft)

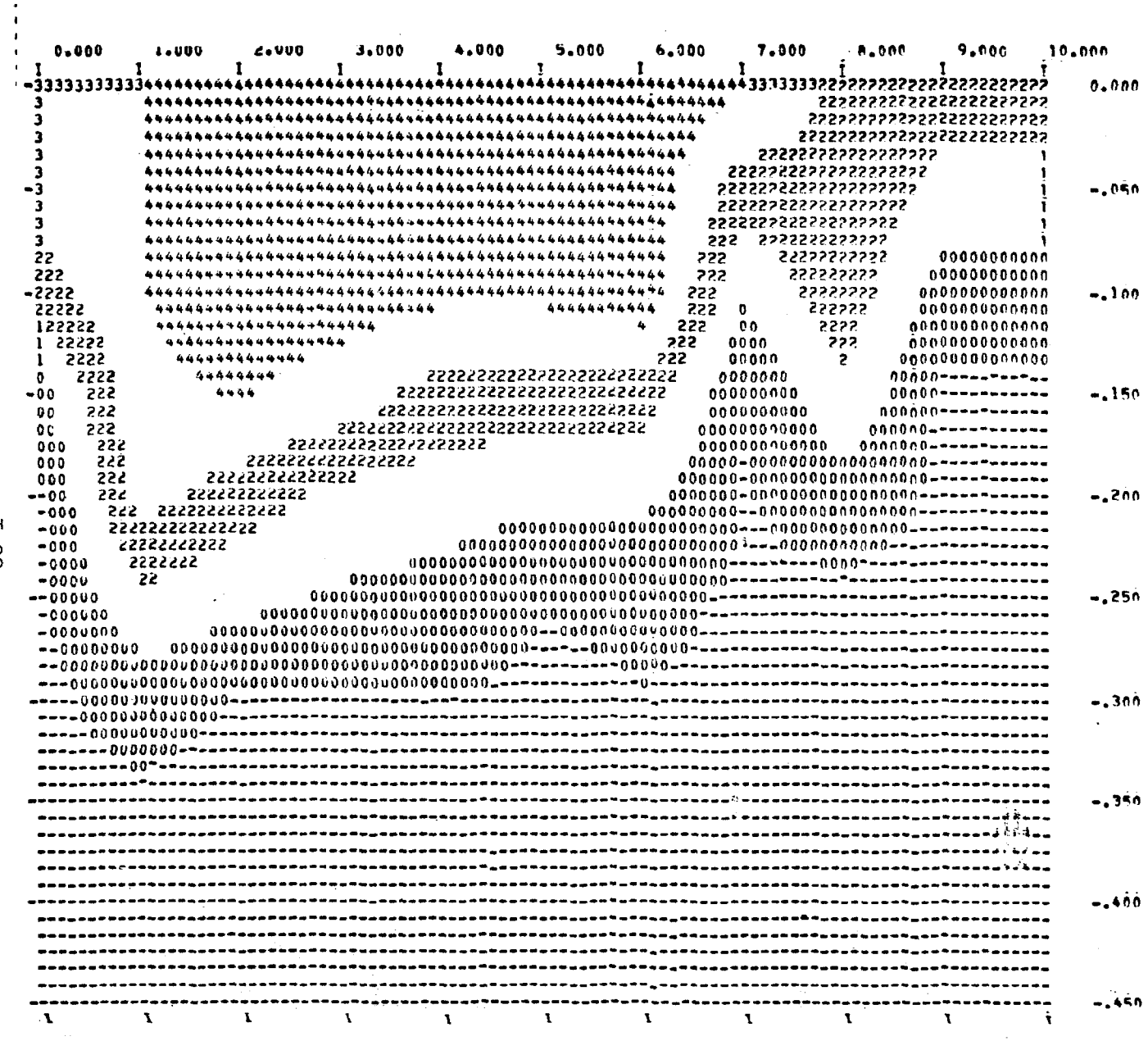


Fig. 36 - Iso-velocity concentrations for Run 207. (Vertical section for y = 0)

values show the velocity decay with distance from the outlet quite well. To illustrate the actual spread of the plume it is helpful to reduce all velocity data with the velocity on the main trajectory as a reference value. Such velocity concentrations then are equal to $u(x,y,z)/u(x,0,0)$. Plots obtained with these concentrations for zero depth were used to find the horizontal standard deviations $b(x)$ by locating the points at which $u(x,b,0)/u(x,0,0) = 0.606$. The results are plotted for three tests in Fig. 37, and a comparison with values predicted by the analytical model is given.

Visual Spread Angles -- In the previous sections the vertical and horizontal spreading of the surface plume were defined quantitatively in terms of spread velocities or the change in standard deviations for temperature and velocity profiles with distance. It is also possible to use visual contours of the buoyant surface jet to measure spread. To define the contour one must use a tracer in the experiment as described in Ref. [53]. Figure 38 is an example of a visual spreading record near the outlet obtained using floating particles and time-exposure photography. More examples can be found in Ref. [53]. The total width of the surface plume measured perpendicular to the main trajectory can easily be recorded as a function of distance from the outlet.

If the shapes of the velocity and temperature distributions in vertical cross sections are approximated by normal distributions such as are specified in Eqs. (1) and (2), the spread of the contour and the spread measured by standard deviations are correlated. If the contour represents a line of iso-velocity concentration of magnitude $k$, the lateral contour spread at the surface $dr_c/ds$ or $dy_c/dx$ is

$$\frac{dy_c}{dx} = \frac{db}{dx}\left[\ell n \frac{1}{k^2}\right]^{1/2} \tag{62}$$

where $db/dx$ is the standard deviation spread. Contour spreads were measured on plots of visual tracers. However, they are difficult to use because it is uncertain how small a value of $k$ should be used to describe the contour of the plume. Therefore visual records of tracers, isotherms, and iso-velocity concentrations were used only to find the initial angle of spread. The tangents drawn to the contours of available surface spreading records define a horizontal spreading angle $\phi_o$ as shown in Fig. 39. This angle was measured on available records in Ref. [53]. Part of the scatter is due to the fact that the experimental tank into which the water was discharged was partially temperature stratified. The spread of the jet will depend on that stratification, and an additional parameter is needed to take it into consideration. Considering largely the velocity data, a very approximate relationship between the outlet spreading angle and the outlet densimetric Froude number appears to be

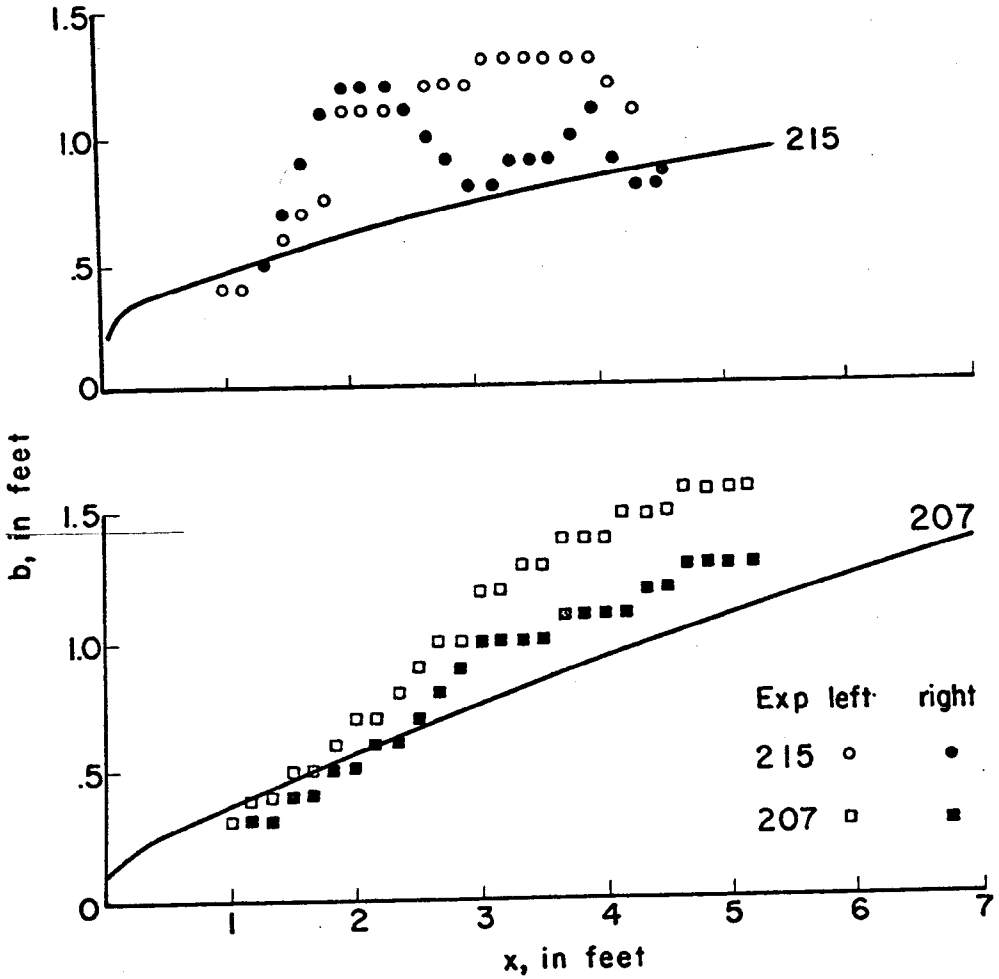


Fig. 37 - Lateral Spread of Heated Water Jet on Water Surface as Illustrated by Values of Standard Deviations b(x) plotted against Distance x from point of Discharge. Analytical Model Predictions (solid lines) and Experimental Data (dotted lines)

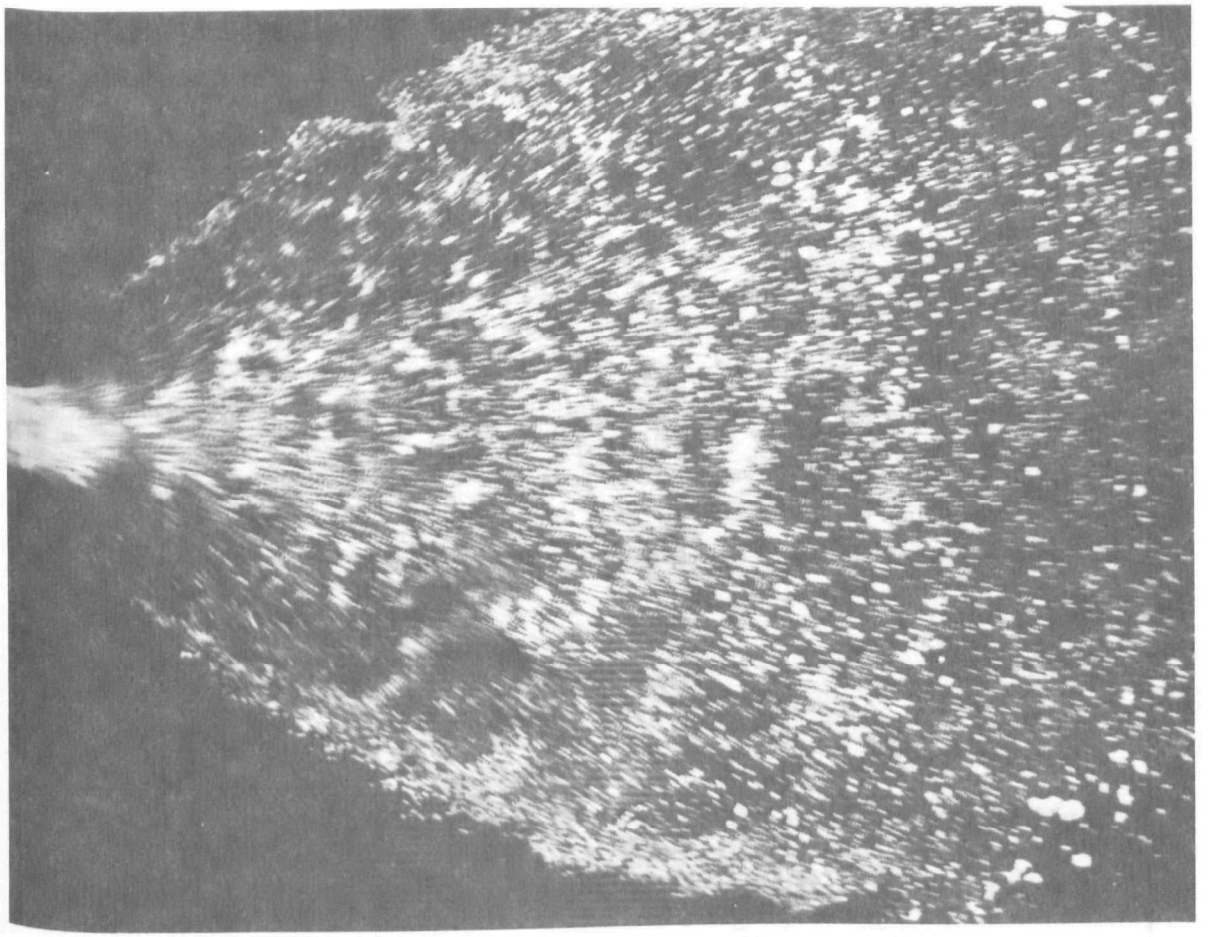

Fig. 38 - Visual Surface Spreading Pattern (Time Exposure of Tracer Particles)

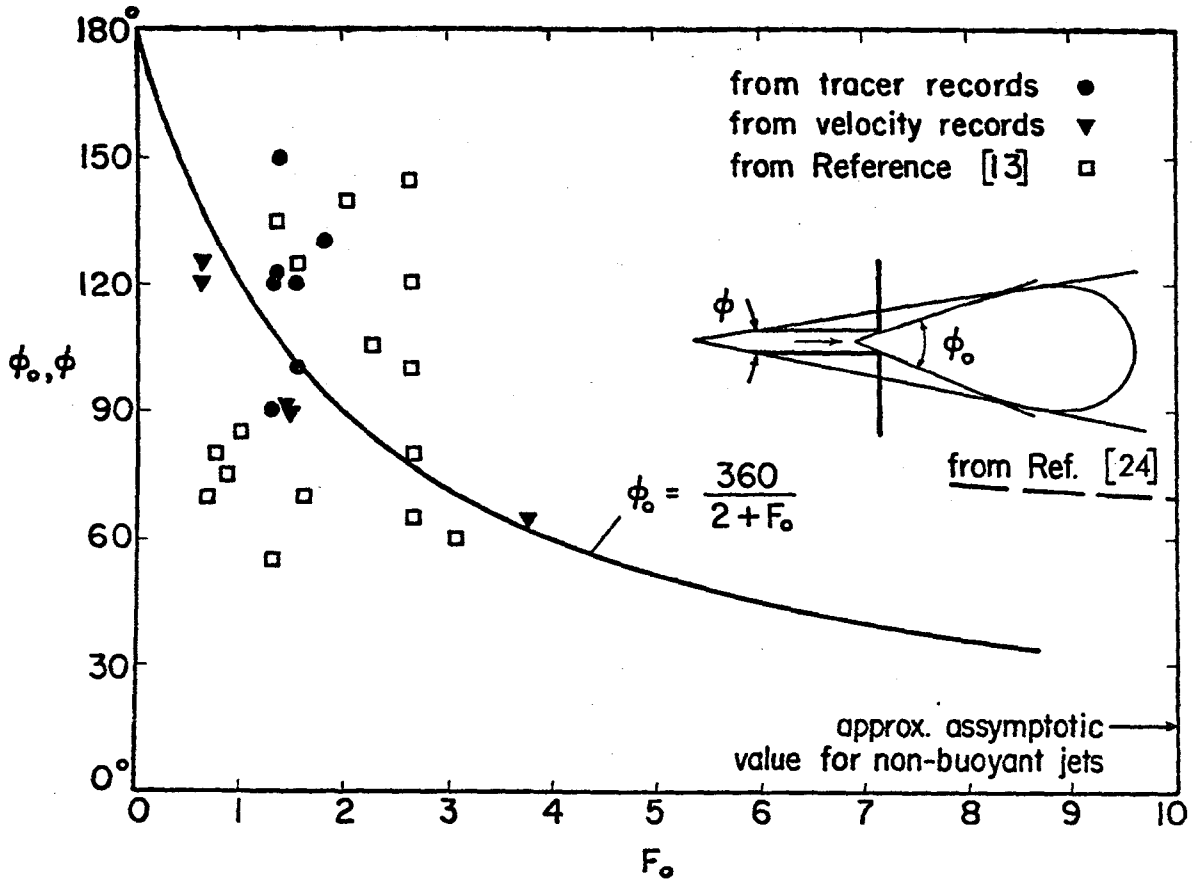


Fig. 39 - Visual Surface Spreading Angle $\phi_o$ of Heated Water Surface Jet. Experimental Data

$$\phi_o = \frac{360^o}{2.5 + F_o} \tag{63}$$

where $\phi_o$ is given in degrees. The data were converted from contour spread values using the simple relationship

$$\phi_o = 2 \arctan\left(\frac{dy_c}{dx}\right) \tag{64}$$

The present data and also those taken from another source show a great deal of scatter, the source of which is believed to be an existing stratification in the tank which was not given sufficient attention. The buoyancy experienced by a jet discharged into a tank will be strongly influenced by an existing temperature stratification.

The same data were also plotted on $\tan \phi_o/2$ versus $1/F_o$ in Fig. 40, and again considerable scatter was obtained. The velocity data appear to fit a straight line with the description

$$\left(\frac{dy_c}{dx}\right)_0 = \frac{c_7}{F_o} + 0.15 \quad \text{for} \quad F_o > 1.0 \tag{65}$$

The boundary or contour of a surface plume was previously estimated to be $y_c \backsimeq mb$, with $m \backsimeq 3$. Thus

$$\left(\frac{dy_c}{dx}\right)_0 = \left(\frac{db}{dx}\right)_0 = \frac{c_7}{3.0}\frac{1}{F_o} + 0.05 \tag{66}$$

By comparison with Eq. (20) one finds that the second part of the right-hand side of the equation is approximately the turbulent spread and the first part is the buoyancy induced spread. By comparing with Eq. (18) it is found that

$$\frac{c_5}{c_6} = \frac{c_7}{3.0} \quad \text{or} \quad c_5 = e^{-0.5}\frac{c_7}{3.0} = \frac{c_7}{4.95} \tag{67}$$

Here $c_7$ is of the order of 1.25 to 2.5, and hence $c_5$ is of the order of from 0.25 to 0.50. These values agree reasonably well with the values found from the lateral velocities in one of the previous sections. A value of $c_5 = 0.40$ was used in the analytical model.

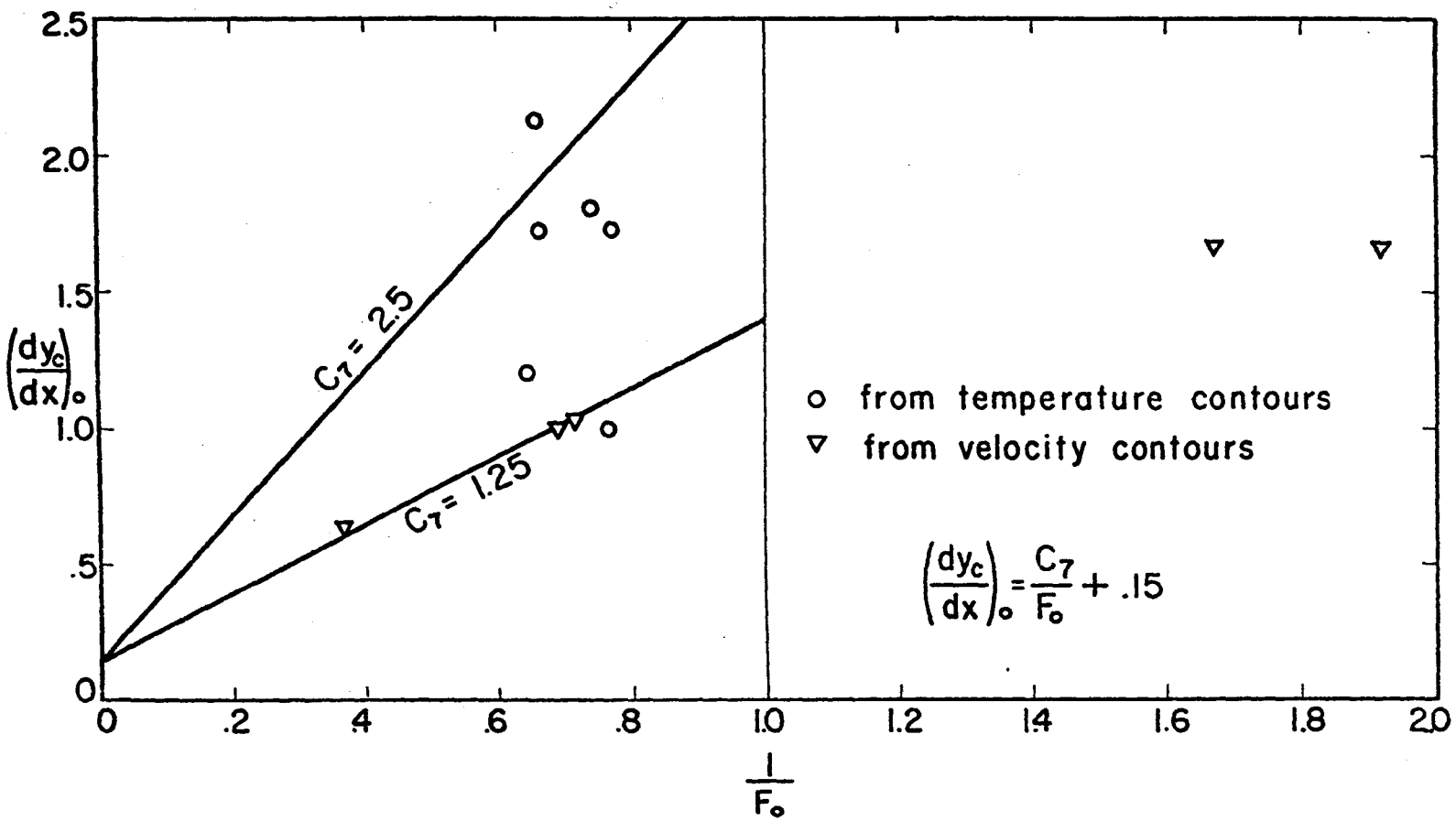


Fig. 40 - Surface Spreading of Visual Contour of Heated Water Surface Jet. Experimental Data

## Entrainment and Mixing near the Outlet

Volumetric Fluxes, Heat Fluxes, and Heat Contents -- The volumetric flux, the heat flux, and the heat content along the main trajectory (main axis of the tank) were calculated by integration of the measured velocity and temperature profiles in cross sections perpendicular to the axis of the tank. The theoretical values of the fluxes are given in Eqs. (5), (6), and (68) with the provision $x = s$, $y = r$.

$$C(x) = \varrho c_p \int_{-\infty}^{\infty} \int_{0}^{\infty} T^*(x,y,z)\, dxdy \tag{68}$$

The limits of integration were changed. Instead of an infinitely large cross section, a finite one defined as that area perpendicular to the main trajectory in which the u-velocity components were all positive was used. The integration was carried out in three steps: integration of individual profiles of velocity (or excess temperature or products of these) with respect to depth; multiplication of each result by distance between midpoints of adjacent profiles; and addition of several of these results for an individual cross section $x = \text{const}$. The results of all integrations were reduced to dimensionless form by using the corresponding outlet values for reference; e.g., $Q_o$ for volumetric flux, $\varrho Q_o c_p (T_o - T_c)$ for heat flux, and $d_o w_o (T_o - T_c)$ for heat content. The results referring to volumetric fluxes are plotted in Fig. 41 versus distances from the outlet.

Primarily because of the small number of vertical profiles measured in each cross section perpendicular to the x-axis, the experimental results show scatter. They show conclusively, however, that there is a substantial amount of entrainment of surrounding water by the heated water jet even if the vertical stratification is strong. Values predicted by the analytical model are also shown in Fig. 41. For further comparison, the theoretical distribution of volume flux for a semi-circular non-buoyant jet is also given. It appears that the measured entrainment was initially larger than that predicted for non-buoyant jets. This observation is quite reasonable considering that the experimental jet had a fully developed velocity distribution at the point of discharge, while the non-buoyant jet theory assumes that the discharge velocity is uniform. The actual zone of flow establishment is therefore much shorter in the experiments than in that theory. For the same reason the analytical model also predicts more initial entrainment than the non-buoyant jet theory. On the other hand, a fully developed non-buoyant circular jet has an entrainment characteristic equal to

$$\frac{Q}{Q_o} = \frac{x}{D_o} \tag{69}$$

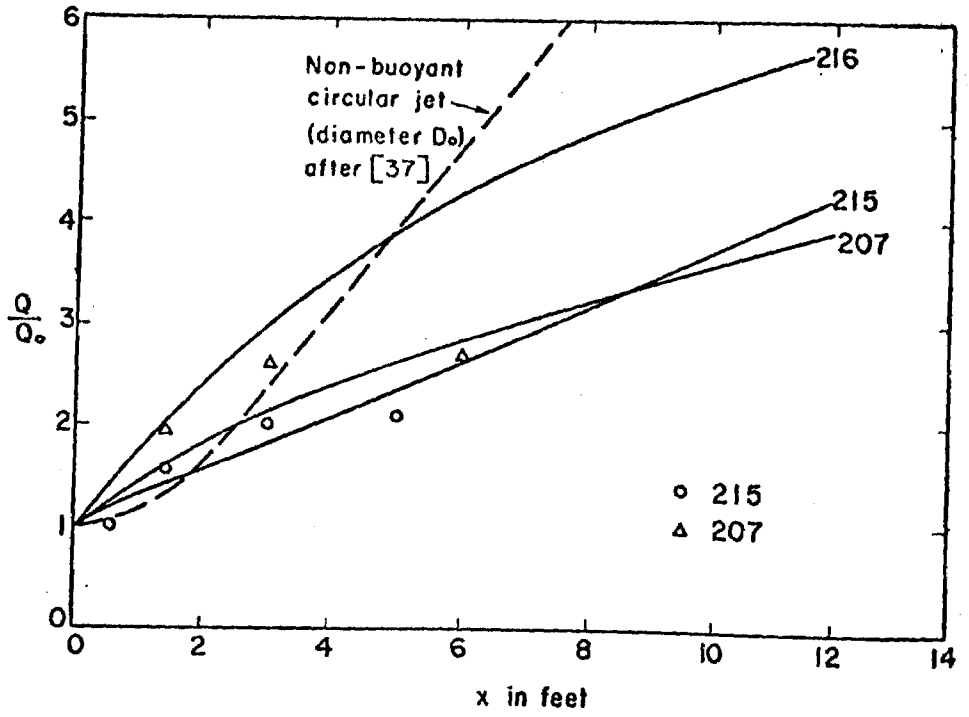


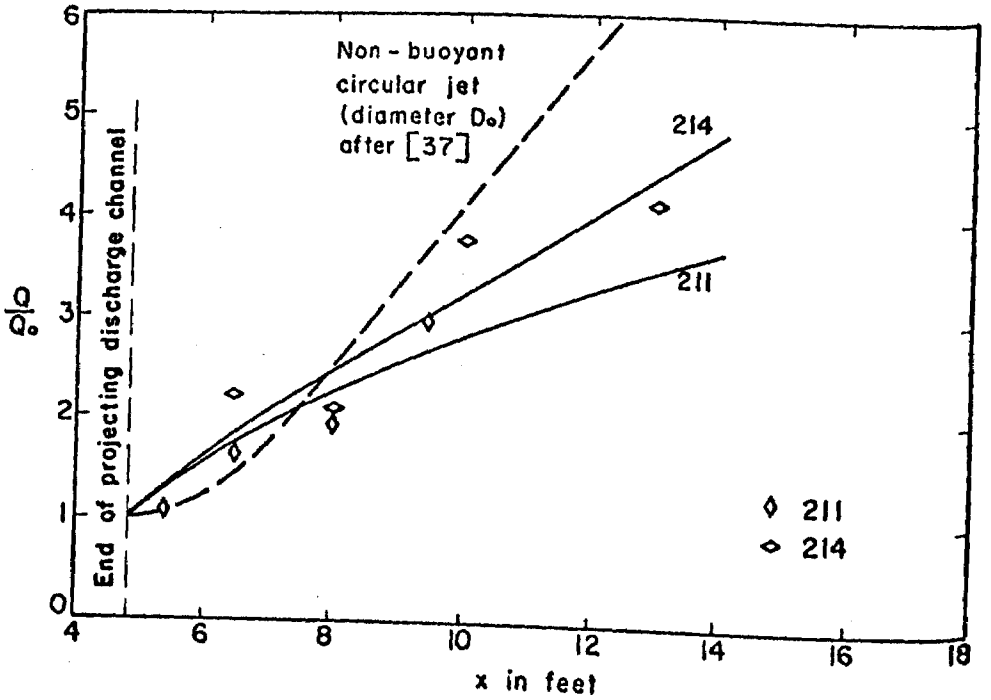


Fig. 41 - Total Volumetric Flow versus Distance from Source of Discharge

In the experiments reported $D_o = 0.4$, and the resulting relationship is shown in Fig. 41. It represents a limiting case of the analytical model ($F_o \longrightarrow \infty$) and is therefore tangent to the result for Exp. 216 ($F_o = 3.75$). It is also evident from Fig. 41 that buoyancy essentially reduces entrainment further downstream from the outlet. Differences in total flow rate between a non-buoyant and a buoyant jet become quite marked.

Heat fluxes, calculated and measured, show only small significant variations with distance. The experiments were carried out in an enclosed and fairly well insulated space. In steady state operation the rate of surface heat transfer was therefore small.

Entrainment and the resulting increase in flow rate as shown in Fig. 41 produce a substantial dilution of the heated effluent and hence a substantial temperature drop. Measured centerline water surface temperatures reported in Fig. 42 show this quite clearly. For comparison, computed temperatures are also shown. The fit between measurements and calculations is strikingly poor, and there are two good reasons for this: first, the failure to account for a zone of flow establishment and second, the stratification of the water in the receiving experimental tank.

It is believed that the length of the zone of flow establishment for velocity distributions is different from that for temperature distributions, because in the discharge cross section the velocity distribution is non-uniform, but the temperature distribution is uniform. The zone of flow establishment for temperature is therefore longer and of the order indicated in Ref. [37]. The zone of flow establishment for velocities is relatively short, if not negligible. The basic analytical model as described does not include a zone of flow establishment.

The second source of disagreement is the temperature stratification in the tank as illustrated by Fig. 31. The water entrained by a surface jet from a temperature stratified reservoir is not of constant temperature. Water entrained laterally is warmer than water entrained vertically. The coldest (bottom) water was taken as a reference, and hence stronger temperature drops have been calculated than were actually measured.

The heat content in a cross section of the plume, as defined by Eq. (68), is a measure of the amount of heat retained in the receiving body of water as a function of location--i.e., distance from the point of discharge. An example of measured results is given in Fig. 43.

Entrainment Mechanisms -- Vertical turbulent mass and momentum transport processes in density stratified fluids depend, as is well known, on the degree of gravitational stability which the fluid shows in the presence of flow induced shear stresses. Generally the Richardson number

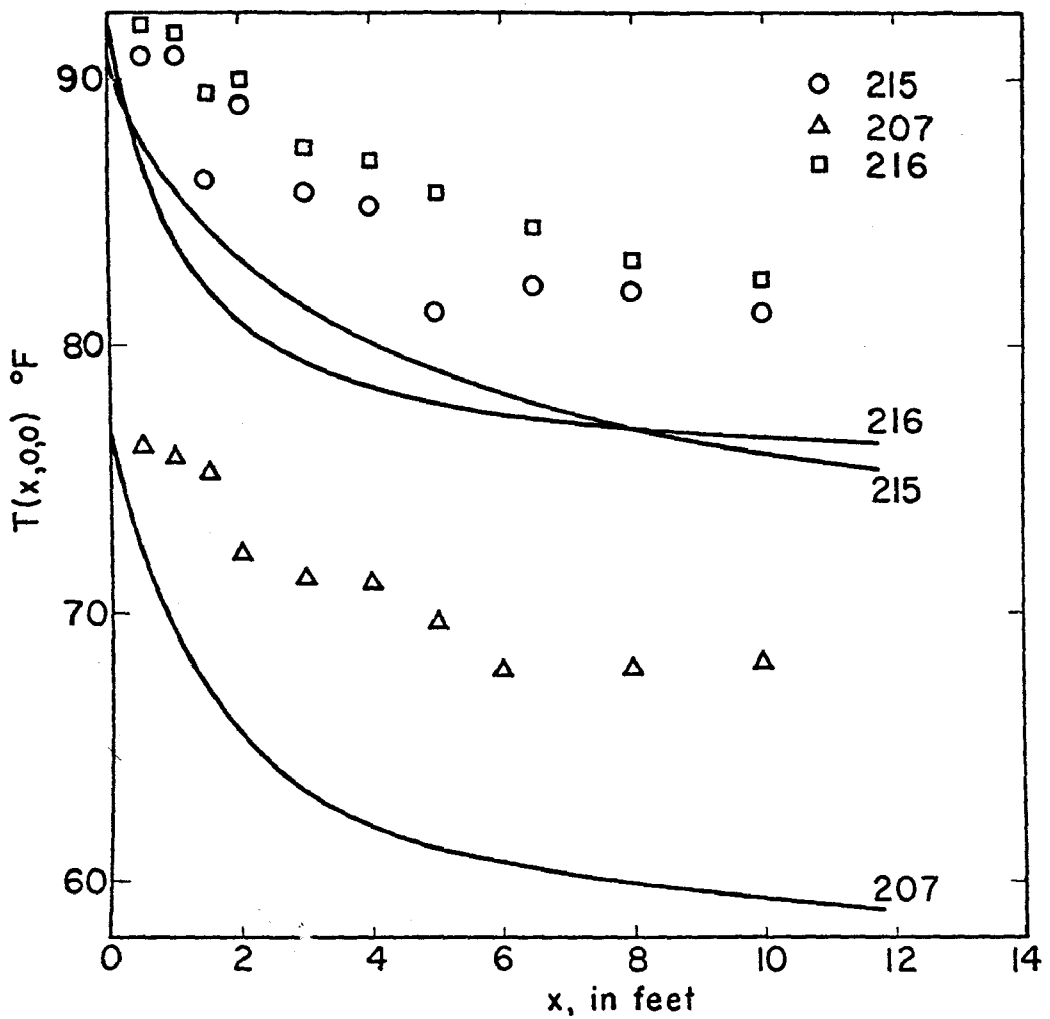


Fig. 42 - Surface Water Temperature Decline along Main Trajectory of Heated Surface Jet

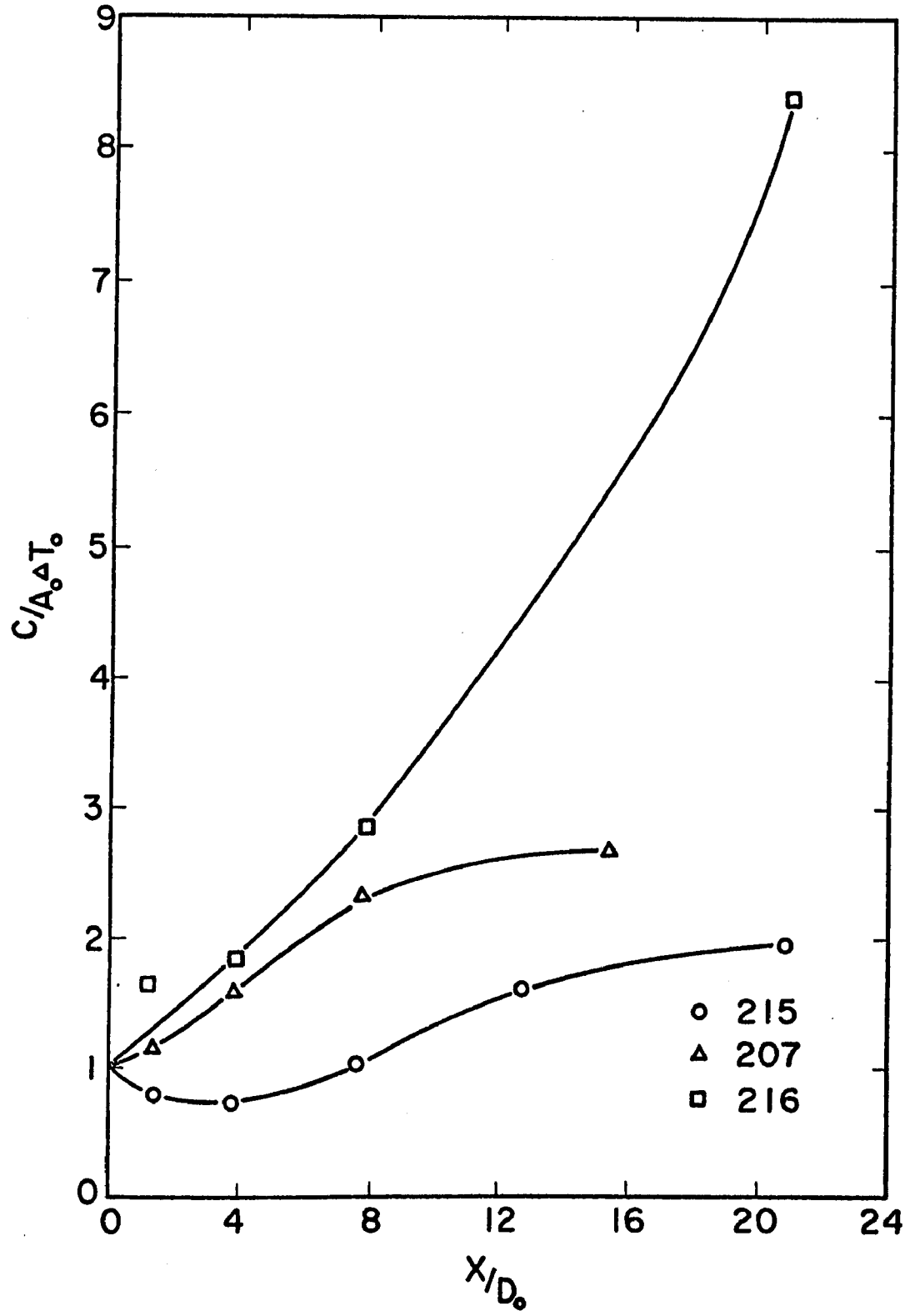


Fig. 43 - Heat Content versus Distance from Source of Discharge

$$Ri = - \frac{g \frac{\partial \varrho}{\partial z}}{\varrho \left(\frac{\partial u}{\partial z}\right)^2} \tag{70}$$

is used as a local stability parameter. The heated water flow from a channel into a reservoir is a density stratified, turbulent flow, and information on the local values of Richardson numbers may shed some light on the vertical mixing process in a plume.

A word of caution is necessary at this point, however, because inherent in the derivation of the Richardson number is the assumption that local turbulence is a function of local mean velocity gradients. This assumption does not necessarily apply to a plume in which the geometrical (depth and width) scale can change drastically with distance from the outlet. There is also turbulence production on the sides of the plume as well as on the bottom. Results given in Ref. [54] suggest caution.

Richardson numbers were calculated numerically. For uniform vertical spacing of measurements, the Richardson number for point $i$ is approximately

$$Ri_i \approx \frac{-2g}{\varrho_i} \left(\frac{\varrho_i - \varrho_{i-1}}{z_i - z_{i-1}} + \frac{\varrho_{i+1} - \varrho_i}{z_{i+1} - z_i}\right)\left(\frac{u_i - u_{i-1}}{z_i - z_{i-1}} + \frac{u_{i+1} - u_i}{z_{i+1} - z_i}\right)^{-2} \tag{71}$$

Since densities were not measured directly, conversion of the temperature measurements to densities was made using the empirical relationship

$$\varrho = 62.43[1 - (6T^2 - 36T + 47)(0.000001)] \tag{72}$$

where $\varrho$ is obtained in $lb_m/ft^3$ if $T$ is given in centigrades. Difficulties arose, of course, in the numerical computations when the velocity gradient $\partial u/\partial z$ took a value of zero. It was therefore decided to have the Richardson number assume special designated values if $\partial u/\partial z = 0$ or $\partial \varrho/\partial z = 0$ or both. All results were obtained in tabular form. To facilitate interpretation a graphical presentation of the numerical results with the aid of program CONTOUR is given in Fig. 44. Since the actual values of Richardson numbers covered a very wide range, and the contour plot could differentiate only between ten different symbols, logarithms (base 10) of Richardson numbers instead of actual values were plotted. The numbers actually printed in Figs. 44 and 45 are equal to $\log_{10} Ri + 4$. Using logarithms was desirable also from another point of view: Velocity measurements with the aid of the tethered sphere probe are probably not precise enough to give accurate values of velocity gradients. This problem exists in part also when measurements are being made with other velocity measuring

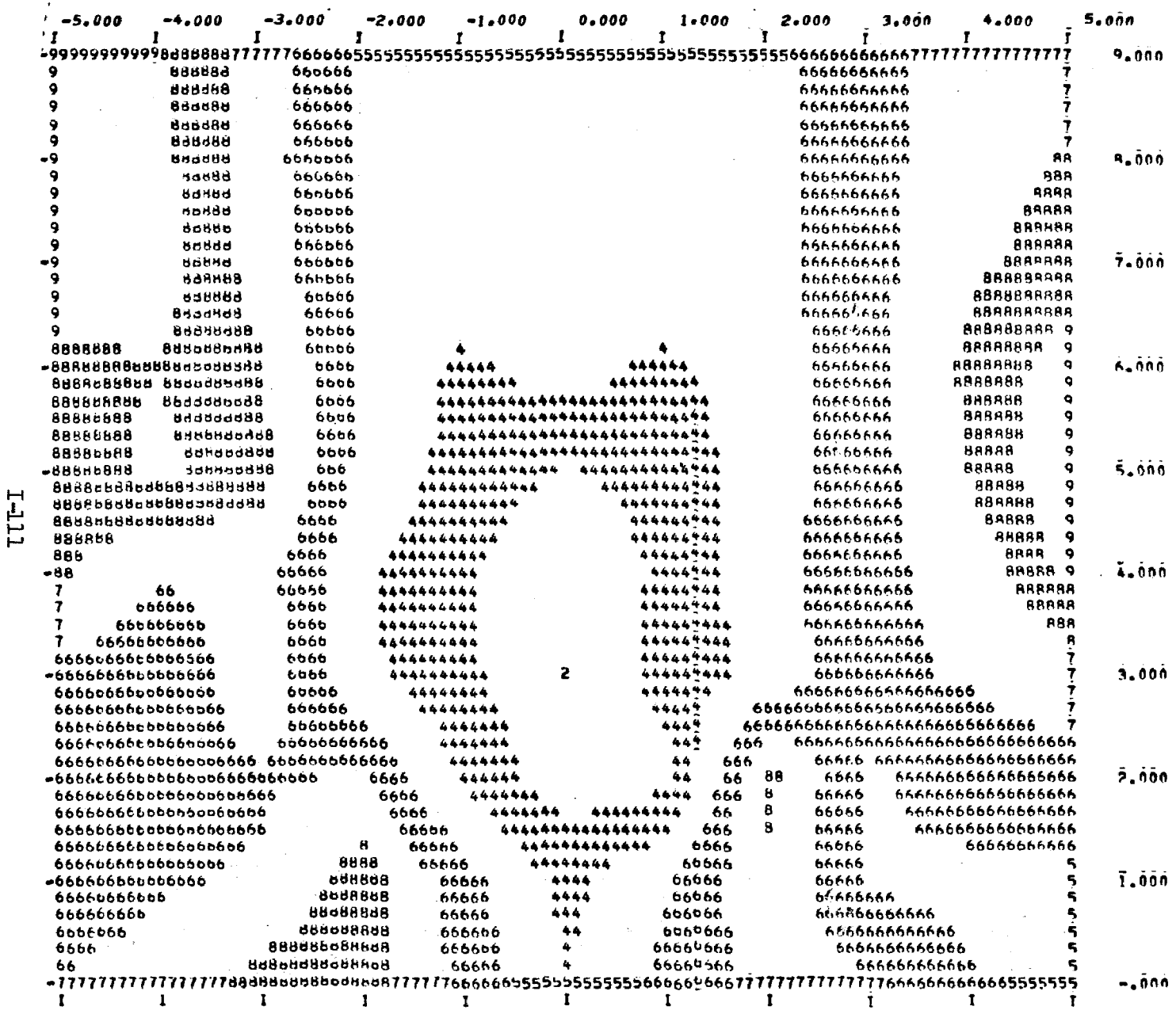


Fig. 44a - Iso-logarithms of Richardson numbers for Run 215. (Horizontal section at z = .05 ft)

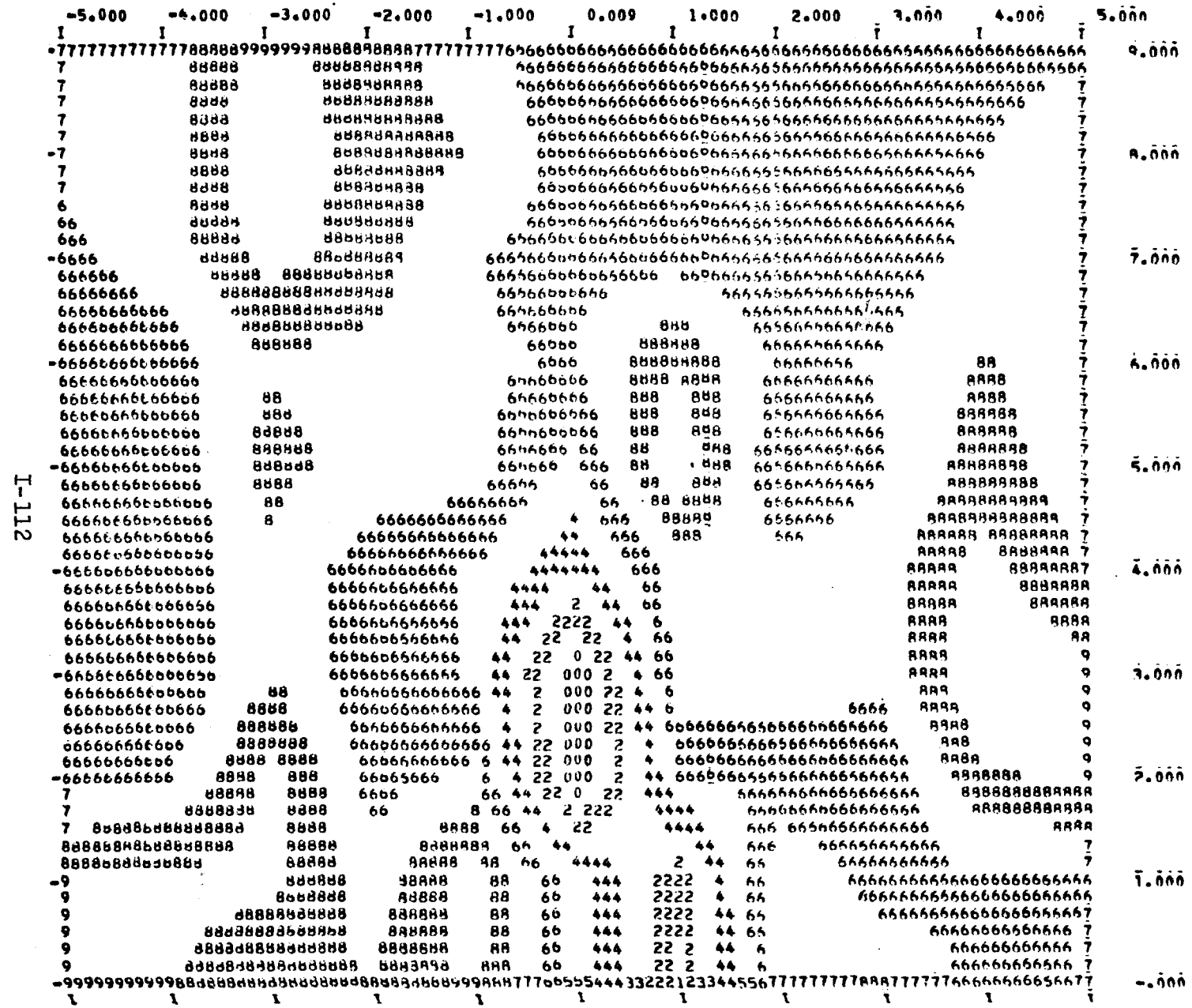




Fig. 44b - Iso-logarithms of Richardson numbers for Run 215. (Horizontal section at z = .14 ft)

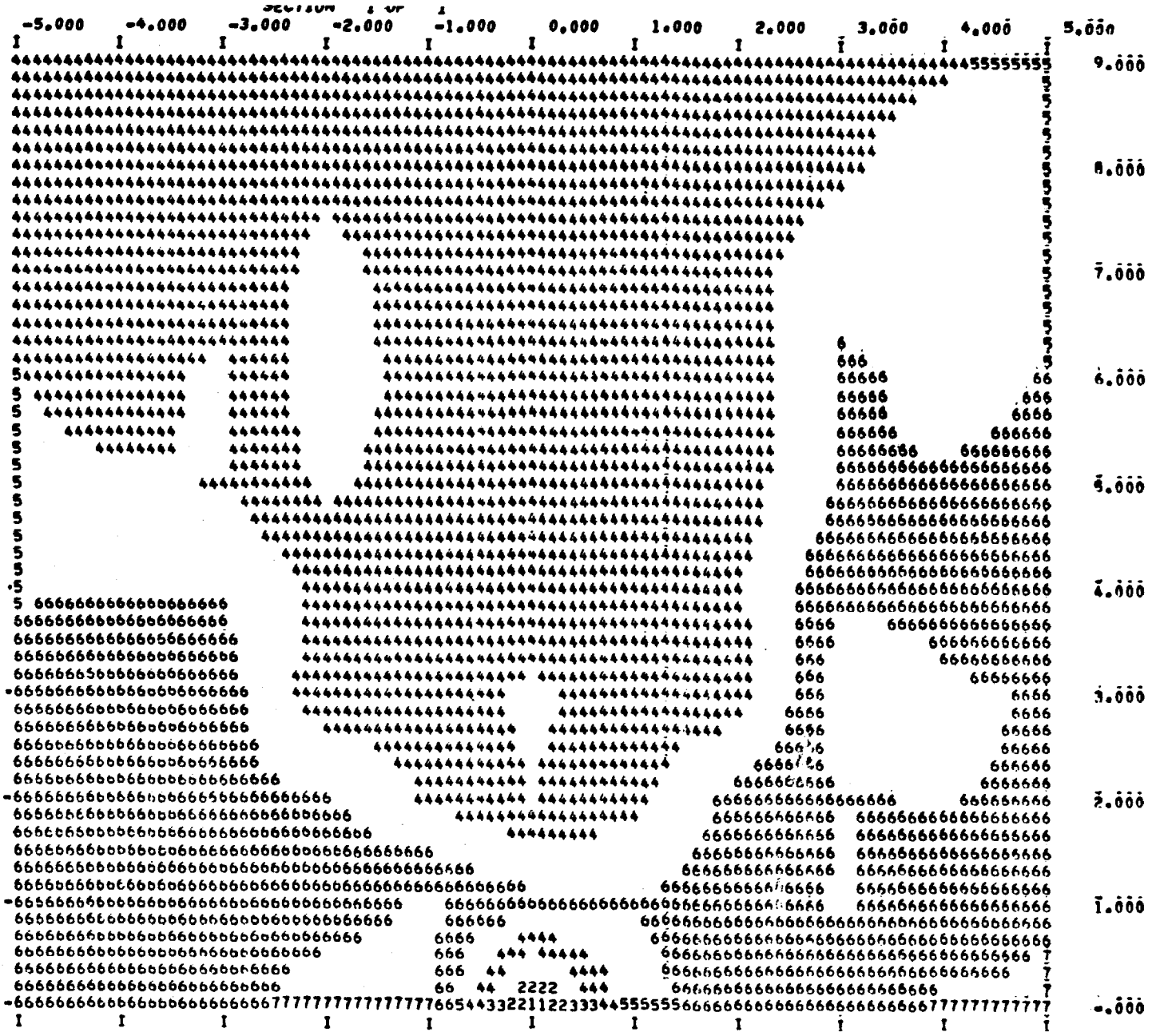




Fig. 44c - Iso-logarithms Richardson num bers for Run 20 (Horizontal sec at z = .05 ft)

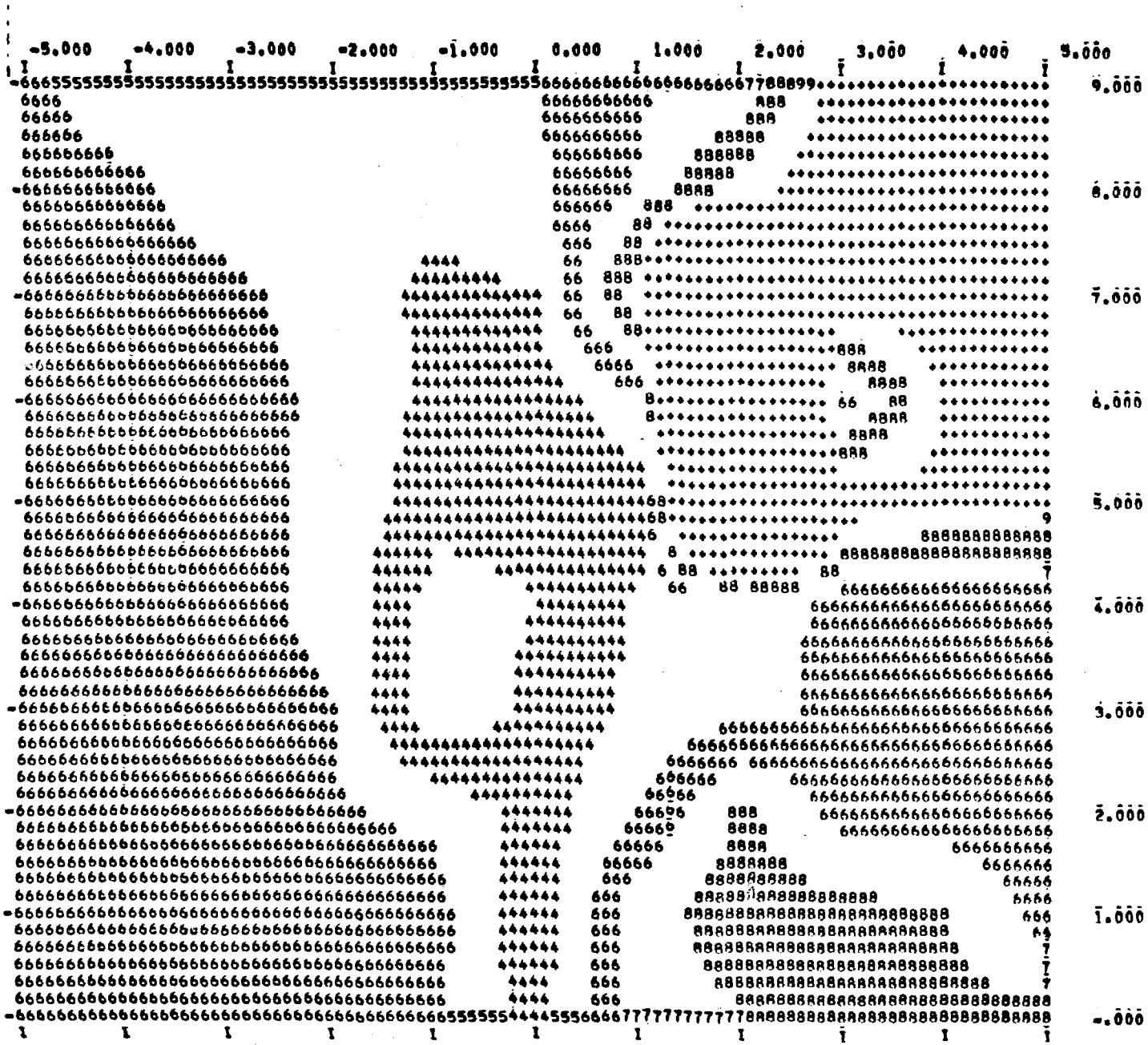




Fig. 44d - Iso-logarithms of Richardson numbers for Run 207. (Horizontal section at z = .14 ft)

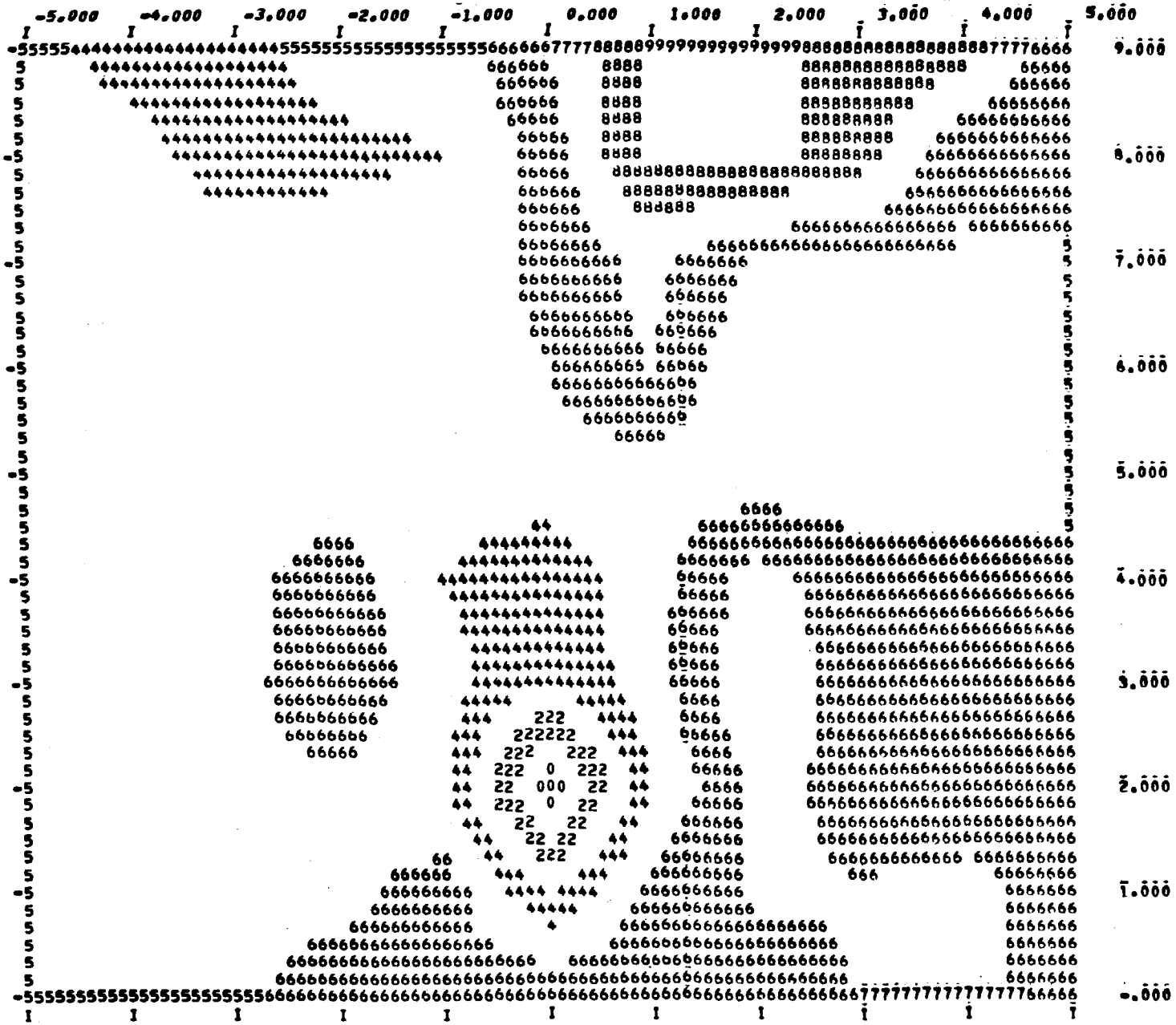




Fig. 44e - Iso-logarithms of Richardson numbers for Run 207. (Horizontal section at z = .20 ft)

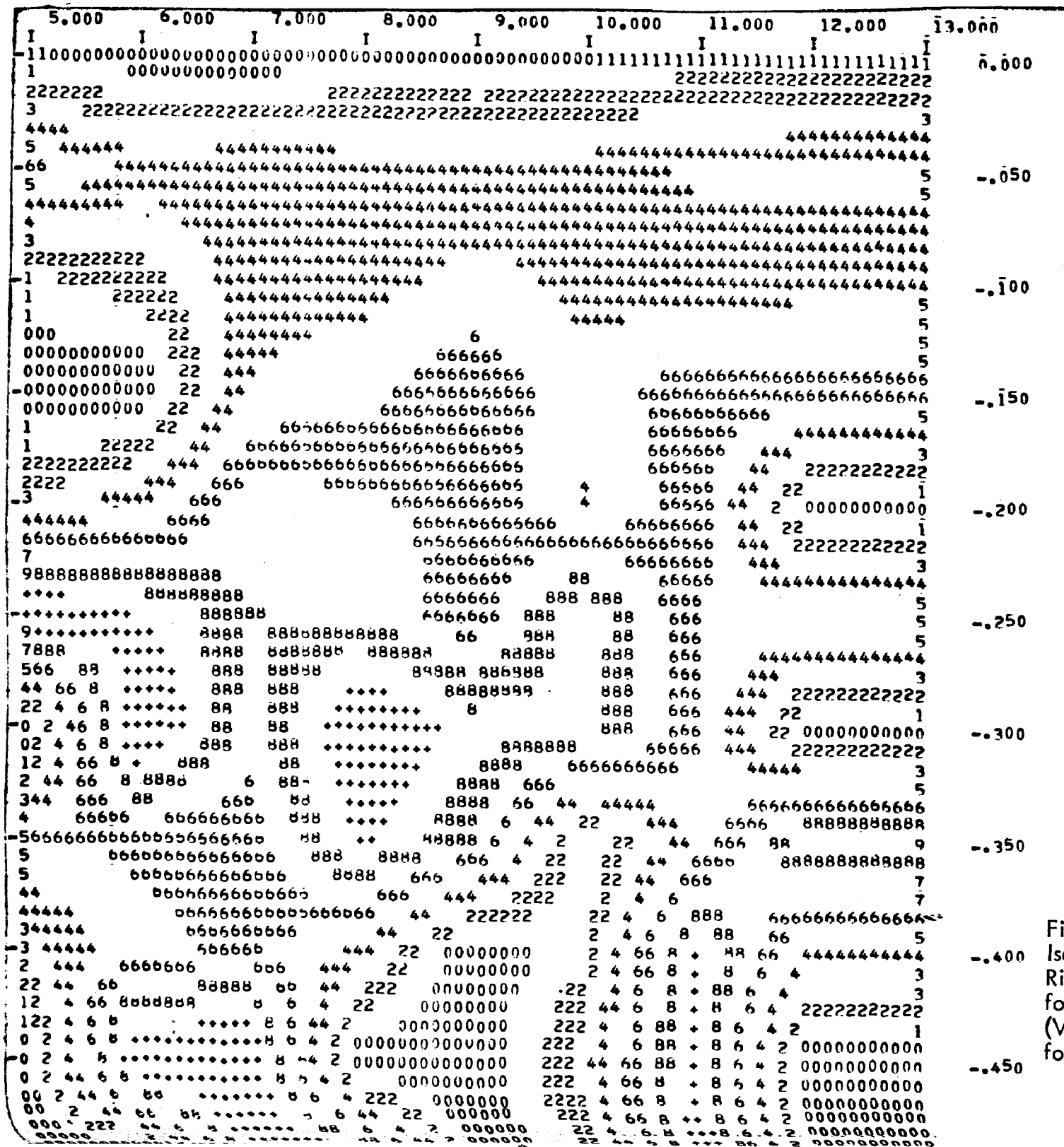


Fig. 45a - Iso-logarithms of Richardson numbers for Run 214. (Vertical section for y = 0)

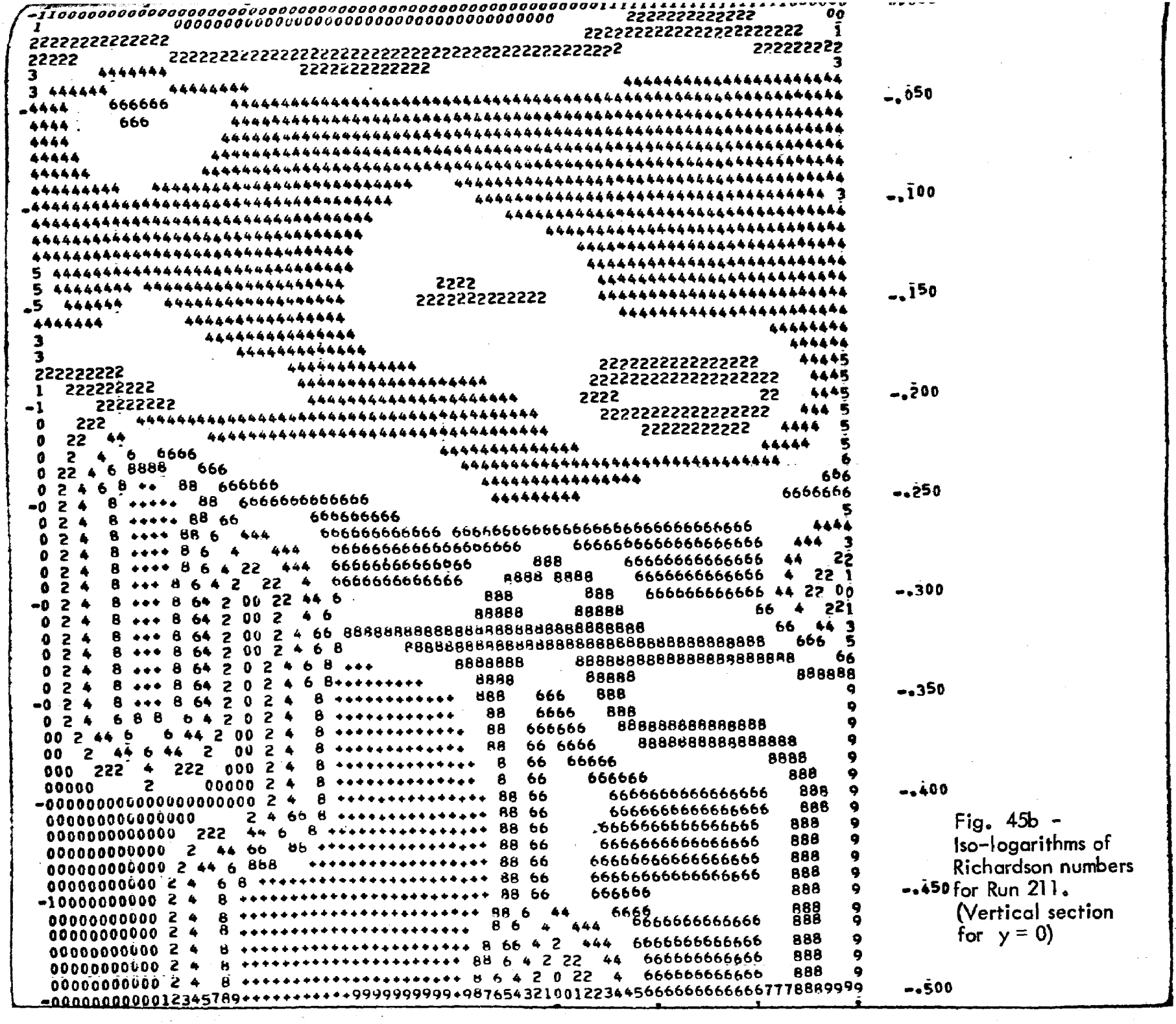


Fig. 45b - Iso-logarithms of Richardson numbers for Run 211. (Vertical section for y = 0)

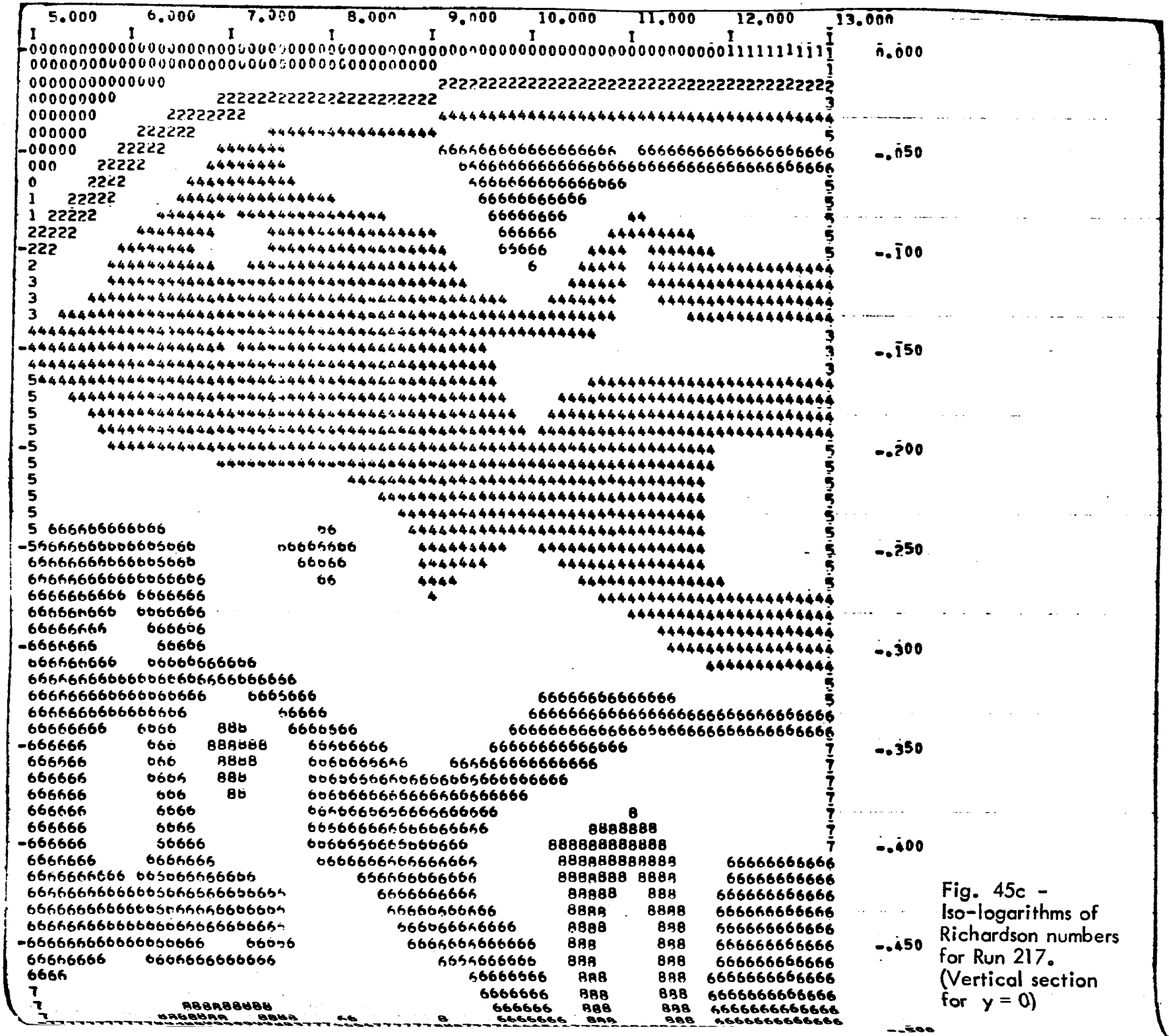


Fig. 45c - Iso-logarithms of Richardson numbers for Run 217. (Vertical section for y = 0)

devices. The logarithm of the Richardson number indicates essentially the order of magnitude and thereby eliminates some of the measurement errors except in those areas in which gradients are very small.

By the above rule Richardson numbers in the range $0.1 < Ri < 1$ obtain the symbol 3. It is generally accepted that a density stratification is stable--i.e., turbulent mixing is absent--when $Ri > 1$. Therefore areas with numbers larger than 3 should represent stably stratified flow regions with little or no vertical mixing. Alternate contour bands have been plotted. Figure 44 represents horizontal cross sections. The outlet is at the middle of the bottom. All scales are in feet.

Figure 45 represents vertical cross sections. The outlet is at the upper left. The first impression of Fig. 45 is of a rather disorganized pattern. A closer examination shows, however, the following typical features:

Near the surface is a thin layer of weak stratification; underneath, a much thicker layer with fairly stable stratification ($1 < Ri < 10$). The thickness of that layer appears to increase with distance from the outlet; underneath that layer more stably stratified fluid and finally the cold water in the tank with Richardson numbers varying rather randomly. In that last layer the velocity and temperature gradients are very small and Richardson numbers are probably meaningless for that reason, because of errors in temperature and velocity measurements.

Near the outlet the patterns differ depending on the outlet Froude number. In Run 214 ($F_o < 1$) a cold water wedge is formed in the channel and its effect on Richardson numbers is clearly apparent. The flow as it leaves the outlet has a stable thermocline at approximately one-third of the depth, but both the top and the bottom are unstable. In Run 211 the stability near the outlet increases from top to bottom of the outlet channel. The lower two-thirds are stably stratified. In Run 217 ($F_o \approx 4$) the major portion of the outlet flow is unstably stratified.

## Flow Regime of Thermal Plume

It has been shown that the heated water surface jet is subject to inertial and buoyant forces, the interplay of which largely determines the behavior of the jet. This interaction is uninhibited by solid walls, and one might therefore expect that the flow regime which the surface jet assumes is one in accordance with the minimum energy principle. In using the analytical model described it was found that the buoyant surface jet tends toward a regime with a specific local densimetric Froude number as defined in Eq. (4). In the absence of currents and wind this number was found to be

close to 3.0. Figure 46 illustrates the situation for the laboratory experiments. The value of 3.0 must be considered representative for an internally critical flow. Usually critical, gravity controlled flows are associated with Froude numbers equal to unity. The value 3.0 arises because of the definition of $F^*$ (on the main trajectory) as given in Eq. (4). If instead of $F^*$ the ratio of inertial to buoyant forces in a cross section is used, one finds that with

$$I = \frac{\rho}{2} u_i^2 \, a_i \, b_i \, f_3 \tag{73}$$

for the inertial forces and

$$B = \int_{-nb}^{nb} \int_{0}^{ma} \rho^*(x,y,z) \, zgdzdr$$

$$= g\rho_i(x,0,0)\lambda_v \, a_i^2 \, b_i \, f_5\{1 - \exp[-\frac{1}{2}(\frac{m}{\lambda_v})^2]\} \tag{74}$$

for the buoyancy forces, the ratio is equal to 0.545 $F^*$. The critical value of the ratio then is close to 1.6. Values of $\lambda_v = \lambda_h = 1.05$ and $m = n = 3$ were used to arrive at this result.

Experimental data on densimetric Froude numbers show them to be somewhat smaller than predicted, as is also shown in Fig. 46. A sharp dropoff in experimental values occurs at approximately 6 ft from the outlet, possibly because of density stratification in the tank.

In the absence of wind and cross-currents the heated water jet thus appears to tend toward a very specific flow regime. In the process the flow appears to reduce its overall entrainment coefficient drastically, as shown in Fig. 47.

When a cross-current or wind is present, it is not clear whether the flow regime should be defined in terms of the total densimetric Froude number $F$ or the relative densimetric Froude number $F^*$ as defined in Eq. (4). It is also questionable whether a specific regime is reached in all situations. Therefore the conclusions of the preceding paragraphs should be applied only to situations without wind or current.

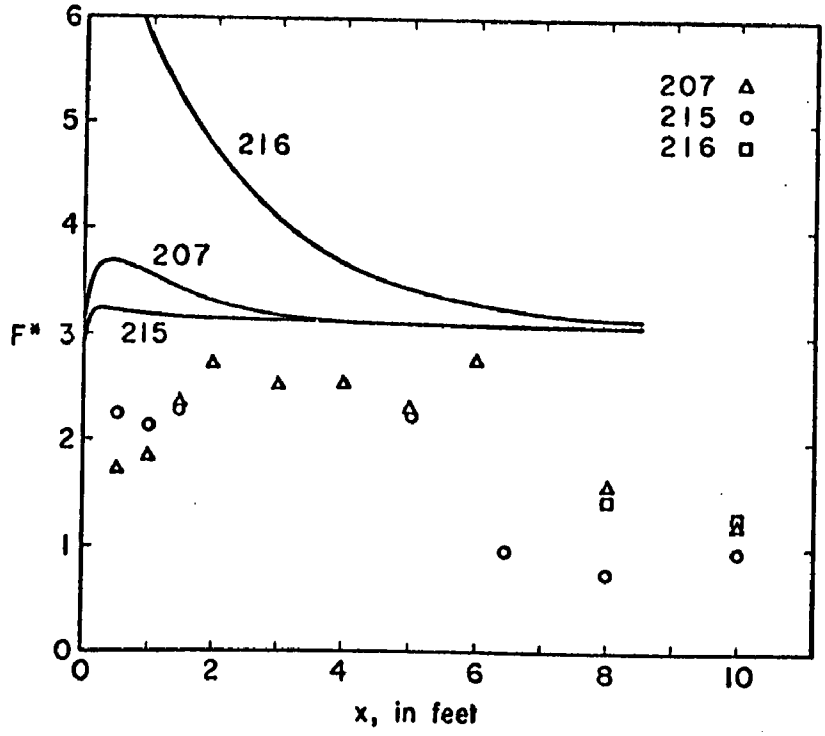


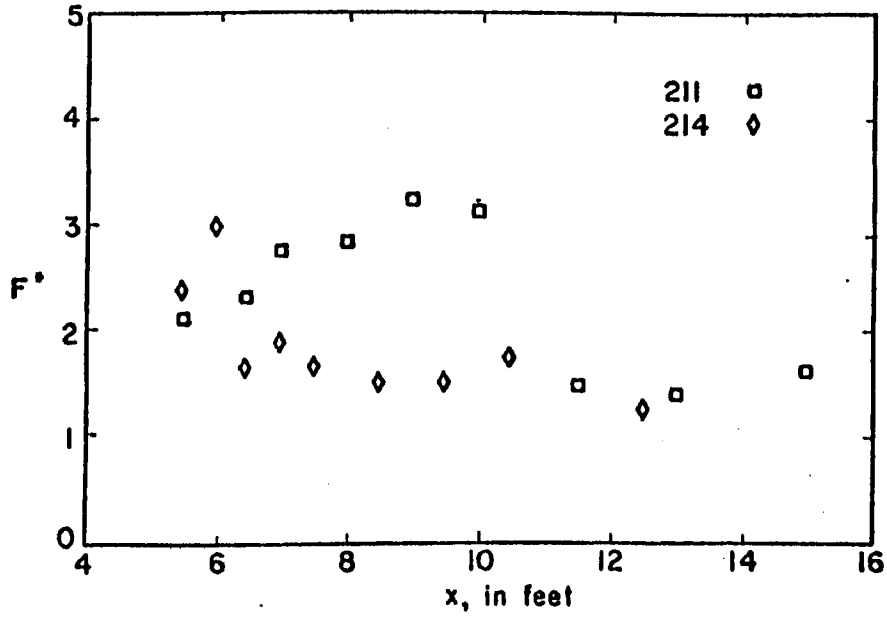


Fig. 46 - Densimetric Froude Numbers versus Distance on Main Trajectory. Analytical Model Predictions (solid lines) and Experimental Data

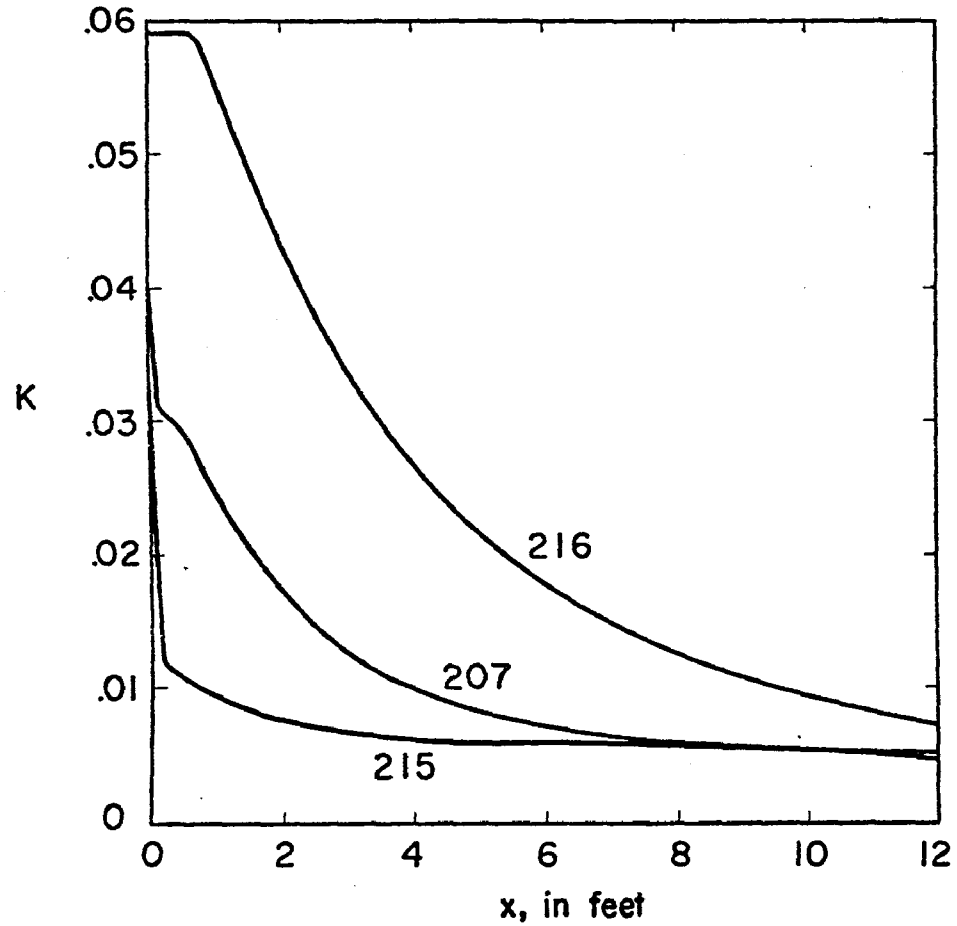


Fig. 47 - Entrainment Coefficients versus Distance along Main Trajectory for several experimental conditions as found from the Analytical Model

## SECTION VII

## ACKNOWLEDGMENTS

In the course of this study Mr. P. Vaidyaraman, Mr. W. Geiger, Mr. Glen Martin, and Mr. K. Streed provided valuable assistance. Their participation in various phases of the project is gratefully acknowledged. The manuscript of this report was edited and typed by Mrs. Shirley Kii.

The help and encouragement of Dr. Mustafa Shirazi, the Project Officer, are gratefully acknowledged.

## SECTION VIII

## REFERENCES


[1] "Biological Aspects of Thermal Pollution," edited by P. A. Krenkel and F. L. Parker, Proc. of the National Symposium on Thermal Pollution, Portland, Oregon, June 1968.

[2] Presentation prepared by the staff of the National Water Quality Laboratory of the FWQA, Duluth, Minnesota, for the Joint Commission on Atomic Energy, November 1969.

[3] Jensen, L. D.; Davies, R. M.; Brooks, A. S., and Meyers, C. D. The Effects of Elevated Temperature upon Aquatic Invertebrates, A Review of the Literature, Res. Rep. No. 4, Res. Proj. RP-49, Department of Geography and Environmental Engineering, The Johns Hopkins University, September 1969.

[4] Parker, F. L. and Krenkel, P. A., Thermal Pollution, Status of the Art, Rep. No. 3, Dept. of Environmental and Water Resources Engineering, Vanderbilt University, December 1969.

[5] Thermal Pollution - 1968, hearings before the Subcommittee on Air and Water Pollution of the Committee on Public Works, U.S. Senate, Parts 1, 2, 3, and 4.

[6] Edinger, J. E. and Polk, E. M., Initial Mixing of Thermal Discharges into a Uniform Current, Rep. No. 1, Department of Environmental and Water Resources Engineering, Vanderbilt University, October 1969.

[7] Wada, A., A Study on Phenomena of Flow and Thermal Diffusion Caused by Outfall of Cooling Water, Tech. Rep. C-66006, Central Research Institute of Electric Power Industry, Tokyo, January 1967.

[8] Wada, A., Numerical Analysis of Distribution of Flow and Thermal Diffusion Caused by Outfall of Cooling Water, Tech. Rep. C-67004, Central Research Institute of Electric Power Industry, Tokyo, January 1969.

[9] Hoopes, J. A.; Zeller, R. W.; and Rohlich, G. A., Heat Dissipation and Induced Circulation from Condenser Cooling Water Discharges into Lake Monona, Rep. No. 35, Eng. Exp. Station, Univ. of Wisconsin, February 1968. (See also Zeller, R. W., Hoopes, J. A. and Rohlich, G. A., "Heated Surface Jets in Steady Cross Current," Proc. ASCE, Jrl. Hydr. Div., September 1971, pp. 1403-1426.)

[10] Carter, H. H., A Preliminary Report on the Characteristics of a Heated Jet Discharged Horizontally into a Traverse Current - Part I - Constant Depth, Tech. Rep. No. 61, Chesapeake Bay Institute, Johns Hopkins University, November 1969.

[11] Motz, L. H. and Benedict, B. A., Heated Surface Jet Discharged into a Flowing Ambient Stream, Rep. No. 4, Dept. of Environmental and Water Resources Engineering, Vanderbilt University, August 1970.

[12] Cederwall, K., "Dispersion Phenomena in Coastal Environments," reprint from the Journal of the Boston Society of Civil Engineers, January 1970.

[13] Hayashi, T. and Shuto, N., "Diffusion of Warm Water Jets Discharged Horizontally at the Water Surface," Proc. 12th Congr., IAHR, Colorado, Vol. 4, September 1967.

[14] Stolzenbach, K. D. and Harleman, D. R. F., An Analytical and Experimental Investigation of Surface Discharges of Heated Water, Rep. No. 135, Ralph M. Parsons Laboratory for Water Resources and Hydrodynamics, Mass. Inst. of Tech., February 1971.

[15] Koh, R. C. Y. and Fan, L. N., Mathematical Models for the Prediction of Temperature Distributions Resulting from the Discharge of Heated Water into Large Bodies of Water, 16130 DWO 10/70, Water Pollution Control Research Series, EPA, October 1970.

[16] Platten, J. L. and Keffer, J. F., Entrainment in Deflected Axisymmetric Jets at Various Angles to the Stream, Mech. Eng. T.P. 6808, Univ. of Toronto, June 1968.

[17] Bowley, W. W. and Sucec, J., "Trajectory and Spreading of a Turbulent Jet in the Presence of a Cross Flow of Arbitrary Velocity Distribution," Tech. Paper 69-GT-33, ASME, March 1969.

[18] Silberman, E. and Stefan, H., Physical (Hydraulic) Modeling of Heat Dispersion in Large Lakes: A Review of the State of the Art, Report ANL/ES-2, Argonne National Laboratory, August 1970.

[19] Wiegel, R. L.; Mobarek, I.; and Jen, Y., Discharge of Warm Water Jet over Sloping Bottom, Rep. HEL 3-4, Hydraulic Engineering Laboratory, Univ. of California, November 1964.

[20] Jen, Y.; Wiegel, R. L.; and Mobarek, I., "Surface Discharge of Horizontal Warm Water Jets," Proc. ASCE, Jrl. Power Div., April 1966.

[21] Tamai, N.; Wiegel, R. L.; and Tornberg, G. F., "Horizontal Discharge of Warm Water Jets," Proc. ASCE, Jrl. Power Div., October 1969.

[22] Stefan, H. and Schiebe, F. R., "Heated Discharge from Flume into Tank," Proc. ASCE, Jrl. Sanitary Eng. Div., December 1970.

[23] Kashiwamura, M. and Yoshida, S., "Outflow Pattern of Fresh Water Issued from a River Mouth," Coastal Engineering in Japan, Vol. 10, 1967.

[24] Wood, I. R. and Wilkinson, D. L., discussion of "Surface Discharge of Horizontal Warm-Water Jet," by Jen, Wiegel, and Mobarek, Proc. ASCE, Jrl. Power Div., Vol. 93, No. PO1, March 1967, pp. 149-151.

[25] Cheney, W. O. and Richards, G. V., Ocean Temperature Measurements for Power Plant Design, Pacific Gas and Electric Company, date not shown.

[26] Fitch, N. R., Temperature Surveys of St. Croix River, 1969-1970, Environmental Monitoring Program, Northern States Power Company, December 31, 1970.

[27] Squire, James L., Jr., Surface Temperature Gradients Observed in Marine Areas Receiving Warm Water Discharges, Tech. Paper No. 11, Bureau of Sport Fisheries and Wildlife, January 1967.

[28] Ackers, P., "Modeling of Heated Water Discharges," Chapter 6 of Engineering Aspects of Thermal Pollution, edited by F. L. Parker and P. A. Krenkel, Proc. of the National Symposium on Thermal Pollution, Vanderbilt University, 1968.

[29] Asbury, J. G.; Grench, R. E.; Nelson, D. M.; Prepejchal, W.; Romberg, G. P.; and Siebold, P., A Photographic Method for Determining Velocity Distributions within Thermal Plumes, Rep. ANL/ES-4, Argonne National Laboratory, February 1971.

[30] Fan, L. N. and Brooks, N. H., Numerical Solutions of Turbulent Buoyant Jet Problems, Rep. No. KH-R-18, W. M. Keck Laboratory of Hydraulics and Water Resources, January 1969.

[31] Rouse, H.; Yih, C. S.; and Humphreys, H. W., "Gravitational Convection from Boundary Source," Tellus, Vol. 4, No. 3, August 1952, pp. 201-210.

[32] Abraham, G., "Horizontal Jets in Stagnant Fluid of Other Density," Proc. ASCE, Jrl. Hydr. Div., July 1965, pp. 139-154.

[33] Fan, L. N. and Brooks, N. H., discussion of "Horizontal Jets in Stagnant Fluid of Other Density," Proc. ASCE, Jrl. Hydr. Div., March 1966.

[34] Abramovich, G. N., The Theory of Turbulent Jets, Massachusetts Institute of Technology Press, Cambridge, Mass., 1963.

[35] Gordier, R. L., Studies on Fluid Jets Discharging Normally into Moving Liquid, Technical Paper No. 28-B, St. Anthony Falls Hydraulic Laboratory, Univ. of Minnesota, 1959.

[36] Stefan, H., "Stratification of Flow from Channel into Deep Lake," Proc. ASCE, Jrl. Hydr. Div., July 1970.

[37] Albertson, M. L.; Dai, Y. B.; Jensen, R. A.; and Rouse, H., "Diffusion of Submerged Jets," Trans. ASCE, Vol. 115, 1950, pp. 639-697.

[38] Folsom, R. G. and Ferguson, C. K., "Jet Mixing of Two Liquids," Trans. ASME, January 1949, pp. 73-77.

[39] Rossby, C. G. and Montgomery, R. B., "The Layer of Frictional Influence in Wind and Ocean Currents," Papers in Physical Oceanography and Meteorology, Vol. 3, No. 3, 1935.

[40] Parr, A. E., "On the Probable Relationship between Vertical Stability and Lateral Mixing Processes," Conseil Permanent International pour l'exploration de la Mer, Jrl. du Conseil, Vol. 11, No. 3, 1936.

[41] Munk, W. H. and Anderson, E. R., "Notes on a Theory of the Thermocline," Jrl. of Marine Research, Vol. 7, 1948.

[42] Ellison, T. H. and Turner, J. S., "Turbulent Entrainment in Stratified Flows," Jrl. of Fluid Mechanics, Vol. 6, Part 3, October 1959.

[43] Kato, H. and Phillips, O. M., "On the Penetration of a Turbulent Layer into a Stratified Fluid," Jrl. of Fluid Mechanics, Vol. 37, Part 4, July 1969.

[44] Wada, A., Numerical Analysis of Distribution of Flow and Thermal Diffusion Caused by Outfall of Cooling Water, Tech. Rep. C 67004, Central Res. Inst. of Electric Power Industry, January 1969.

[45] Sundaram, T. R. and Rehm, R. G., "Formation and Maintenance of Thermoclines in Stratified Lakes Including the Effects of Power-Plant Thermal Discharges," AIAA 8th Aerospace Science Meeting, New York, January 1970.

[46] Fan, Loh-Nien, Turbulent Buoyant Jets into Stratified or Flowing Ambient Fluids, Rep. No. KH-R-15, W. M. Keck Laboratory of Hydraulics and Water Resources, June 1967.

[47] Abbott, M. B., "On the Spreading of One Fluid over Another," La Houille Blanche, Vol. 16, No. 6, 1961, pp. 827-846.

[48] Edinger, J. E.; Duttweiler, D. W.; and Geyer, J. C., "The Response of Water Temperatures to Meteorological Conditions," Water Resources Research, Vol. 4, No. 5, October 1968, pp. 1137-1143.

[49] Roll, H. U., Physics of the Marine Atmosphere, International Geophysics Series, Vol. 7, Academic Press, New York, 1965.

[50] Wada, A., Effect of Winds on a Two-Layered Bay, Tech. Rep. C-66002, Central Research Institute of the Electric Power Industry, Tokyo, September 1966.

[51] Brady, D. K.; Graves, W. L., Jr.; and Geyer, J. C., Surface Heat Exchange at Power Plant Cooling Lakes, Report No. 5, Project RP-49, Department of Geography and Environmental Engineering, Johns Hopkins University, November 1969.

[52] Wilkinson, D. L. and Wood, I. R., "A Rapidly Varied Flow Phenomenon in a Two-Layer Flow," Jrl. of Fluid Mechanics, Vol. 47, Part 2, May 1971, pp. 241-256.

[53] Stefan, H. and Schiebe, F. R., Experimental Study of Warm Water Flow into Impoundments. Part III: Temperature and Velocity Fields Near a Surface Outlet in Three-Dimensional Flow, Project Report No. 103, St. Anthony Falls Hydraulic Laboratory, Univ. of Minnesota, December 1968.

[54] Wada, A., "A Study of Mixing Process in the Sea Caused by Outfall of Industrial Warm Water," Coastal Engineering in Japan, Vol. XII, 1969, pp. 147-158.

# Appendix A

## COMPUTER PROGRAM FOR ANALYTICAL MODEL
## (FORTRAN IV)

```
      PROGRAM PLUME (INPUT,OUTPUT)
C ST CROIX FIELD DATA,  SEPTEMBER 4,1969
      DIMENSION Q(200),T(200),U(200),A(200),B(200),DELRO(200),H(200),
     1 ALFA(200),X(200),Y(200),XL(200),YL(200),XR(200),YR(200),K(200),
     2 MO(200),F(200),AREA(200)
      REAL M,N,L,K1,KS,KH,K,KV,MO,MOO,KRATIO
      N=3.0
      M=3.0
      L=1.05
C INTEGRATION COEFFICIENTS
      F1=3.1415*(ERFN(N/SQRT(2.)))*(ERFN(M/SQRT(2.)))
      F2=F1*(L**2./(L**2.+1.))
      F3= 3.1415*(ERFN(N))*(ERFN(M))/2.
      F4=F1*L**2.
      F5=L*(ERFN(N/SQRT(2.)))*(SQRT(3.1415*2.))
      F6=EXP(-.5)
      PRINT 32
   32 FORMAT (1H1,//,52X,*HEATED WATER PLUME CHARACTERISTICS*,///)
      PRINT 11
   11 FORMAT( //,8X,*F1*,11X,*F2*,11X,*F3*,11X,*F4*,11X,*F5*,11X,*F6*)
      PRINT 20,F1,F2,F3,F4,F5,F6
   20 FORMAT(/,6F13.3,//)
C EMPIRICAL COEFFICIENTS
      C4=0.081
      C5=0.4
      KHAMB=0.082
C DRAGCOEFFICIENT
      CD=1.
C STEP LENGTH
      DS=10.
      NSTEP=200
C CURRENT VELOCITY
      US=.033
C WIND CONDITIONS
      WIND=10.
      BETA=9.*3.1415/8.
C WIND SHEAR STRESS
      ROAIR=0.0030
      W=WIND*(5280.0/3600.)
      IF(W.LE.30.5) GO TO 1
      IF(W.GT.30.5) GO TO 2
    1 STRECO=0.0010
      GO TO 3
    2 STRECO=0.0021
    3 TAUW=STRECO*ROAIR*W**2
      PRINT 53
   53 FORMAT (40X,*US(FT/SEC)*,10X,*W(FT/SEC)*,10X,*TAUW(LBS/SQ. FT)*,/)
      PRINT 104,US,W,TAUW
  104 FORMAT (40X,1F8.2,10X,1F8.3,10X,1F8.4,///)
C SOLAR RADIATION AND DEW POINT TEMPERATURE
      HS=87./3600.
      TD=74.
C INITIAL CONDITIONS
      RINV=1.0E-30
      ALFA0=3.1415/2.
      Q0=660.
      T0=93.1
```

```
      TC=77.5
      DPO=10.
      WIDO=195.
C INITIAL SURFACE HEAT TRANSFER PARAMETERS
      TM=(T(1)+TC+TD)/2.
      BET=.255-.0085*TM+.000204*TM**2.
      FUWI=70.+.7*WIND**2.
      KS=(15.7+(BET+.26)*FUWI)/(3600.*24.)
      EQU=TD+HS/KS
      PRINT 51
   51 FORMAT(40X,*KS (BTU/SQFT SEC DEGF)*,5X,*EQUILIBRIUM TEMP (DEG F)*)
      PRINT 60,KS,EQU
   60 FORMAT(/,33X,2G25.4,//)
C COLD WATER DENSITY
      TCC=(5./9.)*(TC-32.)
      RHOCC=1.-(6.*TCC**2.-36.*TCC+47.)*.0000001
      RHOTC=RHOCC*62.43/32.17
C INITIAL DENSITY DIFFERENTIAL
      TCEL=(5./9.)*(TO-32.)
      RHOC=1.-(6.*TCEL**2.-36.*TCEL+47.)*.0000001
      RHO=62.43*RHOC/32.17
      DELROO=RHOTC-RHO
C INITIAL PARAMETERS
   96 UO=QO/(DPO*WIDO)
      FO =UO/(((DELROO/1.94)*32.2*DPO)**.5)
      MOO=1.94*QO**2/(WIDO*DPO)
C STARTING CONDITIONS
      ALFA(1)=ALFAO
      Q(1)=QO
      T(1)=TO-TC
C INITIAL STANDARD DEVIATIONS
      AA=1.94*Q(1)*F3
      BB=2.*1.94*Q(1)*US*COS(ALFA(1))*F1-MOO*F1
      CC=0.5*1.94*3.1415*US**2*(COS(ALFA(1)))**2*M*N*Q(1)-0.5*MOO*3.1415
     1*US*COS(ALFA(1))*M*N
      CX=BB**2-4.*AA*CC
      U(1)=(-BB+SQRT(CX))/(2.*AA )
      A(1)=DPO/L
      B(1)=Q(1)/(A(1)*(U(1)*F1+0.5*3.1415*US*COS(ALFA(1))*M*N ))
C INITIAL COORDINATES
      X(1)=.0
      Y(1)=.0
C INITIAL HEAT AND MOMENTUM FLUXES
      H(1)=U(1)*T(1)*A(1)*B(1)*F2+US*COS(ALFA(1))*T(1)*A(1)*B(1)*F4
      MO(1)=(U(1)**2.*A(1)*B(1)*F3+2.*US*COS(ALFA(1))*A(1)*B(1)*F1*U(1)
     1+US**2.*COS(ALFA(1))**2.*N*M*A(1)*B(1)*3.1415/2.)*1.94
      I=1
C DENSITY DIFFERENTIAL
  150 TCEL=(5./9.)*(T(I)+TC-32.)
      RHOC=1.-(6.*TCEL**2.-36.*TCEL+47.)*.000001
      RHO=62.43*RHOC/32.17
      DELRO(I)=RHOTC-RHO
C DENSIMETRIC FROUDE NUMBER
      F(I)=U(I)/(((DELRO(I)/1.94)*32.2*L*A(I))**.5)
      IF (F(1) .GE. 3.0)  GO TO 95
      DPO=.95*DPO
      GO TO 96
   95 IF (I .GT. 1) GO TO 97
```

```
      PRINT 501
  501 FORMAT (50X,*U0(FT/SEC)*,10X,*F0*,/)
      PRINT 500,U0,F0
  500 FORMAT (47X,2G15.3,/)
C ENTRAINMENT COEFFICIENTS
   97 IF(U(I)/(US*COS(ALFA(I))).LE.0.1) KH=KHAMB
      KV=(1.0-1.33*ALOG(6.32/F(I)))
      IF (KV.GT.1.0) KV=1.0
       IF(KV.LT.0.0) KV=0.0
      KH=.059
      KV=KH*KV
      K(I)=(KH*A(I)+KV*B(I))/ (A(I)+B(I))
C PRINTOUT OPTION 1
      IF (I .GT.1) GO TO 555
      PRINT 31
   31 FORMAT (3X,*N*,6X,*X(FT)*,6X,*Y(FT)*,6X,*Q(CFS)*,5X,*T(DEG F)*,3X,
     1*A(FT)*,6X,*B(FT)*,6X,*U(FT/SEC)*,2X,*H(BTU/SEC)*,2X,*MO(LBS)*,5X,
     2*ALFA*,10X,*FR*,//)
  555 PRINT 40, I,X(I),Y(I),Q(I),T(I),A(I),B(I),U(I),H(I),MO(I),ALFA(I),
     1F(I)
   40 FORMAT (1X,I3,3X,9F11.2,1F11.4,1F11.2)
C NEW FLOW RATE
      DQ=K(I)*U(I)*(A(I)+B(I))*3.1415*DS*SQRT(2.0)/2.
      Q(I+1)=Q(I)+DQ
C SURFACE HEAT TRANSFER COEFFICIENTS
      TM=(T(I)+TC+TD)/2.
      BET=.255-.0085*TM+.000204*TM**2.
      FUWI=70.+.7*WIND**2.
      KS=(15.7+(BET+.26)*FUWI)/(3600.*24.)
      EQU=TD+HS/KS
C HEATLOSS
      HLOSS=(F5*B(I)*T(I)+(TC-EQU)*2.*N*B(I))*DS*KS/62.4
      H(I+1)=H(I)-HLOSS
C FIND FRICTION FORCE DF
      VISC=.000019142/(.471101+.0143454*(T(I)+TC)+.0000682074*
     1(T(I)+TC)**2.)
      DFLAM=- VISC*EXP(-0.5)*(A(I)**2+B(I)**2)/(A(I)*B(I))*1.965*U(I)
      DF=(KH-K(I))*DFLAM/KH*(-1.)
C FIND WIND FORCE FW
      FW=TAUW*2.*N*B(I)*DS
C NEW MOMENTUM AT I+1
      GAMA=BETA-ALFA(I)
      DMO=DF+FW*COS(GAMA)
      MO(I+1)=MO(I)+DMO
C NEW ANGLE OF MAIN TRAJECTORY AT I+1
      DD=CD*1.94*(US*SIN(ALFA(I)))**2.*M*A(I)*DS/2.
      RINV=(DD-FW*SIN(GAMA))/MO(I)
      DALFA= (ABS(RINV)**.667)*DS*COS(ALFA(I))*RINV/ABS(RINV)
      ALFA(I+1)=ALFA(I)-DALFA
C FIND NEW AREA AT I+1
      K1=US*COS(ALFA(I+1))*2.*N*M
      Z1=F3
      Z2= F1*(K1/(N*M)-MO(I+1)/(1.94*Q(I+1)))
      Z3= 3.1415*K1*(K1/(8.*N*M)-MO(I+1)/(4.*1.94*Q(I+1)))
      ZZ=ABS(Z2)**2.-4.*Z1*Z3
      IF(ZZ.LE.0.0) GO TO 4
      U(I+1)=(-Z2+SQRT(ZZ))/(2.*Z1)
      AREA(I+1)=Q(I+1)/(U(I+1)*F1+K1*3.1415/4.)
```

```
      GO TO 201
 4    PRINT 5
 5    FORMAT(10X,*VALUE OF ZZ IS NEGATIVE*)
 201  CONTINUE
C RATIO OF NEW STANDARD DEVIATIONS AT I+1
      DBB=(C5/(F6*U(I)+US*COS(ALFA(I))))*(32.2*A(I)*L*DELRO(I)/1.94)**.5
     1 *DS
      DAB=-(A(I)*DBB)/(B(I))
      DBT=C4*(U(I)/(U(I)+US*COS(ALFA(I))))*DS
      DAT=DBT*SQRT(KV/KH)
      DB=DBB+DBT
      DA=DAB+DAT
      APROX=A(I)+DA
      BPROX=B(I)+DB
      AXRAT=BPROX/APROX
C   NEW STANDARD DEVIATIONS
      A(I+1)=(AREA(I+1)/AXRAT)**.5
      B(I+1)=AXRAT*A(I+1)
C NEW TEMPERATURE
      T(I+1)=H(I+1)/(U(I+1)*AREA(I+1)*F2+US*COS(ALFA(I+1))*AREA(I+1)*F4)
C NEW COORDINATES OF MAIN TRAJECTORY AT I+1
      ALF=ALFA(I)-DALFA/2.
      DELX=DS*SIN(ALF)
      DELY=DS*COS(ALF)
      X(I+1)=X(I)+DELX
      Y(I+1)=Y(I)+DELY
      IF(I.EQ.NSTEP) GO TO 300
      I=I+1
      GO TO 150
 300  STOP
       END
```

## Appendix B

### ZONE OF FLOW ESTABLISHMENT

The analytical method of plume analysis described previously starts with a fully developed jet. Obviously, this condition will not be found at the real point of discharge. The starting point of the analysis presented has therefore been called the virtual origin ($s = 0$). Between the real origin and the virtual origin of the jet is the outlet region or zone of flow establishment. An analytical treatment of the outlet region is possible only if the geometry is not too complicated. Structures such as levees, as well as the bottom topography in shallow receiving waters, may interfere with the formation of a zone of flow establishment. In many cases it may be necessary to resort to physical experimentation to find the location of the virtual origin and the initial flow conditions of the analytical model. Only if the outlet geometry is fairly regular will it be possible to treat the outlet region analytically. In that case it is possible to draw to some extent on information obtained through studies of non-buoyant jet flows. Buoyancy does introduce some important modifications, however. The zone of flow establishment for neutrally buoyant submerged circular jets with initially uniform velocity and temperature has been well documented [37]. The length of the zone of flow establishment was found to be of the order of 6.2 times the diameter of the discharge nozzle. This value can be found from experimental data; for example, by plotting centerline velocities versus distance. Over the length of the zone of flow establishment the velocity will be constant.

The heated water half-jet under consideration is non-circular, buoyant, and non-uniform with respect to velocity at the point of discharge. Typically it may have the features of a fully developed channel flow before entering the reservoir. The initial conditions for the zone of flow establishment are a temperature distribution of the form

$$T^*(0,r,z) = T^*(0,0,0) = \text{const} \tag{75}$$

$$\text{for} \quad r \leq \frac{w_o}{z} \quad \text{and} \quad z \leq d_o$$

and a velocity distribution

$$u(0,r,z) = u(0,0,0)\ f(r,z) \tag{76}$$

where $f(r,z)$ may be any function suitable for describing the discharge velocity profile, for example

$$f(r,z) = \left[1 - \left(\frac{z}{d_o}\right)^{n_1}\right]\left[1 - \left(\frac{r}{w_o/2}\right)^{n_2}\right] \qquad (77)$$

for a rectangular channel, with $n_1$ and $n_2$ being constants.

In the zone of flow establishment the temperature profile will transit from the form given by Eq. (75) to that given by Eq. (2), while the velocity distribution will transit from Eq. (76) to Eq. (1). The details will be governed largely by the free-shear turbulence generated by shear stresses between discharged and ambient water.

The length of the zone of flow establishment $(x_o)$ for buoyant surface jets cannot be measured as easily as for non-buoyant ones, because buoyancy induces an acceleration in the longitudinal direction near the outlet which masks the end of the zone of flow establishment. To obtain information on $(x_o)$ one must therefore examine velocity distributions rather than centerline velocities. Figure 33 illustrates some of the velocity distributions obtained by computer plotting. For the evaluation of $x_o$ these are not accurate enough due to interpolation errors. Instead, graphs of actually measured velocities such as are given in Figs. 29 through 34 of Ref. [53] must be used. These measurements, all of which refer to strongly buoyant jets, indicate that it takes less than six times the width of the outlet channel to develop a horizontal velocity profile and less than six times the depth to develop a vertical velocity profile. The measurements were not sufficiently detailed to enable evaluation of a dependence between densimetric Froude number at the discharge $F_o$, as defined in Eq. (45), and $x_o$. It appears that for experiments 215, 207, 214, and 211, summarized in Table 1, $x_o$ was very approximately equal to three times the outlet width.

The mechanism which produces this result is probably not horizontal momentum transfer by eddy diffusivity, but rather a secondary effect of the buoyancy-induced horizontal currents shown in Fig. 28. The currents move high-momentum fluid from the center of the plume toward the edges, where the shallow thickness of the flow activates shear stresses in horizontal planes which reduce the momentum of the flow rapidly. The same horizontal transport mechanism applies in part also to heat. Thus the zone of flow establishment for velocity and temperature is shortened by buoyancy effects, as stated earlier.

From some of the data on spreading angles at the outlet presented in Fig. 39 it might be gathered that buoyancy effects become small if $F_o > 10$. Zones of flow establishment for temperature may be somewhat longer than those for velocity. All the above results apply to straight jets rather than curved ones.

Once the length of the zone of flow establishment has been determined, an approximate analytical treatment of the zone of flow establishment can be given analogous to that found in treatments of non-buoyant jet

flows [37]. For high values of $F_o$ ($F_o > 10$ perhaps) results regarding the flow rate and the dimensions of the jet at the end of the zone of flow establishment can be taken directly from the literature [37]. In the intermediate range ($1 < F_o < 10$) the velocity distribution can be approximated by a function of the form

$$u^*(s,r,z) = u^*(0,0,0) = U_o \tag{78}$$

for the inner core region ($r < w/2$ and $z < d$) and

$$u^*(s,r,z) = u^*(0,0,0) \exp\left[\frac{-(z-d)^2}{2a^2}\right] \exp\left[\frac{-(r-w)^2}{2b^2}\right] \tag{79}$$

for the turbulent diffusion region ($r > w/2$ and $z > d$). The dimensions of the core region can be assumed to decrease linearly with distance such that

$$\frac{w}{w_o} = 1 - \frac{x}{x_o} \tag{80}$$

and

$$\frac{d}{d_o} = 1 - \frac{x}{x_{o,d}} \tag{81}$$

where $x_o$ and $x_{o,d}$ are the lengths of the zone of flow establishment for width and depth, respectively, for velocity. Turbulent entrainment in the zone of flow establishment is different from that in fully developed flow. In a turbulent, non-buoyant, circular jet the entrainment coefficient varies linearly from virtually zero to $K = 0.059$ over the length of the zone of flow establishment. A similar variation can be introduced for the zone of flow establishment for buoyant surface jets.

In the total picture the computational scheme developed for fully developed jets can be extended to include a zone of flow establishment. For very low densimetric Froude numbers (tentatively $F_o < 3$) the zone of flow establishment is very short and the computational scheme developed is applicable without further extension. For high densimetric Froude numbers (tentatively $F_o > 10$) the zone of flow establishment can be treated as non-buoyant. Only in the intermediate range would the extension of the analytical model as presented be of value.

PART II: The Two-Dimensional Buoyant Surface Jet and the Internal Hydraulic Jump

by

H. Stefan

and

N. Hayakawa

August 1971

## ABSTRACT

A theoretical and experimental study of the two-dimensional flow of heated water from a channel into a deep reservoir filled with cold water was made. Only flows producing a dilution of warm water by entrainment of cold water were investigated. These flows consisted of a mixing zone near the outlet followed downstream by a stratified flow. The outlet flow characteristics, the type of downstream control, and the geometry of the transition were identified as the essential controlling parameters for the entrainment. The amount of vertical entrainment in the mixing zone at the outlet was calculated and measured. The flow in the mixing zone where the entrainment is produced was found to be a combination of a buoyant half jet with an inverted internal hydraulic jump. The simultaneous presence of both inertial and buoyant forces was responsible for this occurrence. Theoretical and experimental results show that substantial dilution occurred in the outlet mixing zone, but actual rates of entrainment were quite sensitive to changes in flow conditions.



This report was submitted in fulfillment of Project Number 16130 FSU under the sponsorship of the Water Quality Office, Environmental Protection Agency.

CONTENTS

LIST OF FIGURES

LIST OF FIGURES (Cont'd)

## LIST OF SYMBOLS AND UNITS

| | |
|---|---|
| $E_o$ | Initial energy flux of warm water discharge [lb ft/sec] |
| $E_1$ | Final energy flux after mixing [lb ft/sec] |
| $E_2$ | Additional energy flux due to entrainment [lb ft/sec] |
| $F'_o$ | Initial outlet densimetric Froude number [-] |
| $F'_1$ | Final densimetric Froude number [-] |
| $F'_{om}$ | Minimum possible outlet densimetric Froude number for given $H_1$ [-] |
| $g$ | Acceleration of gravity [ft/sec$^2$] |
| $h_o$ | Initial depth of warm water discharge [ft] |
| $h_1$ | Final depth of warm water layer in reservoir after mixing [ft] |
| $h_2$ | Depth of cold water layer [ft] |
| $H_1$ | $h_1/h_o$ [-] |
| $H_2$ | $h_2/h_o$ [-] |
| $\ell$ | Approximate length of mixing zone [ft] |
| p(s) | Static pressure on beach [lb/ft$^2$] |
| $q_o$ | Initial volumetric warm water flux [ft$^3$/sec ft] |
| $q_1$ | Final volumetric warm water flux after mixing [ft$^3$/sec ft] |
| $q_2$ | Cold water volumetric flux [ft$^3$/sec ft] |
| Q | $\frac{q_1}{q_o}$ , flux (entrainment) ratio [-] |
| r | $\frac{\Delta\rho_o}{\rho_2}$ , density deficit ratio [-] |
| s | Coordinate along beach [ft] |
| $u_o$ | Average discharge velocity [fps] |
| $u_1$ | Average flow velocity after mixing [fps] |
| $u_2$ | Average cold water flow velocity [fps] |

$w_1$ Rise of water surface between end of mixing zone and outlet [ft]

$x$ Horizontal coordinate, starting at outlet cross section [ft]

$z$ Vertical coordinate, starting at water surface [ft]

$\alpha_o, \alpha_1, \alpha_2$ Energy flux correction coefficients

$\beta_o, \beta_1, \beta_2$ Momentum flux correction coefficients

$\gamma$ Slope of beach

$\Delta E$ $E_o - E_1$, energy loss in mixing zone

$\Delta\rho_o$ $\overline{\rho}_2 - \rho_o$, density differential between warm and cold water at point of discharge [slugs/ft$^3$]

$\Delta\rho_1$ $\overline{\rho}_2 - \overline{\rho}_1$, density differential between warm and cold water after mixing [slugs/ft$^3$]

$\rho_o$ Initial (discharge) warm water density [slugs/ft$^3$]

$\rho_1$ Final warm water density after mixing [slugs/ft$^3$]

$\rho_2$ Cold water density [slugs/ft$^3$]

$\tau(s)$ Shear stress along beach [lb/ft$^2$]

## SECTION I

## CONCLUSIONS

Theoretical analysis and experimental verification of vertical mixing near a two-dimensional, heated water surface outlet were made. As the heated water is discharged on top of cold water it may entrain and become mixed with cold water near the outlet. If sufficient depth in the receiving reservoir is provided, a stratified flow will result. The following conclusions were reached:

1. The type of flow near the outlet and the amount of entrainment depend on three groups of parameters:

   a. The outlet flow conditions and in particular the outlet densimetric Froude number

   b. The control of the stratified flow from downstream, in particular the depth or thickness of the warm water layer

   c. The geometry of the transition from the outlet channel to the reservoir, in particular the depth of the reservoir and the slope of the beach.

2. The mixing zone near the outlet may be a buoyant half-jet followed by an internal hydraulic jump, a free internal hydraulic jump or a submerged outlet flow as defined in Ref. [2]* The conditions for the occurrence of these flows and the associated entrainment ratios have been derived and are shown in Figs. 4a, 4b, and 4c and 5a, 5b, and 5c for a vertical beach.

3. Theoretical results were derived for a vertical beach face ($90^\circ$ slope) and agree reasonably well with measurements. There is experimental evidence that the results are insensitive to changes in slope angle if the angle varies in the range $23^\circ < \alpha < 90^\circ$.

4. A flat beach of the order of $5^\circ$ or less was observed to inhibit the formation of any surface jet or internal jump and to prevent any mixing.

5. A free mixing internal hydraulic jump requires an outlet densimetric Froude number $F_o' > 2.25$ or $H_1 > 2.73$ if the reservoir has infinite depth. As the reservoir depth is reduced these limiting values shift toward 1.0. A free internal mixing hydraulic jump is characterized by the separation of the interface (thermocline) from the bottom of the outlet channel and the existence of an internal inverted roller.

---

*References for Part II are listed on page II-55.

6. A limiting densimetric Froude number for the onset of submergence of the outlet was established and called $F'_{om}$. It was shown to be a function of the dimensionless warm water depth $H_1$ and the cold water depth $H_2$ (Figs. 4a, 4b, and 4c and Figs. 5a, 5b, and 5c). If an actual $F'_o$ is less than $F'_{om}$, the outlet will be internally submerged.

7. Theoretical analysis predicts that the dimensionless downstream depth $H_1$ of the free mixing internal hydraulic jump has an upper and a lower bound. The upper bound is associated with $F'_{om}$, the lower bound with $Q = 1$.

8. The rate of entrainment of cold water by the warm water was found to be very sensitive to changes in both the outlet densimetric Froude number $F'_o$ and the downstream depth $H_1$, as illustrated by Fig. 18. The achievement of prescribed entrainment rates will therefore require accurate operational controls.

9. Changes in water surface elevation over the length of the mixing zone are quite small. They are, however, essential in the control of buoyancy effects. Consequently, the assumption of a horizontal water surface cannot be accepted in the analysis of the phenomenon.

10. Theoretically it is possible to entrain any amount of cold water, but Figs. 5a, 5b, and 5c indicate that dilution ratios beyond $Q = 2$ (one part warm water to one part cold water) may not be very practical.

11. Lengths of the mixing zone for non-submerged outlets were measured and reported in Fig. 19. In first approximation the length changes linearly with the densimetric outlet Froude number $F'_o$.

12. Turbulent entrainment and mixing by the buoyant jet-internal hydraulic jump mechanism requires considerably less energy than the use of conventional diffuser arrangements.

## SECTION II

## RECOMMENDATIONS

It is recommended that the results presented herein be considered for application to large-scale heated water mixing basins and cooling ponds. The internal hydraulic jump appears to be a mechanism which can be produced easily. It is associated with substantial mixing between warm and cold water resulting in lower discharge water temperatures. Admittedly the rate of entrainment is quite sensitive to changes in the flow conditions, but adequate control of the outlet flow should be possible.

It is also recommended that the study undertaken for a two-dimensional flow herein be extended to the three-dimensional situation.

## SECTION III

## INTRODUCTION

One of the many problems associated with "thermal pollution control" is the rate of dilution of heated water discharges by turbulent mixing with ambient water. Accurate water temperature predictions in the vicinity of cooling water outfalls of power generating plants require among other things an understanding of the flow and mixing processes which occur at or near the source of discharge. Frequently the outlet is an open channel discharging the heated water at the surface of the receiving body of water as shown in Fig. 1. Because such a discharge has not only momentum but also buoyancy, a variety of flows associated with differing amounts of entrainment and mixing may occur. A classification of these flows for a two-dimensional situation has been given in Refs.[1] and [2]. The classification is similar to that given for water surface profiles in textbooks for open channel flow. It hinges on the recognition of the fact that the flow pattern produced by a two-dimensional heated water surface discharge is controlled by the discharge characteristics at the outlet as well as by the downstream flow conditions. Downstream flow control is effective and determines, for example, the maximum thickness of the heated water layer floating on top of the cold water. This downstream control is physically imposed either by a structure (i.e. gate or weir), by a particular geometry of the channel (i.e. sudden channel expansion), or, in the absence of all of these, by the cooling process on the water surface. Near the outlet the upstream controlled flow from the channel joins the downstream controlled internal flow in the receiving body of water. It is at this transition that a variety of flows are observed. A classification and explanation of such two-dimensional patterns was given in Ref. [2] under the assumption of a constant flow rate in the heated water layer. This is well justified for some types of discharge but not for others. A discussion by Wilkinson [3] extended the original paper but excluded free surface effects and finite depths of the receiving reservoir.

This study is concerned with the vertical entrainment and mixing between warm and cold water which occurs in the transition region near the outlet, particularly when the flow resembles that of a buoyant turbulent jet or an internal hydraulic jump. Experiments show that in the two-dimensional situation the initial jet-type flow from the outlet channel usually produces some sort of internal roller at the interface. That portion of the flow associated with the roller is called an irternal mixing hydraulic jump. Between the outlet channel and the roller the flow is strictly a jet flow (half-jet). If the upstream toe of the internal roller reaches the outlet channel, the outlet begins to be internally submerged as schematically shown in Fig. 2. For more details on the flow patterns described the reader may refer to Refs. [1] and [2].

The internal hydraulic jump was previously analyzed by Yih and Guha [4] under the assumption that there is no entrainment across the interface separating the two layers. The momentum equations of the two-layered,

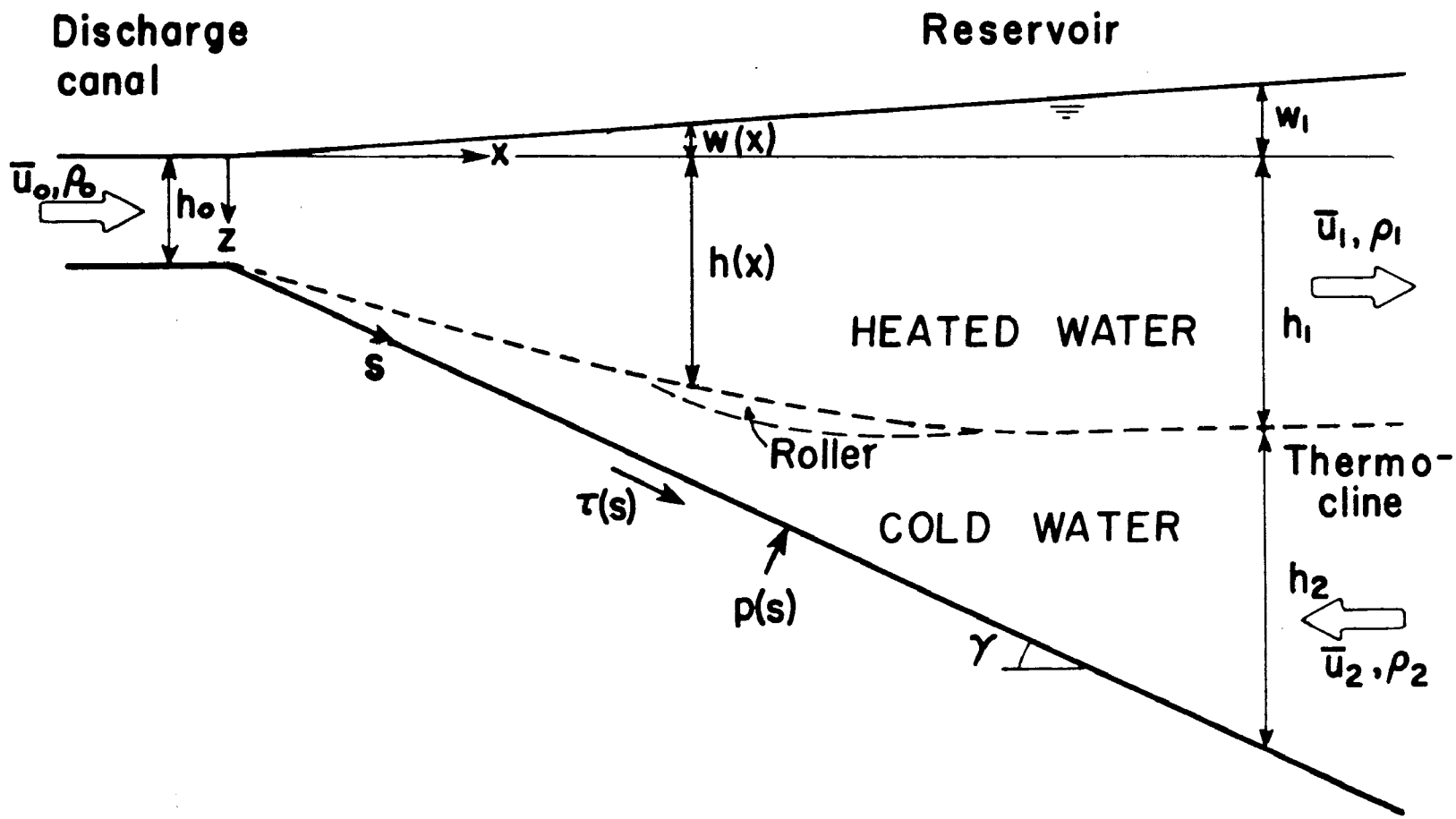


Fig. 1 - Definition Sketch - Two-dimensional, Heated Water Surface Discharge

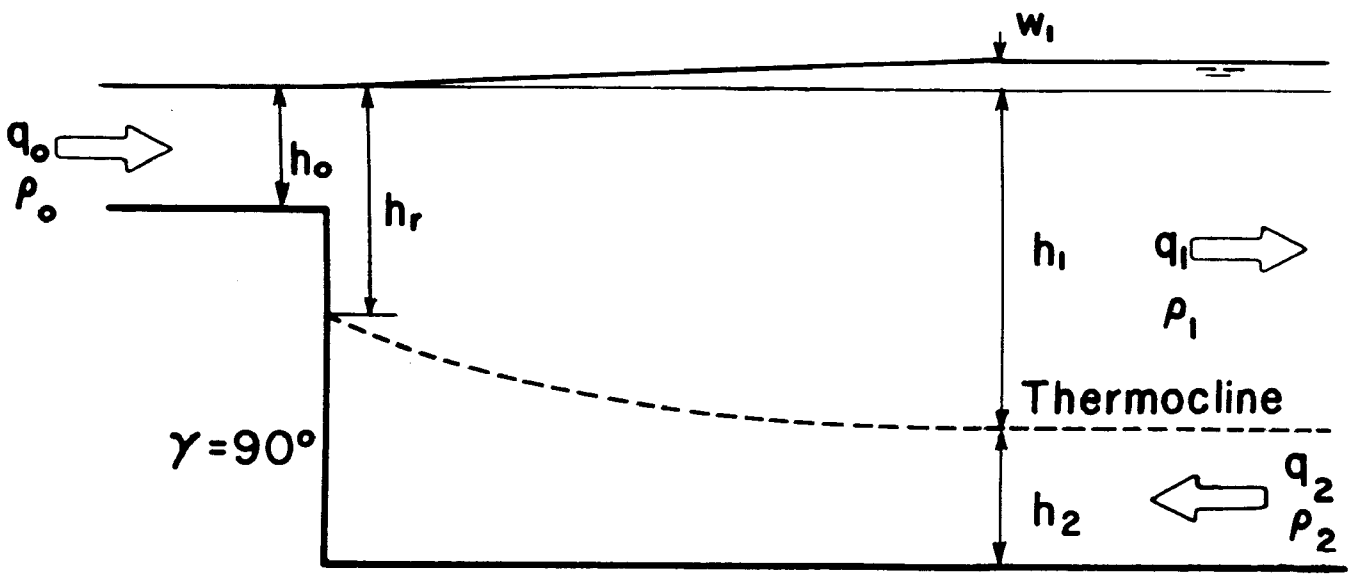


Fig. 2 - Definition Sketch - Internally Submerged Outlet Channel

non-miscible flow system were derived and used to demonstrate the existence of several solutions. A good correlation between experimental data and theoretical predictions for cases with one layer in motion and the other at rest was demonstrated. Hayakawa [5] gave a mathematical refinement of the solutions relating to their physical interpretation.

In the case of hot water flowing on top of cold water a certain amount of flow entrainment exists from one layer to another across the interface, resulting in a more complicated situation than was investigated by Yih and Guha [4]. A more recent short theoretical discussion on the bounds of possible downstream depths of mixing internal hydraulic jumps was given by Wilkinson [3].

In this study the one-dimensional momentum equation for the two-layered transition region from the channel to the downstream stratified flow is given. Theoretical analysis of this equation includes the internal hydraulic jump and the buoyant jet type flow. Laboratory measurements of the vertical entrainment are compared with the theoretical predictions.

## SECTION IV

## BASIC EQUATIONS

The geometrical boundary conditions of the flow problem investigated are shown in Fig. 1. The flow is from an outlet channel into a reservoir, or more precisely into a surface layer (epilimnion) which must form as heated water continues to be discharged under steady flow conditions. The epilimnion is separated from the colder reservoir water by a thermocline which will be replaced by a stable interface in the ensuing calculations. The situation is thus approximated by a two-layered flow. Between the outlet and the stable thermocline there is frequently a mixing zone through which colder water is entrained from beneath. Fig. 3 shows a schematic streamline pattern. Since the flow in both layers is usually a turbulent one, the entrained cold water is rapidly mixed with the upper layer.

The flow in the entrainment zone can be considered either as a buoyant surface jet or as an internal mixing hydraulic jump. Submerged jets and hydraulic jumps can be analyzed using the impulse-momentum theorem. The problem is essentially a hydrodynamic one. Only convective turbulent heat transfer is considered. Conduction, radiation, and evaporation effects are ignored because of the usually short residence time the water is in the mixing zone.

The continuity, momentum, and energy equations can be written for a control volume limited by the following lines: a vertical cross-section through the outlet channel upstream, a vertical cross-section through both layers in the reservoir a short distance downstream from the mixing zone, the free water surface, and the bottoms of channel and reservoir.

The steady flow continuity equation is

$$\rho_o \, q_o + \overline{\rho_2} \, q_2 = \overline{\rho_1} \, q_1 \tag{1}$$

where $\rho_o$, $\overline{\rho_1}$, and $\overline{\rho_2}$ designate the mean densities and $q_o$, $q_1$, and $q_2$ designate the flow rates in the outlet cross section, the warm water layer and the cold water layer downstream, respectively.

The volumetric flow rates are

$$q_o = \int_0^{h_o} u_o \, dz = \overline{u_o} \, h_o \tag{2a}$$

$$q_1 = \int_{+w_1}^{h_1} u_1 \, dz = \overline{u_1}(h_1 - w_1) \tag{2b}$$

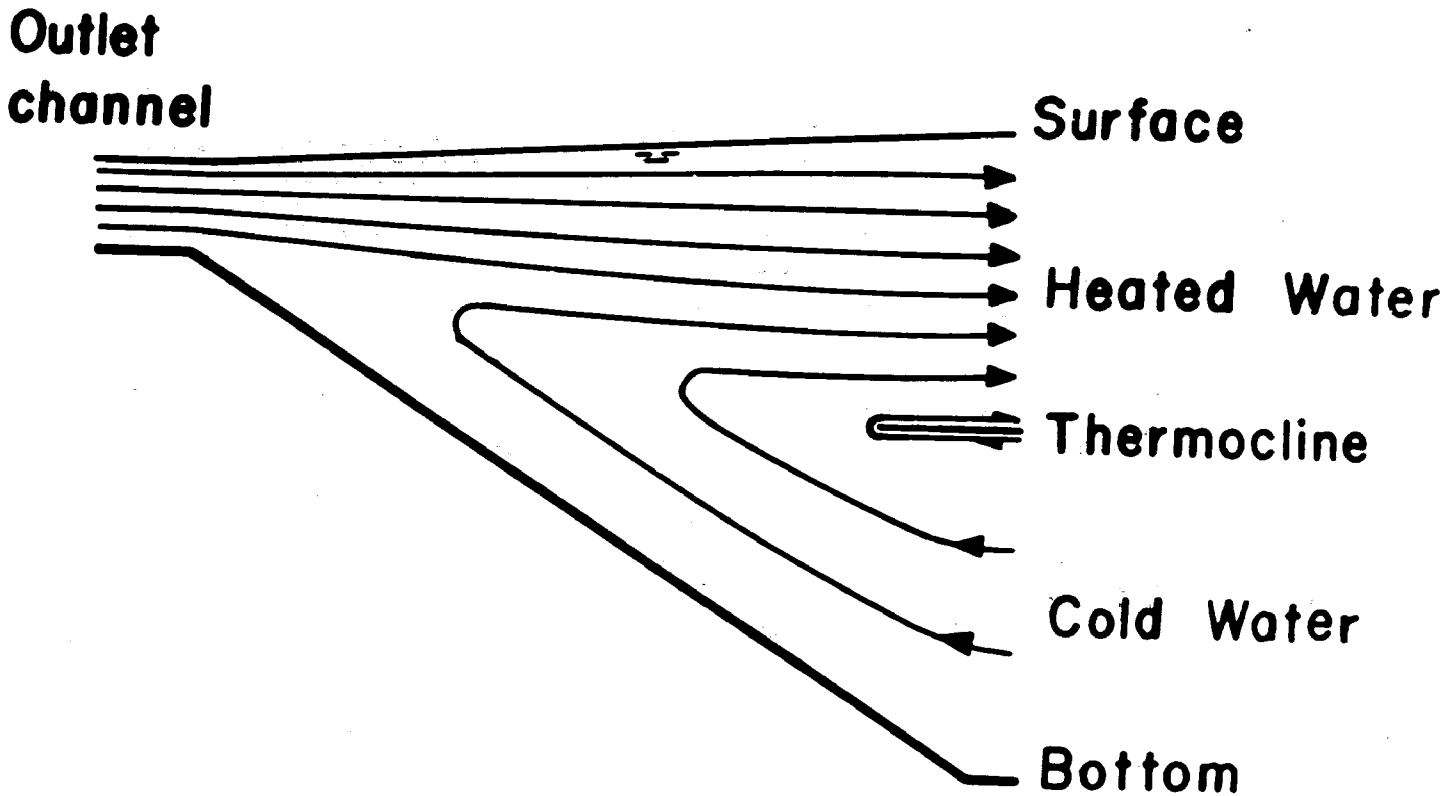


Fig. 3 - Schematic Streamline Pattern Near Outlet

$$q_2 = \int_{h_1}^{h_2+h_1} u_2 \, dz = \overline{u_2} \, h_2 \tag{2c}$$

$u_o$, $u_1$, and $u_2$ designate velocities and $h_o$, $h_1 - w_1$, and $h_2$ designate depths at the outlet and in the warm and cold water layers, respectively. Since the flow is considered incompressible, the volumetric flow rates give

$$q_o + q_2 = q_1 \tag{3}$$

From the previous equations a density deficiency flux equation can be derived:

$$q_o \, \Delta\rho_o = q_1 \, \Delta\rho_1 \tag{4}$$

where $\Delta\rho_o = \overline{\rho_2} - \rho_o$ and $\Delta\rho_1 = \overline{\rho_2} - \overline{\rho_1}$ .

The impulse-momentum equation is

$$\beta_1 \, \overline{\rho_1} \, \overline{u_1}^2 \, (h_1 - w_1) - \beta_o \, \rho_o \, \overline{u_o}^2 \, h_o + \beta_2 \, \overline{\rho_2} \, \overline{u_2}^2 \, h_2 = P_s + F_s + P_o + P_1 \tag{5}$$

where $\beta_1$, $\beta_o$, and $\beta_2$ are momentum correction coefficients; $P_s$, $P_o$, and $P_1$, are static pressure forces; and $F_s$ is a force due to shear stress along the sloping beach. Further definitions are:

$$P_s = \sin\gamma \int_0^{\ell} p(s) \, ds \tag{6a}$$

where $p(s)$ is the static pressure distribution on the sloping beach

$$F_s = \cos\gamma \int_0^{\ell} \tau(s) \, ds \tag{6b}$$

where $\tau(s)$ is the shear stress distribution on the sloping beach,

$$P_o = \frac{1}{2} g \, \rho_o \, h_o^2 \tag{6c}$$

$$P_1 = -\frac{1}{2} g \overline{\rho_1} (h_1 - w_1)^2 - g \overline{\rho_1} (h_1 - w_1) h_2 - \frac{1}{2} g \overline{\rho_2} h_2^2 \quad (6d)$$

The energy fluxes into or out of the control volume are

$$E_o = \frac{1}{2} \alpha_o \rho_o \overline{u_o}^2 q_o \quad (7a)$$

$$E_1 = \left\{\frac{1}{2} \alpha_1 \overline{\rho_1}\, \overline{u_1}^2 + \frac{1}{2} g \overline{\rho_1} (h_1 - w_1) - \frac{1}{2} g \overline{\rho_1} (h_1 + w_1)\right\} q_1$$
$$= \left[\frac{1}{2} \alpha_1 \overline{\rho_1}\, \overline{u_1}^2 - g \overline{\rho_1} w_1\right] q_1 \quad (7b)$$

$$E_2 = \left\{\frac{1}{2} \alpha_2 \overline{\rho_2}\, \overline{u_2}^2 + \left[g \overline{\rho_1} (h_1 - w_1) + \frac{1}{2} g \overline{\rho_2} h_2\right]\right.$$
$$\left. -g \overline{\rho_2} (h_1 + \frac{1}{2} h_2)\right\} q_2 = \left\{\frac{1}{2} \alpha_2 \overline{\rho_2}\, \overline{u_2}^2\right. \quad (7c)$$
$$\left. -g \Delta\rho_1 h_1 - g \overline{\rho_1} w_1\right\} q_2$$

The water surface at the outlet was taken as the datum level.

Since the flow within the control volume is highly turbulent, an energy loss of substantial magnitude must be expected. It can be defined as

$$\Delta E = E_o = E_2 - E_1 \quad (8)$$

but its value cannot be predicted <u>a priori</u>.

The control valume as used in the above equations comprises both the heated water and the cold water layers.

## SECTION V

## THEORETICAL RESULTS

The set of equations derived in the previous section cannot be solved, for example to find the unknown downsteam flow rate $q_2$, without information on the static pressure and shear stress distributions along the sloping beach. Such information, it appears, requires the solution of the equations of motion for the described boundary conditions. Since the flow within the control volume is a highly turbulent shear flow, partly affected by buoyancy, a great many assumptions are necessary to find $\tau(s)$ and $p(s)$.

Instead of proceeding in this direction it was decided to examine two special cases for which the static pressures and shear stresses on the beach could be found more easily: very steep and very flat beaches.

### Steep Beach

On a $90^{\circ}$ beach the shear stresses caused by the entrained cold water flow are likely to be small and directed vertically. As the slope angle goes from zero to $90^{\circ}$, the shear force $F_s$ in the momentum equation therefore goes to zero. At the same time the static pressure force $P_s$ is likely to become a nearly hydrostatic force, at least for the flow schematically shown in Fig. 1, because flow velocities along the beach slope become very small.

$$P_s = [g\,\rho_o\,h_o + \tfrac{1}{2}\,g\,\overline{\rho_2}\,(h_1 + h_2 - h_o)]\,(h_1 + h_2 - h_o) \qquad (9)$$

With these simplifications, substitution of Eqs. (2a), (2b), and (2c) in the momentum equation (5) yields the relationship

$$\frac{\beta_1\,\overline{\rho_1}\,q_1^2}{h_1}\,(1 - \frac{w_1}{h_1})^{-1} - \frac{\beta_o\,\rho_o\,q_o^2}{h_o} + \frac{\beta_2\,\overline{\rho_2}\,q_2^2}{h_2} = \tfrac{1}{2}\,g\,\rho_o\,h_o(2h_1$$

$$+ 2h_2 - h_o) + \tfrac{1}{2}\,g\,\overline{\rho_2}(h_1 - h_o)(h_1 - h_o + 2h_2) - \tfrac{1}{2}\,g\,\overline{\rho_1}$$

$$(h_1 - w_1)(h_1 - w_1 + 2h_2) \qquad (10)$$

For a given set of outflow conditions ($q_o$, $h_o$, $\rho_o$) and a specific downstream control ($h_1$, $h_2$) Eqs. (3), (4), and (10) still contain four unknowns, namely $q_2$, $q_1$, $w_1$ and $\rho_1$. The conservation of volume and mass equations (Eqs. 3 and 4) may be used to remove $q_2$ and $\rho_1$ from Eq. (10),

but one additional condition is needed for a complete solution. This relationship grows out of the following considerations.

The buoyant surface jet is in many respects similar to the turbulent, fully submerged non-buoyant half-jet, but there are also two significant differences: the presence of a free water surface and buoyant forces. The non-buoyant turbulent submerged jet is generally assumed to develop in a hydrostatic pressure field and the flow leaves the pressure field unaffected. It is believed that this hypothesis, well supported by experimental evidence, also applies to the buoyant surface half-jet discharged over a steep beach. This means essentially that the static pressure at all points located in a horizontal plane in the cold water layer must be the same. The following equation is then obtained:

$$g\, h_o\, \rho_o + g(h_1 - h_o)\overline{\rho_2} = g(h_1 - w_1)\overline{\rho_1}$$

or

$$\frac{w_1}{h_o} = \frac{\dfrac{q_1}{q_o} - \dfrac{h_1}{h_o}}{\dfrac{\overline{\rho}_2}{\Delta\rho_o}\dfrac{q_1}{q_o} - 1} \tag{11}$$

when Eq. (4) is substituted.

Using Eq. (11), Eq. (10) was reduced to the following dimensionless form:

$$2\beta_2 F_o'^2 =$$

$$\frac{H_2(H_1 - r)[(H_1 - r)^2 - (1 - r)(Q - r)]}{(Q - r)\left[\dfrac{\beta_o}{\beta_2}(1 - r)H_2 - (Q - 1)^2\right]\left[H_1 - r - \dfrac{\beta_1 H_2 (Q - r)^2}{\beta_o(1-r) H_2 - \beta_2(Q-1)^2}\right]} \tag{12}$$

in which $F_o'$ is the densimetric Froude number defined as

$$F_o' = q_o\, h_o^{-1} \left(\frac{\Delta\rho_o}{\overline{\rho}_2} g\, h_o\right)^{-\frac{1}{2}}$$

and $Q = q_1/q_o$, $H_1 = h_1/h_o$, $H_2 = h_2/h_o$ and $r = \Delta\rho_o/\overline{\rho_2}$. Because the free water surface is nearly horizontal, it is tempting to assume $w_1 = 0$, making the use of Eq. (11) superfluous. This alternate solution

will also be pursued, although it is not likely to yield as good a result as Eq. (12). When Eq. (10) is reduced to the dimensionless form under the assumption of a horizontal water surface or $w_1 = 0$ one obtains

$$\beta_2 F_o'^2 = \frac{H_2 H_1 [H_1^2 + 2(H_2 - Q)H_1 + (1 - 2H_2)Q]}{2Q[\{(Q-1)^2 - \frac{\beta_o}{\beta_2}(1-r) H_2\} H_1 + \frac{\beta_1}{\beta_2} H_2 Q(Q-r)]} \qquad (13)$$

Conditions which satisfy this equation will be compared with those which satisfy Eq. (12). The density differential $r$ is a small positive quantity within the context of this work. It is of the order $10^{-3}$ for a temperature difference of $5 \sim 10^{\circ}$F. $H_1$ and $H_2$ are positive quantities. Because the flow under consideration is two-dimensional, $H_1$ is expected to exceed unity. The ratio $Q$ of flow rates in the warm layer, measured downstream and upstream from the internal jump, is equal to or greater than unity by definition of the problem.

Figs. 4a, 4b, and 4c show plottings of $H_1$ versus $F_o'$ as obtained from Eq. (12) for three reservoir depths $H_2 = \infty$, 8 and 1, respectively. In Figs. 5a, 5b, and 5c the same results are displayed in the form of $Q$ versus $F_o'$ for the same values of $H_2$, respectively. Comparison of Figs. 4a and 4b (or Figs. 5a and 5b) indicates that the flow is not very sensitive to a change in $H_2$ (the dimensionless cold water layer thickness) as long as $H_2$ is considerably larger than one. Under this condition an increase in $H_2$ produces a small increase in the rate of entrainment $Q$. $\beta_o = \beta_1 = \beta_2 = 1.0$ was assumed in the numerical evaluation.

Figs. 4a, 4b, and 4c further indicate that for a given $F_o'$ there exist two $H_1$ values that belong to the same $Q$. The two solutions have different physical meaning. The larger of the two $H_1$ values refers to the internal hydraulic jump, the smaller to a buoyant jet. This can be seen by examination of the lines representing constant downstream densimetric Froude numbers, $F_1'$, which are defined as

$$F_1' = \frac{\bar{u}_1}{\sqrt{\frac{\Delta\rho_1}{\rho_2} g(h_1 - w_1)}} = F_o' \left( \frac{Q}{(H_1 - \frac{w_1}{h_o})} \right)^{\frac{3}{2}} \qquad (14)$$

and which are also plotted in Figs. 4a, 4b, and 4c. It can be shown that the minimum value of $F_o'$ for any curve $Q = \text{const}$ in Figs. 4a, 4b, and 4c corresponds to a downstream densimetric Froude number $F_1'$ equal to unity, which by analogy to the ordinary open channel hydraulic jump may be considered as representative of an internally critical flow

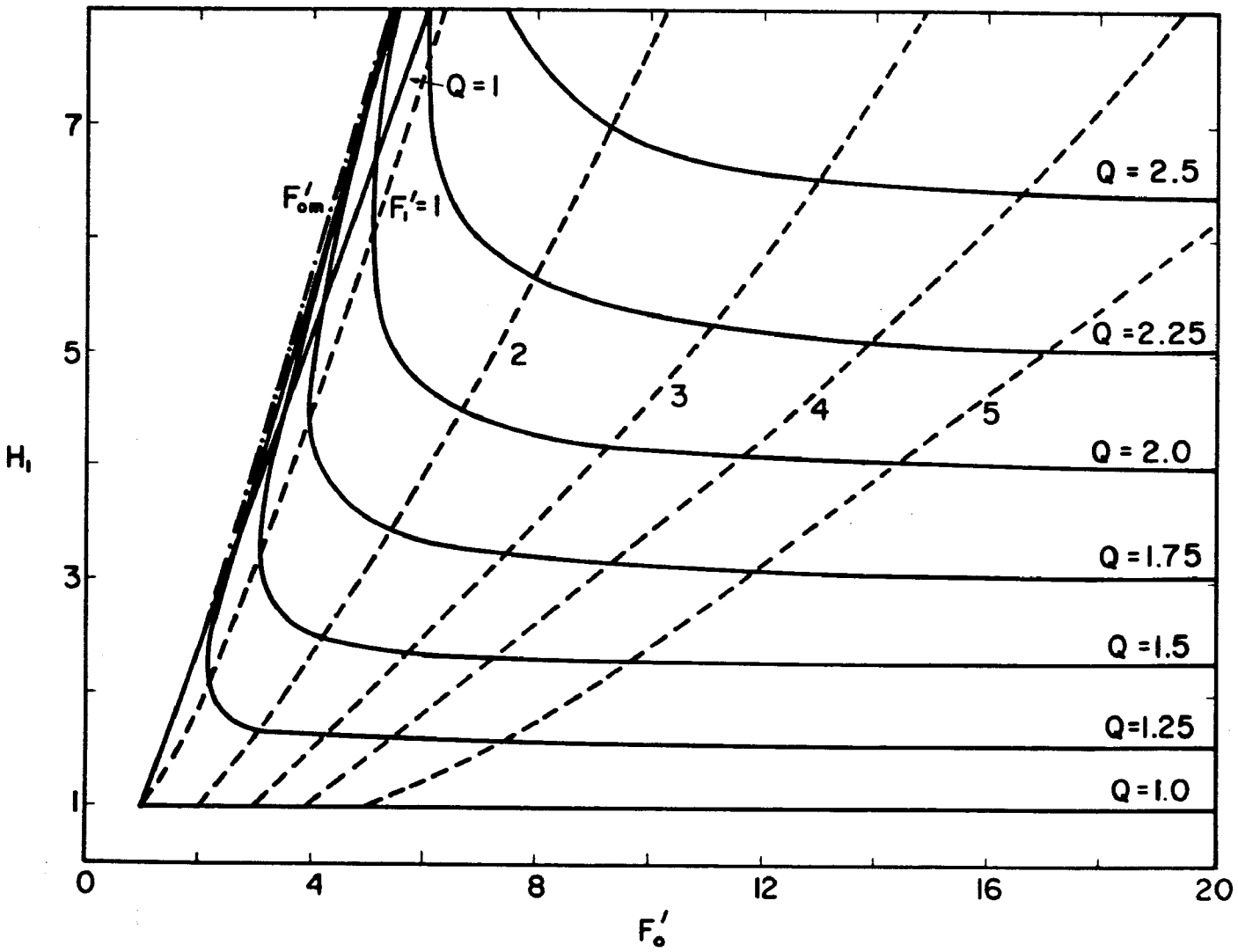


Fig. 4a - $H_1$ versus $F_o'$ for $H_2 = \infty$

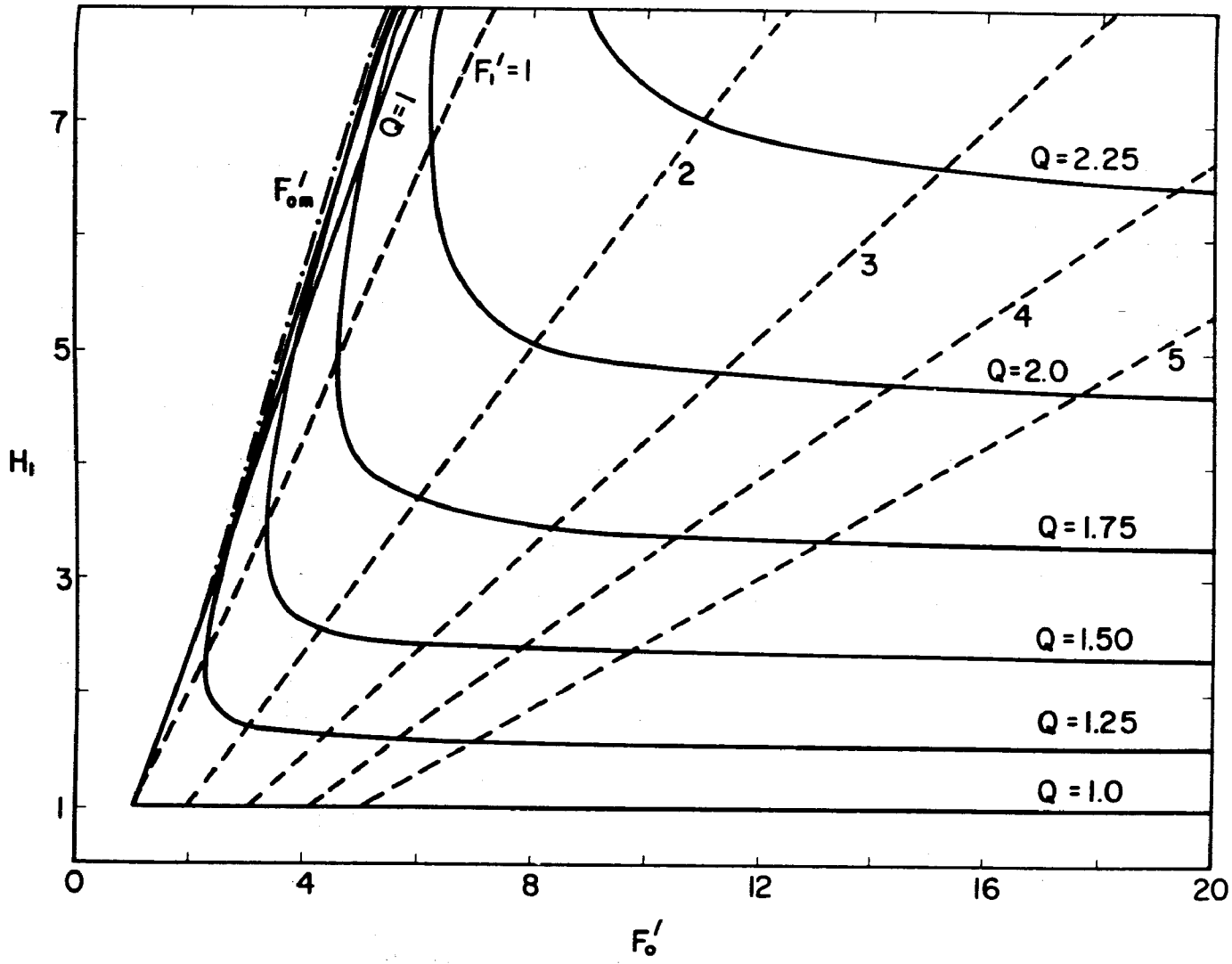


Fig. 4b - $H_1$ versus $F_o'$ for $H_2 = 8$

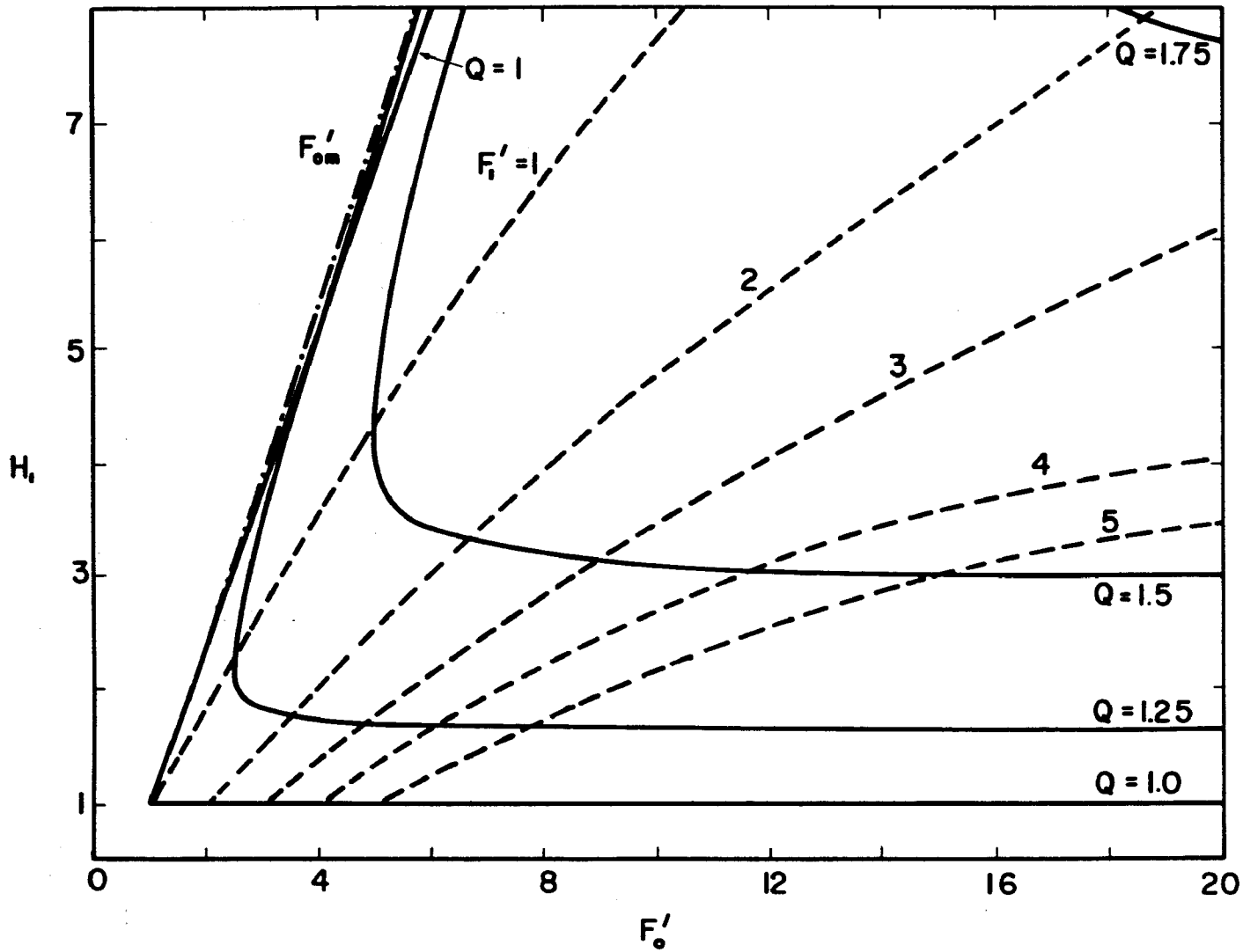


Fig. 4c - $H_1$ versus $F_o'$ for $H_2 = 1$

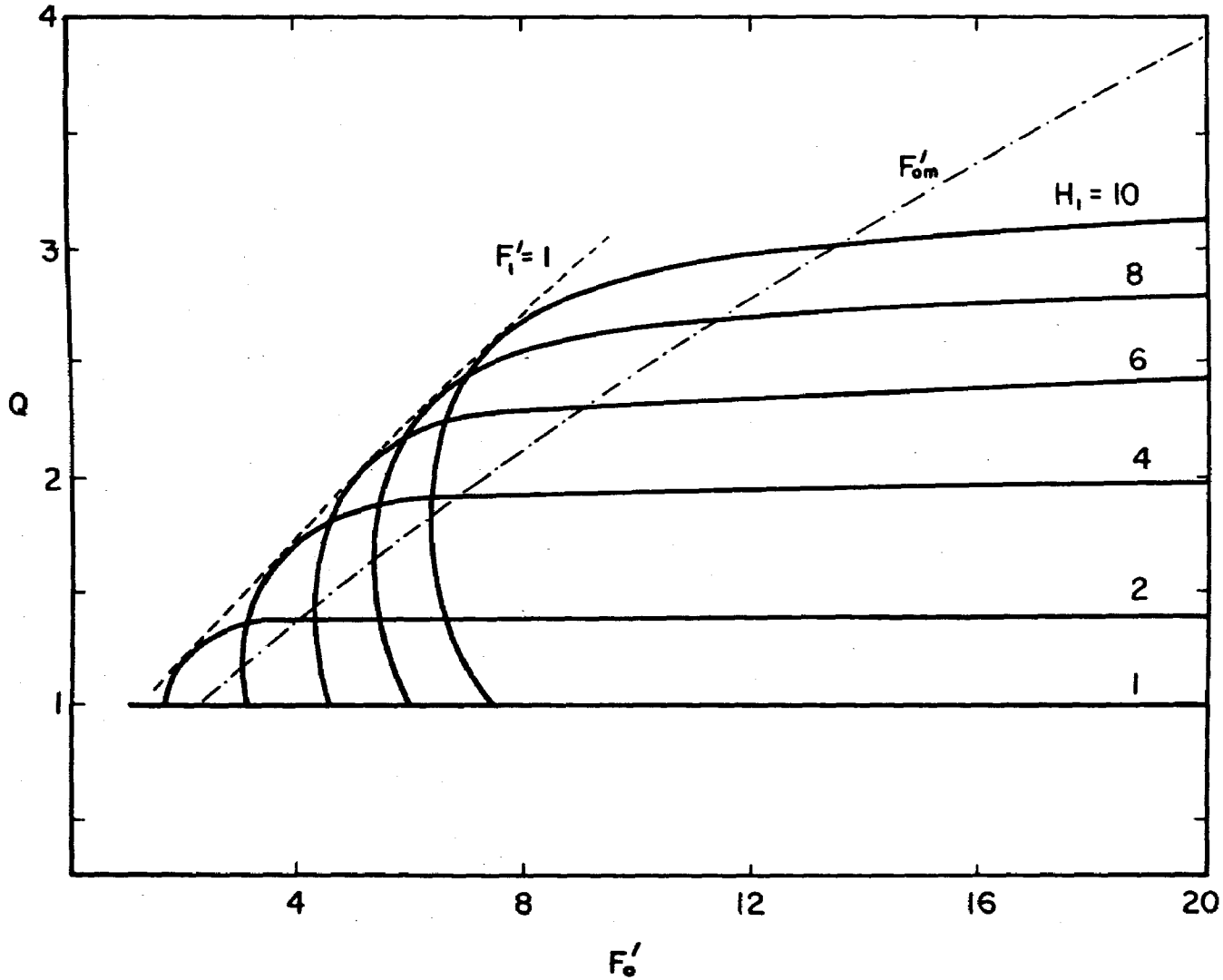


Fig. 5a - Q versus $F_o'$ for $H_2 = \infty$

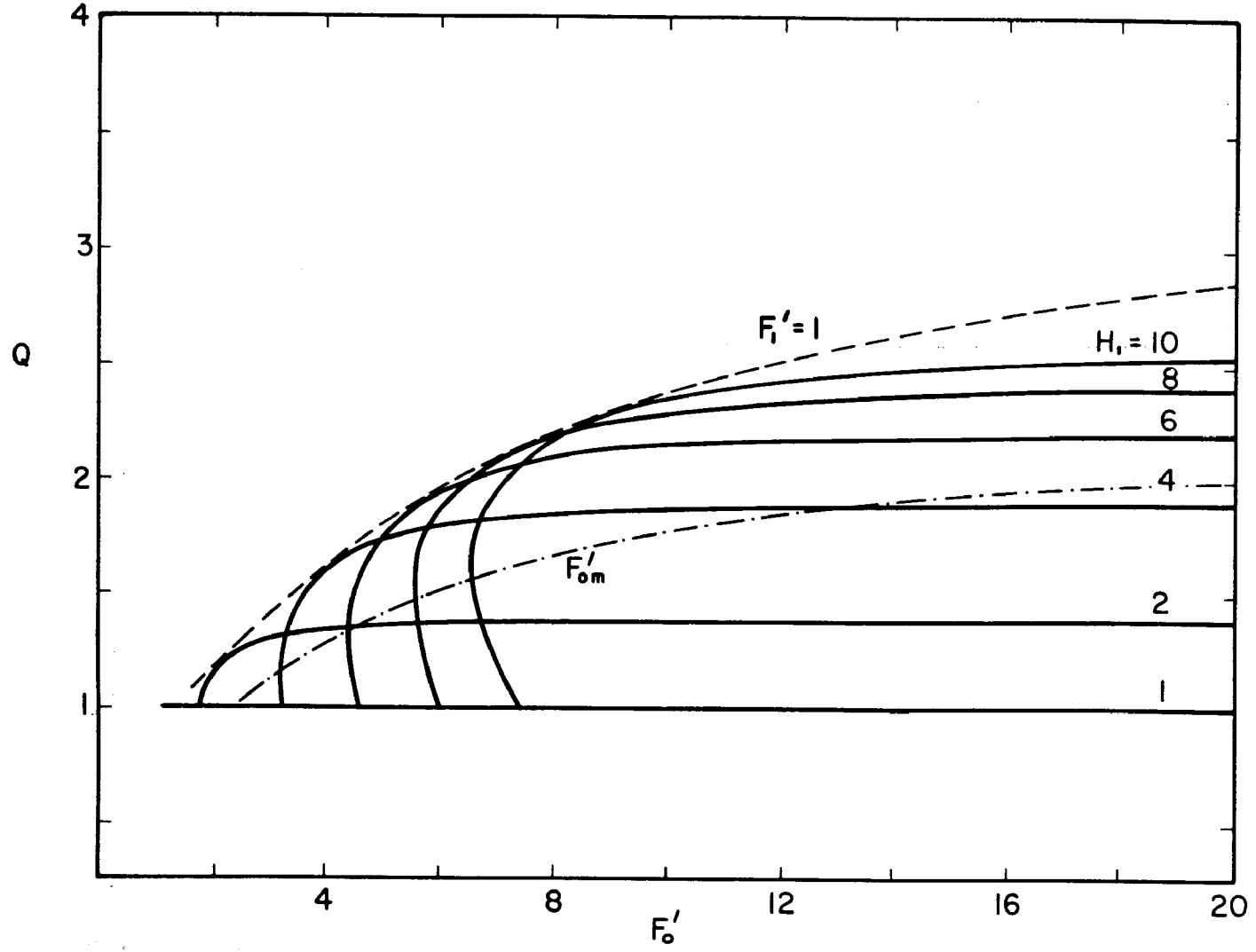


Fig. 5b - Q versus $F_o'$ for $H_2 = 8$

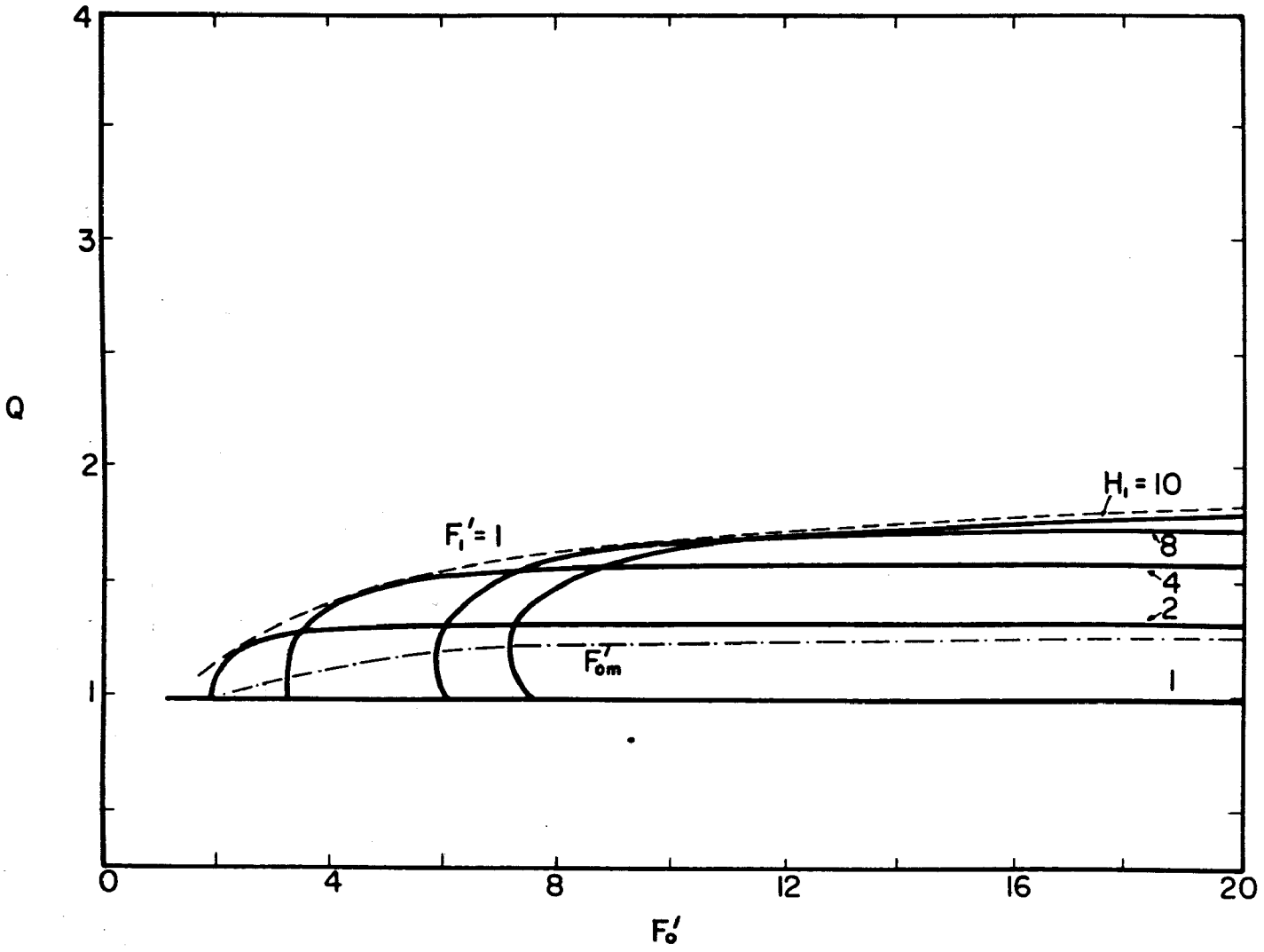


Fig. 5c - Q versus $F_o'$ for $H_2 = 1$

condition. The connection of all minimum values of $F_o$ for different $Q$ values is identical to the line $F_1' = 1$ and represents a separation line between internal hydraulic jumps and surface jets. Considering the two possible values of $H_1$ for a given set of values of $Q$, $F_o'$ and $H_2$, one value of $H_1$ always represents a flow with a downstream densimetric Froude number $F_1' > 1$ and is a buoyant (internally supercritical)half-jet. The other value of $H_1$ represents a flow with a downstream densimetric Froude number $F_1' < 1$ and is an internal hydraulic jump.

A surface buoyant jet is an internally supercritical flow and uniquely controlled by the source (outlet) conditions. The internal hydraulic jump is an internally supercritical flow on the upstream side and internally subcritical on the downstream side. In that case, depth $H_1$ is controlled from downstream. It appears that under steady flow conditions the two-dimensional warm water surface flow will always have a downstream control and therefore an internal hydraulic jump must occur somewhere downstream from the outlet.

Figures 4a, 4b, and 4c show furthermore that for constant entrainment, high values of $F_o'$ are associated with lower values of $H_1$. For an infinitely large outlet densimetric Froude number $F_o'$, asymptotic relationships between $H_1$ and $Q$ were obtained for different $H_2$ values. Fig. 6 shows the results and in particular the special solution

$$Q = \sqrt{H_1} \tag{15}$$

if the reservoir is infinitely deep $(H_2 \longrightarrow \infty)$. This is precisely the relationship arrived at by Albertson et al [6] for non-buoyant, two-dimensional submerged turbulent jets discharged into an infinite fluid medium. Fig. 6 substantiates the assertion that the lower branches of the $H_1$ versus $F_o'$ curves in Figs. 4a, 4b, and 4c represent a jet-type flow.

To the left of the line $F_1' = 1$ in Figs. 4a, 4b, and 4c, two particular lines are of special importance. One is the line representing $Q = 1$ which is given as

$$2F_o'^2 = \frac{(H_1 - r)}{(1 - r)^2}(H_1 + 1 - 2r) \tag{16}$$

Eq. (16) represents the non-mixing internal hydraulic jump and is essentially identical to the relationship given by Yih and Guha [4].

The other line is an envelope of the family of $H_1$ versus $F_o'$ curves which gives the minimum densimetric Froude number, $F_{om}'$, for a given $H_1$. The curve connecting $F_{om}'$ values is also plotted in Figs. 5a, 5b, and 5c.

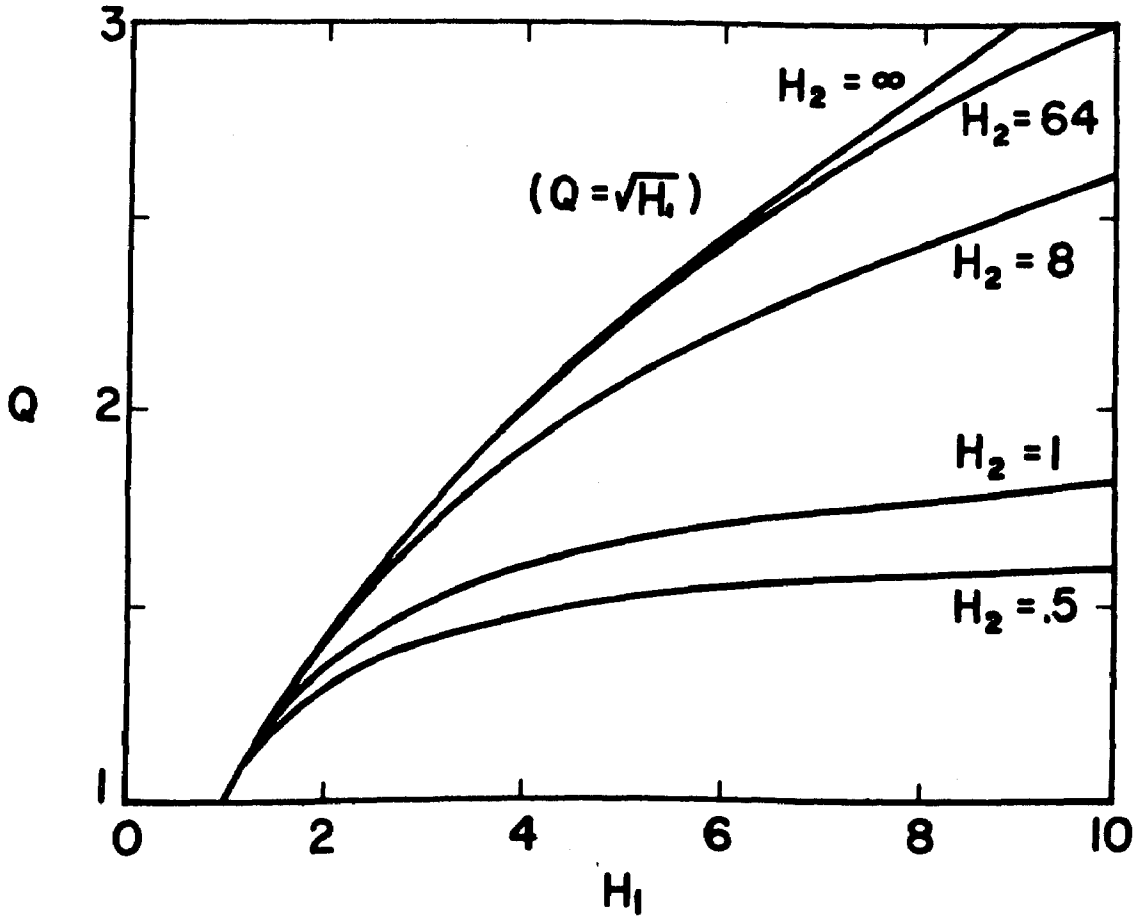


Fig. 6 - Q for infinitely large $F_o'$ as a function of $H_1$ and $H_2$

It is thought that mixing internal hydraulic jumps require larger downstream depths $H_1$ than non-mixing ones for the same $F_o'$ and $H_2$ values. The difference is of course in the entrainment of fluid. Therefore, it is believed that the mixing internal hydraulic jump is seen in the region bounded by the lines $Q = 1$ and $F_{om}'$. In this region, however, there exist two $Q$ values for every given pair of $H_1$ and $F_o'$ values. Figs. 5a and 5b show this even more clearly. Considering the shape of the curves of $H_1$ = constant in Figs. 5a, 5b, and 5c, it can be seen that the smaller $Q$ value approaches $Q = 1$ as $F_o'$ is increased, while the larger one grows to a finite value which is given by the non-buoyant mixing jet theory. It is thought that only the smaller $Q$ value is physically meaningful, but no proof has been established.

To the left of the $F_{om}'$ line in Figs. 4a and 4b is a region where the submerged internal hydraulic jumps should be expected to occur. In the case of the submerged internal hydraulic jump the degree of submergence ($h_r$ in Fig. 2) is a new and unknown variable which must be included in the momentum equations. Consequently these equations cannot be solved without an additional relationship.

Energy losses associated with the entrainment and mixing process have been evaluated using Eqs. (7a), (7b), (7c), and (8).

$$\frac{\Delta E}{E_o} = 1 + \frac{\alpha_2}{\alpha_o}\frac{(Q-1)^3}{(1-r)H_2^2} - \frac{2}{\alpha_o}\frac{H_1(Q-1)}{(1-r)F_o'^2Q} + \frac{2}{\alpha_o}\frac{(Q-r)w_1/h_o}{(1-r)F_o^2Q}$$

$$- \frac{\alpha_1}{\alpha_o}\frac{(Q-r)Q^2}{(1-r)H_1^2} \qquad (19)$$

Results are given in Figs. 7a and 7b for values of $H_2 = \infty$ and 8 which show a minimum positive value of the energy loss at the conjectured transition $F_1' = 1$; $\alpha_o = \alpha_1 = \alpha_2 = 1.0$ has been assumed.

The slope of the free water surface was found to be upward in the flow direction, as indicated in Fig. 1, and small. A plot of the dimensionless water surface elevation $\frac{-w_1}{h_o r}$ is given in Figs. 8a and 8b. A strong dependence of the results on the thickness of the upper layer, $H_1$, is apparent.

Figs. 9 and 10 give results of $H_1$ and $Q$, respectively, versus $F_o'$ using Eq. (13) instead of Eq. (12). Eq. (13) implies that the water surface is horizontal. Comparison of Figs. 9 and 10 with Figs. 4 and 5

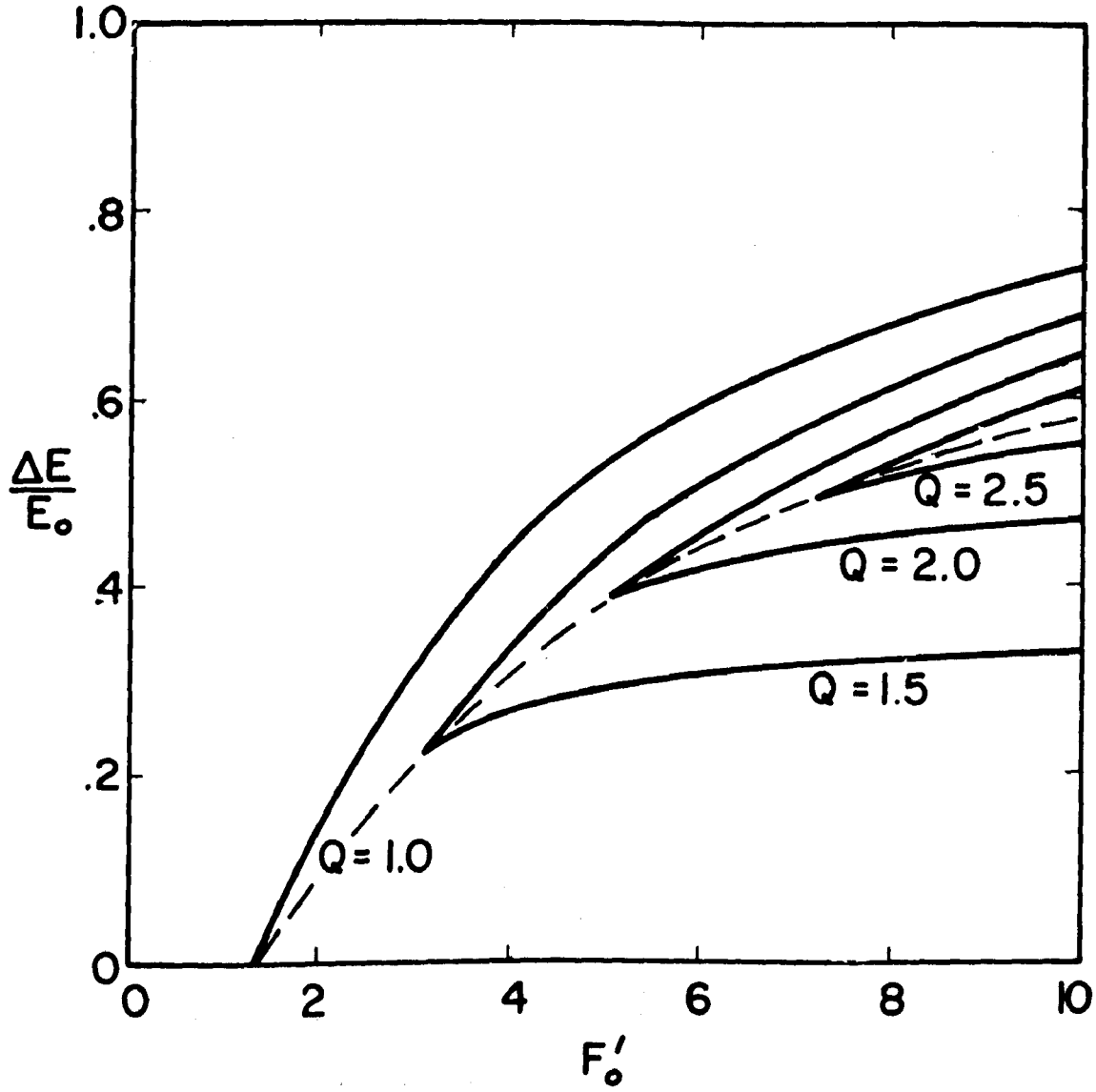


Fig. 7a - $\Delta E/E_o$ versus $F_o'$ for $H_2 = \infty$

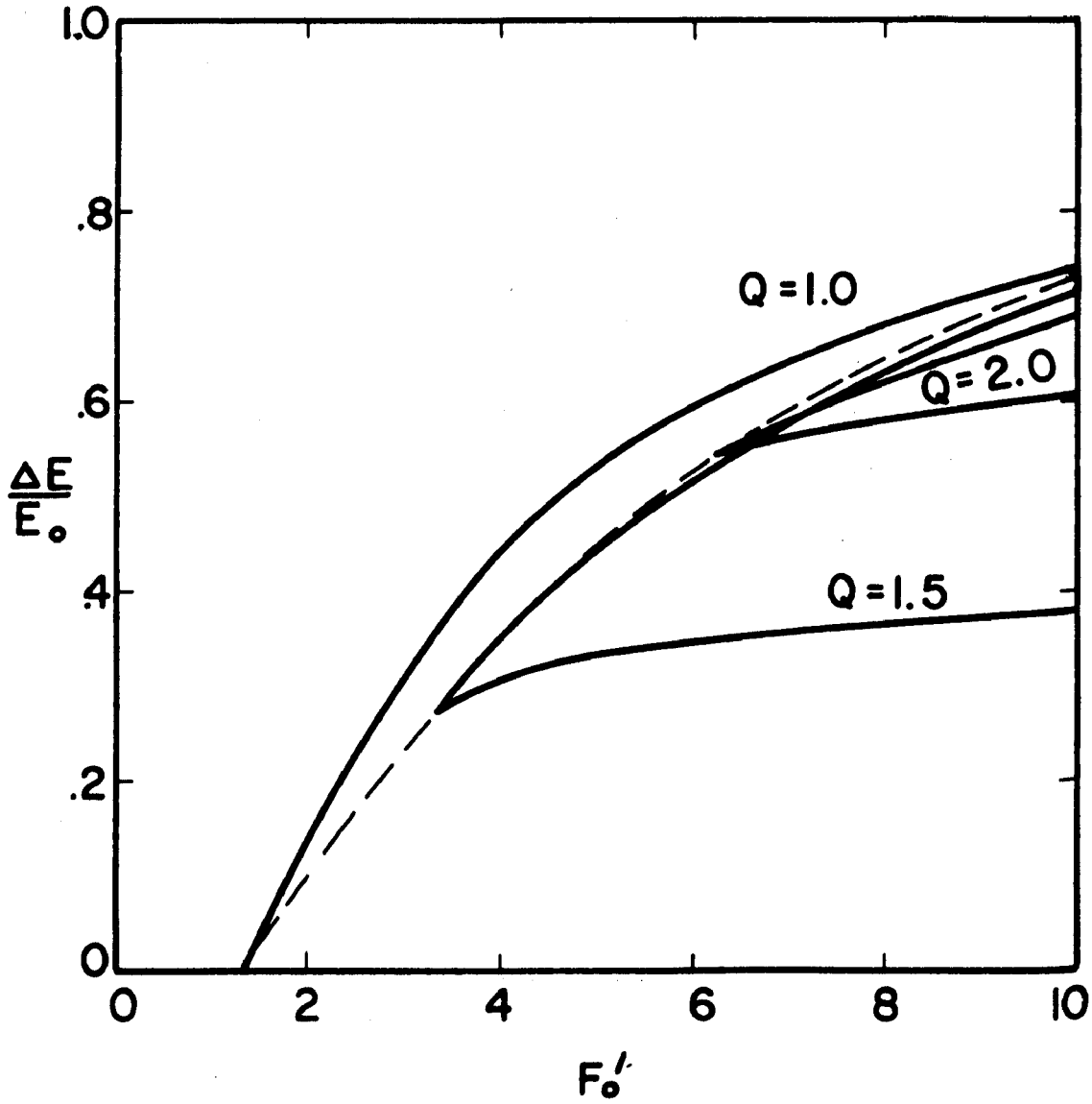


Fig. 7b - $\Delta E/E_o$ versus $F_o'$ for $H_2 = 8$

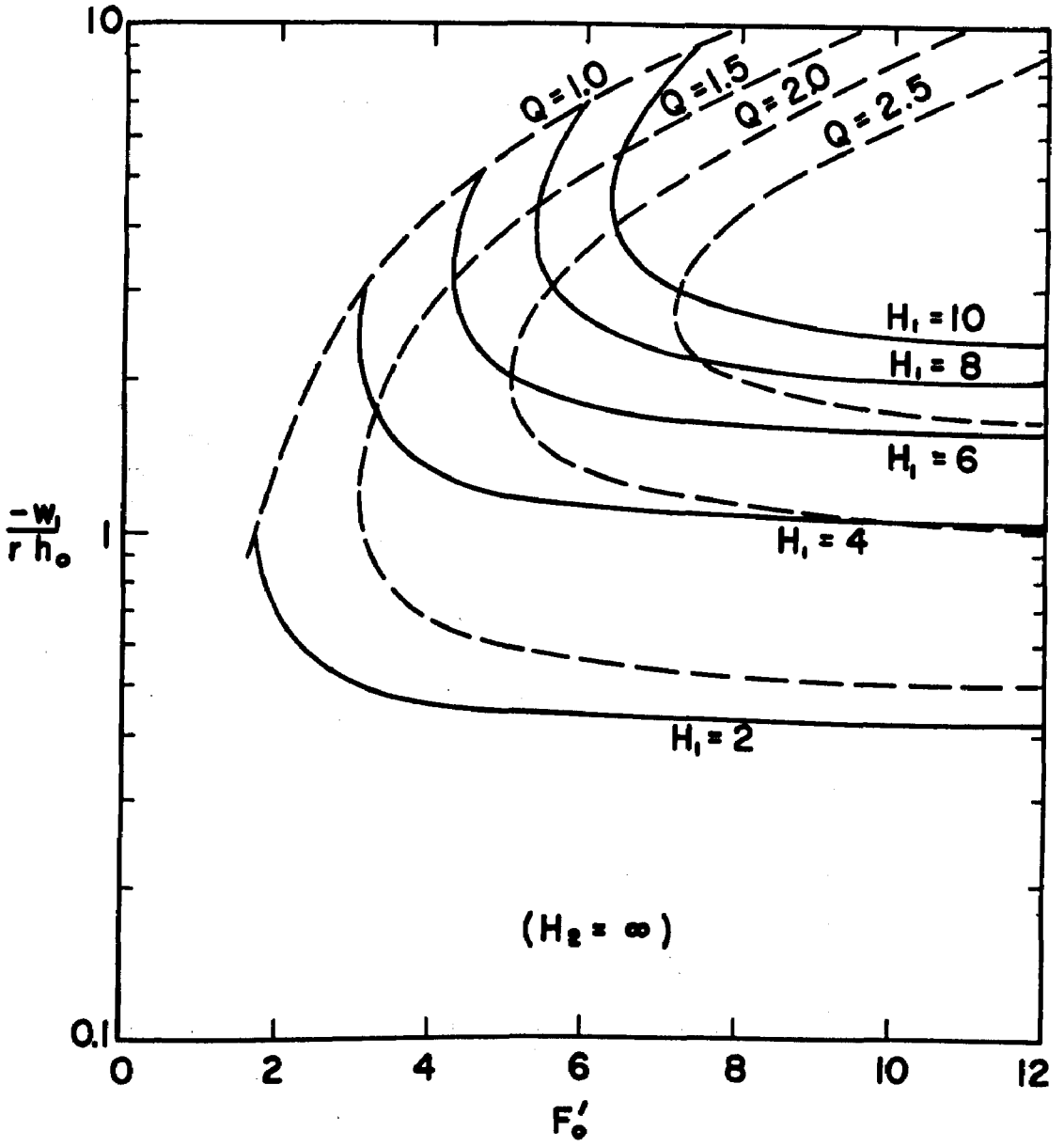


Fig. 8a - Dimensionless water surface elevation $\frac{-w_1}{rh_o}$ versus $F_o'$ for $H_2 = \infty$

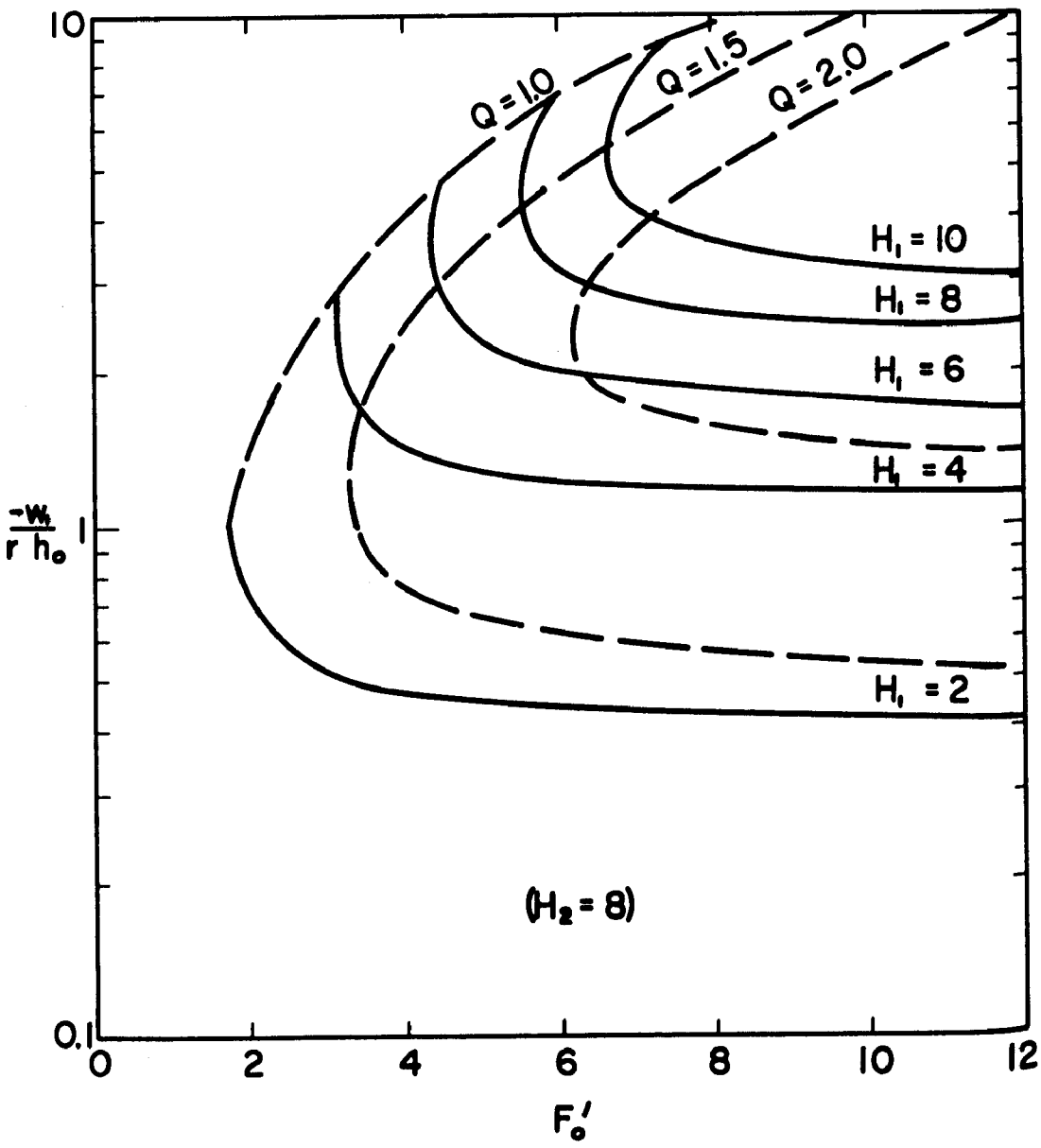


Fig. 8b - Dimensionless water surface elevation $\frac{-w_1}{rh_o}$ versus $F_o'$ for $H_2 = 8$

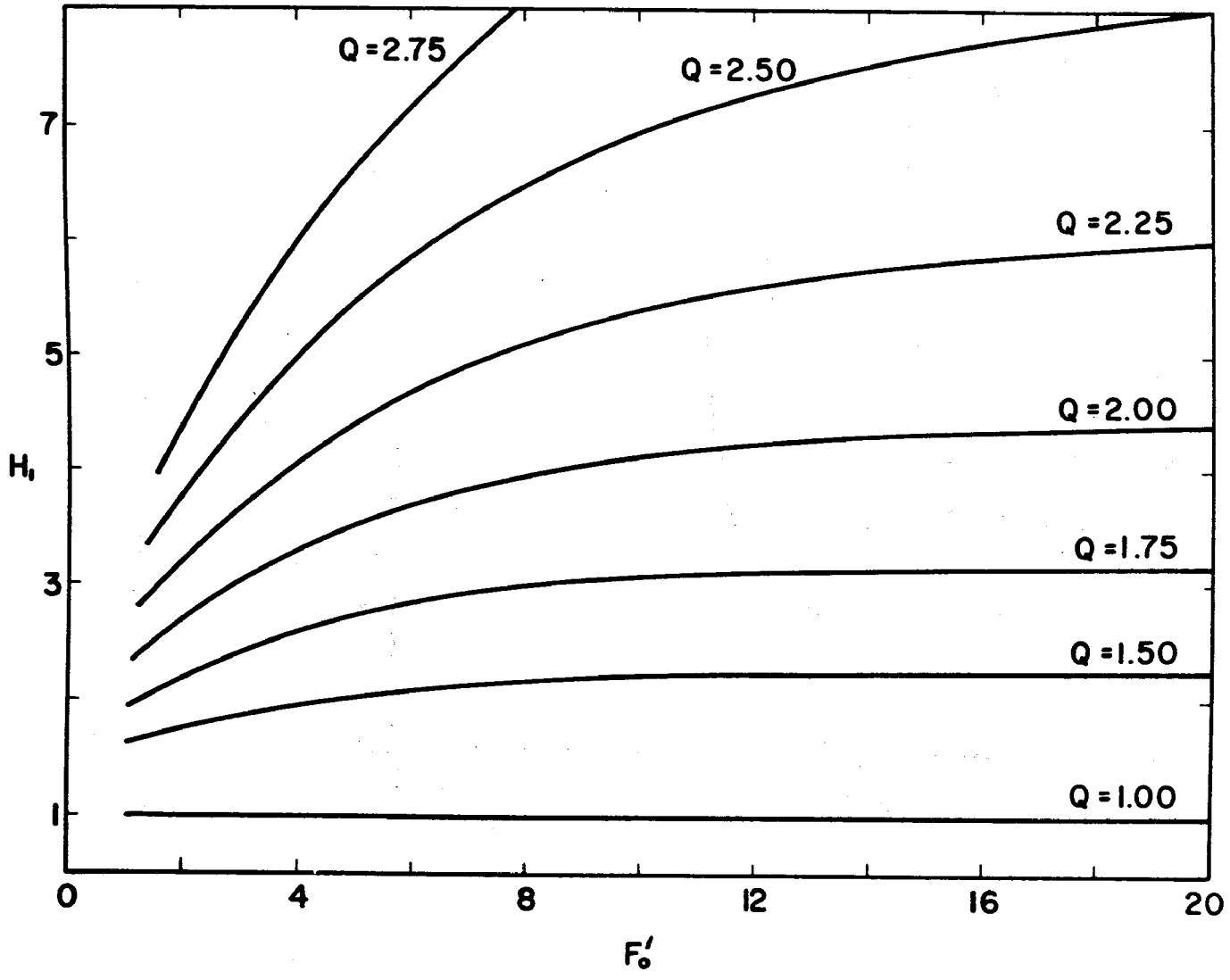


Fig. 9 - $H_1$ versus $F_o'$ for $H_2 = 8$ under the assumption $w_1 = 0$

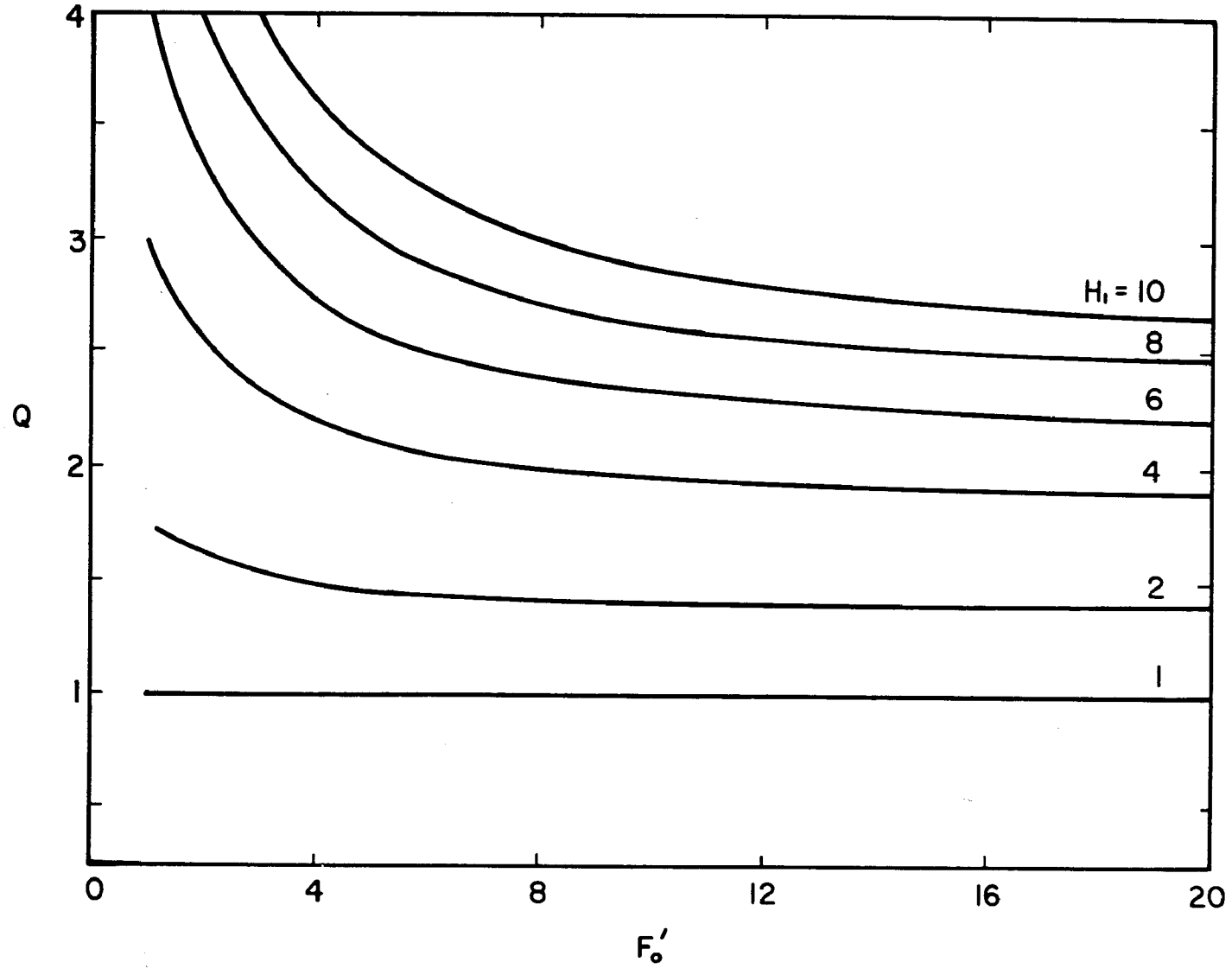


Fig. 10 - Q versus $F_o'$ for $H_2 = 8$ under the assumption $w_1 = 0$

reveals large differences in results, particularly in the lower Froude number range. Eq. (13) does not give Yih and Guha's internal hydraulic jump equations when $Q$ is set equal to unity. It may be concluded that the solutions in Figs. 9 and 10 are valid and useful only when the crucial assumption $w_1 = 0$ is physically imposed by a solid wall such as proposed in Ref. [3]. $w_1 = 0$ is not a valid assumption for the free surface flow under consideration.

Flat Beach

The two-dimensional flow over a flat beach is very similar to that in a diffuser. "Flat" in this context means that there is no separation of the streamlines at the outlet. Further downstream the flow will separate from the beach smoothly because of its buoyancy. This will occur at a depth usually established by downstream conditions. Fig. 11 shows schematically the flow over a flat beach. The entrainment can be expected to be zero or near zero; experimental evidence to this effect will be presented later. Because of this, there was relatively little reason to investigate this flow. The only unknown quantity of interest is the slope of the water surface, and its value was not a prime objective. If it is to be calculated, nevertheless, one can use the momentum equation and a constant flow rate in the upper layer. The pressure distributions are hydrostatic, and the shear stress along the beach can be found from boundary layer theory or from one of the semi-empirical open channel flow equations.

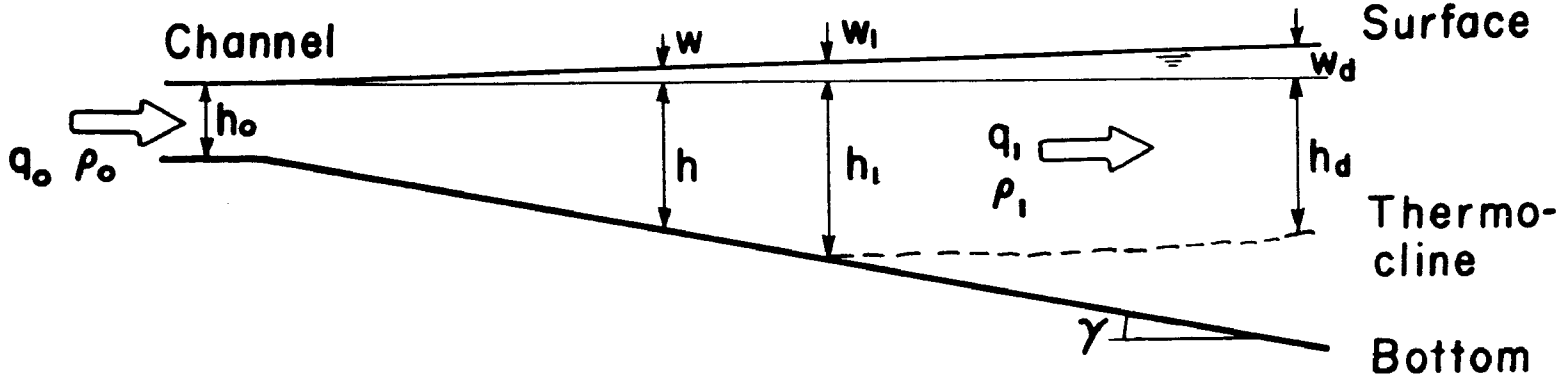


Fig. 11 - Schematic representation of outflow over flat beach

## SECTION VI

## EXPERIMENTAL FACILITY

For the experimental study a 6 in. wide, 15 in. deep, 40 ft long glass walled channel was used. The experimental apparatus is shown schematically in Fig. 12. Heated water was discharged horizontally at the surface. The downstream depth (withdrawal), the heated water discharge rate, the temperature of the heated water, and the temperature of the cold water supply were variable. The flow of the warm water on top of the cold water could be observed over a distance of 13 ft with the aid of minute quantities of dissolved potassium permanganate. Vertical temperature profiles were recorded with a thermistor temperature probe. All measurements were taken in the centerline of the flume. Downstream from the outlet the heated water layer was withdrawn selectively by adjusting the withdrawal plate and the flow rate. The withdrawal flow was metered.

The channel bottom and the flume walls were hydraulically smooth. The downstream gate was adjustable and allowed variation of the inflow depth $h_o$. Heated water temperatures were only a few degrees Fahrenheit above equilibrium temperature--that is, the water temperature at which the net heat exchange through the water surface was zero. Surface heat loss effects on the temperature were small compared to mixing effects mainly because of short residence time.

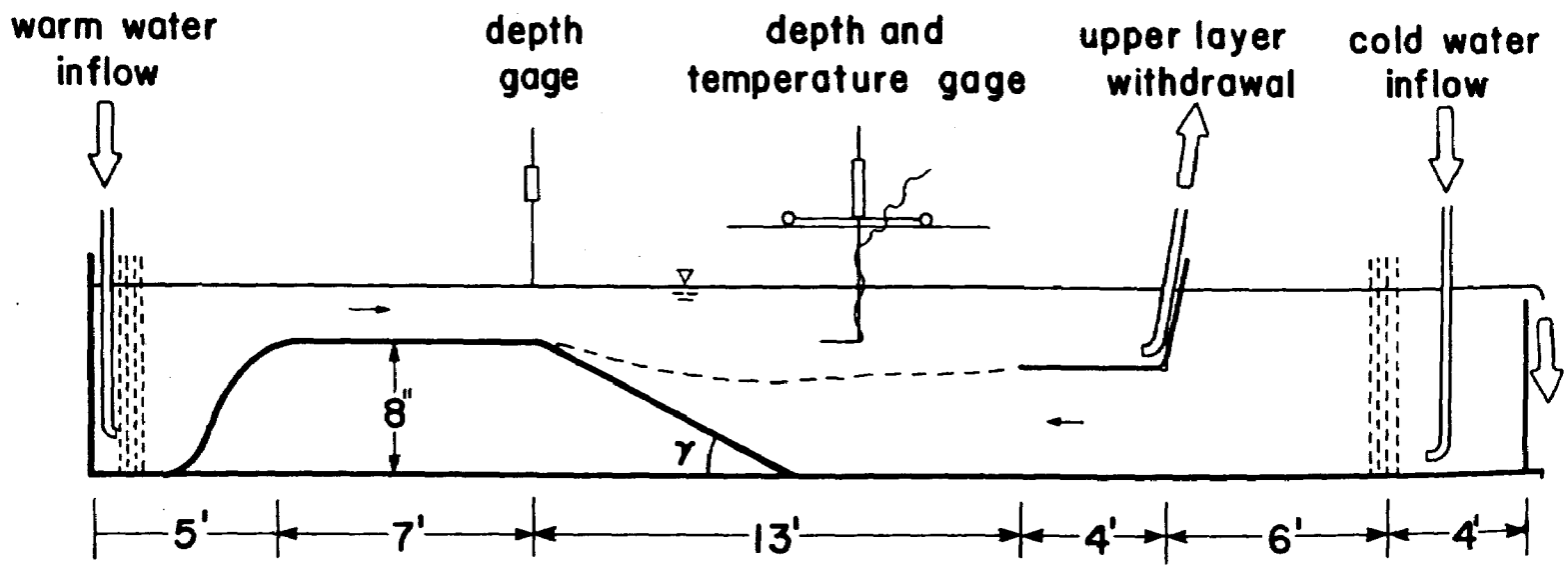


Fig. 12 - Experimental Apparatus

## SECTION VII

## EXPERIMENTAL RESULTS

Figs. 13a through 13d show several typical flow patterns for a $90^{\circ}$ beach. The first example in Fig. 13a is a typical case of buoyant surface jet type mixing. The spread in depth is nearly linear over the first foot or so. Then buoyancy forces begin to bend the interface upward. The second example in Fig. 13b is a typical internal hydraulic jump pattern. The flow along the interface is directed toward the outlet, at least over the first 2 ft.

An example of less violent mixing and internal submergence of the outlet is given in Fig. 13c. It can be seen, although not very clearly, that the discharged heated water spreads jet-like until it reaches the interface. The flow is not exactly a jet, however, because there is a roller on its lower boundary. The roller causes some entrainment of cold water and also generates an eddy beneath the outlet. Fig. 14 shows the associated streamline pattern schematically. The last example in Fig. 13d shows a strong stratification at the outlet. At a short distance from the outlet, the interface becomes unstable and breaks. A not very well defined kind of hydraulic jump follows further downstream. The outlet is slightly submerged. Fig. 13d illustrates the complexity of some flow and mixing patterns at a heated water surface outlet and the problem of interfacial mixing by waves, which will not be pursued further in this study.

Figs. 15a through 15d are temperature profiles which correspond to Figs. 13a through 13d, respectively. All profiles show the well-mixed character (uniform temperature) of the upper layer. Temperature profiles (shown in Figs. 15c and 15d) which are close to the outlet also demonstrate the existence of an intermediate layer between the upper warm layer and the lower cold layer. This intermediate layer is a consequence of the submergence of the outlet as can be seen in Figs. 13c and 13d.

The flow down a flat beach is much less spectacular than for a steep beach, as can be seen in Fig. 16. No measurable amount of entrainment was detected. The separation from the beach is very smooth.

Figs. 17 and 18 show different kinds of plottings of experimental data for a $90^{\circ}$ beach. The dimensionless depth of the lower layer $H_2$ in the experimental channel ranged from 3.5 to 13.5. Theoretical values for $H_2 = 8$ were chosen for comparison. All experimental data points lie above the line $Q = 1$ (Eq. 16) because of entrainment into the moving upper layer. Fig. 17 also displays values of $F'_{om}$, the minimum $F'_o$ value that is expected for a free mixing internal hydraulic jump, for $H_2 = 8$. Flow conditions to the left of that line should represent internally submerged outlets. The experimental data of the observed free hydraulic jumps were generally found on or below the $F'_{om}$ line and above the $Q = 1$ line.


Fig. 13a – Photograph of buoyant surface jet flow downstream from outlet channel. Flow is from left to right. Heated water is dyed and appears darker than cold water. $F_o' = 11.0$, $H_1 = 19.0$, $H_2 = 5.7$, $Q = 1.58$

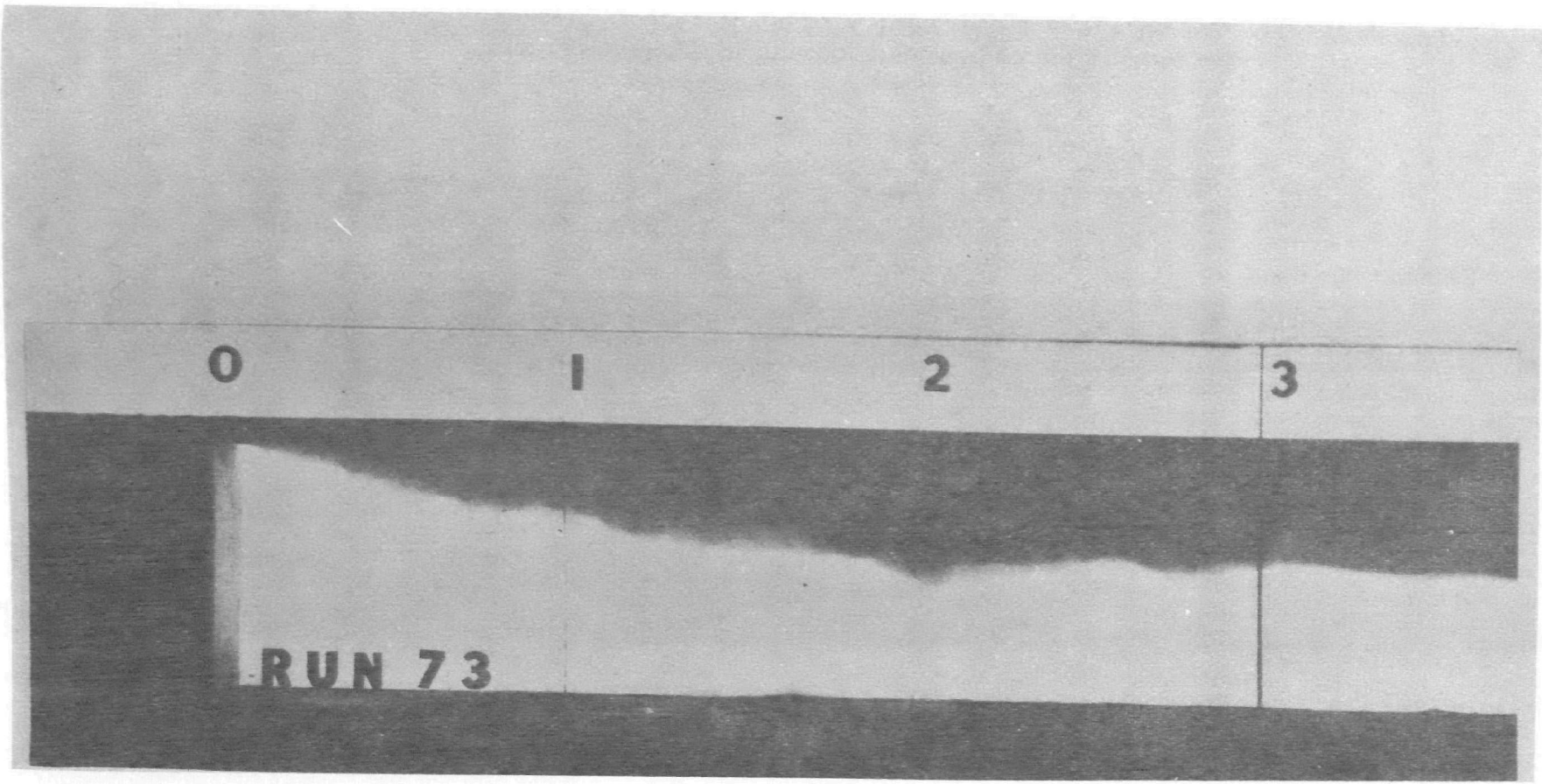


Fig. 13b - Photograph of internal hydraulic jump downstream from outlet.
$F_o' = 4.0$, $H_1 = 5.6$, $H_2 = 6.6$, $Q = 1.20$

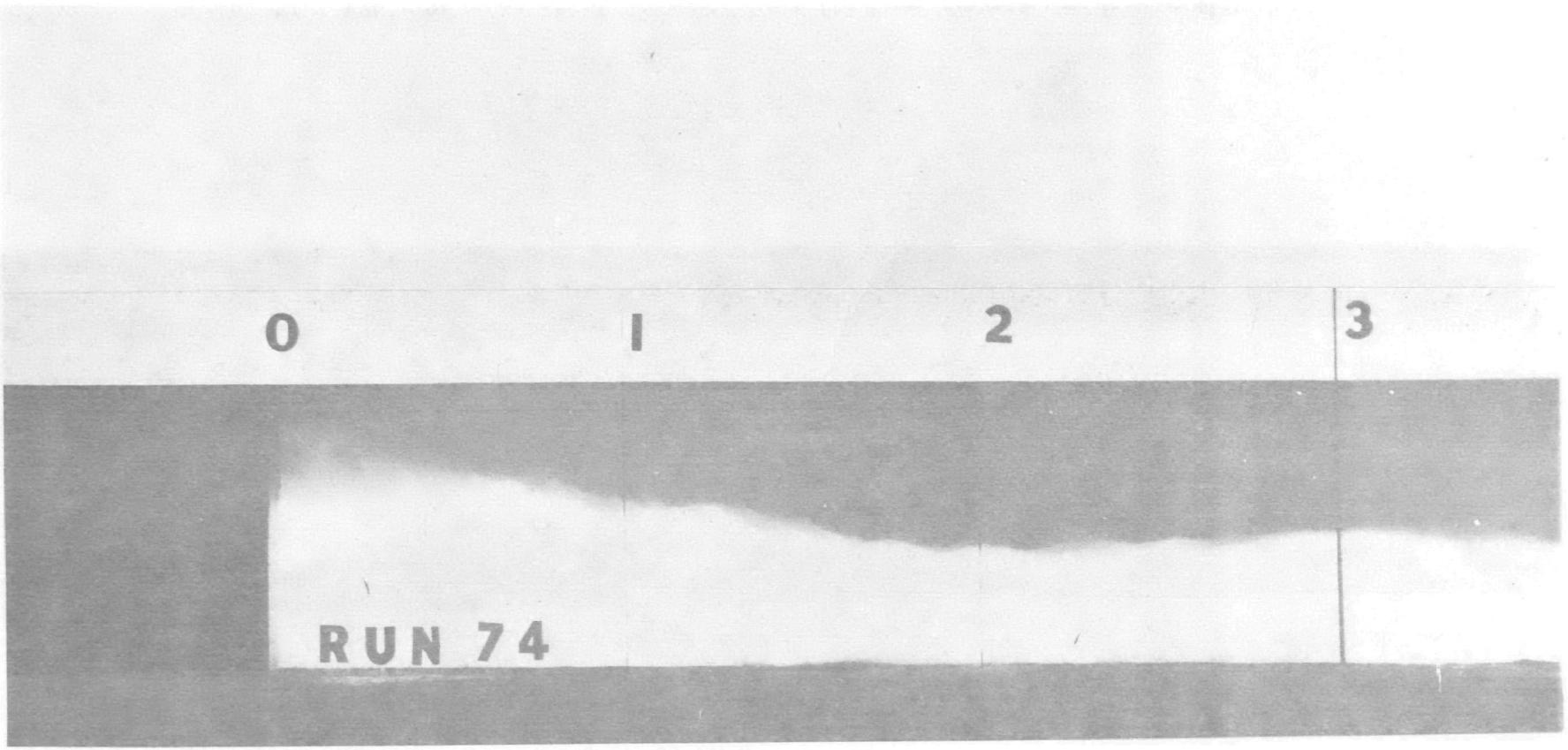


Fig. 13c - Photograph of internally submerged outlet flow.
$F_o' = 3.4$, $H_1 = 6.1$, $H_2 = 5.0$, $Q = 1.06$

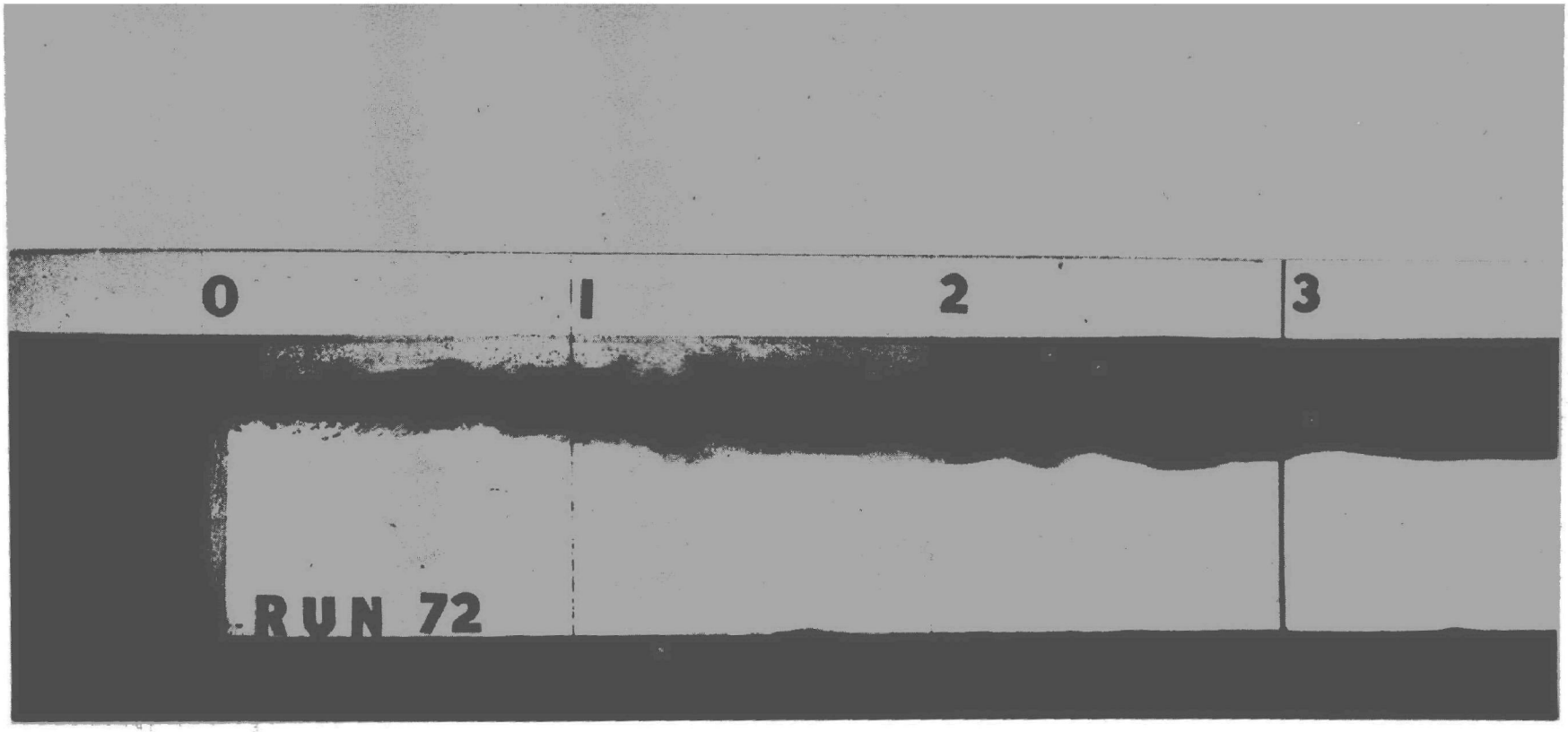


Fig. 13d - Photograph of breaking of internal waves near the outlet.
$F_o' = 1.8$, $H_1 = 2.9$, $H_2 = 4.6$, $Q = 1.08$

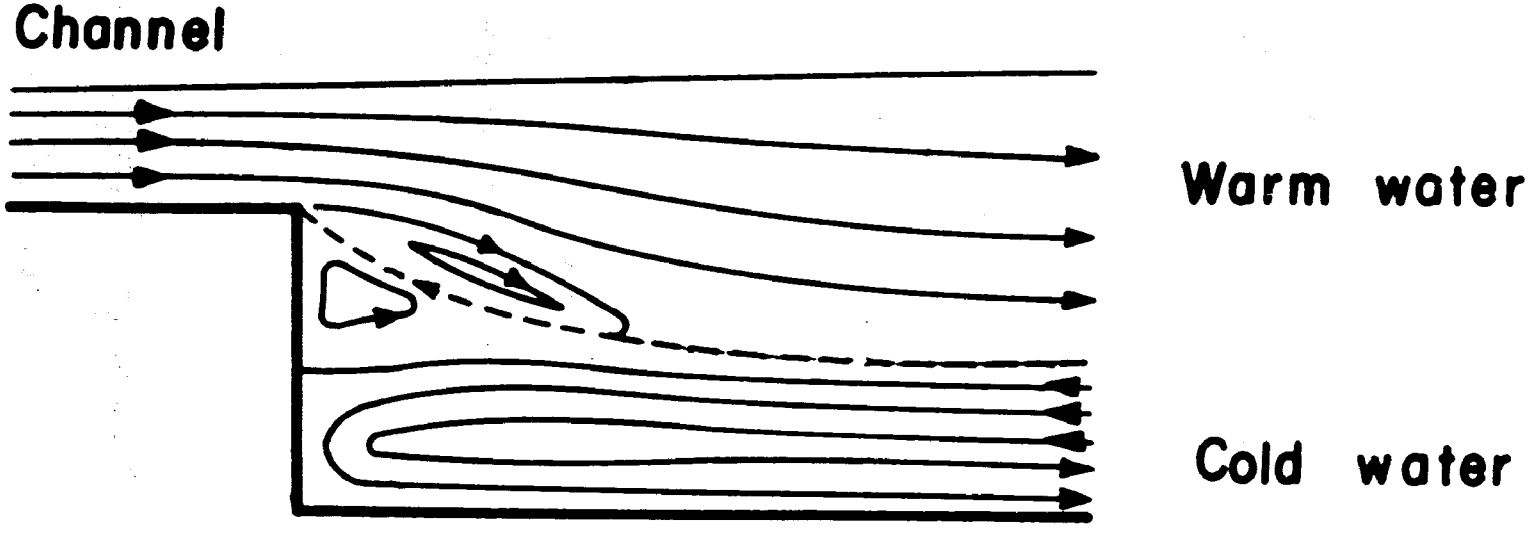


Fig. 14 - Schematic streamline pattern near internally submerged outlet

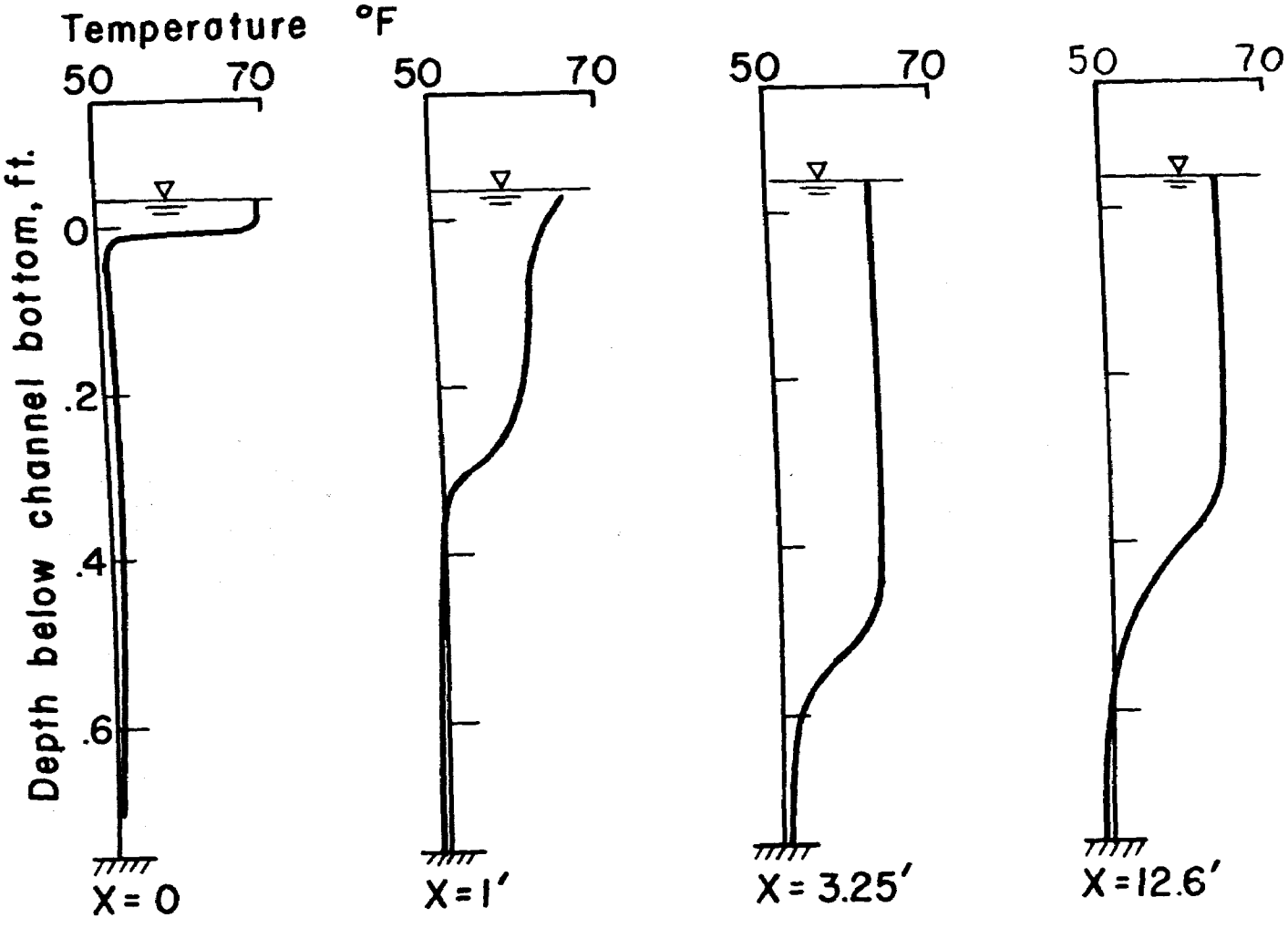


Fig. 15a - Selected vertical temperature profiles associated with flow of Fig. 13a

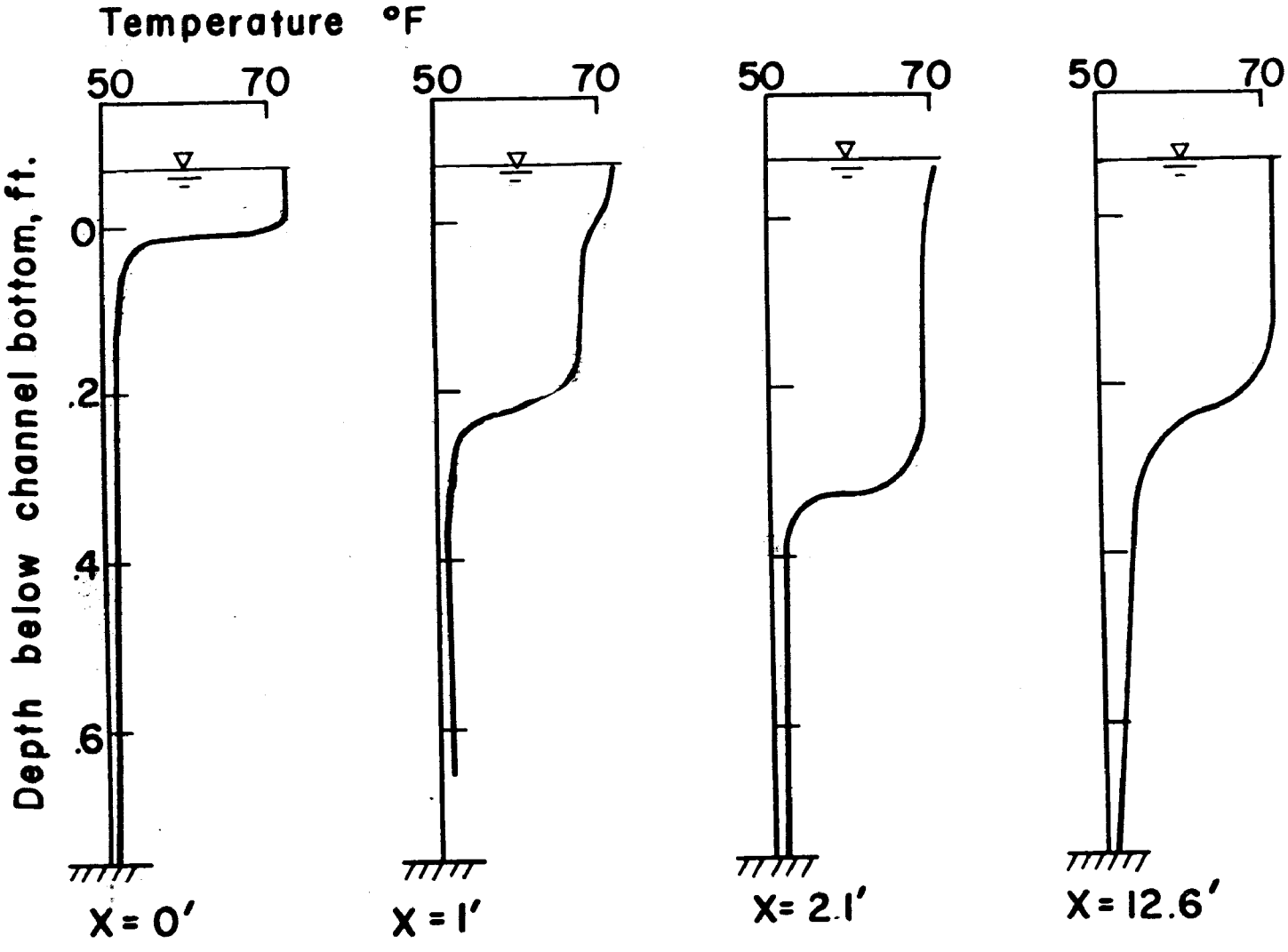


Fig. 15b – Selected vertical temperature profiles associated with flow of Fig. 13b

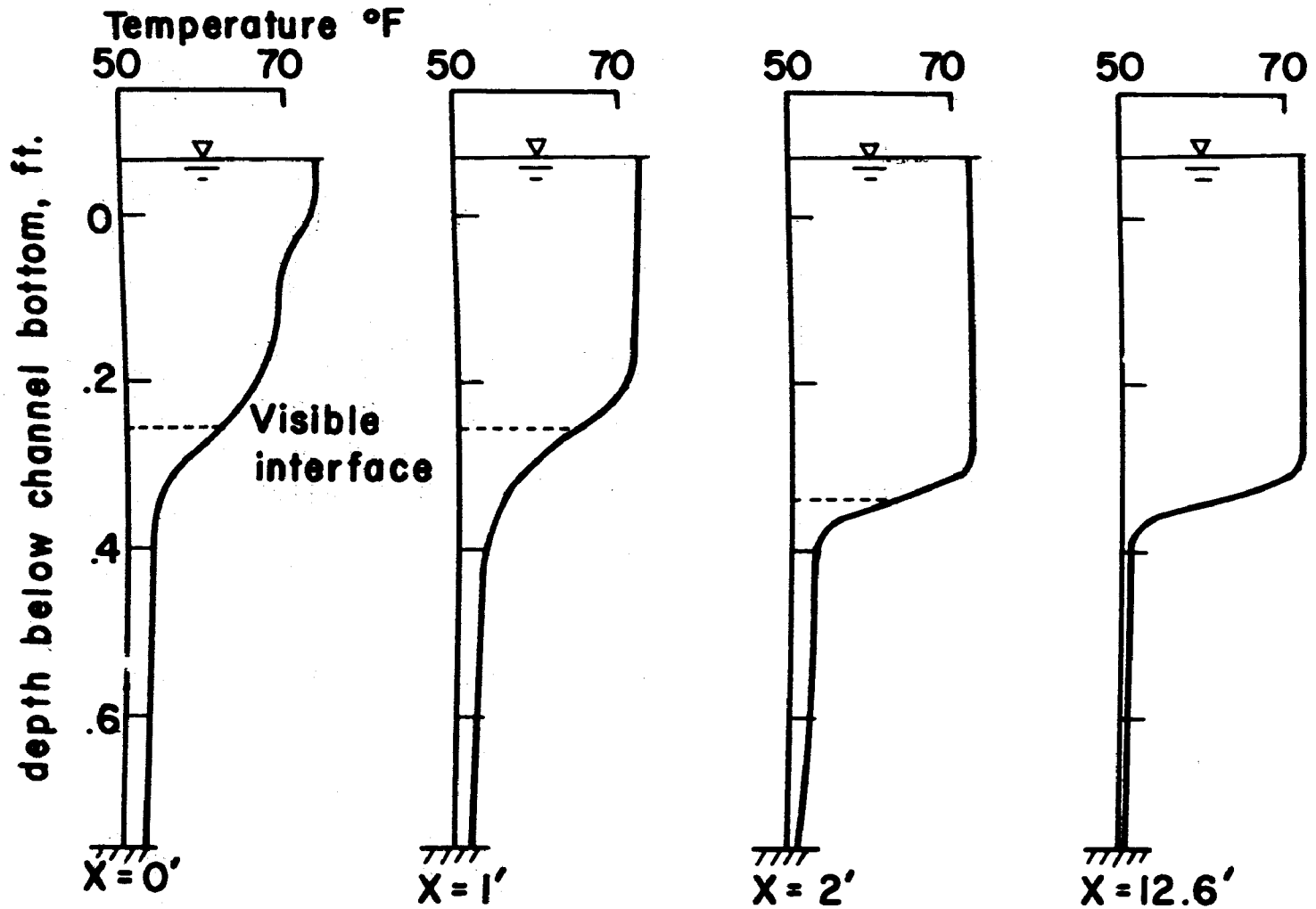


Fig. 15c - Selected vertical temperature profiles associated with flow of Fig. 13c

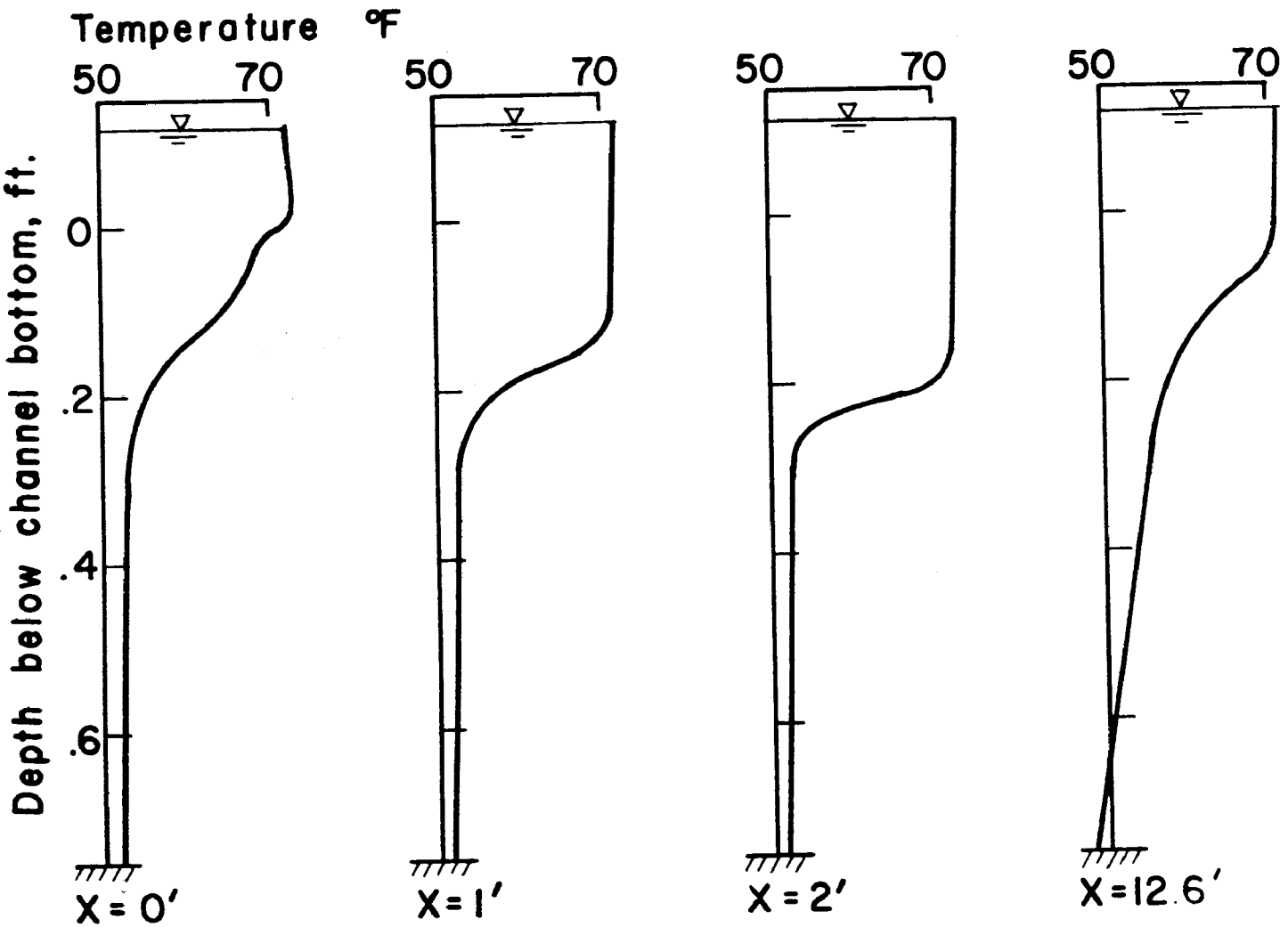


Fig. 15d – Selected vertical temperature profiles associated with flow of Fig. 13d

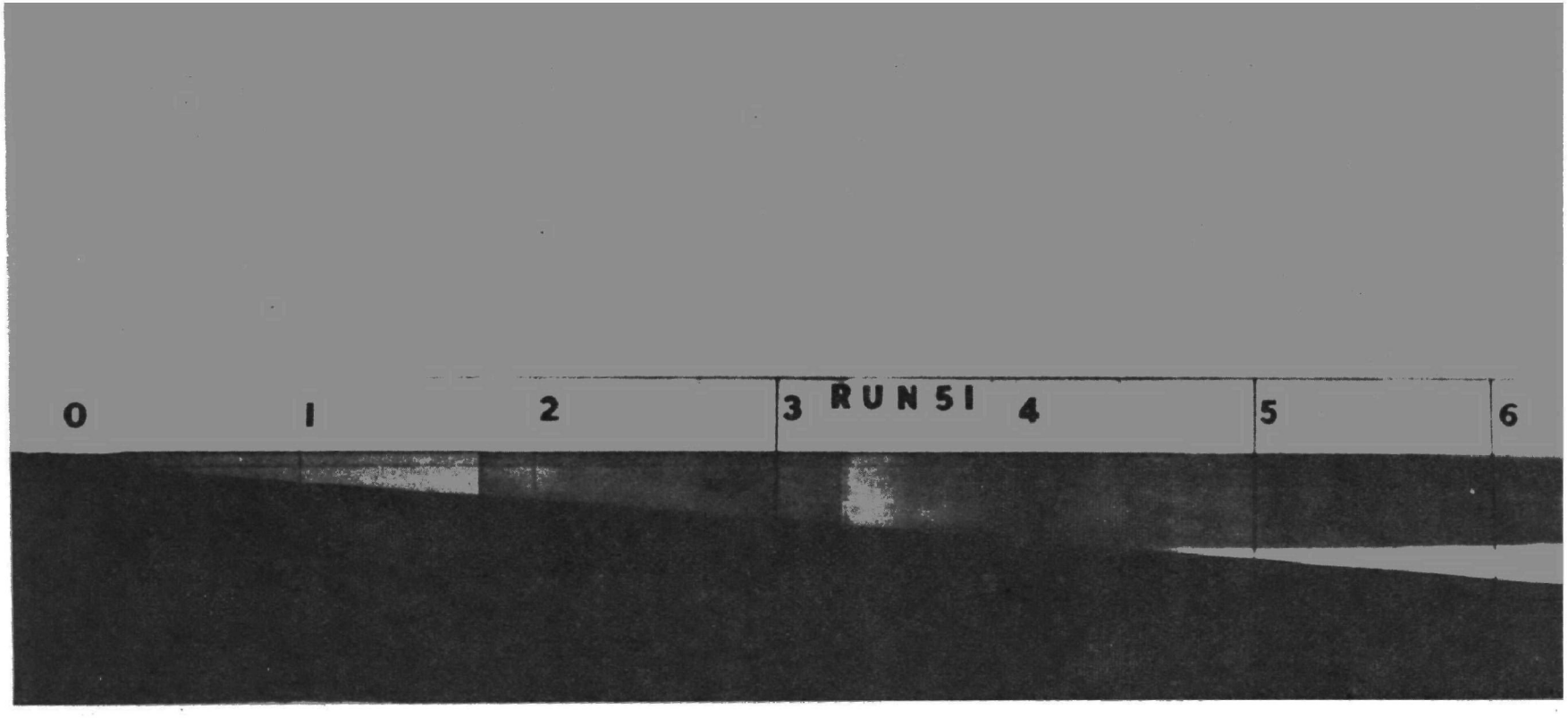


Fig. 16 – Photograph of flow over a flat beach

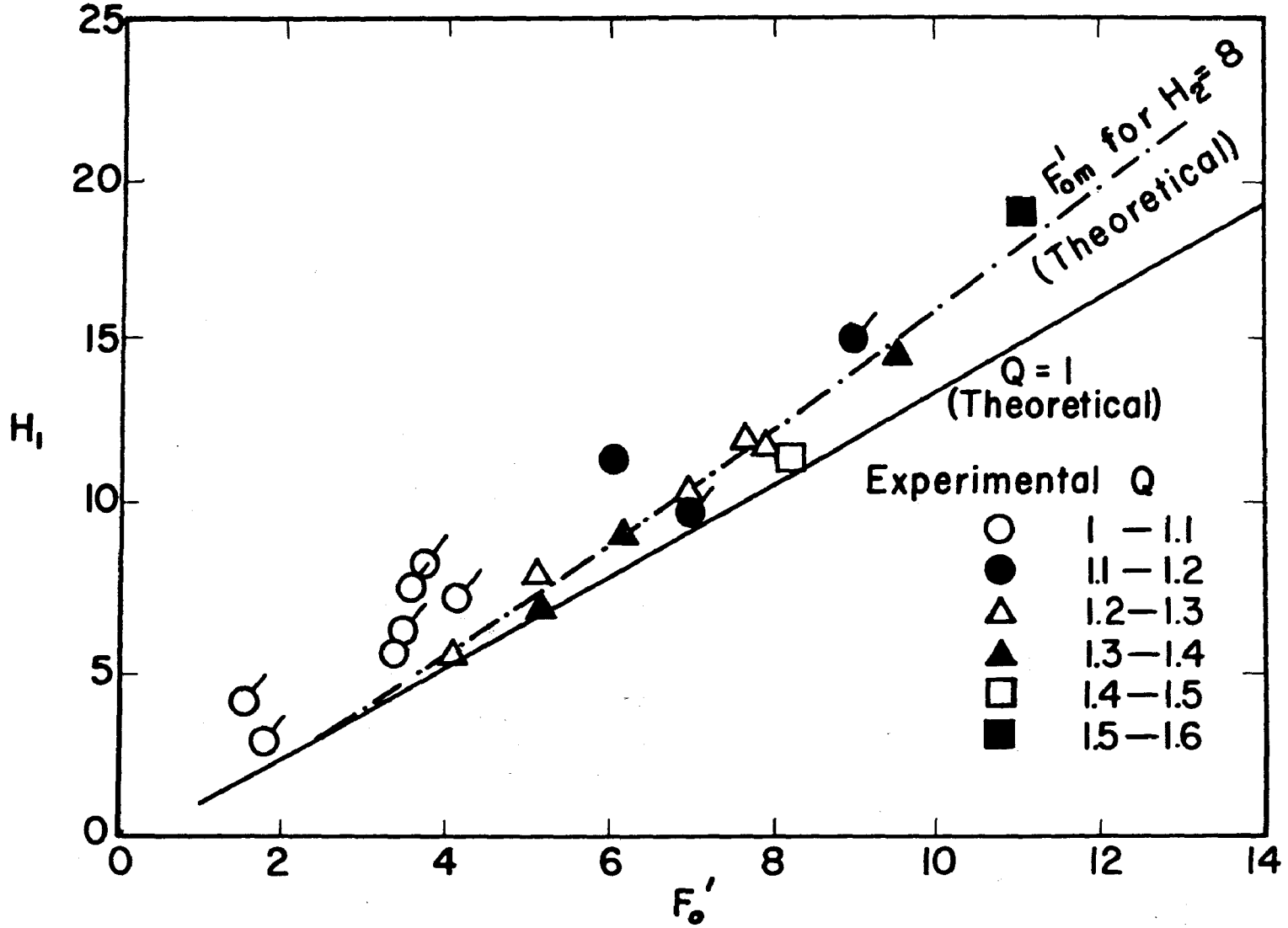


Fig. 17 - Experimental and theoretical data of $H_1$ versus $F_o'$.
(A flag on a symbol designates an internally submerged outlet. The present theory does not apply to this situation.)

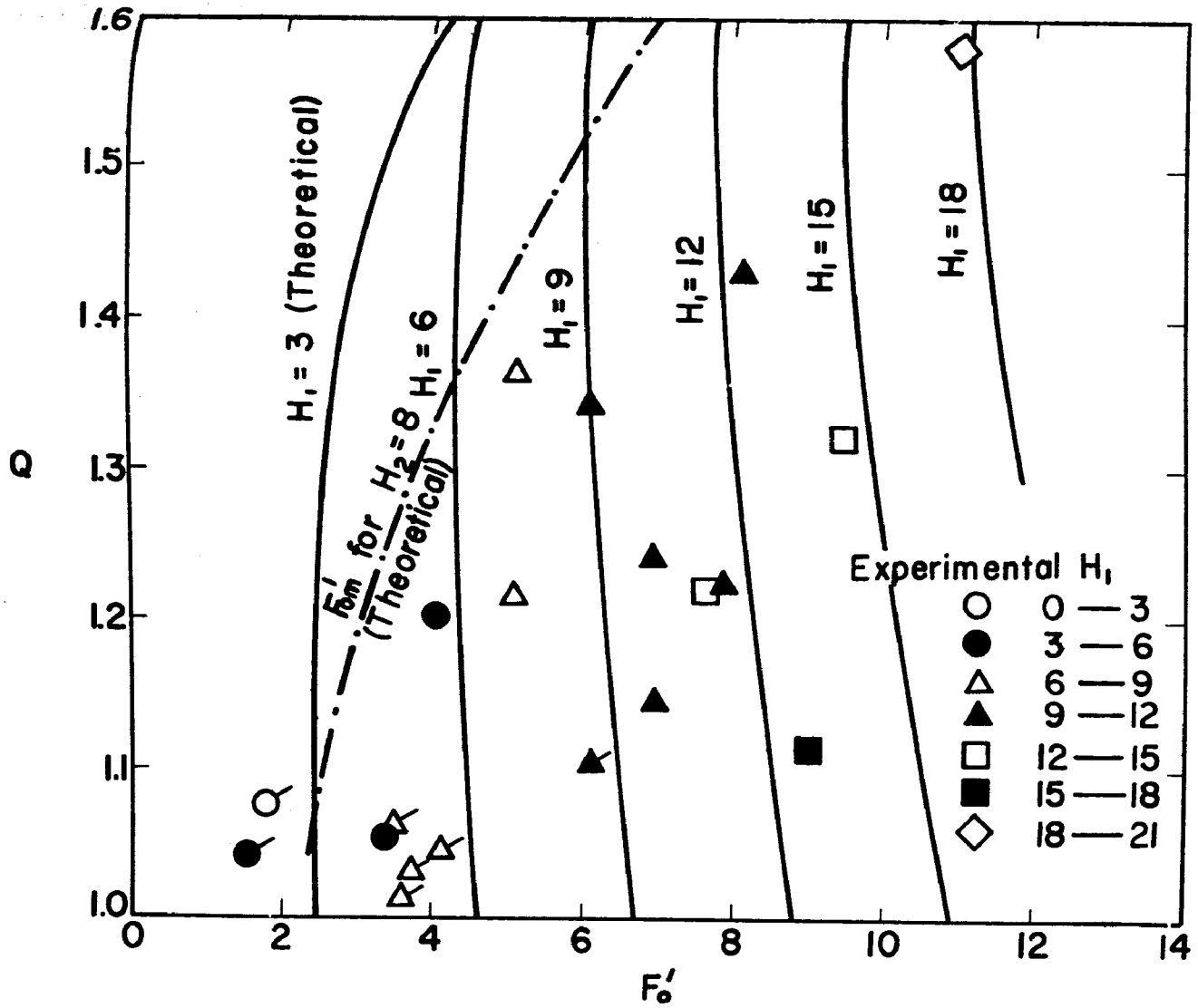


Fig. 18 - Experimental and theoretical data of Q versus $F_o'$.
(A flag on a symbol designates an internally submerged outlet. The present theory does not apply to this situation.)

The rate of entrainment, measured as $Q$, is shown in Fig. 18 as a function of $F_o'$. All data points lie below the $F_{om}'$ line for $H_2 = 8$. Theoretical predictions of flow conditions in terms of $H_1$ and $F_o'$, for $H_2 = 8$ are also shown in Fig. 18. Good agreement with observed experimental data is found. Fig. 18 reveals that $Q$ changes rapidly as either $F_o'$ or $H_1$ is changed while the other parameter is fixed. Because of this high sensitivity of $Q$ values to the parameters $F_o'$ and $H_1$ it may be difficult to accurately control $Q$ in practical cases. Submerged internal hydraulic jump cases, as can be seen in Figs. 17 and 18, are observed to have larger $H_1$ and smaller $Q$ values.

Fig. 19 shows the dimensionless length for the internal mixing zone. Actual lengths, $\ell$, of the internal mixing zone could only be measured with very low accuracy and were frequently close to three feet.

$$\frac{\ell}{h_o} = 10\ F_o' \tag{10}$$

may serve as a first approximation of the results.

Given a choice between different $F_o'$ values for given $H_1$, a maximum of mixing will occur when $F_o' = F_{om}'$. This condition also represents the limits between internally free and submerged outlet conditions, as noted earlier.

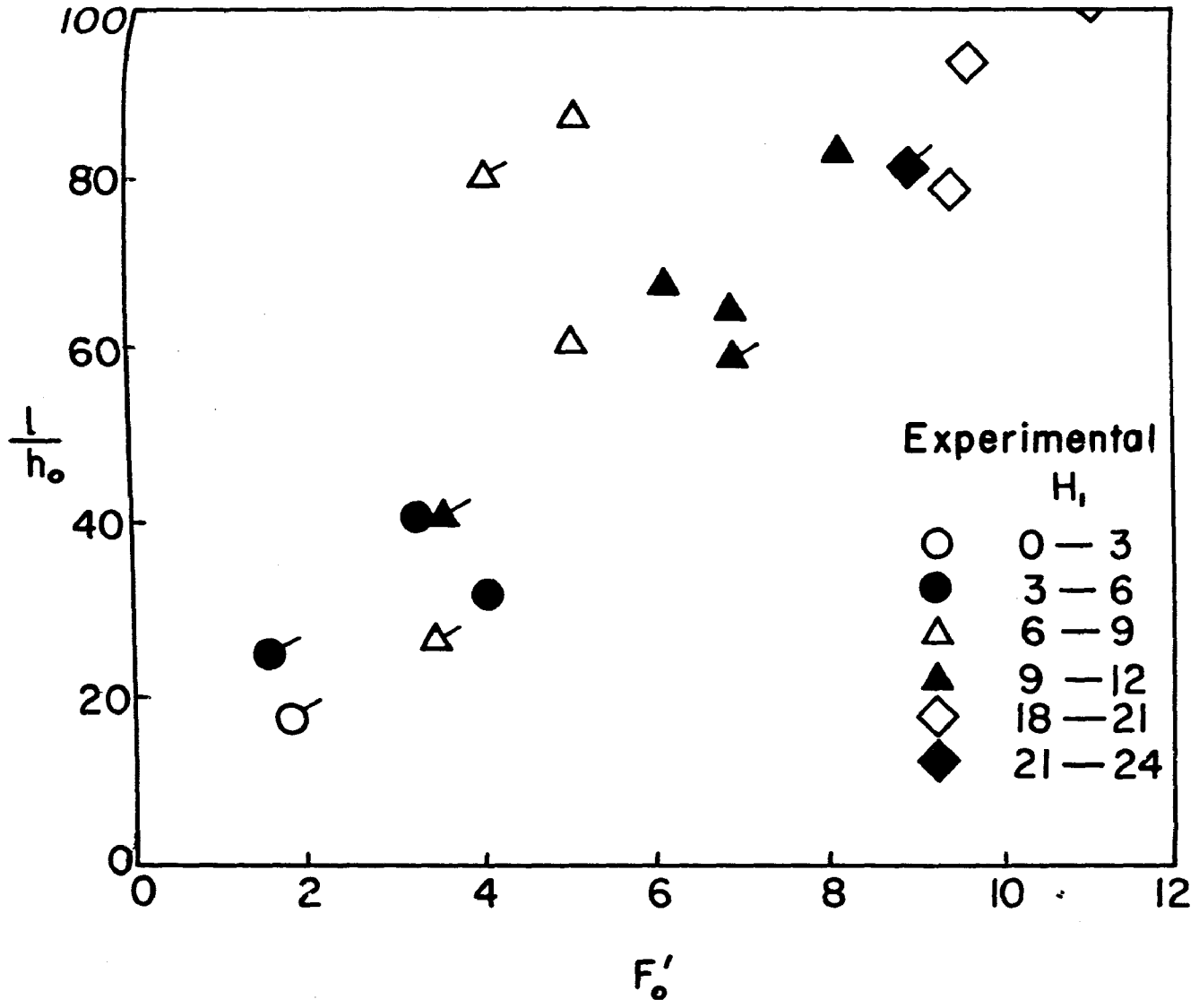


Fig. 19 - Dimensionless length of outlet mixing zone versus $F_o'$.
(A flag on a symbol designates internally submerged outlet flow.)

## SECTION VIII

## APPLICATION OF THEORETICAL AND EXPERIMENTAL RESULTS

The results given in the previous sections may find application in the design of mixing chambers and prediction of outfall temperatures. In this study the flow conditions at the outlet and the depth of the warm water layer downstream from the transition and mixing zone have been treated as independent variables. This requires that no cold water encroaches into the outlet channel, a condition which is easily met at high outlet densimetric Froude numbers, in particular if $F_o' > 1$. The downstream depth $H_1$ is, however, not completely independent of the outlet flow. The thickness of the warm water layer $H_1$ depends on the type of control exerted from downstream as explained in the introduction. It also depends on the flow rate after mixing, $Q_1$, and hence on the entrainment rate itself. Application of the results derived in the previous section will therefore usually require simultaneous consideration of the type of downstream control and entrainment. This point has been clearly made in several references, e.g. [1,2,3]. It has also been shown in those references how the depth $H_1$ can be found if the downstream control is a weir [2], or a submerged sluice gate [3], or the surface cooling process [1]. Other types of downstream controls could be investigated in a similar manner.

The solution of the entraining jump problem for a given outlet condition as investigated in this study and the solution of the stratified flow problem for a given type of downstream control must match where the two flow regions join (cross section 1 in Fig. 1). The matching has to be done essentially in terms of the depth $H_1$ and the flow rate $Q$ at the junction of the two flow regions. This will usually require a trial and error process, but will not impose large difficulties if the necessary separate computations for each zone are carried out numerically or if a set of solutions for each zone is given in graphical form. Figs. 4a, 4b, 4c, 5a, 5b, and 5c may serve as solutions for the entraining jump or outlet mixing region.

The interaction between the outlet entrainment problem and the downstream stratified flow problem suggests that the selection of a desired amount of mixing is possible only if the downstream control is variable. Entrainment is most effectively increased by increasing the downstream depth. A maximum entrainment and mixing rate is achieved at the point of beginning submergence of the outlet. Actual submergence will substantially reduce the amount of entrainment as indicated by experimental data. There will be no entrainment $(Q = 1)$ if $F_o' < 2.25$ and the reservoir is infinitely deep.

A reduction of the depth $H_2$ of the receiving channel adversely affects entrainment, which is important in the design of mixing chambers. The reduction in entrainment is significant when $H_2$ takes values of less than 8.

The effect of beach slope on entrainment was investigated only experimentally. Results obtained with $\alpha = 23^{o}$ slope angle differed little from those obtained for $\alpha = 90^{o}$. Results presented in this study can therefore be applied with some confidence to beach slopes in the range $23^{o} < \alpha < 90^{o}$. At $\alpha = 5.75^{o}$ the beach effect was clearly to produce a flow similar to that in a diffuser and to suppress all mixing.

## SECTION IX

## ACKNOWLEDGMENTS

The authors wish to acknowledge the assistance of Dipl. Ing. W. Geiger in the preparation of the experimental apparatus.

## SECTION X

## REFERENCES


[1] Koh, R. C. Y. "Two-dimensional Surface Warm Jets," Journal of the Hydraulics Division, Proc. of ASCE, Vol 97, No. HY6, 1971, pp 819-836.

[2] Stefan, H. "Stratification of Flow from Channel into Deep Lake," Journal of Hydraulics Division, Proc. of ASCE, Vol 96, No. HY7, 1970, pp 1417-1434.

[3] Wilkinson, D. L. Discussion of "Stratification of Flow from Channel into Deep Lake," Journal of Hydraulics Division, Proc. of ASCE, Vol 97, 1971, pp 602-609.

[4] Yih, C. S. and Guha, C. R. "Hydraulic Jump in a Fluid System of Two Layers," Tellus, Vol 7, No. 3, 1955, pp 358-366.

[5] Hayakawa, N. "Internal Hydraulic Jump in Co-Current Stratified Flow," Journal of the Engineering Mechanics Division, Proc. of ASCE, Vol 96, No. EM5, 1970, pp 797-800.

[6] Albertson, M. L.; Dai, Y. B.; Jensen, R. A.; and Rouse, H. "Diffusion of Submerged Jets," Transactions of ASCE, Paper No. 2409, Vol 115, 1950.

# Part III: Field Measurements in a Three-Dimensional Jet-Type Surface Plume

by
H. Stefan
and
F. R. Schiebe

December 1971

ABSTRACT

Field tests were conducted to measure temperature, velocity, and current direction with depth at several locations in the cooling water plume of the Allen S. King power generating plant on Lake St. Croix. The results of the study compare favorably with data from laboratory and analytical models operated under similarity criteria, specifically geometry and densimetric Froude number similarity.

CONTENTS

LIST OF FIGURES

LIST OF TABLES

## LIST OF SYMBOLS AND UNITS

| | |
|---|---|
| $b$ | Channel width at outlet [ft] |
| $F$ | Local densimetric Froude number based on local absolute velocity |
| $F^*$ | Local densimetric Froude number based on excess velocity |
| $F_o$ | Outlet densimetric Froude number |
| $g$ | Gravitational acceleration [ft $sec^{-2}$] |
| $h$ | Depth of thermocline at outlet [ft] |
| $n$ | Depth constant [ft] |
| $Q$ | Discharge [$ft^3$ $sec^{-1}$] |
| $Ri$ | Local Richardson number |
| $T$ | Temperature [degrees F] |
| $U$ | Average velocity [ft $sec^{-1}$] |
| $V$ | Excess velocity [ft $sec^{-1}$] |
| $z$ | Depth [ft] |
| $\beta_c$ | Slope of density-temperature curve $(\partial\varrho/\partial T)$ [slugs $ft^{-3}$ $^oF^{-1}$] |
| $\lambda$ | Ratio of inflection depths of temperature and velocity profiles |
| $\varrho$ | Density [lbs $sec^2$ $ft^{-4}$] |
| $\sigma$ | Depth of inflection of velocity profile in plume [ft] |

# SECTION I

## CONCLUSIONS

Temperature and velocity distributions resulting from jet-type surface discharges of heated water into near quiescent lakes appear to be little affected by the geometrical scale of the flow field. This implies also that the Reynolds number effect on the flow must be small. Vertical and horizontal spread of the heated water discharge depends primarily on the relative magnitudes of buoyant and inertial forces as conveniently expressed by densimetric Froude numbers specified at the outlet. These observations validate the assumptions made in the analytical model described in Part I of this report.

## SECTION II

## RECOMMENDATIONS

To further improve the predictive ability of either analytical or laboratory models, more extensive and accurate field measurements using improved techniques should be obtained on the same site. The main objective of such investigations would be to more accurately evaluate mixing and entrainment coefficients in both near and far fields of the plume under a variety of hydrological and meteorological conditions.

The processes which control the time-dependent fluctuations of temperature, velocity, and other related mixing and spreading parameters are inadequately understood. Diurnal effects deserve particular attention.

# SECTION III

## INTRODUCTION

In order to verify some of the analytical and experimental findings described in Part I of this report, it appeared desirable to make comparisons with field data. Temperature fields near cooling water outlets have been measured at various sites, and more data are forthcoming. References [25] through [29] in Part I are examples of such measurements. However, few measurements have been taken in thermal plumes with low densimetric Froude numbers at the outlet. For this reason, and in order to develop a better appreciation of prototype problems, it was considered worthwhile to obtain some field measurements. A location particularly suitable for these measurements was found at the cooling water outlet of the A. S. King power generating plant on Lake St. Croix, approximately 30 miles east of Minneapolis. Two surveys were taken, on June 18 and July 30, 1971.

## SECTION IV

## THE SITE

With one unit installed the A. S. King plant has a capacity of 550 MW. When operating at full capacity the cooling water flow rate is of the order of 630 cfs. The intake is through a skimmer wall from the bottom of the lake and the discharge through a canal 10 to 12 ft deep, approximately 1300 ft long and 45 ft wide at the bottom, with side slopes of 3:1. Before entering the lake the channel widens to approximately 145 ft at the bottom. The discharge into the lake is at an angle of nearly 90 degrees to one shoreline and 45 degrees to the other as shown in Fig. 1. The lake is actually a natural basin of the St. Croix River. Near the cooling water outlet the basin is approximately 3000 ft wide and up to 40 ft deep. A major portion of the lake is 25 to 30 ft deep. The shore is moderately steep with a slope of the order of 5:1 near the cooling water outlet channel. Figure 1 shows the channel and shoreline configurations. Because the discharge is from an exposed point on the shoreline and because the slope of the shore is not too flat, the heated water discharge forms a buoyant surface jet very similar to that described in the analytical and experimental studies.

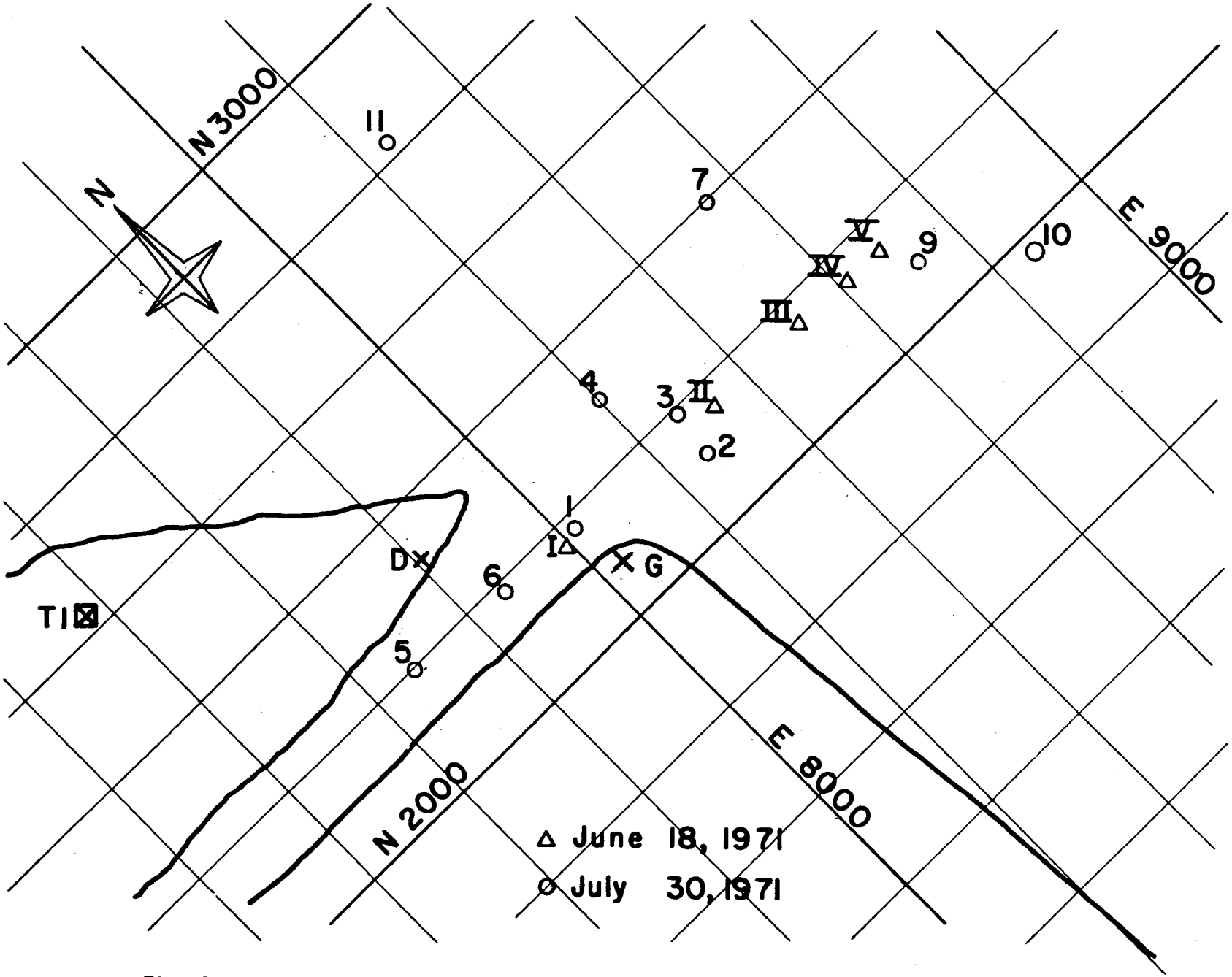


Fig. 1 - Cooling water discharge channel at Allen S. King power generating plant. Location of measuring stations

## SECTION V

## HYDROLOGICAL AND METEOROLOGICAL CONDITIONS

At the time of the survey the lake cooling water and meteorological conditions were as shown below in Table 1.

Table 1

HYDROLOGICAL, METEOROLOGICAL, AND PLANT OPERATING CONDITIONS

| | June 18 | July 30 |
|---|---|---|
| Elevation | close to 675 ft | 675 ft[2] |
| Surface water temp. upstream from discharge | -- | 73.3°F[2] |
| Surface flow velocity upstream from discharge | -- | 0.4 fps[2] |
| Cooling water flow rate | 583[1] | 560 cfs[1] |
| Plant load | 560 | 274 to 400 Mw[1] |
| Cooling water discharge temperature | ≈ 80°[2] | 79.1° to 80.4°F |
| Solar radiation | -- | 1.1 to 1.3 cal $cm^{-2}$ $min^{-1}$[1] |
| Wind velocity at 35 ft | 0 to 1[3] | 4 to 7 fps[1] |
| Wind direction | -- | NNW to NNE[1] |
| Dry bulb temp | 81° to 86°[1] | 64° to 68°F[2] |
| Wet bulb temp | -- | 57.5° to 58.5°F[2] |
| Sky | clear[2] | clear to 50% cover[2] |
| Duration of survey | 13:30 - 17:00 | 10:45 - 16:00 |

Sources of information: [1]NSP, [2]measurement, [3]estimate

## SECTION VI

## INSTRUMENTATION

Water temperature, flow velocity, and direction of flow were measured at selected stations shown in Fig. 1 and depths shown on the graphs to follow. Locations were determined by triangulation with transits from a base line on shore between points D and G in Fig. 1. Several reference points, such as the tower T1, were available. Depths were measured by distance from the water surface. A Yellow Spring Tele-Thermometer (thermistor), a Gurley current meter, and a current direction vane similar to that described in Ref. [1]* were used to find water temperatures, current magnitudes, and current directions, respectively. Only horizontal current velocities were measured.

The instruments were assembled on a triangular base as shown in Fig. 2 and lowered from a boat. The orientation of the instrumentation assembly was fixed with the aid of a telescope and a solid support system. The electrical signals of all meters were transmitted to the water surface, read, and manually recorded.

---

*References for Part III are listed on page III-35.

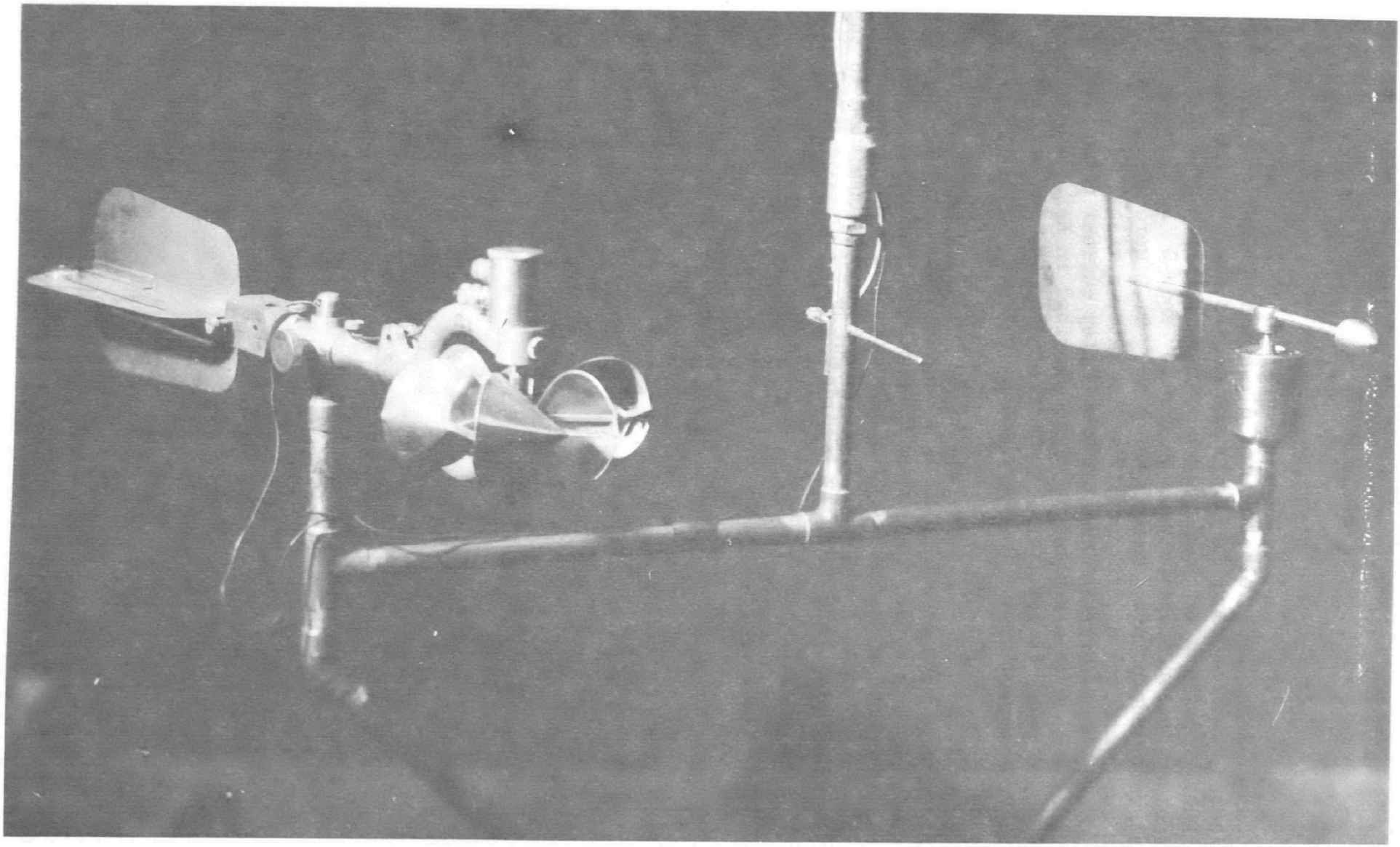

Fig. 2 - Instrument arrangement. Current meter (left), thermistor (center), and current direction vane (right)

## SECTION VII

## RESULTS

The measured temperature profiles with depth are shown in Fig. 3. A strong temperature stratification exists near the outlet which can be made even more apparent by plotting isotherms in a vertical cross section through the centerline of the discharge channel such as is shown in Fig. 4. For comparison, similar plots derived from much more extensive measurements carried out by Northern States Power Company (NSP) in previous years [2] are shown in Fig. 5. Figures 4 and 5 illustrate the type of stratification which develops when heated water is discharged at very low densimetric Froude numbers. A cold water wedge penetrates or attempts to penetrate into the outlet channel. The situation is very similar to the arrested salt water wedge which is encountered in rivers and channels discharging fresh water into the sea. Analyses of the salt (cold) water wedge phenomenon are given in Refs. [3], [4], and [5]. Observations of the phenomenon are reported in Ref. [6].

A mixing layer (metalimnion) of substantial thickness between the cold water and the heated water effluents can be observed in Figs. 4 and 5. This layer is probably caused by entrainment from the upstream toe of the cold water wedge. Although the outlet flow is not exactly two-layered, it is of interest to calculate densimetric Froude numbers at the end of the outlet channel for the field conditions using the depth from the water surface to the thermocline, h, defined as the inflection point of the vertical temperature profile, as the characteristic depth. The results are shown in Table 2.

Table 2

SUMMARY OF OUTLET CONDITIONS

| Date | Q (cfs) | h (ft) | b (ft) | $T_{max}$ ($^{o}F$) | $T_{min}$ ($^{o}F$) | $\frac{\Delta\rho}{\rho}$ (-) | $F_o$ (-) |
|---|---|---|---|---|---|---|---|
| 6-18-71 | 583 | 6. | 199. | 85. | 79. | 0.00111 | 1.06 |
| 7-30-71 | 560 | 7. | 196. | 80.8 | 70.2 | 0.00139 | 0.73 |
| 6-18-69 | 650 | 4.3 | 195.1 | 81. | 68.4 | 0.00159 | 1.65 |
| 9-4-69 | 660 | 4.0 | 205 | 88.2 | 72.5 | 0.00237 | 1.45 |
| 8-13-70 | 624 | 3.7 | 205.9 | 93.4 | 79.0 | 0.00242 | 1.50 |

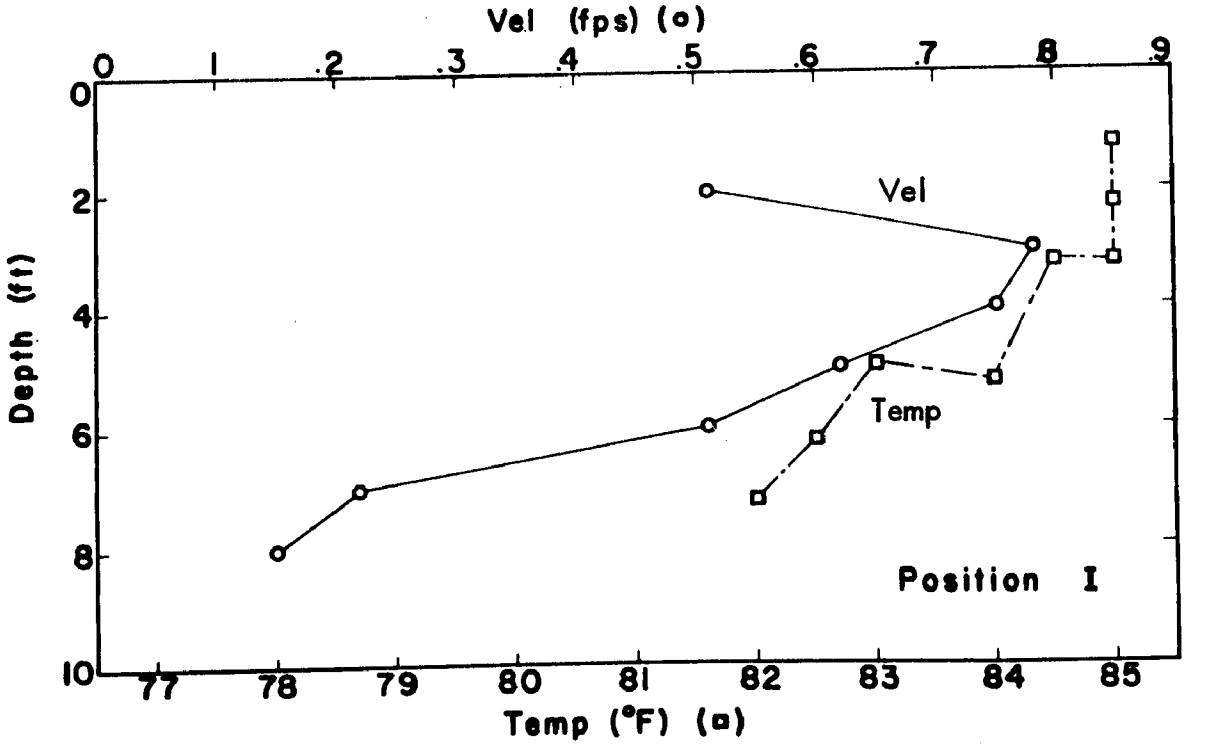


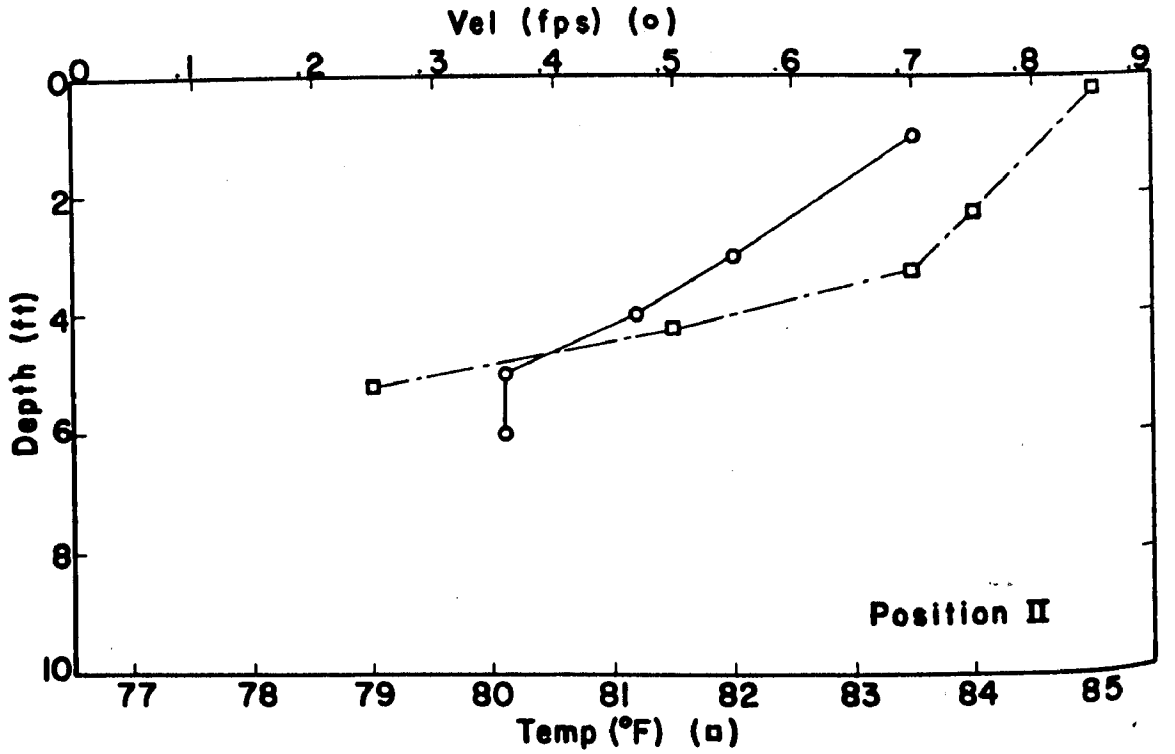


Fig. 3a - Profiles of measured velocities and temperatures
6-18-71

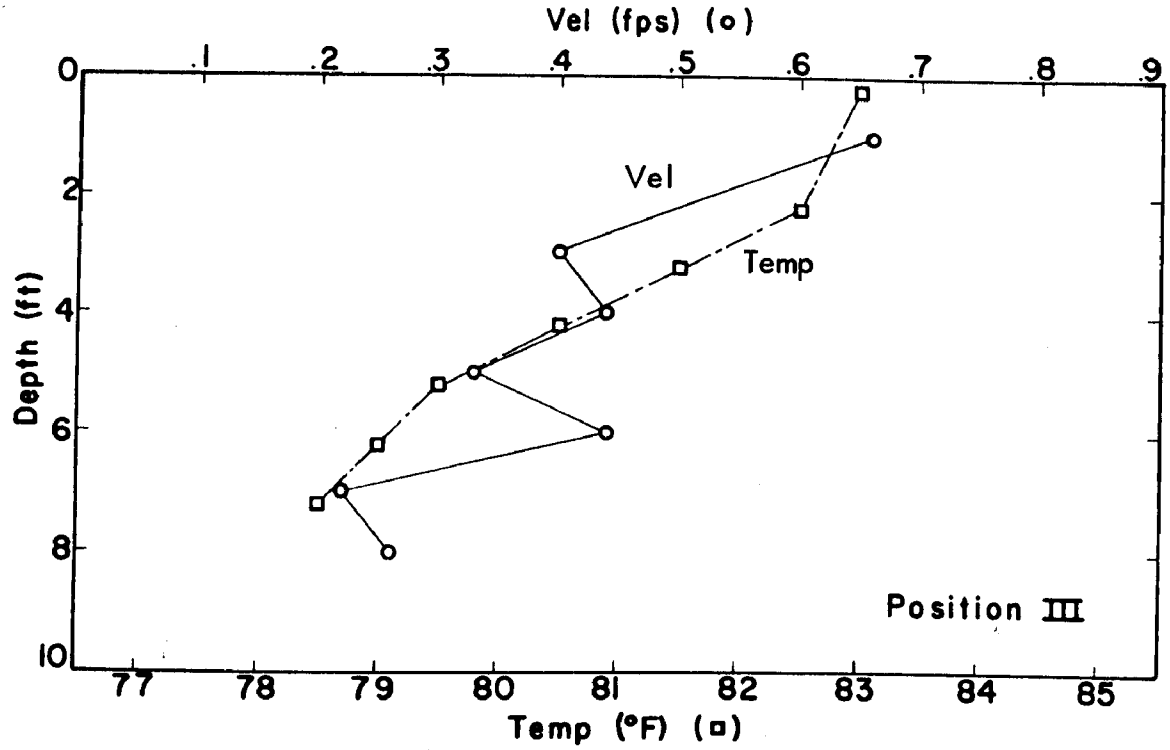


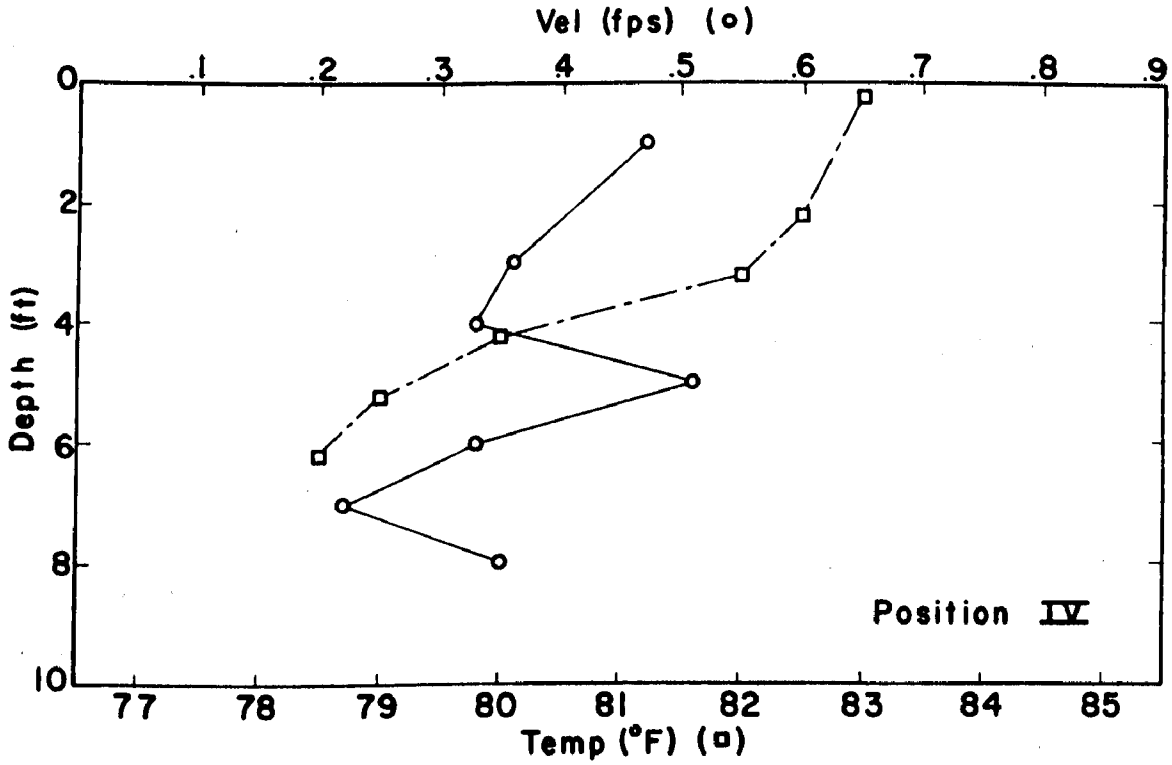


Fig. 3b - Profiles of measured velocities and temperatures (continued)
6-18-71

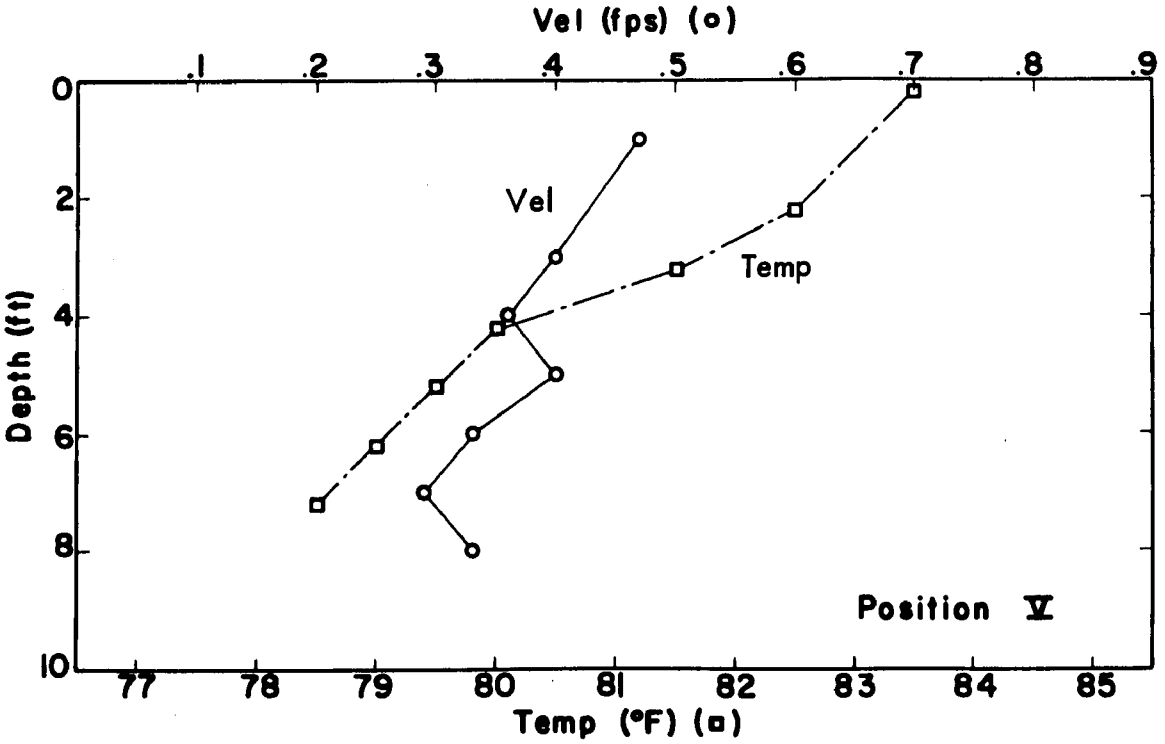


Fig. 3c - Profiles of measured velocities and temperatures (continued)
6-18-71

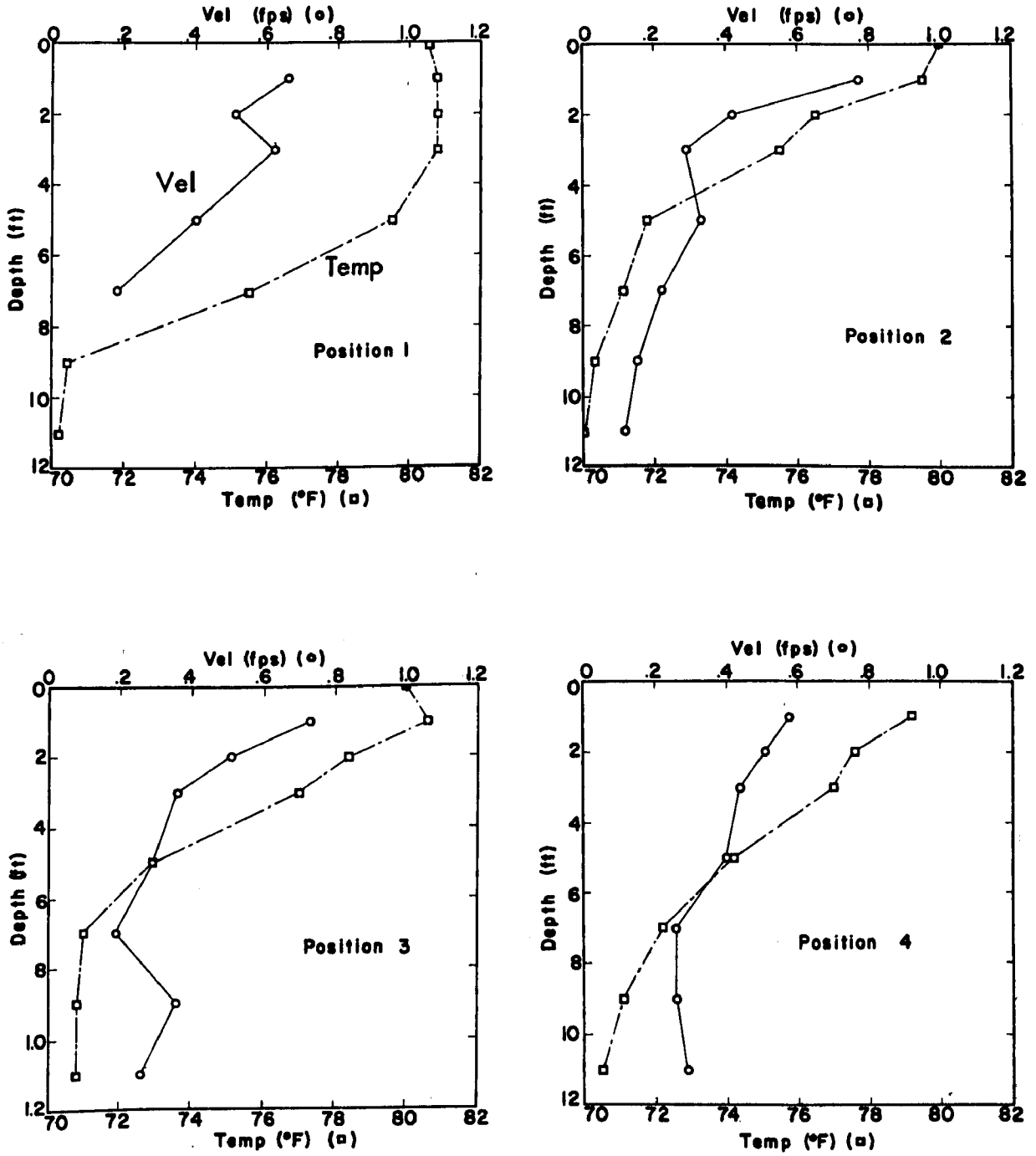


Fig. 3d - Profiles of measured velocities and temperatures (continued)
7-30-71

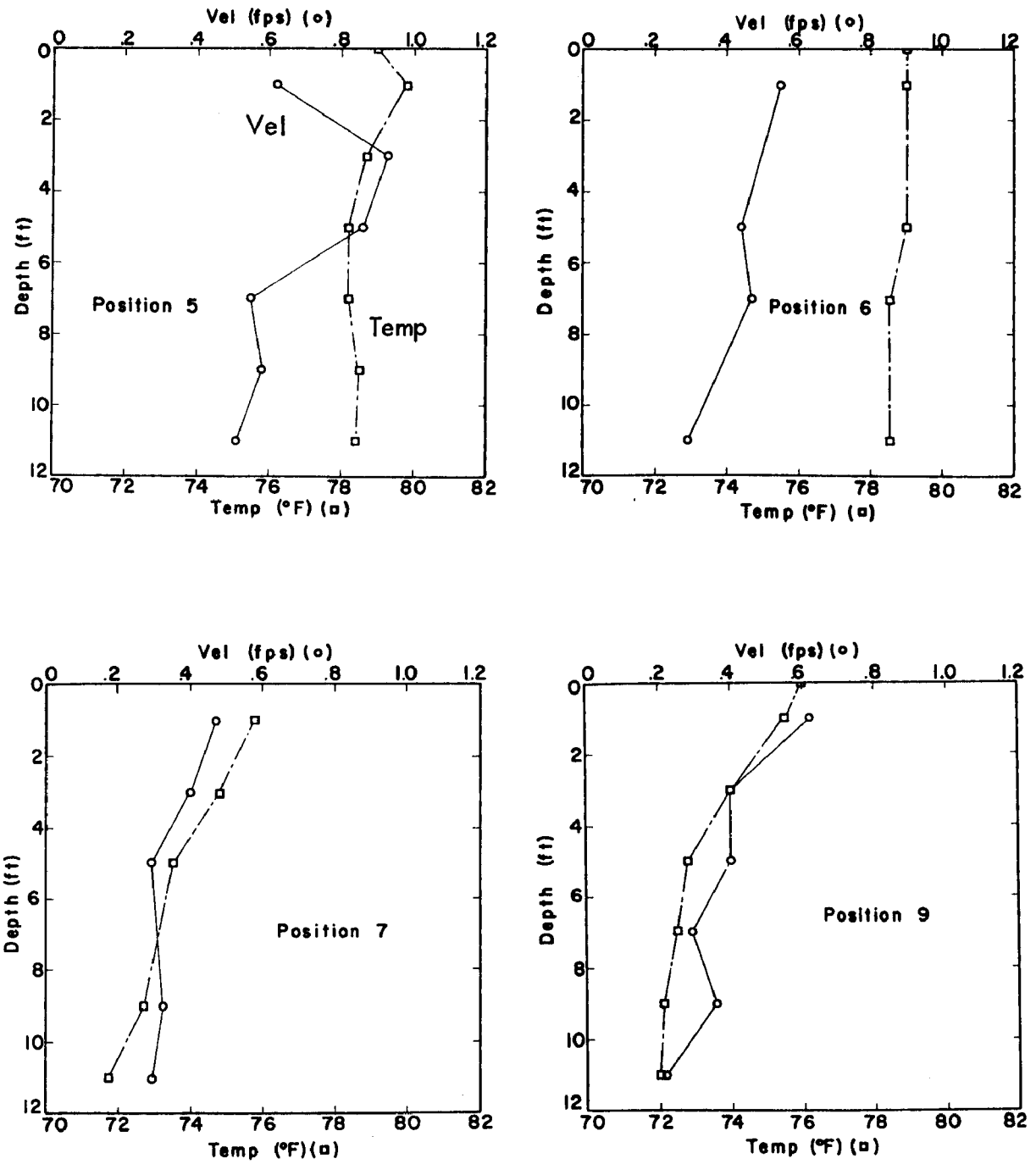


Fig. 3e - Profiles of measured velocities and temperatures (continued)
7-30-71

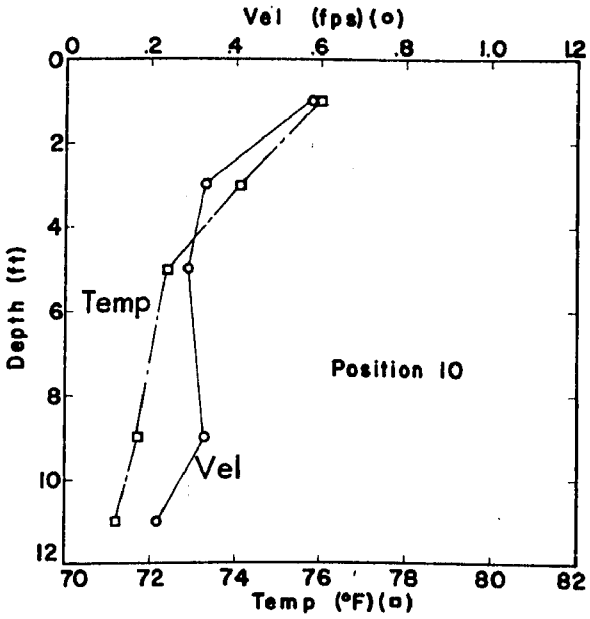


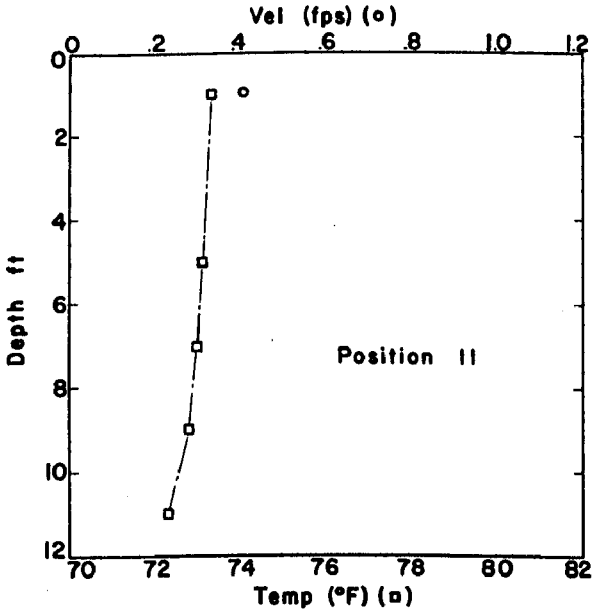


Fig. 3f - Profiles of measured velocities and temperatures (continued)
7-30-71

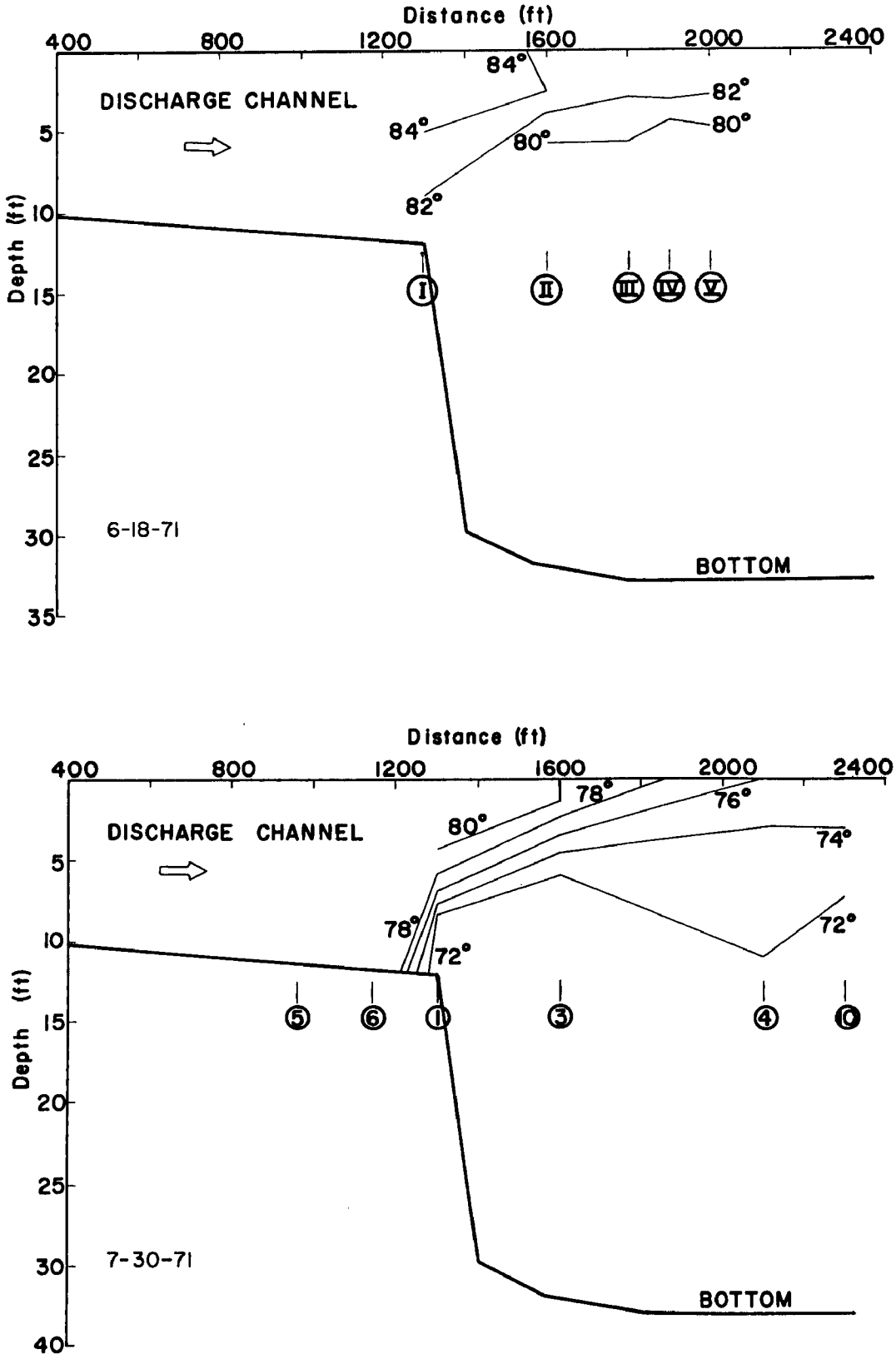


Fig. 4 - Isotherms in vertical cross section through centerline of discharge channel

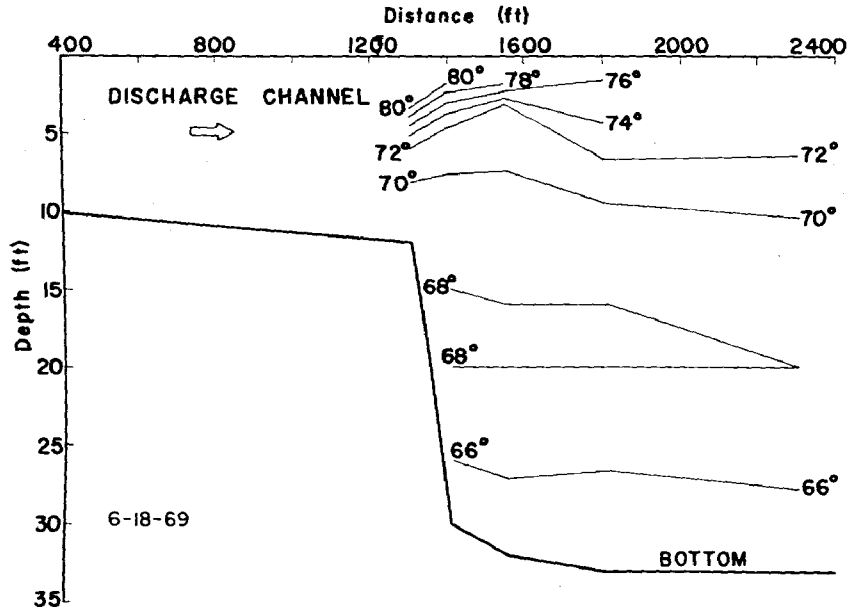


Fig. 5a - Isotherms in vertical cross section through centerline of discharge channel as derived from NSP measurements in 1969 and 1970

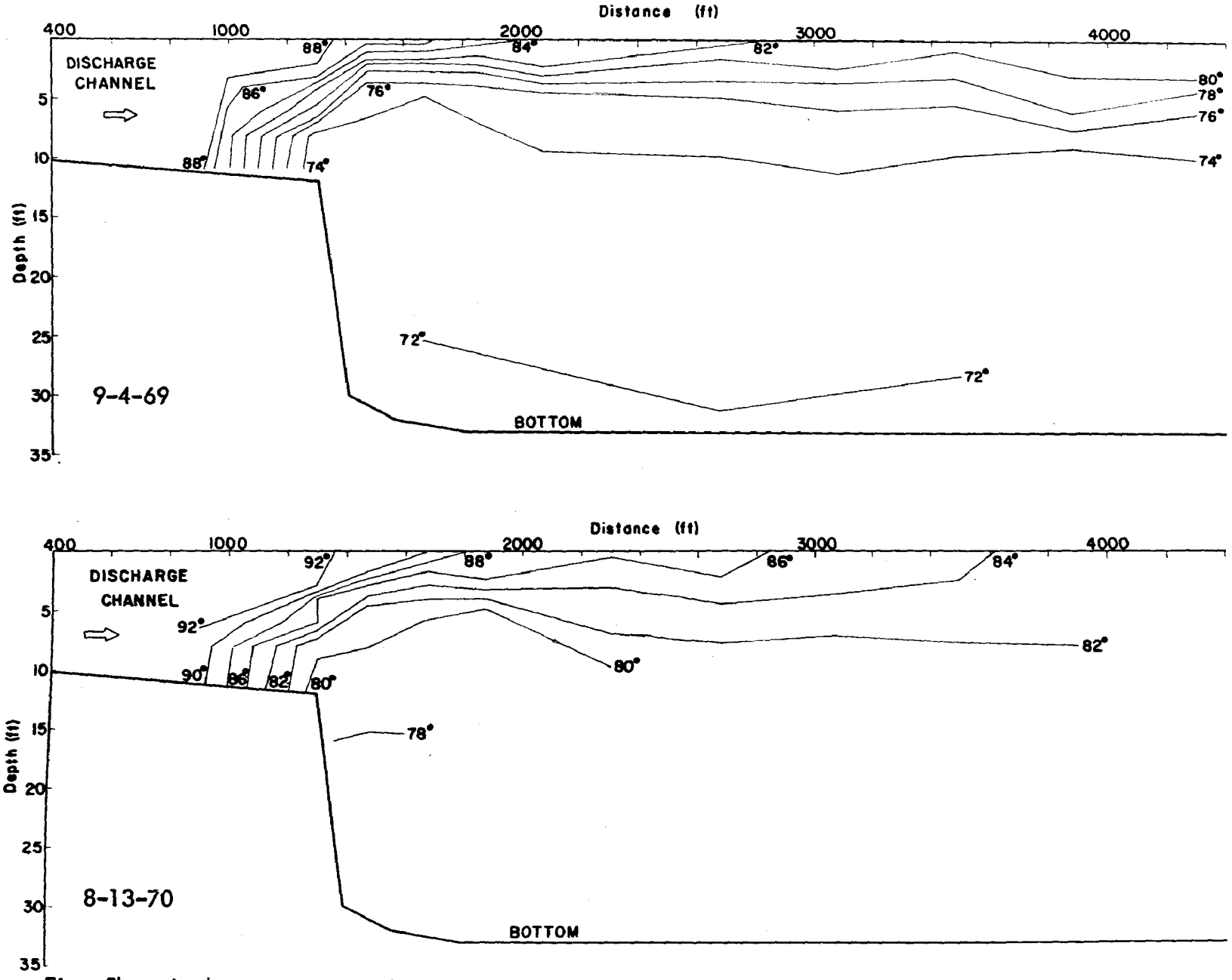




Fig. 5b - Isotherms in vertical cross section through centerline of discharge channel as derived from NSP measurements in 1969 and 1970 (continued)

The densimetric Froude number, $F_o$, is defined by

$$F_o = \frac{U}{\sqrt{\frac{\Delta\varrho}{\varrho} gh}} = \frac{Q}{bh\sqrt{\frac{\Delta\varrho}{\varrho} gh}} \qquad (1)$$

where $Q$ is the heated water discharge rate, $b$ is the width of the heated water layer at the outlet, $h$ is the depth of the thermocline below the water surface, and $\Delta\varrho$ is the density difference between the warmest and the coldest water in the outlet cross section. Isothermal patterns at the water surface were not derived from the present experiments because of the small number of measurements. Measurements of these patterns in previous years have been well documented by Northern States Power Company in Ref. [2].

The temperature stratification measured is also reflected in the velocity measurements. Although velocities below 0.10 fps could not be measured satisfactorily, it is already apparent from the results in Fig. 3 that the heated water forms a surface shear flow with a strong velocity gradient near the thermocline.

The resultant velocity vectors were decomposed into components which are respectively parallel (u) and perpendicular (v) to the discharge channel for the second survey (7-30-71); u and v are positive in easterly and southerly directions, respectively (see Fig. 1). The results given in Fig. 6 show strong gradients of both components with depth. The buoyant spread perpendicular to the main direction of the flow is evident in the velocity profiles measured at positions 2, 3, and 4. The plume is injected into a weak cross-current which is essentially produced by the breeze blowing from the north along the main orientation of the lake. At positions 2, 3, and 4 there is a reversion of the flow direction of the v-velocity component with depth. This was also observed at positions 9 and 10, but not at 7.

Since the v-velocity component is essentially a spread velocity perpendicular to the main direction of the flow, the measurements at stations 2, 3, 4, 7, and 9 illustrate the buoyancy-induced lateral spread. The distributions of the spread velocities with depth are very similar to those found in laboratory experiments in a tank and reported in Part I of this report.

The data shown in Fig. 3 can also be used to calculate Richardson numbers at various depths. The velocity and temperature measurements are approximated by functions of the form

$$T^* = T_m^* \exp\left[-\frac{z^2}{2\lambda^2\sigma^2}\right] \qquad (2)$$

$$V = V_m \exp\left[-\frac{z^2}{2\sigma^2}\right] \qquad (3)$$

where $z$ is the depth. The Richardson number will then follow the function

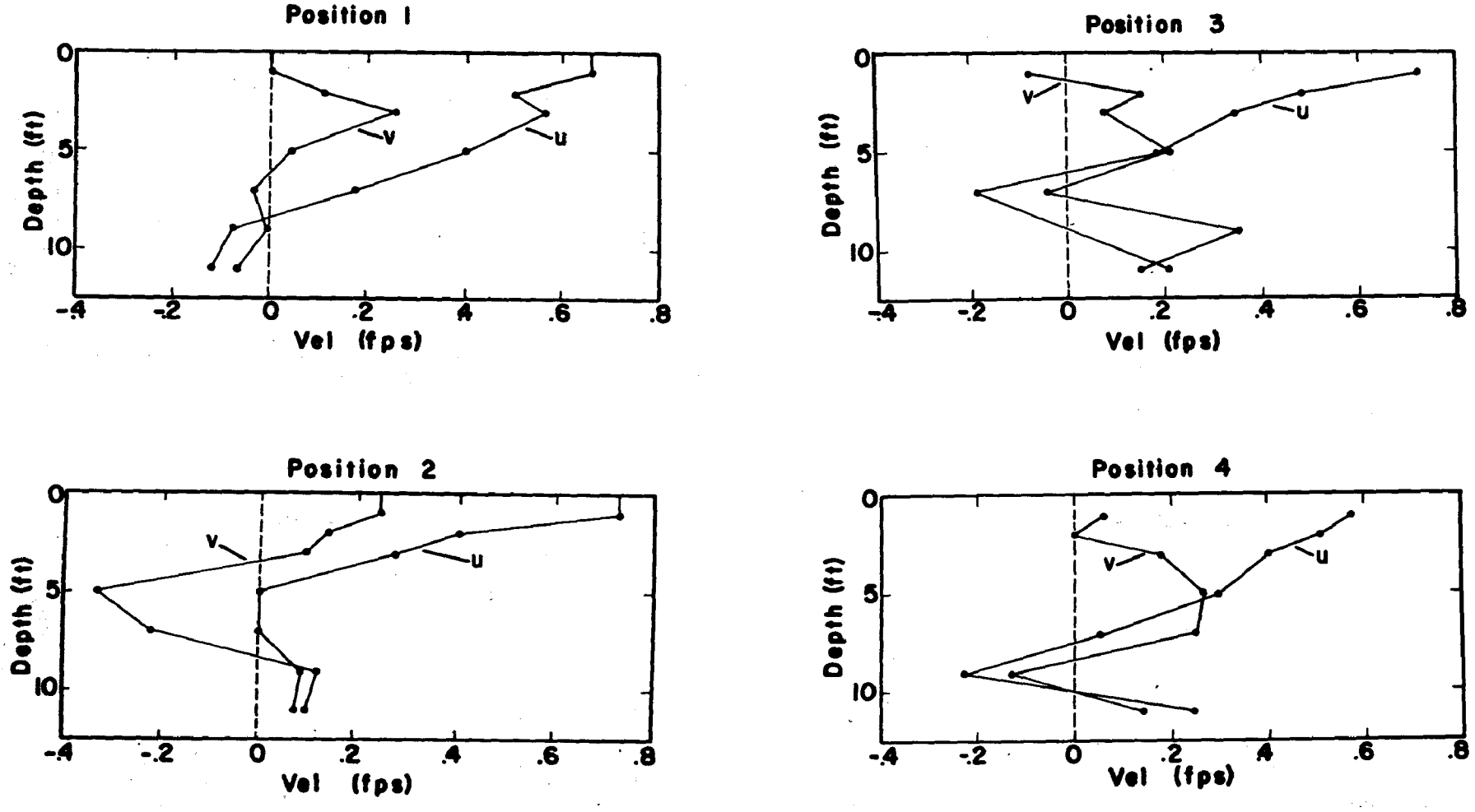


Fig. 6a - Velocity components u and v in direction of discharge and perpendicular to it, respectively

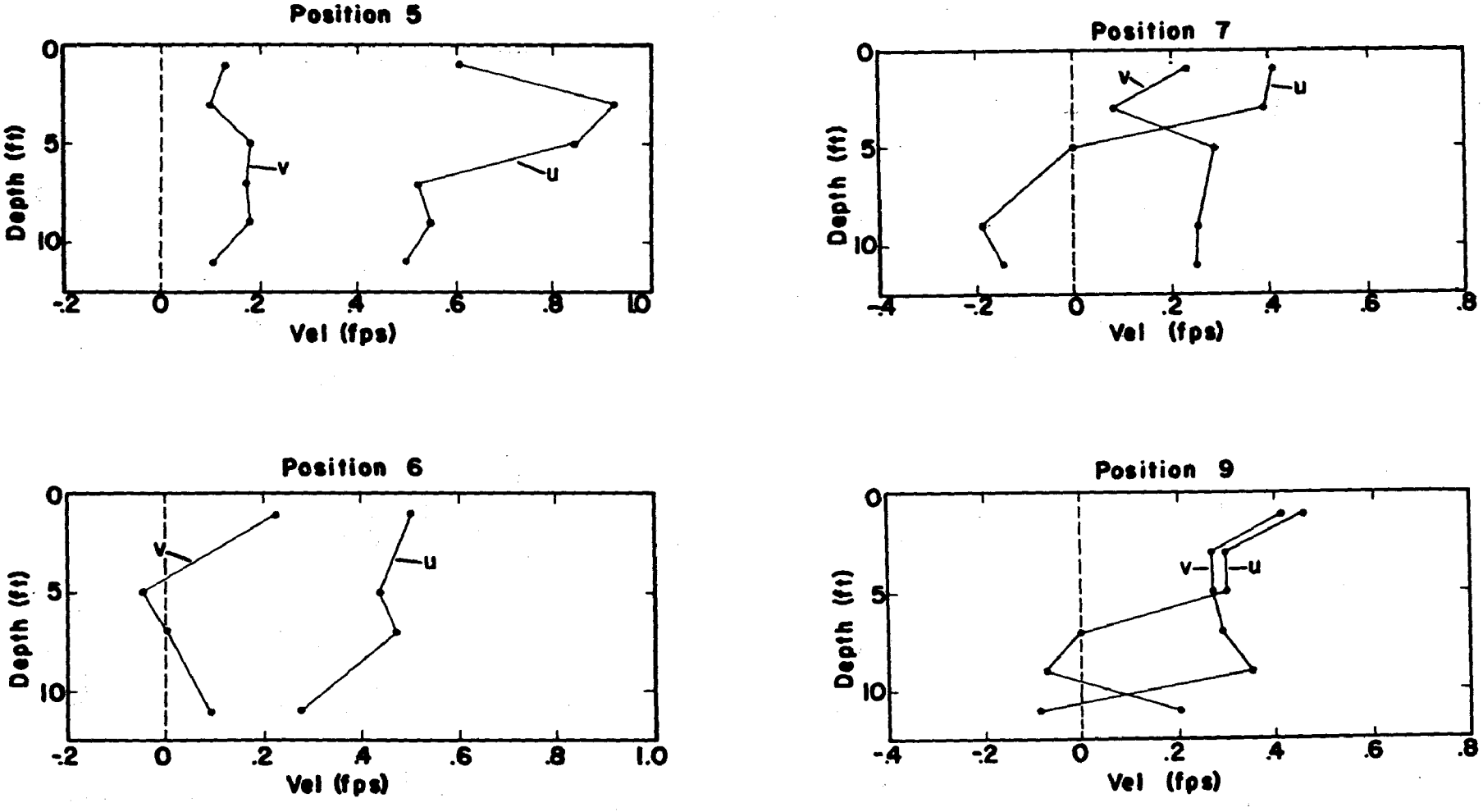




Fig. 6b - Velocity components u and v in direction of discharge and perpendicular to it, respectively (continued)

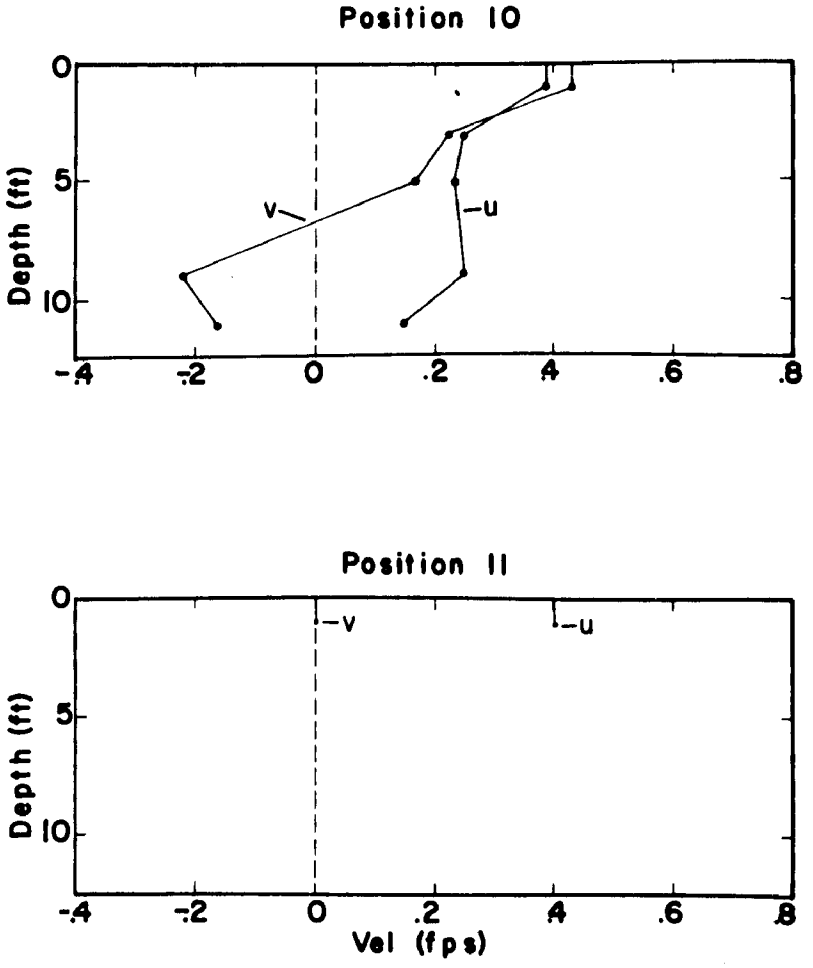


Fig. 6c - Velocity components u and v in direction of discharge and perpendicular to it, respectively (continued)

$$Ri = \frac{g\frac{d\rho}{dz}}{\rho\left(\frac{du}{dz}\right)^2} = \frac{g\,T_m^*\,\beta_c z}{\rho\,V_m^2\,\lambda^2}\left(\frac{\sigma}{z}\right)^2 \exp\left[\frac{z^2(2\lambda^2 - 1)}{2\lambda^2\sigma^2}\right] \qquad (4)$$

where the density-temperature relationship in the range under consideration has been assumed to be linear. In these equations $d\rho/dT = \beta_c$ (slugs $ft^{-3}$ $^oF^{-1}$), $T^*$ is the temperature excess above the cold lake temperature, $V$ is the excess velocity above the ambient lake current velocity at large depths below the surface layer of heated water, subscript $m$ refers to the maximum values of these variables in a given vertical profile, and $\lambda\sigma$ and $\sigma$ are the distances from the water surface to the inflection points of the temperature and the velocity profiles, respectively. These constants cannot be determined with great accuracy from the available data. Nevertheless some crude estimates for three stations are given in Table 3. Richardson numbers were then computed from Eq. (4). The results obtained were not satisfactory. The lowest Richardson numbers (ranging from 0.1 to 2.0) were found near the thermocline, while very high values occurred near the free surface and below the thermocline. This is an unacceptable result because it would mean that the stability of the stratification is weakest near the thermocline and stronger above and below. It can be shown that this result is due to the description of the temperature and velocity profiles by normal distribution functions. It must therefore be concluded that such functions adequately describe the overall features of the thermal plume, but are not satisfactory for the computation of local properties.

Table 3

SUMMARY OF CONDITIONS WITHIN THE PLUME

| Position | $T_m^*$ $^oF$ | $\beta_c$ slugs-$ft^{-3}sec^{-1}$ | $V_m$ $ft\ sec^{-1}$ | $\lambda$ (-) | $\sigma$ ft | n ft | F* (-) | F (-) |
|---|---|---|---|---|---|---|---|---|
| 2 | 10 | $2.48\times10^{-4}$ | .65 | 1.7 | 1.4 | 6.2 | 2.074 | 2.459 |
| 3 | 9.2 | $2.48\times10^{-4}$ | .54 | 1.7 | 1.8 | 6.2 | 1.584 | 2.141 |
| 4 | 8.7 | $2.48\times10^{-4}$ | .36 | 1.0 | 4.0 | 6.2 | 0.950 | 1.529 |
| 9 | 4.0 | $2.48\times10^{-4}$ | .32 | 1.5 | 2.0 | 6.2 | 1.438 | 2.781 |
| 10 | 4.8 | $2.48\times10^{-4}$ | .29 | 1.5 | 2.0 | 6.2 | 1.190 | 2.380 |

The selection of an exponential function to describe the measured velocity distribution with depth will remedy the above discrepancy. An exponential function of the form

$$V = V_m \exp[\frac{-z}{n}] \tag{5}$$

fits experimental data almost as well as the normal distribution function. It results in a Richardson number distribution of the form

$$Ri = \frac{g\, T_m^*\, \beta_c z}{\varrho\, V_m^{\,2}\, \lambda^2} \left(\frac{n}{\sigma}\right)^2 \exp\left(\frac{2z}{n} - \frac{z^2}{2\lambda^2\sigma^2}\right) \tag{6}$$

Numerical results given in Fig. 7 appear to be reasonable. Richardson number values are obviously extremely sensitive to minor changes in input data. The numerical field data must therefore be regarded and used with great caution. Calculated Richardson numbers give orders of magnitude at best.

Considering that a stable stratification, inhibiting vertical mixing, forms at a Richardson number value near unity, the results obtained from the field measurements suggest that the horizontal stratification was quite strong at all five locations for which data are shown. This result is in agreement with findings from the laboratory experiments and from the analytical model.

It is also of interest to calculate the overall densimetric Froude numbers from the data. In accordance with Eq. (4) in Part I of this report, the number is defined as

$$F^* = \frac{V_m}{\left(\frac{T_m^*\, \beta_c}{\varrho}\, g\sigma\lambda\right)^{1/2}} \tag{7}$$

Selected values are shown in Table 3.

Another set of densimetric Froude numbers can be calculated by considering measured absolute flow velocities $U_m$ instead of excess velocities $V_m$. If $U_m$ is the measured absolute water surface velocity at a station, the new densimetric Froude number is

$$F = F_* \frac{U_m}{V_m} \tag{8}$$

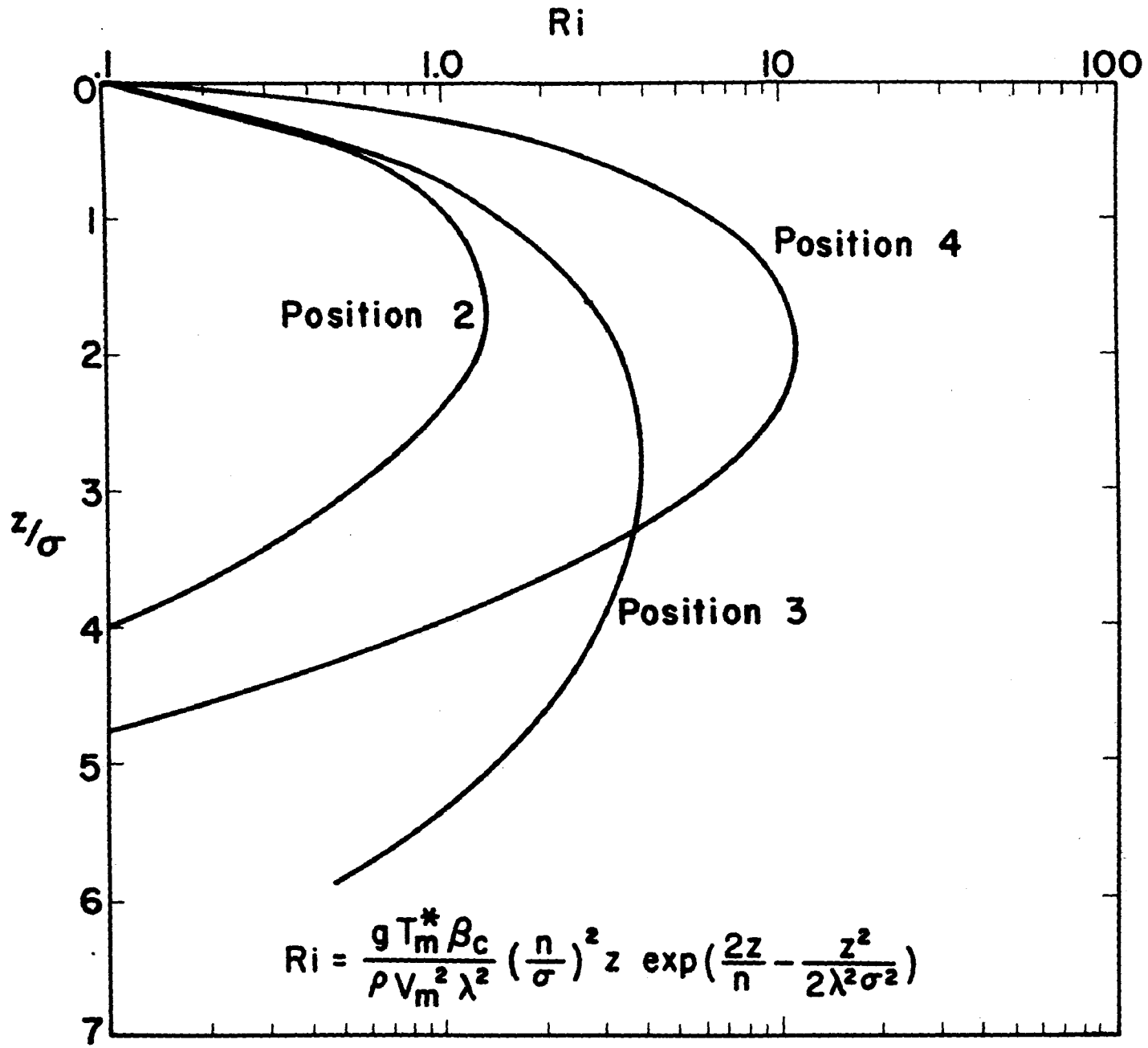


Fig. 7 - Richardson number distribution with depth for selected locations

Results are shown in the last column of Table 3. The average value is 2.26, which is close to the values obtained in laboratory experiments and shown in Fig. 46 of Part I.

## SECTION VIII

## SUMMARY

A small number of temperature and velocity measurements were taken near the cooling water outlet channel of the A. S. King power generating plant on Lake St. Croix on two occasions during the summer of 1971. The results were analyzed in terms of

1. Temperature profiles with depth
2. Velocity components in direction of discharge with depth
3. Velocity components perpendicular to direction of discharge (spread velocities)
4. Isotherms in a vertical plane through the center of the discharge channel
5. Densimetric Froude numbers for individual stations
6. Richardson numbers as a function of depth

All the field results agree within reason with experimental laboratory data obtained for the same outlet densimetric Froude numbers. For instance, temperature, velocity, and Richardson number profiles show the same type and degree of stratification; the horizontal spread is of the same nature as in the laboratory; and densimetric Froude numbers at locations near the outlet are of the same magnitude as found through laboratory experiments and analysis.

## SECTION IX

## ACKNOWLEDGMENTS

The authors were assisted in the field surveys by students from the Department of Civil and Mineral Engineering, in particular Messrs. Glen Martin, David Ford, and Loren Bergstedt. Mr. Karl Streed prepared some of the figures. Professor E. Silberman helped in making the arrangements for the surveys. Northern States Power Company kindly provided a boat and operator. The manuscript of this report was edited and typed by Mrs. Shirley Kii.

## SECTION X

## REFERENCES


[1] Csanady, G. T. and Mekinda, M., "Rapid Fluctuations of Current Direction in Lake Huron," Proceedings of the Thirteenth Conference on Great Lakes Research, Part I, International Association for Great Lakes Research, 1970.

[2] Fitch, N. R., Temperature Surveys of St. Croix River, 1969-1970, Northern States Power Company, December 1970.

[3] Ippen, A. T. and Harleman, D. R. F., Steady-State Characteristics of Subsurface Flow, Circular 521, U.S. National Bureau of Standards, 1952, pp. 79-93.

[4] Harleman, D. R. F., "Stratified Flow," Section 26 of Handbook of Fluid Dynamics, edited by V. L. Streeter, McGraw-Hill Book Company, 1961.

[5] Keulegan, G. H., "The Mechanism of an Arrested Saline Wedge," Section 11 of Estuary and Coastline Hydrodynamics, edited by A. T. Ippen, McGraw-Hill Book Company, 1966.

[6] Keulegan, G. H., An Experimental Study of the Motion of Saline Water from Locks into Fresh Water Channels, Report 5168, U.S. National Bureau of Standards, March 1957.

| 1 Accession Number | 2 Subject Field & Group | SELECTED WATER RESOURCES ABSTRACTS<br>INPUT TRANSACTION FORM |
|---|---|---|
| W | 05G | |

5 Organization

Minnesota Univ., Minneapolis, St. Anthony Falls Hydraulic Lab.

6 Title

SURFACE DISCHARGE OF HEATED WATER

10 Author(s)

Stefan, H.
Hayakawa, N.
Schiebe, F. R.

16 Project Designation

Project No. 16130 FSU

21 Note

22 Citation

23 Descriptors (Starred First)

*Outfalls, *Thermal Pollution, *Mathematical Model, Thermal Plume Data

25 Identifiers (Starred First)

*Thermal Outfalls, *Surface Discharge

27 Abstract

A comprehensive analytical model has been developed to describe the flow of heated water from a channel onto the surface of a lake or reservoir. This analytical tool can be used to predict depth, width, temperature, and flow velocity in a heated water surface jet. Weak cross-currents and winds are included. The model also predicts the total amount of heat actually lost to the atmosphere and the amount of ambient water entrained As presented, the analytical method is simple and inexpensive to apply. It assumes fully established buoyant jet flow into a homogeneous environment. It can be extended to include, for example, an outlet zone (zone of flow establishment) or stratification in the ambient water. Experimental (laboratory) data have been analyzed for comparison with the analytical method and also to illustrate the physical features of heated water surface discharges, particularly those with low densimetric Froude numbers. The two-dimensional mixing internal hydraulic jump has been analyzed theoretically and experimentally. Criteria for the existence of the phenomenon and the rates of entrainment which it may produce have been established theoretically and verified with a limited number of experimental data. The results of two field surveys in a thermal plume are presented. Comparisons with laboratory data illustrate the outstanding significance of the densimetric Froude number and the relative insignificance of the Reynolds number as modeling parameters. (Stefan-Minnesota)

Abstractor: Heinz G. Stefan
Institution: St. Anthony Falls Hydr. Lab., U. of Minn., Minneapolis

WR:102 (REV. JULY 1969) WRSIC
SEND, WITH COPY OF DOCUMENT, TO: WATER RESOURCES SCIENTIFIC INFORMATION CENTER U.S. DEPARTMENT OF THE INTERIOR WASHINGTON, D. C. 20240
*U.S. GOVERNMENT PRINTING OFFICE: 1972-484-484/158 1-3
GPO: 1970 - 407 -891